

TECHNISCHE UNIVERSITÄT MÜNCHEN

Lehrstuhl für Entwicklungsgenetik



Nedd8 in the brain -
Its impact on synaptic function and
the role of PSD-95

Marisa Brockmann

Vollständiger Abdruck der von der Fakultät Wissenschaftszentrum Weihenstephan für Ernährung, Landnutzung und Umwelt der Technischen Universität München zur Erlangung des akademischen Grades eines

Doktors der Naturwissenschaften

genehmigten Dissertation.

Vorsitzender:

Univ.-Prof. Dr. E. Grill

Prüfer der Dissertation:

1. Univ.-Prof. Dr. W. Wurst

2. Univ.-Prof. Dr. V. Stein (Rheinische Friedrich-Wilhelms-Universität Bonn)

3. apl. Prof. Dr. J. Beckers

Die Dissertation wurde am 04.11.2013 bei der Technischen Universität München eingereicht und durch die Fakultät Wissenschaftszentrum Weihenstephan für Ernährung, Landnutzung und Umwelt am 02.04.2014 angenommen.

Ehrenwörtliche Versicherung

Ich versichere hiermit ehrenwörtlich, dass diese Dissertation mit dem Titel “Nedd8 in the brain – Its impact on synaptic function and the role of PSD-95” selbständig und ohne unerlaubte Beihilfe angefertigt habe. Ich habe mich dabei keiner anderen als der von mir ausdrücklich bezeichneten Hilfen oder Quellen bedient.

Erklärung

Hiermit erkläre ich, dass ich mich nicht anderweitig einer Doktorprüfung ohne Erfolg unterzogen habe. Die Dissertation wurde in ihrer jetzigen oder ähnlichen Form bei keiner anderen Hochschule eingereicht und hat noch keinem sonstigen Prüfungszweck gedient.

München, im Oktober 2013

Marisa Brockmann

Preface

The present study was conducted as a collaboration in two different labs. The biochemical experiments were obtained in the laboratory of Dr. Damian Refojo at the MPI of Psychiatry, whereas the electrophysiological experiments were conducted in the laboratory of Prof. Dr. Valentin Stein at the University of Bonn. All experiments shown in this PhD Thesis were performed by myself. Whenever others contributed to the work, the individual researchers are stated in the figure legends.

Contents

Preface	vii
Abstract	1
Zusammenfassung	5
1 Introduction	9
1.1 The Excitatory Synapse	9
1.1.1 The Pre-Synapse	10
1.1.2 The Post-Synapse	11
1.2 Synaptic Plasticity	16
1.3 The Inhibitory Synapse	18
1.4 Ubiquitin-Like-Pathways	19
1.4.1 The Ubiquitin Pathway	19
1.4.2 The Nedd8 Pathway	20
1.4.3 Nedd8 Targets – Functional Impact of Protein Neddylation	21
1.5 Ubiquitin-Like Pathways in the Brain	23
1.5.1 UBLs in the Pre-Synapse	23
1.5.2 UBLs in the Post-Synapse	24
1.6 Theory	25
1.6.1 The Hippocampus	25
1.6.2 Modes of Recording	27

2	Material and Methods	33
2.1	Material	33
2.1.1	Buffers	33
2.1.2	Chemicals and Reagents	36
2.1.3	Antibodies	37
2.2	Methods	38
2.2.1	Cell Culture	38
2.2.2	Primary Hippocampal Cell Culture	38
2.2.3	Molecular Biology	41
2.2.4	Biochemistry	45
2.2.5	Affinity Purification and Mass Spectrometry	48
2.2.6	Animal Experiments	50
2.2.7	In-Utero Electroporation	50
2.2.8	Organotypic Hippocampal Slice Preparation	51
2.2.9	Semliki Forest Virus Preparation	52
2.2.10	Infection of Organotypic Hippocampal Slices with SFV	54
2.2.11	Image Acquisition and Live Cell Imaging	54
2.2.12	Acute Hippocampal Slice Preparation	55
2.2.13	Electrophysiology Field Recordings	55
2.2.14	Whole Cell Recordings	56
2.2.15	Somatic Outside-Out Patches	59
2.2.16	Data Analysis	59
3	Aim	61
4	Results	65
4.1	Neddylated Proteins in the Mature Synapse	65
4.2	Interference with the Ned8 Pathway	67
4.3	PSD-95: The First Described Synaptic Target of Neddylation	70
4.3.1	Neddylation of PSD-95	70

4.3.2	Blocking PSD-95 Neddylation - Genetic Approaches	72
4.3.3	Blocking PSD-95 Neddylation - Pharmacological Approach	74
4.3.4	PSD-95 Neddylation is Mediated via the E3 Ligase Mdm2	75
4.4	GKAP is not Neddylated	76
4.5	Structural Characteristics of PSD-95 Promote its Neddylation	78
4.6	PSD-95 is Ubiquitylated	80
4.7	Functional Impact of PSD-95 Neddylation	81
4.7.1	PSD-95 Ubiquitylation vs. Neddylation	81
4.7.2	PSD-95 Multimerization is Diminished after MLN-4924 Treatment . .	83
4.8	Neddylated Lysine Residues of PSD-95	84
4.8.1	A new Mass-Spectrometry Method for the Unambiguous Identification of Neddylated Lysine Residues	85
4.8.2	Mass Spectrometry Analysis Revealed Neddylated and Ubiquitylated Lysine Residues of PSD-95	87
4.8.3	Location of Neddylated and Ubiquitylated Lysine Residues in PSD-95	90
4.8.4	Nedd8 and ubiquitin Compete for K393 Modification	92
4.8.5	Generation of PSD-95 Neddylation Mutants	93
4.9	Morphological and Functional Analysis of PSD-95 Neddylation Mutants . . .	94
4.9.1	Morphological Analysis of PSD-95 Mutants in Primary Neurons . . .	95
4.9.2	Morphological Analysis of PSD-95-K202R during Spine Development in Hippocampal Slices	96
4.9.3	PSD-95-K202R has a Dominant Negative Effect on Excitatory Synapse Function during Spine Development	98
4.9.4	PSD-95-K202R Exerts a Dominant Negative Effect on mEPSC Frequency in Mature Excitatory Synapses	100
4.10	Ubc12-C111S in Electrophysiology	103
4.10.1	Blocking the Nedd8 Pathway Affects Synaptic Transmission - Genetic Approach	103

4.11	Acute Effects of Neddylation Inhibition on Synaptic Transmission - Pharmacological Approach	105
4.11.1	Acute MLN-4924 Treatment Affects Spine Morphology and Function in Primary Hippocampal Neurons	105
4.11.2	Acute MLN-4924 Treatment has no Effect on Spine Size in Hippocampal Neurons from Acute Brain Slices	107
4.12	Nedd8 Effects on Basal Synaptic Transmission	108
4.13	Neddylation Effects on the Pre-Synapse of Excitatory Synapses	110
4.13.1	Pre-Synaptic Neurotransmitter Release is Altered in MLN-4924-Treated Acute Brain Slices	111
4.13.2	MK-801 Effect is Decreased in MLN-4924-treated Brain Slices	113
4.13.3	Vesicle Depletion and Recovery after High Frequency Stimulation is Reduced in MLN-4924-Treated Slices	115
4.14	Neddylation Effects on the Post-Synapse of Excitatory Synapses	116
4.14.1	MLN-4924 Reduces Synaptic Transmission in Acute Brain Slices	117
4.14.2	AMPA/NMDA Ratios are Increased upon Neddylation Inhibition	118
4.14.3	AMPA EPSCs are Decreased when the Nedd8 Pathway is Blocked	120
4.14.4	NMDA EPSCs are Decreased when the Nedd8 Pathway is Blocked	121
4.14.5	Decay Times of AMPA and NMDA Currents	123
4.14.6	The Current Amplitude of Somatic Outside-Out Patches Increases upon MLN-4924 Treatment	125
4.15	Neddylation Effects on Inhibitory Synapses	126
4.16	Neddylation in Synaptic Plasticity	128
4.16.1	Glutamate Treatment Increases PSD-95 Neddylation	129
4.16.2	MLN-4924 Prevents LTP Induction	132
4.16.3	Ubc12-C111S Interferes with LTP Induction	133
4.16.4	MLN-4924 Prevents LTD Induction	134

5 Discussion	137
5.1 Neddylated is Active in Neurons	138
5.2 PSD-95 is a Target of the Nedd8 Pathway	139
5.3 Identification of Neddylated Lysine Residues	143
5.4 PSD-95-K202R Impact on Neuronal Morphology and Function	147
5.5 Functional Impact of Neddylated on Basal Synaptic-Transmission at Excitatory Synapses	150
5.5.1 Neddylated is Involved in Pre-Synaptic Functions	151
5.5.2 Nedd8 Controls AMPA Receptor Distribution	154
5.5.3 Nedd8 Control AMPA Receptor Kinetics	157
5.5.4 Nedd8 Controls NMDA Receptor Distribution	157
5.6 Functional Impact of Neddylated on Synaptic-Neurotransmission at Inhibitory Synapses	159
5.7 Activity-Dependent Changes of Target Protein Neddylated	160
5.8 The Nedd8 Pathway is Involved in the Induction of Synaptic Plasticity	162
5.9 The Impact of MLN-4924 on Different Synaptic Sites	163
6 Conclusion	165
List of Figures	167
List of Tables	171
Nomenklatur	173
References	177
Acknowledgments	I
Curriculum Vitae	III
Publications	V

Abstract

Post-translational modifications, like ubiquitin and SUMO, have been implicated in the regulation of neuronal function under basal conditions and during synaptic plasticity. Dysfunction of the ubiquitin and the SUMO pathway, has been shown to alter synaptic transmission and synaptic plasticity. Additionally, ubiquitin-like pathways have been associated with neurological diseases, such as Alzheimer's and Parkinson's disease. In neuronal and glia inclusions, besides ubiquitylated and sumoylated proteins, also neddylated proteins have been found. But so far, neddylated proteins in neurons or the impact of neddylation on neuronal function remains unexplored.

The aim of this thesis was to identify neddylated proteins in synaptic compartments and to characterize the impact of neddylation on synaptic function.

First, protein analyses of the synapse revealed that the Nedd8 pathway is active in pre- and post-synaptic compartments, where many neddylated proteins are present. Immunoprecipitation experiments revealed the first neuron-specific target of the Nedd8 pathway: PSD-95.

Detailed analysis of PSD-95 neddylation proved that the activating enzyme Nae1 and the conjugating enzyme Ubc12 are involved in PSD-95 neddylation. Additionally, PSD-95 is neddylated *via* the E3 ligase Mdm2. Biochemical analyses of PSD-95 revealed that the PEST domain, located at the N-terminus of PSD-95, is necessary for the recruitment of Ubc12 and thus mediates PSD-95 neddylation. Deleting the PEST domain prevents PSD-95 neddylation proving that this protein sequence in PSD-95 is essential for its modification by the Nedd8 pathway. In addition, we provided here the first description about the function of PSD-95 neddylation. The lack of PSD-95 neddylation reduced PSD-95 oligomerization and by this means destabilizes the synapse. These results suggest an opposed effect of Nedd8 and ubiquitin on PSD-95 function: whereby PSD-95 is ubiquitylated upon NMDA activation and consequently degraded *via* the proteasome

and PSD-95 neddylation is triggered upon glutamate treatment and stabilizes PSD-95 in the post-synapse.

In a subsequent set of experiments, the neddylation of PSD-95 was investigated more precisely, aiming to identify neddylated lysine residues of PSD-95 *via* mass spectrometry. Although this approach is the state of the art in the identification of ubiquitylated targets, the identification of neddylated residues is impracticable under conventional settings, since Nedd8 and ubiquitin modifications result both in -GG remnants after trypsination and consequently cannot be differentiated by mass spectrometry. To overcome this limitation, Nedd8 mutants were designed that generate a mass shift for Nedd8 after trypsin digestion and consequently allow the differentiation between Nedd8 and Ubiquitin. Western Blot experiments sufficiently proved the efficiency of the generated Nedd8 mutants which allowed the identification of neddylated lysine residues in PSD-95. Mass spectrometry revealed five neddylated lysines in PSD-95 of which K202 was the most consistently modified residue. Morphological analysis during spine development revealed that spine maturation was impaired in neurons expressing the Nedd8 deficient mutant PSD-95- K202R. These morphological defects were supported by electrophysiological recordings, showing that PSD-95-K202R has a dominant-negative effect on mEPSC amplitude in developing neurons.

In addition, neddylation strongly impacts on pre-synaptic function by regulating pre-synaptic neurotransmitter release and the refilling of vesicles after sustained activity.

At the post-synaptic site, neddylation inhibition results in decreased AMPA and NMDA currents which might result from a decreased number of post-synaptic AMPA and NMDA receptors. Furthermore, neddylation inhibition alters AMPA receptor kinetics. This effect might be provoked by altered pre-synaptic vesicle release, altered neurotransmitter re-uptake, or it might be that neddylation favors the interaction between the AMPA receptors and auxiliary proteins such as TARPs or Cornichons and consequently increases the decay time of AMPA currents.

Besides the effects the Nedd8 pathway exerts on basal synaptic neurotransmission, neddylation also impacts on synaptic plasticity. When neddylation is blocked neither long-term potentiation nor long-term depression is induced. Furthermore, neuronal activity increases target protein neddylation including PSD-95. In conclusion, neddylation is triggered by neuronal activity and

might control changes in synaptic strength.

In summary, this thesis describes the first neuron specific target of the Nedd8 pathway: PSD-95. Furthermore, a new mass spectrometry approach revealed PSD-95-K202 to be neddylated and we observed that K202 neddylation is essential for neuronal development. In addition, it was demonstrated for the first time that the Nedd8 pathway impacts on basal neurotransmission by influencing neurotransmitter release from the pre-synapse and AMPA as well as NMDA receptor distribution in the post-synaptic membrane. Therefore, this thesis opens a new field in synaptic research describing the synaptic function of a new post-translational modification in the brain.

Zusammenfassung

Posttranslationale Proteinmodifikationen wie Ubiquitylierung und SUMOylierung steuern wichtige neurobiologische Prozesse wie die Signalübertragung an Synapsen und die synaptische Plastizität. Die Dysfunktion des Ubiquitin und Sumo- Signalweges wurde bereits mit vielen neurodegenerativen Krankheiten in Verbindung gebracht in denen synaptische Funktionen sowie synaptische Plastizität gestört sind. Hierzu zählen neurologische Erkrankungen wie Alzheimer oder Parkinson, bei denen Ubiquitin und Sumo in Plaques nachgewiesen werden konnte. Ebenfalls wurde Nedd8, ein Ubiquitin-ähnliches Protein, in Neuronen nachgewiesen dessen Rolle im Gehirn zurzeit noch völlig unerforscht ist.

Das Ziel dieser Arbeit lag darin, spezifisch neddylierte Proteine in Synapsen nachzuweisen sowie den Einfluss der Neddylierung auf synaptische Funktionen zu untersuchen.

Zunächst konnte gezeigt werden, dass die Neddylierung in der Präsynapse sowie in der Postsynapse stattfindet. Ebenfalls konnten durch Western Blot Analysen, neddylierte Proteine in Synapsen nachgewiesen werden. In einer Reihe von Immunpräzipitations-Experimenten konnte gezeigt werden, dass PSD-95 neddyliert werden kann. Somit beschreibt diese Arbeit mit PSD-95 das erste neuronenspezifische Protein welches direkt neddyliert wird.

Weitere Experimente konnten zeigen, dass das Nedd8-aktivierende Enzym Nae1 und das konjugierende Enzym Ubc12 an der Neddylierung von PSD-95 beteiligt sind. Des Weiteren wurde Mdm2 als E3 Ligase bestimmt, welche Nedd8 direkt an PSD-95 bindet. Strukturanalysen von PSD-95 konnten zeigen das die PEST-Domäne, die sich am N-terminalen Ende von PSD-95 befindet, mit Ubc12 interagiert und somit die Neddylierung von PSD-95 unterstützt. PSD-95 Mutanten, denen die PEST-Domäne fehlt, können nicht mehr durch Nedd8 modifiziert werden. Funktionelle Analysen zeigten, dass die Neddylierung von PSD-95 an der Dimerisierung

von PSD-95 beteiligt ist. Folglich kann PSD-95 nicht mehr mit sich selbst interagieren wenn seine Neddylierung geblockt wurde. Die verhinderte Dimerisierung von PSD-95 kann zu der Destabilisierung von Synapsen führen, wie für Synapsen gezeigt wurde in denen die Neddylierungskaskade unterbrochen wurde. Weitere Ergebnisse belegen, dass Glutamat die Neddylierung von PSD-95 erhöht, wobei NMDA Zugabe die Ubiquitylierung von PSD-95 fördert. Dies deutet darauf hin, dass Nedd8 und Ubiquitin entgegengesetzte Auswirkung auf die Funktion von PSD-95 haben könnten, wobei Ubiquitin die Degradation von PSD-95 einleitet und Nedd8 PSD-95 in der Postsynapse stabilisiert.

Des Weiteren wurde eine neue Methode entwickelt, die die Unterscheidung von neddylierten und ubiquitylierten Lysinen mit Hilfe von Massenspektrometrie erlaubt. Das Problem bei herkömmlicher Massenspektrometrie liegt darin, dass sie nicht in der Lage ist neddylierte von ubiquitylierten Lysinen zu unterscheiden, da diese nach Trypsinierung beide -GG Überhänge erzeugen. Aus diesem Grund wurden Nedd8-Mutanten hergestellt welche eine Veränderung der Masse von Nedd8 nach der Trypsinierung hervorrufen und somit die Identifikation von neddylierten Lysinen in PSD-95 erlauben. In der Proteinsequenz von PSD-95 konnten 5 neddylierte Lysine nachgewiesen werden, wobei K202 der konsistenteste Kandidat in allen Experimenten war. Morphologische Analysen der PSD-95 Mutante K202R ergab, dass die Mutation einer einzigen Aminosäure, welche die spezifische Neddylierung von PSD-95 an der Position K202 unterbindet, die Entwicklung von dendritischen Dornfortsätzen stark behindert. Diese Beobachtung wurde elektrophysiologisch bestätigt, da PSD-95-K202R einen dominant-negativen Effekt auf die Amplitude von mEPSCs ausübte.

Weiterhin wird in der Arbeit beschrieben, dass die Neddylierung einen starken Einfluss auf präsynaptische Funktionen hat. Dabei führt die Inhibition der Nedd8-Kaskade zu einer reduzierten Transmitterausschüttung. Zudem können präsynaptische Vesikel nach starker Aktivierung nicht so schnell wieder aufgefüllt werden. In der Postsynapse führt die Inhibition der Neddylierung zu einer verminderten Anzahl von AMPA- und NMDA-Rezeptoren in der postsynaptischen Membran, wobei in extrasynaptischen Membranen die Konzentration an AMPA Rezeptoren zunimmt. Ebenfalls konnte gezeigt werden, dass sich die Kinetik der AMPA Rezeptoren verändert, welches unter anderem auf die Änderung der Interaktion von AMPA

Rezeptoren mit Hilfsproteinen wie TARPs oder Cornichons zurückzuführen sein kann.

Neben dem Einfluss auf basale synaptische Funktionen ist die Neddylierung auch an synaptischer Plastizität beteiligt. Hierfür konnte gezeigt werden, dass die Inhibition der Neddylierungskaskade die Induktion der Langzeit-Potenzierung sowie der Langzeit-Depression verhindert. Interessanterweise wurde beobachtet, dass die Neddylierung von PSD-95 bei starker neuronaler Aktivität zunimmt. Somit lässt sich Schlussfolgern, dass Neddylierung bei ansteigender neuronaler Aktivität zunimmt und dadurch Veränderungen der neuronalen Signalstärke kontrolliert werden.

Zusammenfassend lässt sich sagen, dass diese Doktorarbeit das erste neuronenspezifische Protein beschreibt, welches neddyliert wird: PSD-95. Außerdem konnte gezeigt werden, dass Neddylierung einen starken Einfluss auf synaptische Funktionen hat, indem prä- und postsynaptische Vorgänge sowie synaptische Plastizität kontrolliert werden.

Diese Arbeit gibt einen ersten Überblick über die Funktion des Nedd8-Signalweges im Gehirn.

1 Introduction

The human brain is a highly complex system of hundreds of billions of neurons making up trillions of connections. A central goal in neuroscience research is to understand the mechanisms controlling neuronal development, synaptic plasticity, and how behavior is altered by these processes.

It is fascinating that each synapse is individually regulated and modified to adapt neuronal circuits to external stimuli. Information processing and storage have to be acutely balanced to guarantee the equilibrium between circuit plasticity and stability.

Recent studies indicate that post-translational modifications play an important role in synapse formation, elimination, and functional plasticity. Therefore, synaptic protein function is controlled by post-translational modifications that are removed or added to synaptic proteins.

1.1 The Excitatory Synapse

Synapses are specialized structures transferring signals from one neuron to another neuron. Chemical synapses can be divided into excitatory and inhibitory connections. In chemical synapses, the pre- and post-synapse are separated by the synaptic cleft. In an excitatory pre-synapse, glutamate filled vesicles are stored. Upon an action potential glutamate is released into the synaptic cleft and binds to receptors that are located in the post-synaptic membrane. The activation of post-synaptic receptors from an excitatory synapse will generate excitatory post-synaptic currents (EPSCs), which will increase the probability of generating an action potential in the post-synaptic cell.

1.1.1 The Pre-Synapse

The main function of an excitatory pre-synapse is to convert electrical activity into a chemical signal in the form of neurotransmitter release. Glutamate, the neurotransmitter of most excitatory synapses, is stored in small round membrane compartments called synaptic vesicles (SVs). Upon the arrival of an action potential at the pre-synapse voltage gated Ca^{2+} -channels open. The channel opening results in an influx of calcium ions that bind to calcium sensors and therefore trigger the release of neurotransmitter by vesicle exocytosis into the synaptic cleft (Wu et al., 2007).

The pre-synapse contains an electron-dense protein network called active zone. The active zone comprises three different protein groups that perform distinct functions during neurotransmitter release: Voltage-gated calcium channels make up the first group of proteins that induce the synaptic vesicle release. Secondly, scaffold proteins build up the cytomatrix of the active zone (CAZ) that anchors cell adhesion molecules to the pre-synapse and thus assures the precise alignment with the post-synaptic density (PSD) (Ziv and Garner, 2004). Additionally, the CAZ supports the synaptic vesicle transport and restricts the synaptic vesicle release to the active zone (Schoch and Gundelfinger, 2006). Especially Munc-13s, RIMs, ELKSs, leprins- α s, piccolo, and bassoon are enriched in the CAZ but also interact with numerous other pre-synaptic proteins (Schoch and Gundelfinger, 2006). The last group is made up of SNARE proteins that are crucial for the synaptic vesicle fusion with the plasma membrane (Sudhof and Rizo, 2011). Once synaptic vesicles reach the plasma membrane they are docked and primed for release. During the priming, a four-helix bundle is formed between synaptic vesicles and SNARE complexes that consist of syntaxin, SNAP25, and synaptobrevin. Upon calcium influx, the calcium sensor synaptotagmin becomes activated and replaces complexin to the four-helix bundle and thus relieves the SNARE complex from the fusion clamp (Giraudo et al., 2006, Schaub et al., 2006). In the case of spontaneous synaptic vesicle release Doc2b acts as a calcium sensor that has a much higher calcium affinity compared to synaptotagmin. The high calcium affinity allows the synaptic vesicle release upon small changes of intracellular calcium levels (Groffen et al., 2010).

1.1.2 The Post-Synapse

The post-synapse of a glutamatergic synapse is a complex structure that receives glutamate signals from the pre-synapse. In the post-synaptic membrane glutamatergic receptors, such as AMPA and NMDA receptors, are located that will open upon glutamate binding. On the intracellular side, the post-synaptic density (PSD) is localized, a complex protein network that is involved in the localization of synaptic receptors. Additionally, the PSD organizes post-synaptic signaling pathways.

Glutamatergic receptors at excitatory synapses are divided into three major classes: ionotropic-, metabotropic-, and kainate receptors. Of these three classes, the ionotropic receptors amino-3-hydroxy-5-methyl-4-isoxazolepropionic acid (AMPA) receptors, along with N-methyl D-aspartate (NMDA) receptors are particularly important for synaptic function. Especially the AMPA receptor trafficking and distribution in the post-synapse are highly regulated.

AMPA receptors are composed of four highly similar subunits called GluA1-4 (Keinanen et al., 1990, Hollmann and Heinemann, 1994, Rosenmund et al., 1998). The subunit composition of AMPA receptors varies depending on neuronal maturity and on the brain region and thus contributes to differences in functional properties of AMPA receptors (Hollmann and Heinemann, 1994). First, all AMPA receptor subunits are alternatively spliced, resulting in flip and flop variants of each AMPA subunit (Sommer et al., 1990). The splice variants are differentially expressed during neuronal hippocampal maturation. Flip variants are mainly expressed before birth, while flop variants are expressed in mature hippocampal neurons (Monyer et al., 1991). As a functional consequence, the flop variant of the AMPA receptor deactivates and desensitizes the receptor more rapidly than the flip variant (Mosbacher et al., 1994). In addition, GluA2 subunits undergo RNA editing that exchanges glutamine to arginine at position 607. GluA2Q subunits containing AMPA receptors display altered kinetics, calcium permeability, and neurotransmitter affinity (Burnashev et al., 1992). In brief, AMPA receptors containing edited GluA2 subunits are impermeable for Ca^{2+} and show a linear current-voltage (I-V) curve (non rectifying) (Fig. 1.1). In mature hippocampal neurons mainly GluA1/GluA2 and GluA2/GluA3 receptor combinations are found. The AMPA receptor subunits differ in the length of their intracellular

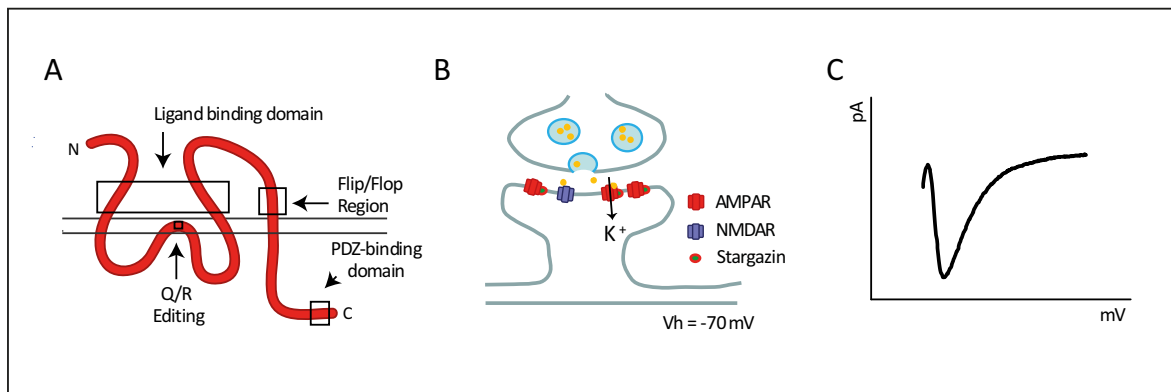


Figure 1.1: Physiological and morphological properties of AMPA receptors. **A)** Schematic diagram of an AMPA receptor subunit. Depicted are the C- and N-terminals of the protein sequence, the ligand-binding-domain (LDB), flip/flop splicing region, Q/R editing site, and the PDZ binding domain. **B)** When clamped at -70 mV, NMDA receptors are impermeable for Ca^{2+} -ions, since a negative membrane potential sucks Mg^{2+} into the pore and thus blocks the NMDA receptor. AMPA receptors open upon glutamate binding and become permeable for Na^{+} - and K^{+} -ions. **C)** Typical sample trace for AMPA EPSC recordings. At -70 mV, glutamate evokes excitatory post-synaptic currents (EPSC) that are almost entirely mediated by AMPA receptors.

C-terminus. While GluA1 and GluA4 have long intracellular tails, the tails of GluA2 and GluA3 are shorter. The subunit composition determines the regulation of AMPA receptor recruitment to the post-synaptic side. While GluA2/GluA3 AMPA receptors are rapidly cycled in and out of the synapse even under basal conditions, GluA1/GluA4-containing AMPA receptors are mainly inserted into the post-synapse upon NMDA receptor activation (Passafaro et al., 2001, Shi et al., 2001).

The differences in trafficking are related to intracellular proteins that bind to the distinct C-terminals of AMPA receptor subunits. For example GluA2 interacts with PICK1 that mediates AMPA endocytosis and recycling and with NSF that mediates insertion and stabilization of AMPA receptors in the post-synaptic membrane (Nishimune et al., 1998, Xia et al., 1999). GluA1 interacts directly with SAP97 and anchors GluA1 in the synapse (Sans et al., 2001). Additionally, GluA1 also interacts with the cytoskeleton by binding 4.1N in a palmitoylation-dependent manner (Hayashi et al., 2005).

TARPs have been shown to directly interact with AMPA receptors, including stargazin that is involved in AMPA receptor trafficking and also modifies the functionality of AMPA receptors (Chen et al., 2000, Priel et al., 2005, Nicoll et al., 2006). Stargazin guides AMPA receptors to

the cell surface and clusters them in the post-synaptic membrane through the interaction with PSD-95 (Schnell et al., 2002). In addition, stargazin alters AMPA receptor kinetics by slowing AMPA receptor activation, deactivation and desensitization (Priel et al., 2005, Tomita et al., 2005b, Turetsky et al., 2005).

NMDA receptors also belong to the glutamatergic receptors in excitatory synapses. NMDA receptors are activated voltage-dependently and thus play a critical part in synaptic plasticity. In brief, under basal conditions NMDA receptors cannot be activated by glutamate release due to an Mg^{2+} block (Cull-Candy and Leszkiewicz, 2004, Traynelis et al., 2010). For that reason, AMPA-lacking synapses that only contain NMDA receptors are referred to as “silent synapses”, since no ion influx is induced by single glutamate activation. At positive membrane potentials, the Mg^{2+} block is removed and glutamate binding that opens NMDA channels results in Ca^{2+} influx. Depending on the pattern of synaptic stimulation, Ca^{2+} influx leads to different forms of synaptic plasticity, for example long-term potentiation (LTP) or long-term-depression (LTD) (Fig. 1.2).

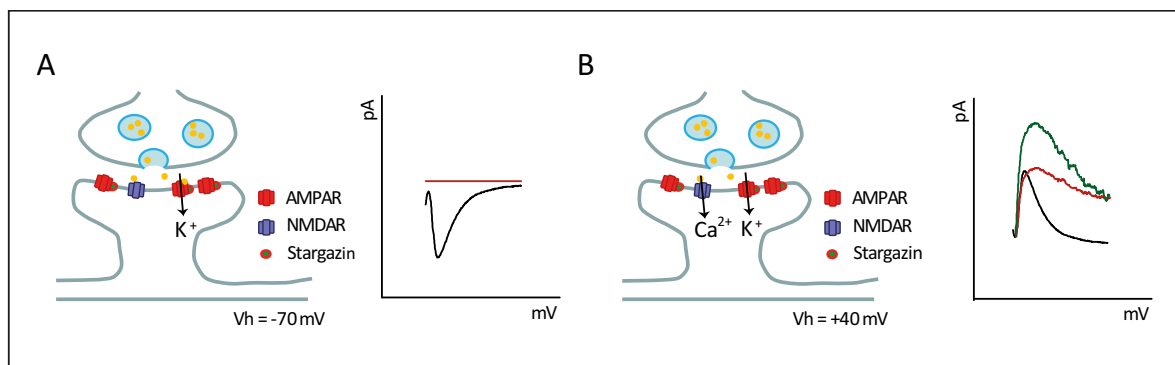


Figure 1.2: Physiological properties of AMPA and NMDA receptors. **A)** At negative membrane potentials, glutamate only evokes AMPA receptors, which subsequently results in potassium influx into the post-synapse (black line). NMDA receptors are silent at negative membrane potentials since an Mg^{2+} block prevents ion influx (red line). **B)** At positive membrane potentials, +40 mV, the Mg^{2+} block is removed from NMDA receptors and subsequently glutamate activation will result in both AMPA and NMDA receptor activation (green line). Selective antagonists for AMPA and NMDA receptors allow the isolation of both currents (AMPA: black line; NMDA: red line).

Like AMPA receptors, NMDA receptors are tetramers and compose of three subunits, NR1, NR2 (A-D), and NR3. In the hippocampus, NMDA receptors assemble to heterodimers or heterotrimers. NR2B-containing NMDA receptors are expressed in early development, while

the number of NR2A-containing NMDA receptors increases during development. NR2B- and NR2A-containing receptors differ in their receptor kinetics; NR2B-containing receptors have a slower decay time compared to NR2A-containing receptors (Dumas, 2005, Paoletti, 2011). NMDA receptor gating is regulated by different ligands, for example glycine that binds to NR1 for channel opening.

NMDA receptors interact with PDZ domains of different molecules, such as PSD-95, S-SCAM, and SAP-102 which are important for the anchoring and intracellular trafficking of NMDA receptors (Kim and Sheng, 2004).

MAGUKs (Membrane-associated guanylate kinase) are a scaffold protein family involved in the function of glutamatergic synapses. The best-studied member of this protein family is the post-synaptic density protein of 95 kDa, **PSD-95**. Additional members of the protein family include PSD-93, SAP-102, and SAP-97 (reviewed in Funke et al., 2005).

All MAGUKs share a common protein domain structure containing three N-terminal PDZ domains, a Src-homology 3 (SH3) domain, and a C-terminal catalytically inactive guanylate kinase (GK) domain. PDZ domains occur in around 350 proteins which can be typically found at cell-cell contact sites. The interaction with target proteins takes place with the last for amino acids of the target protein's C-terminus or can heterodimerize. The SH3 and GK domains of PSD-MAGUKs are also interaction modules that bind many proteins such as guanylate kinase-associated protein (GKAP), microtubule-associated protein 1A (MAP1A), or AKAP79 (Kim et al., 1997, Bhattacharyya et al., 2009).

MAGUK expression is highly regulated during neuronal development. In young mice, before postnatal day 10, SAP102 is highly expressed in neurons, whereas PSD-95, PSD-93, and SAP97 are only slightly expressed. PSD-95, PSD-93, and SAP97 expression increases at later developmental stages and promotes synaptic development (Petralia et al., 2002, van Zundert et al., 2004, Elias et al., 2006, 2008). For example, the switch of NMDA receptor subunits during development that change from NR2B- to NR2A-containing NMDA receptors is dependent on different MAGUKs expressions (Elias et al., 2008).

PSD-95 is the major protein of the post-synaptic density (PSD) and associates with neurotransmitter receptors like NMDA, adhesion molecules like neuroligins, and signaling enzymes like

nNOS (reviewed in Han et al., Xu, Yokoi et al.). PSD-95 has a number of different functions throughout post-synaptic development up to spine stability. The N-terminus of PSD-95 and PSD-93 can be palmitoylated at two cysteine residues which are necessary for synaptic targeting and receptor clustering (Topinka and Brecht, 1998). The PEST domain of PSD-95 is located close to the two cysteine residues. This domain is a polypeptide sequences enriched in proline (P), glutamic acid (E), serine (S), and threonine (T) and flanked by lysine (K), arginine (R) or histidine (H) residues. PEST sequences can be found in many proteins and are distributed once or even more often anywhere along the polypeptide chain. Especially in the 1990s, the PEST domain became of special interest, since it was described as a proteolytic signal that regulates protein concentrations (Ghoda et al., 1992). Additionally, it was shown that the degradation upon the PEST domain *via* the 26S proteasome needs the ubiquitylation of the target protein (Schork et al., 1995). Later it was proven that PSD-95 is ubiquitylated and consequently degraded *via* the proteasome upon NMDA receptor stimulation (Colledge et al., 2003).

PSD-95 is located near the post-synaptic membrane, multimerizes and thus forms a network which also includes other proteins that cluster receptors in the post-synaptic membrane. Through its protein interactions PSD-95 stabilizes AMPA receptors *via* TARPs or directly NR2 in the post-synaptic membrane. Through its interaction with AMPA receptors, PSD-95 controls synaptic neurotransmission. PSD-95 overexpression increases AMPA-mediated EPSCs, whereas NMDA currents are unaltered (Schnell et al., 2002). In contrast, the acute knockdown of PSD-95 *via* shRNAs decreases AMPA EPSCs (Funke et al., 2005).

Additionally, PSD-95 impacts on synaptic plasticity thus the overexpression of PSD-95 converts silent synapses into functional synapses by stabilizing GluA1-containing AMPA receptors in the post-synapse (El-Husseini et al., 2000). The overexpression of PSD-95 does not increase LTP induction, which might be due to the increase in AMPA receptors upon PSD-95 overexpression (Stein et al., 2003). In contrast, PSD-95 strongly regulates LTD, since PSD-95 overexpression augments and PSD-95 knockdown impairs LTD induction (Stein et al., 2003, Beique and Andrade, 2003).

1.2 Synaptic Plasticity

In the brain, billions of neurons communicate with each other *via* thousands of synapses. This system stays flexible during adulthood and can be re-modeled. This process is called ‘plasticity’ and describes the ability of synapses to undergo a morphological change in order to adapt to external stimuli.

The first systematic study of long-term potentiation was achieved by Terje Lomo in 1966 who observed “frequency potentiation of excitatory synaptic activity in the dentate area of the hippocampus” (Lomo, 1966) . Later, it was shown by studies on the sea slug *Aplysia* that synaptic strengthening and weakening is related to memory formation (Kandel and Schwartz, 1982). These studies showed that habituation or sensitization is based on the weakening or strengthening of synaptic connections, whereas long term storage is related to an increase in synapse numbers (Bailey and Kandel, 1993).

Additionally, various studies have been done on adult rodents that include motor training or memory tasks. All these learning paradigms lead to a change in the number and size of dendritic spines in the specific brain region (Keck et al., 2008, Hofer et al., 2009, Yamahachi et al., 2009, Majewska et al., 2006). Thus, synaptic plasticity is thought to be the basis for learning and memory.

The strengthening and weakening of existing contacts play a crucial role in synaptic plasticity. These findings go back to Donald Hebb (1949), who established the Hebbian Rules which state that cells that fire together also wire together. He emphasized that a repeated and persistent stimulation of a pre-synaptic cell is needed to induce synaptic plasticity in the post-synaptic cell. Later, Bliss and Lomo (1973) were able to prove that EPSPs potentiate after high-frequency stimulation. Thus, increased synaptic activity strengthens synaptic contacts and is called long-term potentiation (LTP), whereas low activation results in synaptic weakening and is called long-term depression. At CA3-CA1 synapses in the hippocampus, LTP and LTD require NMDA receptor activation and the subsequent influx of Ca^{2+} -ions into the post-synaptic cell [Bear and Malenka, 1994]. LTP and LTD require different kinetics of Ca^{2+} -influx: whereby LTP is dependent on a brief increase of intracellular Ca^{2+} , LTD requires a prolonged increase of intracellular Ca^{2+} .

concentration.

During LTP, large increases in Ca^{2+} -concentration result in the activation of protein kinases, such as PKC and CaMKII (Malenka and Bear, 2004). Phosphorylation of AMPA receptors increases the receptor concentration in the post-synaptic membrane due to the insertion of new receptors. Increased AMPA receptor insertion into the post-synaptic membrane is a main mechanism for LTP induction (Shi et al., 1999, Pickard et al., 2001, Lu et al., 2001). In support, the inhibition of AMPA receptor exocytosis blocks LTP induction (Bredt and Nicoll, 2003).

LTD is induced by a low and sustained increase of the Ca^{2+} -concentration in the post-synapse and leads to the activation of protein phosphatases such as protein phosphatase 1 (PP1) (Malenka and Bear, 2004). LTD induces the dephosphorylation of Ser-845 of the GluA1 subunit and consequently reduces the open probability of AMPA receptors (Banke et al., 2000). Additionally, AMPA receptors are internalized in a dynamin- and clathrin-dependent manner after LTD induction (Carroll et al., 1999, Ehlers, 2000) and the inhibition of AMPA receptor endocytosis sufficiently blocks LTD (Bredt and Nicoll, 2003).

Furthermore, scaffold proteins, such as PSD-95 have been shown to impact on synaptic plasticity (Schnell et al., 2002, Stein et al., 2003, Ehrlich and Malinow, 2004). PSD-95 anchors AMPA receptors in the post-synaptic membrane and thus a reduction of PSD-95 would also negatively affect the AMPA receptor concentration during LTD. PSD-95 levels are controlled by palmitoylation (El-Husseini Ael et al., 2002), which anchors PSD-95 to the post-synaptic membrane and ubiquitylation which in contrast removes PSD-95 from synaptic sites (Colledge et al., 2003). In conclusion, post-translational modifications on PSD-95 could influence LTP and LTD. In addition, PSD-95 might act as a signaling scaffold connecting NMDAR-mediated Ca^{2+} -influx to downstream signaling cascades that trigger LTD. PDZ domains of PSD-95 are required to mediate the interaction with NMDA and AMPA *via* stargazin, while the SH3 and the GK domain interact with various signaling molecules (Kameyama et al., 1998, Tavalin et al., 2002, Bhattacharyya et al., 2009). These results indicate that the regulation of other proteins, like PSD-95 upon LTP or LTD induction, impacts on AMPA receptor distribution (Xu et al., 2008).

1.3 The Inhibitory Synapse

Inhibitory chemical synapses decrease the chance to generate an action potential by creating a more negative post-synaptic potential upon activation, in contrast to excitatory synapses that depolarize the post-synaptic neuron.

The main neurotransmitter involved in inhibitory post-synaptic currents is γ -aminobutyric acid (GABA) that binds to ionotropic GABA_A receptors and hyperpolarizes the neuron by Cl⁻-influx (Misgeld et al., 1986). GABA_A receptors mediate the fast inhibitory actions of GABA in the brain (Rudolph and Mohler, 2004) whereas GABA_B receptors are G protein-coupled receptors, also known as metabotropic receptors which mediate the slow response to GABA. GABA release from the pre-synaptic terminals *via* calcium-dependent vesicle fusion to the pre-synaptic membrane does not differ from glutamate release.

GABA_A receptor subunits are composed of four transmembrane domains (TMs) with a large intracellular domain between TM3 and TM4. Based on their sequence homology, 18 GABA_A receptor subunits have been described that are separated into seven subunit classes: α (1-6), β (1-3), γ (1-3), δ , ϵ (1-3), θ , and π (Bormann and Feigenspan, 1995). Most GABA_A receptors expressed in the brain consist of two α -subunits, two β -subunits and one γ -subunit, whereby the γ -subunit can be replaced by δ , ϵ , θ , or π (Fritschy et al., 1998, Bettler and Tiao, 2006). The rapid influx of Cl⁻ is triggered by GABA binding between the α - and γ -subunit. Depending on their subunit composition, GABA_A receptors are located at synaptic or extra-synaptic sites.

GABA_A receptor clustering at inhibitory synapses is mediated by the multifunctional protein gephyrin that binds to the β -subunit (Meyer et al., 1995, Kneussel et al., 1999). Reduced gephyrin expression results in more mobile GABA_A receptors that decrease the mIPSC amplitude, since GABA_A receptors cannot be stabilized in the post-synaptic membrane (Jacob et al., 2005). The $\alpha 2$ -subunit directly interacts with gephyrin, which then binds to microtubules and actin interactors such as collybin, mena/VASP, and profilin1+2 (Mammoto et al., 1998, Kins et al., 2000, Giesemann et al., 2003). Removal of GABA_A receptors from synaptic sites is accomplished by endocytosis in a clathrin-dependent manner or by microtubule-dependent trafficking (Kittler et al., 2004).

1.4 Ubiquitin-Like-Pathways

There are several ubiquitin-like proteins (UBLs), including Nedd8, SUMO, ISG15, FAT10, Atg12, and Atg8 that conjugate to target proteins in a manner analogous to ubiquitin (Haas et al., 1987, Loeb and Haas, 1992, Kamitani et al., 1997, Mizushima et al., 1998, Liu et al., 1999, Ichimura et al., 2000, Yeh et al., 2000, Bawa-Khalife and Yeh, 2010). UBLs are post-translational modifications that are covalently conjugated to target proteins *via* an enzymatic cascade (Kerscher et al., 2006, Dye and Schulman, 2007).

1.4.1 The Ubiquitin Pathway

Ubiquitin is a small 76 amino acid protein that is coupled *via* an isopeptide bond to target proteins. The transfer of ubiquitin to its target proteins is mediated *via* an enzymatic cascade consisting of ubiquitin activating-enzymes (E1s), ubiquitin conjugating enzymes (E2s), and ubiquitin ligases (E3s) (Hershko and Ciechanover, 1998, Hoppe, 2005). Before ubiquitin can be bound to target proteins it has to be processed at its C-terminus. De-ubiquitylating (DUBs) enzymes process ubiquitin-precursors and expose glycine carboxylate, representing the target conjugation site. In an ATP-dependent manner, activating enzymes adenylate ubiquitin at its C-terminus and therefore ubiquitin can bind to the E1 active site (Haas et al., 1982). In the next step, ubiquitin is transferred from the E1 to an active-site cysteine of an E2 enzyme. Finally, with the help of E3 ligases, ubiquitin is coupled *via* an isopeptide bond to the ϵ -amino group of lysine in substrates (Eletr et al., 2005, Huang and Schulman, 2005). Two E3 ligase classes can be differentiated: the first class contains Really Interesting New Gene (RING) finger domain classes and the second class is the Homologous to E6-AP Carboxyl Terminus (HECT) (Hotton and Callis, 2008, Deshaies and Joazeiro, 2009). The E3 ligases determine target protein specificity. The high specificity of E3 ligase target recognition is reflected in the enormous number of putative E3s in humans, which is estimated to be 700 (Ardley and Robinson, 2005, Deshaies and Joazeiro, 2009) (Fig. 1.3).

Ubiquitylation exerts different functions by protein modification depending on the linked chain of ubiquitin. Poly-ubiquitin chains are formed *via* lysine 48 (K48) and typically target proteins

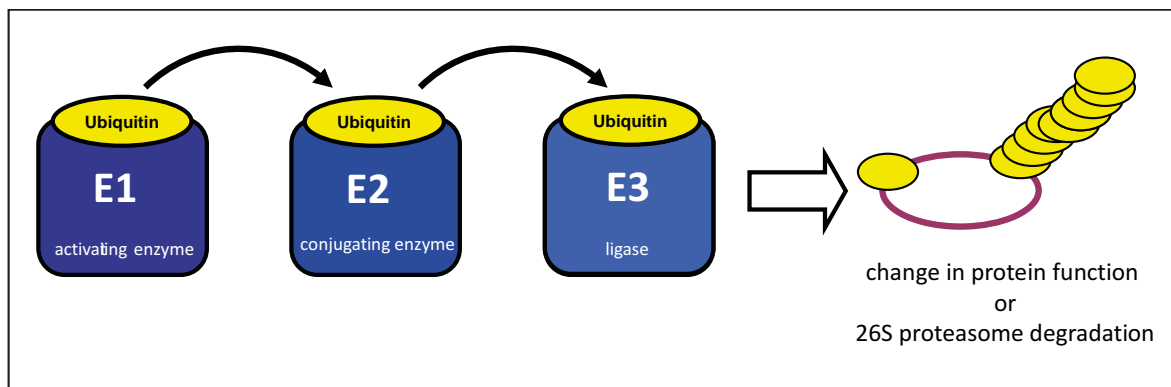


Figure 1.3: The Ubiquitin pathway. The 8.5 kDa protein ubiquitin is conjugated to target proteins *via* an enzymatic cascade. First, ubiquitin is activated *via* an activating enzyme E1 which transfers ubiquitin to the E2 conjugating enzyme. The E3 ligase conjugates ubiquitin from the E2 to target proteins. Mono-ubiquitylation of target proteins will lead to a change in protein function, whereas poly-ubiquitylation sends target proteins to the 26S proteasome for degradation.

for degradation by the 26S proteasome (Thrower et al., 2000). Mono- or poly-ubiquitylation *via* other lysine residues for example K63 does not target proteins for degradation but instead changes the protein function or subcellular localization (Chan and Hill, 2001, Haglund et al., 2003, Welchman et al., 2005, Mukhopadhyay and Riezman, 2007).

In addition, ubiquitin is removed from target proteins by de-ubiquitylating enzymes (DUBs). DUBs are proteases that reverse ubiquitylation and poly-ubiquitylation and thus present an additional mechanism to control protein function (Kim et al., 2003, Reyes-Turcu et al., 2009).

1.4.2 The Nedd8 Pathway

A subtractive cloning screen between the cDNA library derived from mouse neuronal precursors and mRNAs from adult mouse brains identified 10 developmentally down regulated genes (NEDD) (Kumar et al., 1992). One of these genes, NEDD8, is an 81 amino acid polypeptide, 60 % identical and 80 % homologous to ubiquitin (Kamitani et al., 1997) and is found in various organisms from mammal's to yeast (Callis et al., 1995, Hochstrasser, 1996, Kamitani et al., 1997, Kumar et al., 1992). Also, the crystal structure of Nedd8 and Ubiquitin are fairly analogous (Whitby et al., 1998).

Like ubiquitin, Nedd8 is synthesized as 81 kDa precursor protein. Before Nedd8 can be attached to its target proteins, it has to be cleaved by C-terminal hydrolases. This process is catalyzed by

NEDP1 (also known as DEN1 and SENP8) a cysteine protease with high specificity for Nedd8 (Wu et al., 2003, Shen et al., 2005). After the cleavage, the conserved glycine (76) residue remains, which serves as the attachment site to form isopeptide linkage to lysine residues of target proteins (Kamitani et al., 1997, Gong and Yeh, 1999).

After its processing, Nedd8 is coupled to its target proteins using a cascade of E1, E2, and E3 enzymes. First, Nedd8 is adenylated in an ATP-dependent manner *via* the activating enzyme E1, which is a heterodimer composed of Nedd8-activating enzyme 1 (Nae1), also called APP-BP1, and ubiquitin-activating enzyme 3 (Uba3) and thus transferred to the E1 cysteine side chain *via* thiolester linkage (Liakopoulos et al., 1998, Osaka et al., 1998). Afterwards, the activated Nedd8 is transferred to the E2 conjugating-enzyme, Ubc12, by forming another thiolester linkage (Gong and Yeh, 1999). Besides Ubc12, another E2 has been described recently that preferentially promotes the neddylation of Cul5. It is called Ube2F (Huang et al., 2009). Finally, Nedd8 is transferred *via* an E3 ligase to its target proteins forming an isopeptide bond (Fig. 1.4). In contrast to the ubiquitin pathway where multiple E3 ligases are described, only a few E3 ligases are described for the Nedd8 pathway. These E3 ligases are described to be involved in the ubiquitin as well as in the Nedd8 pathway, showing that they are not restricted to one conjugation pathway. E3 ligases shown to be involved in the neddylation of proteins contain Really Interesting Novel Gene (RING) finger domains, e.g. Ring Box Protein (Rbx)1 and Rbx2, murine double mutant 2 (Mdm2), casitas b-lineage lymphoma (c-CBL) protein, and Skp1-Cullin-F box protein SCFFBX011 (Kamura et al., 1999, Morimoto et al., 2000, Xirodimas et al., 2004, Oved et al., 2006, Abida et al., 2007, Huang et al., 2009).

Neddylation is a reversible process which is mediated by Nedd8 de-conjugating enzymes. The best studied de-conjugating enzyme is the CSN5, a subunit of the zinc-metalloprotease complex COP9 (Lyapina et al., 2001). NEDP1, already mentioned to be involved in the process of the Nedd8 precursor, also functions as a Nedd8 peptidase (Yamoah et al., 2005).

1.4.3 Nedd8 Targets – Functional Impact of Protein Neddylation

The best-characterized targets for the Nedd8 pathway are the cullins (Cul1, 2, 3, 4A, 4B and 7, PARC, Apc2) which are scaffold proteins regulating protein ubiquitylation and proteasomal

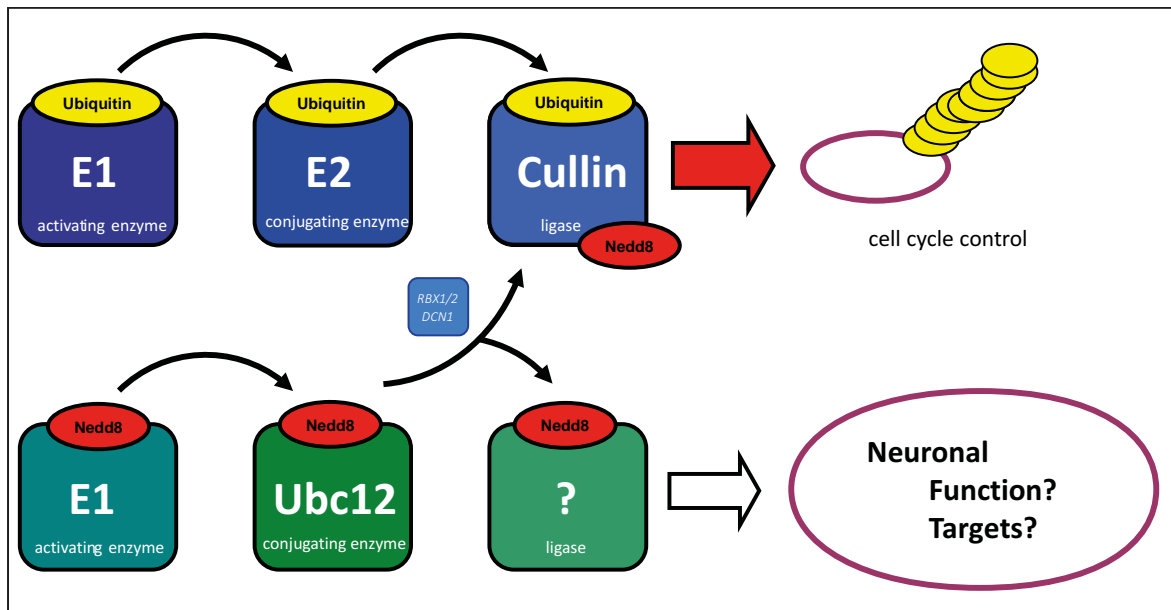


Figure 1.4: The Nedd8 pathway and its interaction with the ubiquitin pathway. Analogous to the ubiquitin pathway, Nedd8 is coupled *via* an enzymatic cascade, including an E1 activating enzyme, an E2 conjugating enzyme, and an E3 ligase to its target proteins. Cullins, E3 ligases of the ubiquitin pathway, are neddylated by the E3 ligase complex of Rbx1 (RING box protein 1) and DCN 1 (Defective in Cullin Neddylatation 1). Neddylatation of cullins control their E3 ligase activity. Cullin neddylatation will increase their activity and therefore increase UPS-dependent target protein degradation. Only a few additional targets for Nedd8 have been described. In the brain, E3 ligases and possible targets of the Nedd8 pathway are so far completely undescribed.

degradation of proteins involved in cell-cycle control (Hori et al., 1999). Neddylatation of cullins is mediated by the interaction of Ring-domain Rbx1 or Rbx2 with Ubc12 or Ube2f (Kamura et al., 1999, Huang et al., 2009). When Nedd8 binds to cullins their structural conformation is changed, subsequently bringing ubiquitin closer to its substrate and thereby increasing its ubiquitylation and consequently its degradation *via* the proteasome (Pan et al., 2004, Duda et al., 2008, Saha and Deshaies, 2008). In addition, neddylatation prevents the interaction of cullin and Cullin-Associated and Neddylatation-Dissociated 1 (CAND1) (Liu et al., 2002).

Like other post-translational modifications, neddylatation changes the three-dimensional surface of target proteins and hence their biochemical properties. These bindings can be classified into three categories: The first example is based on findings from cullin neddylatation. Here, Nedd8 attachment induces conformational changes in the C-terminus of cullins and frees cullins in a catalytically active conformation (Duda et al., 2008). A similar mechanism can be found by EGFR

neddylation, where conformational changes upon neddylation, expose previously buried lysine residues to the surface for further modification (Oved et al., 2006). In a second mechanism, neddylation can prevent the interaction of the target protein with other interacting molecules. For example, CAND1 perfectly binds to un-neddylated cullins but fails to bind to neddylated cullins (Goldenberg et al., 2004). Along this line, neddylation can also compete with other post-translational modifications for example an excessive neddylation of EGFR prevents its ubiquitylation (Oved et al., 2006). The third category is based on the idea that neddylation provides new binding surfaces to recruit new interaction partners (Duda et al., 2008). For example, neddylated EGFR recruits proteins of the endocytic machinery and thus induces EGFR down-regulation (Oved et al., 2006).

1.5 Ubiquitin-Like Pathways in the Brain

Ubiquitin-like proteins, such as ubiquitin and SUMO, have been described to influence neuronal development and function, including neurogenesis, axon and dendrite outgrowth, synaptogenesis, pre- and post-synaptic function, and activity dependent plasticity (reviewed in Yi and Ehlers, 2007, Haas and Broadie, 2008, Schwartz and Ciechanover, 2009, Kawabe and Brose, 2011). Furthermore, ubiquitin-like proteins have been associated with diseases of the central nervous system (Tai and Schuman, 2008, Schwartz and Ciechanover, 2009). Also, many substrates have been described that are targeted by the ubiquitin and SUMO pathway. In this context, a few examples are stated that control pre- or post-synaptic function by UBL protein modification.

1.5.1 UBLs in the Pre-Synapse

Various targets of the ubiquitin pathway have been described in the pre-synapse (Yi and Ehlers, 2007, Haas and Broadie, 2008). Blocking the proteasome causes a significant increase in neurotransmitter release *via* pre-synaptic mechanisms (Speese et al., 2003). Rim-1, a pre-synaptic protein of the CAZ, is described to be ubiquitylated by the E3 ligase SCRAPPER and controls neurotransmitter release (Yao et al., 2007). Other pre-synaptic proteins, such as synaptophysin

and syntaxin-1 are ubiquitylated as well, but the impact ubiquitylation has on their function has to be explored further (Chin et al., 2002, Wheeler et al., 2002). In general, many pre-synaptic proteins could be identified as being targets of the ubiquitin pathway. Nevertheless, a clear picture about the functional impact of ubiquitylation on pre-synaptic function is still missing.

For SUMO not so many pre-synaptic targets are described, although numerous pre-synaptic proteins have SUMO-consensus sequences (Wilkinson et al., 2008). More importantly, it was shown that neuronal activity increases the sumoylation of pre-synaptic proteins and that increased sumoylation decreased the glutamate release evoked by KCl (Feligioni et al., 2009). One of the rare targets of SUMO2/3 in the pre-synapse is tomosyn, a protein that interacts with syntaxin-1A. Tomosyn sumoylation enhances the inhibition on pre-synaptic exocytosis (Williams et al., 2011). Additionally, mGluAs had been found to be sumoylated in bacteria assays, however no modification has so far been detected in neurons (Tang et al., 2005, Niswender and Conn, 2010, Wilkinson and Henley, 2011). A newly developed knock-in mouse model, expressing tagged SUMO1 might uncover more synaptic-targets in the future and might give a more comprehensive idea about the impact of sumoylation on pre-synaptic function (Tirard et al., 2012).

1.5.2 UBLs in the Post-Synapse

The PSD is responsible for the organization of neurotransmitter receptors, scaffolding proteins, and signaling enzymes. During neuronal activity, the molecular composition of the PSD is highly dynamic, which is partially mediated by the ubiquitin system. Sustained neuronal activity or decreased neuronal activity dramatically changes the composition of the PSD (Ehlers, 2003). Some proteins of the PSD undergo activity-dependent ubiquitylation, including Shank, GKAP, AKAP79/150, and PSD-95 (Colledge et al., 2003, Ehlers, 2003, Hung et al., 2010). For example, PSD-95 ubiquitylation *via* Mdm2 decrease the number of AMPA receptors in the post-synapse, whereas ubiquitin-defective mutants of PSD-95 inhibit AMPA receptor endocytosis (Colledge et al., 2003). Besides scaffolding proteins, glutamatergic receptors are also ubiquitylated. It was demonstrated that ubiquitylation controls AMPA receptor trafficking by GluA-1 modification *via* the E3 ligase APC/C (Burbea et al., 2002, Juo and Kaplan, 2004). However, GluA-1 abundance

at the synapse is also controlled by the ubiquitylation of β -catenin *via* the E3 ligase LIN-23. Therefore, β -catenin ubiquitylation decreases GluA1 receptor concentration in the post-synaptic membrane (Dreier et al., 2005).

In addition, GluA1 and GluA2 have been found to be directly ubiquitylated. GluA1 ubiquitylation *via* the E3-ligase Nedd4 results in receptor internalization and subsequent degradation *via* the proteasome (Lin et al., 2011). In contrast, GluA2 ubiquitylation results in lysosome degradation (Lussier et al., 2011).

NMDA receptors are ubiquitylated at different subdomains, including GluN1, GluN2, and GluN2B. NMDA receptor ubiquitylation is mediated by different E3 ligases, like CHIP, mind-bob2, and SCFFBx2 and always leads to a decrease in receptor concentration in post-synaptic membranes (Kato et al., 2005, Nelson et al., 2006, Jurd et al., 2008).

For SUMO a few post-synaptic targets are described for example CASK (Chao et al., 2008). CASK sumoylation decreases its interaction with the 4.1 protein and consequently reduces spine size and spine density (Chao et al., 2008). Furthermore, increased levels of sumoylated proteins are necessary to induce long-term potentiation. A lot of proteins like AMPA receptors and downstream molecules like Arc have been identified as potential targets of the SUMO pathway, since their protein sequences contain consensus sumoylation sites (Waung et al., 2008, Craig and Henley, 2012). Nevertheless, the direct proof that these proteins are sumoylated is still missing. The kainate receptor subunit GluK2 was found to be sumoylated directly at K886 in response to kainate stimulation. As a consequence, kainate receptors are removed from the post-synaptic side by endocytosis (Martin et al., 2007).

1.6 Theory

1.6.1 The Hippocampus

Located in the medial temporal lobe of the cerebral cortex, the hippocampus is part of the limbic system and is involved in memory formation.

The importance of the hippocampus was discovered in 1957 when Scoville and Milner removed

the hippocampi of H.M to treat epilepsy. Removal of the hippocampus resulted in severe memory deficits (Scoville and Milner, 1957). Since that time, the hippocampus has become one of the best studied brain structures and its morphology and function are well characterized. The detailed knowledge of the hippocampal function makes it an ideal model to study synapse formation and synapse physiology.

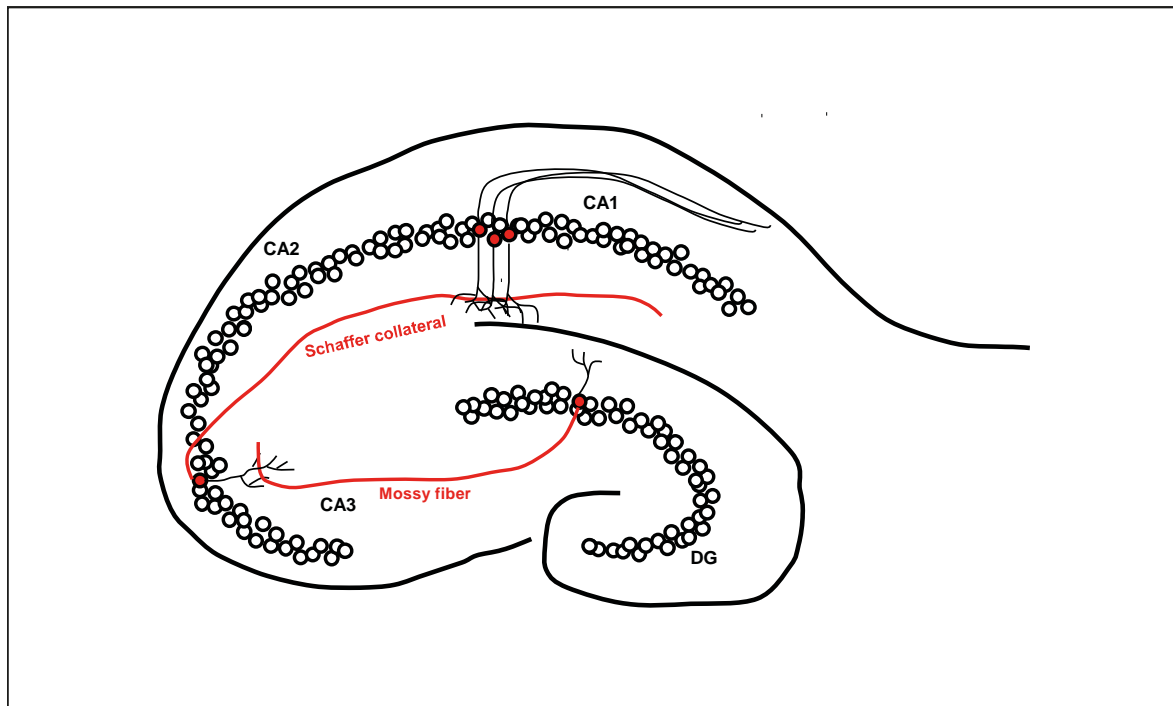


Figure 1.5: Simple schematic illustration of the projections and connections in the hippocampus. Neurons from the dentate gyrus, called granular cells, project to pyramidal neurons of CA3 *via* mossy fiber connections. CA3 neuron projections terminate in the CA1 area of the hippocampus and are called Schaffer collaterals. From CA1, neurons project out of the hippocampus mainly to the subiculum.

The hippocampus comprises distinct structures that have the shape of a curved tube, called ram's horn (Cornu Ammonis) (Fig. 1.5). Most inputs into the hippocampus originate from the entorhinal cortex and project to granular cells of the dentate gyrus (DG). Granular cells are located in the stratum granulosum of the DG and project onto pyramidal neurons of region three of the Cornu Ammonis (CA3). This synapse is called the mossy fiber synapse due to the large pre-synaptic terminals. CA3 pyramidal neurons project to pyramidal neurons in the region one of the Cornu Ammonis (CA1). Finally, CA1 pyramidal neurons send their axons to the subiculum, the main output region of the hippocampus (Fig. 1.5).

The hippocampus is an ideal brain structure to study synaptic connections, since axonal projections and post-synaptic neurons are mostly found on the same plane. Consequently, a bundles of Schaffer collaterals that all project from CA3 and CA1 are present in a hippocampal brain slice. The synapse between the CA3 and CA1 pyramidal neuron is very well described in its function and regulation especially during synaptic plasticity. In this study, the CA3-CA1 synapse was used as a model synapse to describe the effect of neddylation on basal synaptic function and on synaptic plasticity.

Dependent on the scientific question, acute hippocampal brain slices or organotypic slice cultures were used to study the effect of Nedd8 on synaptic transmission. Acute hippocampal brain slices can be used for six hours, before neurons start to die. Neddylation in acute brain slices was blocked by the Nae1 inhibitor MLN-4924 that can be applied by the artificial cerebrospinal fluid (ACSF). Organotypic slice cultures can be cultured for several weeks and allow for various experimental manipulations. For example, organotypic slice cultures can be treated for long time periods with pharmaceuticals or can be infected with viruses to genetically alter synaptic protein expression.

1.6.2 Modes of Recording

Two different kinds of recordings could be obtained to characterize electrophysiological properties of neurons: extracellular field recordings and patch clamp recordings.

In this study, extracellular field recordings were exclusively conducted at CA3-CA1 synapses in acute hippocampal brain slices. Since pyramidal neurons in the hippocampus are organized in a laminar array in which soma point in one direction and dendrites in the other, it is possible to record sum potentials of different cells at one time. The laminated pattern of inputs and outputs makes the hippocampus an ideal structure to obtain field recordings (Fig. 1.6A, B).

For hippocampal field recordings, Schaffer collaterals are activated *via* a stimulation electrode and post-synaptic responses recorded in the pyramidal and radial layer of CA1 (Fig. 1.6A, B).

The electrode stimulation opens ion-channels at the axons that make up the Schaffer collaterals. The resulting ion-influx depolarizes the axon and thus the axon is at a different potential from the rest of the neuron e.g. the soma. Consequently, current flows from the soma to the depolarized

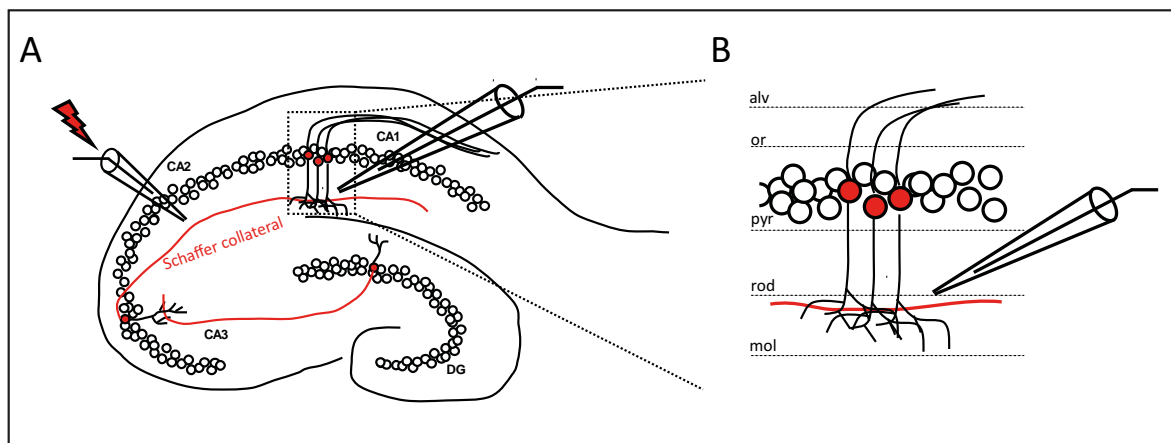


Figure 1.6: Illustration of extracellular recordings in the hippocampus by Schaffer collaterals activation. **A)** Illustration of an hippocampal slice that indicates the position of the stimulation electrode that will generate action potentials in the Schaffer collaterals. The Recording electrode is placed in CA1. **B)** Enlarged view of pyramidal neurons in CA1 and CA1-layers (alv = alveus; or = oriens; pyr = pyramidal cell layer; rad = radiatum, mol = molecular layer). Recordings were obtained from rod and pyr layers in CA1.

axon. Since the potential in the extracellular space is opposite to the intracellular potential, extracellular electrodes record a negative potential at the axon and a positive potential at the soma. Thus, when the recording electrode is placed in CA1, action potentials generated in the Schaffer collaterals are detected as negative potential. The negative potential generated by Schaffer collaterals is called fiber volley. The size of the fiber volley give information about the number of activated Schaffer collaterals. The activation of the Schaffer collaterals results in pre-synaptic glutamate release that opens glutamate receptors at the post-synaptic membrane. The consequent influx of ions depolarizes the post-synaptic neuron that is detected as a negative potential by the recording electrode. In conclusion, the field recordings (EPSP) correspond to the depolarization of the post-synaptic neurons (Fig. 1.7), while a corresponding action potential is called pope spike (not shown in the picture).

Especially in the hippocampus, field recordings are a powerful tool to study influences on synaptic neurotransmission. Nevertheless, field recordings do not allow for studying single cells, or current flow at synaptic membranes. To obtain intracellular recordings, sharp microelectrodes are inserted into the cell and thus allow the determination of the membrane potential. Sharp electrodes do not allow for the recording of the ion-flux at single ion channels since the background

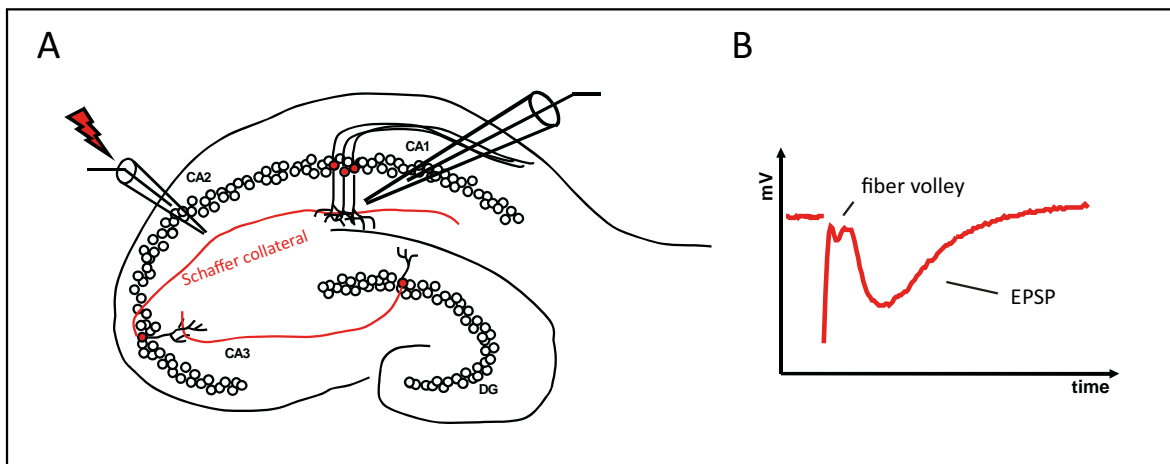


Figure 1.7: Sample trace for extracellular field recording. **A)** Illustration of the positioning of the activating electrode at the Schaffer collaterals and the recoding electrode in CA1. **B)** Sample recording trace showing the fiber volley that represents the action potential in the Schaffer collaterals and the EPSP, which represents the sum of the post-synaptic potentials.

noise is too high. Therefore, patch clamp recordings were invented by Erwin Neher and Bert Sakmann that allow for the recording of single ion channels (Hamill et al., 1981).

In this study, patch clamp recordings were obtained from primary hippocampal neurons, organotypic slices, and from acute brain slices. Depending on the scientific question, different systems are suited to answer individual questions.

In brief, to obtain patch clamp recordings, glass microelectrodes are filled with an internal solution that mimics the intracellular ion-concentrations. These microelectrodes are guided to neuronal somas with a continuously outflow of internal solution. The overpressure results in a typical light on the cell that shows the experimenter that the patch-microelectrode is near enough to the cell surface. Suction is applied to assist the formation of a high resistance seal between the glass electrode and the cell membrane (gigaseal). This so-called cell-attached configuration has to be achieved for all patch-clamp modes and enables the recording of single ion channels that are located in the patch of the membrane (Fig. 1.8). The best known configuration is the whole-cell configuration and is achieved by applying suction to the cell-attached configuration that ruptures the membrane patch. The intracellular space of the cell is connected with the microelectrode and consequently the intracellular solution mixes with the intracellular solution of the patched cell. Whole-cell recordings enables the altering of properties of the patched cell by

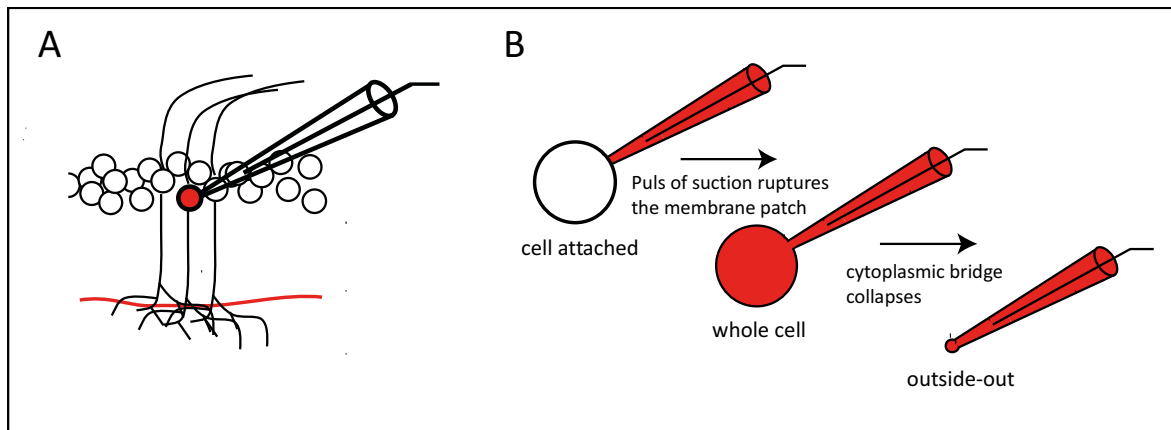


Figure 1.8: Illustration of a patched CA1 neuron and patch-clamp configurations. **A)** Illustration of CA1 of the hippocampus. Patch-clamp recordings measure the current flow over the cell membrane from one individual cell. **B)** Patch-clamp configurations. After obtaining a gigaseal the recording electrode and the patched cell are in the cell attached configuration. Whole cell recordings are obtained by breaking the cell membrane in the patch-pipette. By slowly removing the patch-pipette, the cell membrane blebs, detach and form a convex membrane, thus outside-out patches are obtained.

applying substances to the intracellular space of the cell. In some experiments of this study, the Nae1 inhibitor MLN-4924 was applied to the internal solution to restrict its action to the patched cell (Fig. 1.8).

After obtaining whole cell recordings, the microelectrode can be slowly withdrawn from the cell. Thereby, the membrane blebs out from the cell and the bleb detaches and forms a convex membrane when the membrane is pulled far enough away from the cell-body. This configuration is called outside-out patch and allows for the examining of ion channel properties. In this study, extra-synaptic AMPA currents were obtained *via* this configuration. In addition, substances can be applied to the extracellular surface to e.g. detect differences in ion-channel properties.

To measure the current flow through the membrane of excitatory cells, the membrane voltage is held to a set level. This kind of recording is called voltage-clamp. The manipulation of the membrane voltage enables the studying of current-voltage relationships of membrane channels. This is accomplished by monitoring the voltage across the membrane and simultaneously injecting of current to clamp the trans-membrane voltage to the set level.

Additionally, current-clamp recordings can be performed that are used to study the behavior of membrane potentials. Voltage-clamp recordings allow for the specific analysis of different

currents separately, but this is limited to studying excitation of neurons under physiological conditions. In current-clamp, current pulses are repetitively injected into the cell which allows the determination of the membrane resistance.

2 Material and Methods

2.1 Material

2.1.1 Buffers

Media for General Cell Culture and Primary Cell Culture

Table 2.1: Media for General Cell Culture and Primary Cell Culture

Name	Recipe/Supplier
HEK293 cells medium	500 ml Dulbecco's modified eagle medium (DMEM)(Gibco), 50 ml fetal calf serum (FCS) (Gibco), 5 ml 100 mM Glutamine (Gibco), 10 ml Penicilin/Streptomycin (Gibco)
BHK cells medium	Glasgow MEM BHK-21 medium (Gibco), 10 % Fetal bovine serum, 1 % Penicilin/Streptomycin
Freezing medium	95 % FCS (Gibco), 5 % dimethylsulfoxide (DMSO) (Gibco)
Dissection media	500 ml HBSS (Gibco), 5 ml Penicilin/Streptomycin (Gibco), 3.5 ml 1 M HEPES (Gibco), 5 ml 200 mM L-Glutamine (Gibco)
Serum media	50 ml DMEM (Gibco), 10 % FCS (Gibco)
Growth media	500 ml Neurobasal A (Gibco), 10 ml B27 (Gibco), 1.25 ml 200 mM L-Glutamine (Gibco)
Washing Media	HBSS (Gibco), 0.01 M HEPES
2 xBBS-buffer	50 mM BES; 280 mM NaCl, 1.5 mM Na ₂ HPO ₄ , pH 7.26

Media for Bacteria Cultures

Table 2.2: Media for Bacteria Cultures

Name	Recipe/Supplier
Lysogeny broth (LB) medium	1 % (w/v) bacto-tryptone (BD), 0.5 % (w/v) bacto-yeast-extract (BD), 1.5 % (w7v) NaCl, pH 7.4 with NaOH
LB agar plates	1 % (w/v) bacto-tryptone (BD), 0.5 % (w/v) bacto-yeast-extract (BD), 1.5 % (w7v) NaCl, 1.5 % bacto-agar (BD)pH 7.4 with NaOH
Super optimal broth (SOC) medium	2.0 % (w/v) bacto-tryptone (BD), 0.5 % (w/v) bacto-yeast-extract, 10 mM NaCl, 2.5 mM KCl, 10 mM MgSO ₄ , 10 mM mgCl ₂ , 20 mM glucose

Buffers for Biochemistry

Table 2.3: Buffers for Biochemistry

Name	Recipe/Supplier
RIPA lysis buffer	50 mM Tris, pH 8.0, 150 mM NaCl, 0,1% SDS, 1 % NP-40 or Triton X-100 and 0.5 % Sodium deoxycholate
NP40 lysis buffer	150 mM NaCl, 1.0 % NP-40 and 50 mM Tris, pH 8.0
Loading Buffer (4x)	50 % Glycerol, 125 mM Tris-HCl pH 6.8, 20 % SDS, 1 % bromphenol blue, 5 % β-mercaptoethanol
Running buffer (10x SDS PAGE)	30.3 g Tris, 144 g glycine, 50 ml 20 % SDS, adjust to 1 l with H ₂ O
Transfer buffer	400 ml methanol, 6.06 g Tris, 28.8 g glycine, fill up with H ₂ O up to 2 l, pH 8.3
10x TBS	12.11 g Tris, 87.66 g NaCl, pH 7.6
1x TBS	900 ml H ₂ O, 100 ml 10x TBS, 0.1 ml tween-20
5 % milk in 1x TBS	5 g milk, 100 ml 1x TBS

Media for Organotypic Slice Cultures and SFV Generation

Table 2.4: Media for Organotypic Slice Cultures and SFV generation

Name	Recipe/Supplier
slice-dissection media	MEM medium (Gibco), 1 % Penicilin/Streptomycin (Gibco), 1 % 1M Tris/HCl pH 7.2
Slice-culturing medium	50 % MEM medium (Gibco), 25 % HBSS (Gibco), 25 % Horse serum, 0.5 % L-Glutamine 200 mM
TBS-5 Buffer	50 mM 1 M Tris/HCl pH 7.8, 130 mM 5 M NaCl, 10 mM 1 M KCl, 5 mM 1 M MgCl ₂

Buffers for Electrophysiology

Table 2.5: Media used for Electrophysiology

Name	Recipe/Supplier
ACSF	in mM: 130 NaCl, 2.75 KCl, 1.43 MgSO ₄ , 1.1 NaH ₂ PO ₄ , 28.8 NaHCO ₃ , 2.5 CaCl ₂ , 11 glucose
HEPES-Ringer	in mM: 140 NaCl, 2.4 KCl, 10 HEPES, 10 Glucose, 4 CaCl ₂ , 4 MgCl ₂
Internal Solution	in mM: 150 Cs-Gluconate, 10 HEPES, 2 MgCl ₂ , 4 NaATP, 0.2 EGTA, 5 QX-314, 8 NaCl. pH 7.2 (290 mOSm/L)
High Chloride Internal	in mM: 90 CsCl, 20 Cs-Gluconate, 8 NaCl, 2 MgCl ₂ , 10 HEPES, 1 EGTA, 2 QX-314, pH 7.2 (290 mOSm/L)

2.1.2 Chemicals and Reagents

Table 2.6: Chemicals and Reagents

Name	Recipe/Supplier
(+) MK-801 hydrogen maleate	SIGMA
(2R)-amino-5-phosphonopentanoate (APV)	BioTrend
(S)- α -Amino-3-hydroxy-5-methylisoxazole-4-propionic acid (AMPA)	Sigma
2,3-dihydroxy-6-nitro-7-sulfamoyl-benzo[f]quinoxaline-2,3-dione (NBQX)	BioTrend
6-cyano-7-nitroquinoxaline-2,3-dione (CNQX)	Tocris
Adenosine 5'-triphosphate magnesium salt (MgATP)	Sigma
Aprotinin	Carl Roth
Laminin	Invitrogen
MG-132	Merck
MLN-4924	Active Biochem
N-Ethylmaleimide (NEM)	Sigma
Picrotoxin (PTX)	Sigma
Poly-D-Lysine	Sigma
Tetrodotoxin citrate (TTX)	BioTrend
Trichlormethiazide (TCM)	Sigma
α -chymotrypsin	Sigma

2.1.3 Antibodies

Primary Antibodies

Table 2.7: Primary Antibodies

Name	Recipe/Supplier
α -Cullin1	Invitrogen #322400 (mouse; 1:1000)
α -Flag M2	Sigma Aldrich #F3165 (mouse; 1:2000)
α -GFP	Abcam #ab6556 (rabbit; 1:2000)
α -GFP	Abcam #ab13970 (chicken; 1:2000)
α -Nedd8	Epitomics #1571-1 (rabbit; 1:5000)
α -Nedd8	Alexis #ALX-210-194 (rabbit; 1:500)
α -PSD-95	Neuromab #75-028 (mouse, 1:1000)
α -PSD-95	Cell Signaling Technology #2507 (rabbit; 1:1000)
α -Synaptophysin	Abcam #ab14692 (rabbit; 1:1000)
α -Ubc12	Lifespan BioScience #LS-B432 (rabbit; 1:500)
α -Tubulin	Sigma Aldrich #5168 (mouse; 1:2000)
α - β -Actin	Cell Signaling Technology #4967 (rabbit; 1:5000)

Secondary Antibodies

Table 2.8: Secondary Antibodies

Name	Recipe/Supplier
α -mouse-IgG HRP	Cell Signaling Technology #7076 (1:2000)
α -rabbit-IgG HRP	Cell Signaling Technology #7074 (1:2000)
α -rat-IgG HRP	Cell Signaling Technology #7077 (1:2000)

2.2 Methods

2.2.1 Cell Culture

All cell culture reagents were purchased from Invitrogen except as otherwise stated.

Mammalian Cell Lines

HEK293 (human embryonic kidney) cells were grown in Dulbecco's modified Eagle's medium (DMEM) supplemented with 10 % heat-inactivated FCS, Penicillin (100 units/ml), Streptomycin (100 µg/ml) and 2 mM L-Glutamine at 37 °C, 5 % CO₂. Every second day cells were passaged. Therefore, medium was removed and cells washed using 1 x DPBS. 1 ml 0.5 % trypsin/EDTA was added to the cell culture plate and incubated for 2 min in at 37 °C until the cells were detached from the culture plates. To inactivate the trypsin, 9 ml of media was added and 1 ml of the cell suspension transferred on another plate containing 9 ml of fresh media to generate a new passage of cells. For some experiments, cells were transiently transfected with expression plasmids using lipofectamine 2000 (Invitrogen). Cells were seeded at a desired concentration and transfected 24 hours later according to the manufacturer protocol. 24 hours later cells were harvested and used for further analysis. For long term storage, cells from one 10 cm cell culture plate were trypsinized and centrifuged. The resulting cell pellet was resuspended in 1.5 ml of freezing media. The suspension was aliquoted in cryo tubes and slowly cooled in an isopropanol-filled freezing container at -80 °C. After 2 days cryo tubes were stored in liquid nitrogen.

2.2.2 Primary Hippocampal Cell Culture

Coating of Coverslips

Coverslips (CVS) were washed for 5 min in Chloroform and afterwards washed 3 times with 100 % Ethanol. CVS were dried overnight at 80 %. Afterwards, CVS were placed into 24-well plates and coated with 1 mg/ml Poly-D-Lysine (SIGMA) and if necessary with 1 µg/ml Laminin (Invitrogen). After the incubation CVS were washed 3 times with PBS.

Primary Neuronal Cell Culture

Primary neuronal cell cultures were obtained from rat embryos as described (Dotti et al., 1988, Banker et al., 1974, Kaech and Banker, 2006). Before starting the preparation, cell culture dishes and glass-coverslips were covered with Poly-D-Lysine (0.05 mg/ml, 30.000-70.000 MW, Sigma Aldrich) and Laminin (1 µg/ml, Invitrogen) to ensure proper attachment of primary cells for 5 hours. Afterwards, dishes were washed 3 times with PBS to remove the Poly-D-Lysine/Laminin, filled with serum media and stored in the incubator (37 °C, 5 % CO₂) for equilibration. Primary hippocampal and cortical neurons were prepared from embryos (E 18.5-19.5) from Sprague Dawley rats. Therefore, embryos were removed from their pregnant mother, decapitated and heads collected in ice cold dissection media. Carefully the brains were removed the cortices and the hippocampi were separated and collected in 15 ml tubes on ice filled with 14 ml of dissection media. Thus, the dissection media was replaced by pre-warmed 0.25 % trypsin containing 1 mM EDTA and tissue pieces digested for 20 min at 37 °C. Tissue pieces were washed 3 x with 10 ml DMEM supplemented with 10 % FCS. Afterwards the tissue was homogenized in 1.5 ml of serum media using a fire-polished Pasteur pipette. Cells were centrifuged at 90 x g for 5 min, the supernatant removed and cells resuspended in pre-warmed growth medium. Cell number and viability was assessed by counting the number of living cells using a Trypan Blue staining. Cells were plated at desired density (105 cells/well in a 12-well plate, 5-10x10⁶ cells/10 cm plate) on the pre- incubated cell culture dishes at 37 °C and 5 % CO₂.

CaPO₄ Transfection of Primary Hippocampal Neurons

Primary neurons were transfected at different DIV's with expression plasmids using a modified calcium phosphate protocol (Jiang and Chen, 2006). To transfect 4 wells of a 24 well plate, 1 ml of transfection reagent is needed that contains 900 µl fresh growth media, 37.5 µl water and DNA (6-9 µg) mix, 12.5 µl 1 M CaCl₂ and 50 µl BBS. To avoid any damage of the primary neurons, the procedures have to be done quickly to minimize the time the cells were out of the incubator. Growth media is placed into the incubator (37 °C, 5 % CO₂) for equilibration 30 min before

transfection. The sterile water is mixed with 12.5 ml of 1 M CaCl₂ in a 1.5 ml sterile eppendorf cup. 6-9 µg of DNA is added and gently mixed by pipetting 10 times. During slow vortexing, 50 ml of 2 x BBS was added by dropping to the mixture. Finally, 900 ml of pre-incubated growth media was supplemented and the mix was vortexed at full speed for 10 seconds. The mixture was incubated for 15 min at RT. Afterwards the conditioned culture media on the cells was carefully removed and quickly replaced by 250 µl of transfection mixture. Thus the neurons were placed in the incubator. The conditioned media was collected, sterile filtered by passing through a 45 µm pore filter and put in the incubator together with the cell transfection. Primary neurons were transfected between 2-4 h depending on the DIV's of the neuronal culture as well as on the appearance of precipitate. Meanwhile, the washing solution, to stop the transfection, was pre-warmed. The cells were carefully washed with the washing solution until all precipitate was removed up to 10 times. Afterwards, the conditioned culture medium was placed back on the cells. Transfection efficiency was assessed one day after transfection, by the co-expression of fluorescent proteins.

Immunocytochemistry on Primary Neurons

Primary hippocampal neurons were grown on Poly-D-Lysine-coated coverslips in a 24-well. Cells were fixed in pre-warmed PFA 4 % in 4 % sucrose/PBS buffer for 20-30 min at RT. Afterwards cells were washed three times with PBS and then permeabilized with PBS-0.1 %-Triton X-100 3 x for 5 min. Cells were washed 5 min with PBS and consequently blocked with 5 % BSA (w/v) in PBS-0.1 %-Triton X-100 for 1 h at RT. The first as well as the second antibody was diluted in an appropriate concentration in 5 % BSA (w/v) in PBS-0.01 %-Triton-100. Incubation with the first antibody was carried out overnight at 4 °C followed by 3 x washing in PBS-0.01 %-Triton-100 for 10 min. The second antibodies were diluted 1:1000 in PBS-0.01 %-Triton-100, placed on the neurons and incubated for 2 h at RT. Coverslips were washed 3 x 10 min with PBS-0.01 %-Triton-100 and mounted with antifade mounting media (Vector Labs).

Cell Stimulation

For primary neuron stimulation, conditioned media was removed from cells and replaced by cell culture media containing 10 μ M of glutamate. After the time of treatment cells were washed with pre-warmed HBSS and conditioned media was given back to the cells.

2.2.3 Molecular Biology

Preparation and Transformation of Electrocompetent Bacteria

To generate electrocompetent bacteria, a pre-culture was inoculated from a frozen glycerol-stock of DH5 α and vigorously shook overnight (o.n.) at 37 °C. The next day, the pre-culture is transferred to an Erlenmeyer flask containing 500 ml LB media and incubated again at 37 °C until bacteria have grown to an optical density (OD) of 0.5-0.6 at 600 nm (DU530 photometer, Beckmann Coulter, Krefeld, Germany). The bacteria suspension was transferred into two pre-chilled centrifuge bottles (Beckmann Coulter) and cooled down on ice for 30 minutes. To prevent re-warming of the bacteria all following procedures were performed at 4 °C. After centrifugation at 4000 x g for 15 min at 4 °C (Avanti J-25 centrifuger, Beckmann Coulter) the supernatant was decanted and the pellets gently resolved in 1 l of ice-cold sterile water (Ampuva, Fresenius, Bad Homburg, Germany). Bacteria were centrifuged again at 4000 x g for 15 min at 4 °C, the supernatant discharged and the bacteria pellet resolved in 500 ml of ice cold sterile water. After a third centrifugation step bacteria were resuspended in 40 ml sterile water added with 10 % glycerol. Bacteria aliquots (20 μ l) were frozen on dry-ice and stored at -80 °C. Electrocompetence of the bacteria was tested by electroporating 10 pg of pUC19 vector (Invitrogen) into 20 μ l bacteria. Therefore, an aliquot of electrocompetent bacteria was thawed on ice and plasmid DNA was added. After 1 min of incubation, bacteria suspension was mixed carefully and transferred into a 1 mm electroporation cuvette (VWR). Bacteria were electroporated at 1.8 kV, 25 μ F capacitance and 200 Ω resistance in an electroporation system (Gene Pulse Xcall, BioRad, Munich, Germany). 1 ml of SOC medium was added and transformed bacteria were shaken for 30 min at 37 °C before plating on pre-warmed LB agar plates containing the appropriate antibiotics (100 μ g/ml ampicillin or 50 μ g/ml kanamycin) for selection. The next day colonies were

counted and the competence of the bacteria calculated.

Preparation and Transformation of Chemically Competent Bacteria

DH5 α bacteria were grown over night in 5 ml of LB medium. The next day, the pre-culture was added to 100 ml of fresh LB-media and incubated on a shaker at 37 °C until bacteria suspension reaches an optical density of OD_{550 nm} \square 500. Bacteria were put on ice to stop their growing and centrifuged for 15 min at 5000 rpm at 4 °C. The supernatant was decanted and the pellet resolved in 30 ml of ice-cold TBF1 buffer. Bacteria suspension was incubated on ice for 20 min and centrifuged again for 5 min at 4000 rpm at 4 °C. Afterwards, the pellet was resuspended in 3.6 ml of TBF2 buffer, bacteria aliquoted and stored at -80 °C. For transfection, chemically competent bacteria were thawed on ice. DNA was added to the bacteria, gently mixed by pipetting and incubated on ice for 30 min. The DNA was placed in the bacteria *via* heat-shock. Therefore, the bacteria-DNA mix was incubated for 90 seconds at 42 °C and subsequently put on ice. 1 ml of pre-warmed SOC media was added and bacteria were incubated for 1 h at 37 °C before plated on LB plates. Electrocompetence was determined as described before (Section (2.2.3); Preparation and Transformation of Chemically Competent Bacteria).

Preparation of Plasmid DNA

Plasmid DNA was prepared from liquid bacteria cultures. Therefore, one colony was picked from an agar plate and inoculated in LB medium supplemented with the appropriate antibiotics (100 μ g/ml ampicillin or 50 μ g/ml kanamycin). Bacteria grew o.n. at 37 °C on a shaker for subsequent DNA preparation. Plasmid preparation were carried out by means of the respective DNA amount using plasmid isolation kits from Qiagen following the manufacturer's instructions.

Determination of DNA Concentration

DNA concentration was determined in a UV photometer (DU640, Beckmann Coulter). Therefore, DNA was diluted 1/200 in water filled in a cuvette (thickness of 1 cm) and the optical density (OD) was measured at a wavelength of 260 nm. DNA concentration was calculated using the following equation:

DNA concentration = OD₂₆₀ nm x dilution factor x n
(n = 0 µg/ml for double stranded DNA).

Agarose Gel Electrophoresis

To separate DNA fragments of different size or to determine their length, DNA was run by agarose gel electrophoresis. Therefore, agarose were boiled in 1 x TAE buffer with an agarose concentration depending on the DNA fragment size (between 1-2 % agarose). 0.1 µg/ml ethidiumbromide was added to the liquid agarose, spilt in a gel electrophoresis chamber (PeqLab) and cooled to RT while polymerizing. DNA samples were mixed with 1/6 with 6 x sample buffer, loaded into gel pockets and separated by electrophoresis for 1-2 h at 80-140 V depending on the size of the DNA fragment. After electrophoresis DNA fragments were detected with a UV light camera (Biometra, Göttingen. Germany).

Polymerase Chain Reaction (PCR)

To amplify cDNA fragments for expression analysis or to clone PCR products into expression vectors, polymerase chain reactions were obtained using Thermoprime Plus DNA polymerase (ABgene, Hamburg, Germany) in a standardized 50 µl PCR reaction mix, containing: 1 µl of cDNA; 5 µl 10 x reaction buffer IV (ABgene), 3 µl MgCl₂ solution (25 mM, ABgene), 1 µl forward primer (10 pmol), 1 µl reverse primer (10 mol), 1 µl dNTPs (10 mM each, Roch) and 0.5 µl of Thermoprime Plus DNA polymerase (5 U/µl, ABgene). Routinely a standard PCR program was carried out as followed: 95 °C 5 min, 35 cycles of 98 °C for 45 sec, 58-60 °C for 30 sec, 72 °C for 20 sec to 1 min, followed by 72 °C for 10 min then holding at 8 °C. Annealing time and elongation time had to be adapted in dependence of the melting temperatures of the primers and the amplicon size. Successful DNA amplification was verified by agarose gel electrophoresis.

DNA Cleavage by Restriction Enzymes

DNA fragments or PCR products were cleaved using restriction enzymes from Fermentas or New England Biolabs (NEB). For preparative purpose 2-3 µg of DNA was digested with 10 U (1 µl) of restriction enzyme in the appropriate buffer (1 x) for 4-5 h at 37 °C (unless a differ-

ent temperature was stated by the company). The reaction was stopped following manufacturer's instructions and successful digestion was verified by agarose gel electrophoresis.

DNA Fragment Dephosphorylating

To prevent unwanted re-ligation of opened vectors, the 5'-termini is removed *via* Antarctic phosphatases, which is required by ligases. Therefore, 10 U of Fast phosphatase (CIP, Fermentas) and 1 x CIP buffer were added to the linearized plasmid and incubated at 37 °C for 45 min followed by head inactivation for 20 min at 75 °C.

Isolation of DNA Fragments

To purify DNA fragments after enzymatic restriction, samples were separated *via* agarose gel electrophoresis. The DNA was visualized using UV light and the appropriate bands were cut out using a scalpel. DNA was isolated using Qiagen Gel Extraction Kit following manufacturer's instructions. Afterwards DNA concentration and quality was determined by agarose gel electrophoresis using DNA marker smart ladder.

Ligation of DNA Fragments and Target Vectors

For Ligations, the T4 ligase (Fermentas) was used which catalysis the formation of a phosphodiester bond between 5'-phosphate and 3'-hydroxyl termini of double stranded DNA. Therefore, a molar ratio of 1:3 or 1:9 of linearized vector: insert was used and 5 U of T4 ligase in 1 x T4 ligase buffer was added to a total volume of 10 μ l. The reaction mix was incubated o.n. at 16 °C followed by head inactivation of the enzyme at 65 °C for 10 min. 1 μ l of the ligation was transformed into electrocompetent bacteria and plated on LB plates. Colonies were checked by plasmid prep and restriction digestion using the appropriate restriction enzymes or by sequencing (Sequiserve).

Topo TA Cloning

Topo TA cloning from Invitrogen was used to clone PCR products directly into a target vector. Therefore, PCR products were amplified using a Taq DNA polymerase (5 U/ μ l, Abgene)

that produces 3'-A overhangs. These A-overhangs are inserted into a cut vector which carries T-overhangs with covalently bound topoisomerase. The PCR product was mixed with TOPO pcRII vector and salt solution, following the manufacturer's protocol. The reaction was incubated at RT for 30 min before transformed into electrocompetent bacteria. For blue-white selection, bacteria were plated on LB plates supplemented with X-Gal (1 mg/ml). White colonies were analyzed by MiniPrep and restriction digestion with EcoR1.

Side Directed Mutagenesis

Mutagenesis PCRs were done either by Site-directed Mutagenesis Kit (Stratagene) according to the manufacturer's protocol.

2.2.4 Biochemistry

Sample Preparation

Cells or brain tissue for immunoprecipitation or immunoblotting were lysed in an appropriate chilled lyses buffer (RIPA or NP40 lysis buffer) supplemented with protease inhibitors (complete protease inhibitor tablets, Roche). When protein neddylation was analyzed 20 mM N-Ethylmaleimide (NEM) (Sigma Aldrich), an inhibitor of cysteine peptidases, and 2 mM 1,10-Phenanthroline monohydrate (OPT) (Sigma Aldrich), an inhibitor of metalloproteases were added to the lysis buffer. Therefore, cells were taken out of the incubator placed on ice and washed 2 times with chilled PBS. An appropriate amount of lysis buffer was added to the cells e.g. 1 ml ice-cold lysis buffer to a 10 cm plate and cells collected using a cell scraper. Cells or tissue were homogenized *via* ultrasound or insulin syringes. Cells were rotated for 1 h at 4 °C to let the lysis proceed. Thereafter, cells were centrifuged at 4 °C, 13.000 rpm for 30 min to remove cell debris. Now, proteins were used for Western blot analysis or co-immunoprecipitation studies.

Immunoprecipitation Analysis

Protein lysates were prepared as described before (Section 2.2.4; Sample Preparation). Before starting the immunoprecipitation procedure, 50 μ l of the protein lysate was taken for western blot analysis as “lysate”, to prove the accuracy of cell transfection. Afterwards, protein lysates were pre-cleared by adding 5 μ l of Dynabeads Protein G (Invitrogen) and let them rotate for 30 min at 4 °C. Thereafter, Dynabeads were removed *via* a magnet and the appropriate antibody added to the protein lysate rotated over night at 4 °C. For Flag-immunoprecipitations, Flag-M2-beads were added to the protein lysate and incubated equally. For non-conjugated antibodies, the antibody-protein complex was immunoprecipitated with Dynabeads Protein G, by an incubation of 4 h at 4 °C. Next, immunoprecipitated proteins were washed with 3 times for 15 min PBS added with 0.05 % Triton at 4 °C. Proteins were eluted by either boiling the samples in 1 x Laemmli-buffer (5 min at 95 °C), or in case of the Flag beads, by incubating with 3 x Flag peptide (150 ng/ μ l) for 30 min. Samples were analyzed by immunoblotting analysis.

Immunoblotting

For western blot analysis protein samples were separated by 8 %, 10 % or 12 % SDS-PAGE (Sodium Dodecyl Sulfate PolyAcrylamide Gel Electrophoresis). Before loading the samples, protein concentration was determined using Bradford assay (Bio-Rad). The appropriate amount of protein lysate and a pre-stained protein ladder (PageRuler™, Fermentas) were loaded on the SDS gel and separated *via* SDS-PAGE. The separated proteins were transferred using a wet-blot-system (Bio-Rad) to a 0.45 μ m PVDF membrane (Millipore). The membranes were blocked for 1 h in 5 % milk (Roth) and solved in 1 x TBS-T. Afterwards, the membranes were incubated with the appropriate primary antibody overnight at 4 °C. Membranes were washed 3 times for 10 min with TBS-T and incubated with the secondary-HRP coupled antibody, for 1 h at room temperature, diluted in 5 % milk in TBS-T. After again washing the membranes for 3 times with TBS-T, the signal was visualized using chemiluminescent reagent ECL (Millipore) and Kodak films developed in an automated development machine (XP 2000, Kodak). To quantify the signals, films were scanned and analyzed by Image J software (NIH, <http://rsbweb.nih.gov/ij/>).

Synaptosome Preparation

Synaptosomes were prepared as previously described (Cho et al., 1992, Lau et al., 1996). All experiments were performed at 4 °C and all buffers used were supplemented with protease inhibitor cocktail (Roche), phosphatase inhibitor cocktail I and II (Sigma Aldrich), and 5 mM of Sodium Orthovanadate. C57BL/6 mice were decapitated, hippocampi and cerebral cortex tissue dissected and homogenized in ice-cold HEPES-sucrose buffer I (Sucrose 0.32 M, 4 mM HEPES, pH 7.4) using a manual glass Dounce homogenizer. It is important to notice that from each fraction a protein-sample has to be stored at -20 °C to allow later analysis. To remove the nuclear fraction as well as cell debris (P1), the homogenate was centrifuged at 1,000 x g for 5 min at 4 °C. The supernatant was centrifuged at 10,000 x g for 15 min to obtain the crude synaptosomal fraction as pellet (P2). The pellet was carefully resuspended in 10 volumes of HEPES-sucrose buffer I and centrifuged again at 10,000 x g for 15 min to receive a purified crude synaptosomal fraction (P2'). The P2' was resuspended in 0.32 M sucrose, layered onto 4 ml of 1.2 M sucrose and centrifuged at 230,000 x g for 15 min. The interphase of the gradient was collected *via* a glass pipette, diluted in 8 volumes of 0.32 M sucrose, layered on 4 ml of 0.8 M sucrose and centrifuged again at 230,000 x g for 15 min. The resulting pellet contained the purified synaptosomes (P2''). In the next step the synaptosomes have to be lysed by a hypo-osmotic shock. Therefore, the P2'' pellet is resuspended in 9 volumes of H₂O supplemented with protease and phosphatase inhibitors and passed through a G32 syringe 3 times. The pH was adjusted to pH 7.4 by adding HEPES to a concentration of 4 mM. The mixture was incubated for 30 min at 4 °C to guarantee the complete lysis. After another centrifugation step (25,000 x g for 20 min) the crude synaptic vesicles (S3) have been separated from the synaptosomal membranes present in the pellet (P3; pre- and post-synaptic membranes). Synaptic vesicles were obtained by centrifugation at 165,000 x g for 2 h of S3. The synaptic membranes can still be purified into pre- and post-synapse by resuspending P3 in 0.32 M sucrose layered on a sucrose gradient 0.8 M to 1 M to 1.2 M (pH 7.4) and centrifugation at 150,000 x g for 30 min. Thereby, the plasma membrane fractions could be found between layer 1 M and 1.2 M sucrose. The sucrose concentration was adjusted to 0.32 M by adding 4 mM HEPES and centrifuged again at 150,000 x g

for 40 min to obtain the synaptic plasma membranes (P4). The pellet was resuspended in 5 ml of chilled 50 mM HEPES buffer supplemented with protease and phosphatase inhibitors plus 2 mM EDTA and 0.5 % Triton X-100. The solution is incubated for 15 min at 4 °C by rotating and afterwards centrifuged at 32,000 x g for 20 min to receive the PSD-1T fraction. The PSD-1T was resuspended in 50 mM HEPES supplemented with 2 mM EDTA and 0.5 % Triton X-100 and incubated at 4 °C for 15 min. The suspension was thereafter centrifuged at 200,000 x g for 20 min to obtain the PSD-2T fraction. All pellets received (P1-4, PSD-1/2T) were directly lysed in SDS containing lysis buffer and stored at -80 °C.

2.2.5 Affinity Purification and Mass Spectrometry

In-gel Tryptic Digestion

The gel band detected at 100 kDa was cut and subjected to in-gel tryptic digestion protocol. Briefly, the gel band was destained twice with a solution of acetonitrile (ACN)/25 mM ammonium bicarbonate (NH_4HCO_3) pH 8.5 (1/1, v/v) at 37 °C for 30 min. Then the gel slice was dried at room temperature, rehydrated with the addition of 25 mM NH_4HCO_3 and the proteins were reduced with 10 mM dithiothreitol (DTT) for 30 min at 56 °C in darkness. After removing the supernatant, 55 mM iodoacetamide (IAA) in 25 mM NH_4HCO_3 was added. The reaction of carboxyamidomethylation proceeded for 30 min at room temperature (RT) in darkness. For the enzymatic digestion 200 ng of trypsin in 20 mM NH_4HCO_3 pH 8.5 was added to the slice. The enzymatic reaction occurred at 37 °C overnight. To quench the enzymatic reaction 1 % aqueous acetic acid was added. After the digestion, peptides were extracted by incubating the slice with 2 % aqueous formic acid/ACN (1/1, v/v) at RT for 20 min and then sonication for 5 min. The extraction procedure was repeated twice. Supernatants were pooled and then dried using a Savant Speedvac Plus SC210A apparatus (Thermo Scientific).

LC-ESI-MS/MS Analysis

The extracted peptides were dissolved in 0.1 % HCOOH aqueous solution and separated using a nano-LC system (Eksigent, Dublin, CA, USA), consisting of autosampler and 2D-nano

HPLC devices, coupled to LTQ-Orbitrap XL mass spectrometer (Thermo Scientific, Bremen, Germany) equipped with a nano-ESI source. The sample was loaded onto a Zorbax-300 SB-C18 trapping column (5 μm , 5 x 0.3 mm i.d., Agilent Technologies, USA) and washed for 10 min with 0.1 % HCOOH at 3 $\mu\text{L}/\text{min}$. The peptides were separated on a nano column, 75 μm i.d x 15 cm, PicoFrit capillary column (New Objective, USA) packed in-house with 3 μm C18 coated particles (Dr. Maisch, Germany). For the liquid chromatography, 0.1 % HCOOH aqueous solvent (A) and ACN/0.1 % HCOOH (95/5, v/v) solvent (B) were used. The peptides were eluted with a linear gradient of solvent B from 2 to 10 % in 5 min and from 10 to 40 % in 98 min at flow rate of 200 nL/min. The eluted peptides were analyzed on-line in ESI-MS and -MSMS positive mode. The mass spectrometer was set so that one full scan was acquired in the Orbitrap parallel to the MSMS scans in the LTQ linear ion trap. The resolving power of the Orbitrap mass analyzer was set at resolution 60000 (FMHW, m/z 400) for the precursor ion scan in the mass range from 150 to 2000 Da. The fragmentation spectra (MSMS mode) were acquired in data dependent mode. The five most intensive signal ions (m/z) in each scan were selected for fragmentation with 30 s repeat duration time, 60 s exclusion duration time, 2 uma isolation width (m/z), 30 ms activation time, 35 V normalized collision energy and activation Q was set 0.250. The chromatographic separation and the spectra acquisition were performed in automatic mode, controlled and monitored by X calibur software (version 2.0.7, Thermo Scientific, San José CA, USA).

Protein Identification and Ubiquitylation/Neddylaton Localization

Prior to the submission to protein database (DB) search the MSMS spectra were converted in mzData format using a conversion tool embedded in Bioworks software (version 3.1, Thermo Scientific, San José, CA, USA). The protein database searches were performed using the Mascot engine (www.matrixscience.com). The Tandem spectra were searched against the protein SwissProt 15.3 database (uniprot 9.05.09), choosing for taxonomy specimen *Rattus norvegicus* for primary rat neurons and *Mus musculus* for the samples generated in HEK cells. The peptide and the fragment mass accuracies were set to 20 ppm and 0.6 Da, respectively. Full tryptic peptides including one missed cleavage side were accepted. Carboxyamidomethylation at cysteine

was set as a static modification. Methionine oxidation, serine, thymosine, threonine phosphorylation and lysine modification by GG- and LGG- tags, were set as variable modifications. The modification GG- tag (m/z 114) at lysine residue can result by trypsin cleavage of ubiquitin or Nedd8, the LGG- (m/z 383) tag results specifically from ubiquitin in case of a missed cleavage. In case of searches of data set generated from mutants Nedd8 mutants, AGG- (m/z185) or LGG- (m/z 227) modification tags were added to the list of the variable modifications. In proteomics experiments 10-15 % of all tryptic peptides of a given protein are identified 32. To enlarge the sequence coverage we repeated the protein database search by setting SemiTrypsin as enzyme. The semitryptic peptides include more than 90% of non-tryptic peptides generated during the trypsin digestion, diverse proteomics studies report their existence which is related to the solutions used for the digestion 33-35. The Mascot database search was performed with a confidence index over 95 %. The Mascot score threshold for the peptide score and the expected peptide score were set higher than 20 and lower than 19, respectively. The tandem spectra of the peptides modified by GG- and LGG-, AGG- and LGG- were manually inspected before being accepted.

2.2.6 Animal Experiments

All animal experiments were conducted under standard laboratory conditions (22 ± 1 °C, 55 ± 5 % humidity, 12 h light-dark cycle) with water and food ad libitum. Littermates were weaned at the age of 4 weeks and tail biopsies were taken for genotyping if necessary.

2.2.7 In-Utero Electroporation

Timed, E13.5-E15.5, pregnant female CD1 mice were anesthetized using isoflurane (Baxter), the eyes protected from drying using eye cream (Bepanthen eye and nose cream) and the abdomen shaved. Surgical instruments were disinfected as well as the abdomen of the mice using 70 % ethanol. A midline abdominal incision, approximately 3 cm in length, was made using a scissor. Sterile gauze was placed on the mice, before the uterine horns were carefully exposed. During the whole surgery the uterine horns had to be hydrated with saline (0.9 %NaCl solution), prewarmed to 37 °C. Glass micro-pipette was filled with a mixture of, high concentrated expression

plasmid (2-4 $\mu\text{g}/\mu\text{l}$) and fast green (for visualization), and 1 μl injected into the lateral ventricle of the embryos. After the DNA injection, electroporations were performed using an Electro Square Porater ECM830 and tweezerrodes (BTX Genetronics). The developing cortex or hippocampus was targeted using a 7-mm diameter tweezerrodes (BTX Genetronics) and application of 5 pulses with 40 V, 50 ms and with 950 ms interval (Nakahira and Yuasa, 2005). After the electroporation, the embryos were placed back into the uterus and the abdominal wall and the skin closed with surgical sutures (Johnson & Johnson). At the end of the surgery, the wound was disinfected with iodine (Braunol) and antibiotics was applied (Enrofloxacin, 100 mg/ml, Bayer, Leverkusen) intraperitoneally and painkiller subcutaneously (Carprofen, Boehringer Ingelheim). After birth, the embryos were allowed to grow up and were used for electrophysiological recording between P18 and P22. Electroporation efficiency was assessed by a fluorescent microscope.

2.2.8 Organotypic Hippocampal Slice Preparation

Organotypic hippocampal slice cultures are an intermediate between acute brain slices and primary hippocampal neurons. They allow the culturing of neurons in a hippocampal network. Neurons can be genetically modified by plasmid transfection *via* electroporation or viral infection. Hippocampal Slices were prepared according to Stoppini and Buchs (Stoppini et al., 1991). Before starting the organotypic slice preparation, culture plates had to be prepared. Therefore, 30 mm petri dishes were filled with 1 ml of the slice-culturing medium. Millicell culture plate inserts (Millipore) were located into the petri dishes and 4 confetti of Biopore 0.4 μm membrane (Millipore Corporation) placed on each insert. The prepared cultures were put into the incubator (35 $^{\circ}\text{C}$, 5 % CO_2) for one hour to equilibrate. Hippocampal slices were prepared from 7 day old C57BL/6 mice. Mice were decapitated, brains removed and placed into a dish filled with chilled slice-dissection media. The Hippocampus was removed and cut into 400 μm slices using a McIlwain tissue culture chopper (The Mickle Laboratory Engineering). Brain slices were transferred into a Falcon tube and separated by gentle shaking. Afterwards undamaged slices were positioned on the confetti of the pre-incubated petri dishes, excess slice-dissection media removed and returned to the incubator. Slice-culturing media had to be changed the day after preparation and then every second day.

2.2.9 Semliki Forest Virus Preparation

The Semliki Forest Virus (SFV) belongs to the alpha-viruses which are able to infect animal and men and are characterized by their positive single stranded RNA genome. They have an icosahedral capsid which is enveloped by a lipid bilayer derived from the host cell and makes up 40 nm. The virus is covered by E1 and E2 glycoproteins arranged in interconnective trimmers. The DNA is made up of ~12000 base pairs, where the 5' -end codes for the cap-structure and non-structural proteins (nsP1 –nsP4) whereas the structural proteins are encoded at the 3' -end which is additionally polyadenylated. The non-structural proteins are involved in the replication and translation of the viral proteins which build up the RNA-replication-complex. For scientific approaches, structural and non-structural proteins were split on two different plasmids. Whereat, pSFV codes for the non-structural, responsible for RNA replication, and pSVF-Helper for all structural proteins. Therefore, infective viruses are just generated when RNA of both plasmids were co-transfected. After one round of infection, no new virus particles can be found, therefore they are called “suicide vectors”.

pSFV Plasmid and SFV-mRNA Generation

After cloning the cDNA of the gene of interest into the multiple cloning region of the pSVF vector, RNA of both plasmids had to be generated. Both plasmids contain a SP6 RNA polymerase promoter site. For in vitro transcription plasmids were linearized with the restriction enzyme SpeI and RNA was generated using mMessage mMachine transcription kit (Ambion). The correct length of the transcript was verified by agarose gel electroporation. RNA was precipitated by LiCl at -20 °C, washed with Ethanol and suspended in nuclease-free water.

BHK Cell Transfection with the SFV System

Baby hamster kidney cells (BHK-21) are used to generate infectious virus particles. BHK-21 cells grown to 90 % confluence on a 10 mm dish were plated on a 150 mm dish in a 1:5 dilution. When BHK-21 cells reached 80 % confluence, cells were detached from the plates by adding 3 ml of trypsin/EDTA for 2 min. BHK-21 cells were transferred into a 50 ml Falcon, 3 ml of

medium added to inhibit trypsin activity and centrifuged for 2 min at 330 g. The supernatant was removed and the cell pellet washed with 10 ml chilled RNase free PBS. Cells were again centrifuged for 2 min at 330 g, the supernatant removed and the pellet resuspended in 0.5 ml of chilled RNase free PBS. The dissociated BHK-21 cells were mixed with the RNA of pSFV containing gene of interest and pSFV-helper (ratio 1:1) and transferred to a sterile electroporation cuvette. Cells were electroporated twice with an interval of 10 sec using a Bio-Rad electroporator with the following settings: voltage 1.5 kV, capacitance 25 μ F and infinity resistance. Between the electroporations cells had to be mixed gently. A time constant of 0.7-0.8 s revealed a sufficient electroporation. After electroporation cells were left at room temperature for 10 min before they were plated in 9.5 ml of medium on a 100 mm dish. The dish was kept at 37 °C, 5 % CO₂.

Virus-Harvesting

36 h after electroporation, viral particles were released from the BHK-21 cells and were present in the supernatant. These were collected in a Falcon and centrifuged at 3000 g for 15 min to remove all cell rests. To further clean and concentrate the viral particles, the supernatant was spun in an ultracentrifuge for 1.5 h at 50.000 g using a SW41 rotor. The supernatant was aspirated, dried and resuspended in 300 μ l TBS-5 buffer over night at 4 °C. Afterwards, the virus was aliquoted and stored at -80 °C.

Virus Activation

To avoid uncontrolled infection, the pSVF-helper plasmid contains point mutations in its genes coding for structural proteins. These structural proteins form spikes that are necessary for the infection. Under normal conditions spine-forming proteins are cleaved by endogenous proteases. This process could be prevented by the inserted mutations, making the proteins resistant to the endogenous proteases. Therefore, the viral particles have to be treated with exogenous proteases to be infectious. For the activation, the viral solution was incubated with α -chymotrypsin (ratio 1:20) for 45 min at room temperature. Afterwards, α -chymotrypsin was inactivated with aprotinin (ratio 1:15) for 10 min at room temperature. The activated virus was aliquoted and stored at -80 °C.

2.2.10 Infection of Organotypic Hippocampal Slices with SFV

Organotypic brain slices were infected with the SFV one day before recording. Depending on the scientific question the day in vitro (DIV) is important. Thus, if one wants to look at spine development, slices were transfected at DIV1-2 when the dendrites of the neurons are covered with filopodia. When experiments should be conducted when spines are stable, neurons will be transfected at later DIVs' when spines are mature (DIV7-8). Therefore, injection pipettes (World Precision Instruments, Sarasota, Florida) were filled with mineral oil and placed into Nanoinjector II (Drummond Scientific Company). 1 μ l of the SFV of interest was aspirated into the injection pipette. The hippocampi were taken out of the incubator and 46 nl of the SVF injected into the CA3 region of the hippocampus. Slices were laid back in the incubator and used the next day.

2.2.11 Image Acquisition and Live Cell Imaging

To analyze the morphology of synapses in acute hippocampal brain slices, images were obtained using an Olympus IX81 inverted laser scanning confocal microscope and Fluoview 1000 software. As objective a 10x UPlanSApo, 0.40 numerical aperture (NA), 20 x UPlanSApo, 0.75 NA, 40x PlanApo, 0.9 NA WLSM or 60 x UPlanSApo, 1.2 NA W Olympus objective were used. Pictures were captured randomly in a blind manner. Z-stack of pictures with 0.4-1.2 μ m step size were collected and analyzed with open access Image J software (freeware: <http://rsbweb.nih.gov/ij/>).

Live cell images from organotypic brain slices were obtained by a custom built 2-photon microscope. Organotypic slices were placed in an imaging chamber perfused with ACSF. Image stacks of a dendritic region were acquired using a 2-photon microscope controlled by scanimage (<http://scanimage.org>) with a Chameleon Vision-S (Coherent) femtosecond laser as light source. The laser was driven at 910 nm with an output power of approximately 50 mW. Objective was a LUMPLFLN 40XW (Olympus) water immersion lens with a numerical aperture of 0.8. Images were taken every 5 minutes for 2.5 hours. After 30 minutes of baseline imaging 1 μ M of MLN-4924 was added to the ACSF.

Images were analyzed with MATLAB-based software. In principle, maximum projections of the images were registered, spines were marked and their mean intensity was read for the different time points. The mean intensity for each spine was divided by the mean intensity of the dendrite of the corresponding time point to identify changes in spine size.

2.2.12 Acute Hippocampal Slice Preparation

Acute hippocampal brain slices were obtained from P14-P21 C57BL/6 mice. Therefore, animals were anesthetized with Isoflurane, decapitated, the brains removed and placed into ice-cold ACSF gassed with carbogen (95 % O₂, 5 % CO₂) for 1 min. The hippocampi were dissected and transversally sliced (400 μM) with a vibratome (Leica VT1200S) in chilled, carbogenated ACSF. Slices were equilibrated in slice-chambers containing continuously gassed ACSF for 30 min at 32 °C and thereafter kept at room temperature.

2.2.13 Electrophysiology Field Recordings

Field excitatory post synaptic potentials (fEPSP) were recorded from acute hippocampal slices placed on PDL-coated glass cover slights. Schaffer collaterals were disconnected using a scalpel in CA3 to prevent recurrent excitation. To record synaptic responses in CA1, Schaffer collaterals were stimulated in CA3 using a glass microelectrode (Science Products GB150TF-8P, Hoffenheim, Germany) filled with ACSF. Same electrodes were used to record evoked responses in the stratum radiatum of the CA1. fEPSP data were acquired using a Multiclamp 700B amplifier (Axon Instruments) and digitized on a Digita 1322A (Axon Instruments). Traces were visualized and fEPSP slope was analyzed using Clampex software (Axon Instruments). All experiments were conducted at room temperature (21-23 °C) and the recording chamber was continuously perfused with carbogenated ACSF. Pre-baseline recordings were taken until fEPSP reached stable slopes for 20 min. Thus, baseline recordings for single experiments could be started.

Input-Output curves

Basal synaptic transmission at CA3-CA1 synapses was assessed by measuring the input-output relation at the synapse. Thereby, the input is defined as the amplitude of the fiber volley,

representative for the strength of action potential triggered in the Schaffer collaterals. The slope of the resulting fEPSP was defined as output. Thus, fiber volley amplitudes of 0.05, 0.1, 0.15, 0.2 and 0.25 mV were evoked and the resulting fEPSC plotted.

Paired-Pulse-Facilitation (PPF)

Paired-Pulse-Facilitation, an experiment to analyze pre-synaptic neurotransmitter release, was assessed. Thereby, the stimulation electrode was placed in CA3 and Schaffer collaterals were stimulated using stimulus intervals of 20, 40 and 100 ms. fEPSP were recorded in CA1.

Vesicle Depletion Experiments

After 10 min of stable baseline fEPSP recordings, long repetitive stimuli, 300 pulses at 10 Hz, were applied to Schaffer collaterals and resulting fEPSP measured in CA1. Post fEPSP were recorded for 5 min and normalized to the mean slope of the baseline.

Long-Term-Potentiation (LTP)

After 20 min of baseline fEPSP recording, Long-term potentiation was induced by a high-frequency stimulus (100 Hz for 1 s). Post-fEPSPs were recorded for 60 min and normalized to the mean slope of the baseline.

Long-Term Depression (LTD)

Long-term depression was induced by low-frequency stimulation (1 Hz for 15 min). Post-fEPSPs were recorded for 60 min and normalized to the mean slope of the baseline.

2.2.14 Whole Cell Recordings

Patch-clamp recordings were conducted in primary hippocampal neurons, organotypic hippocampal brain slices as well as in acute brain slices. Primary hippocampal neurons as well as pyramidal cells in tissues were visualized using differential interference contrast camera on an upright microscope (Olympus, BX51WI). All recordings were done at room temperature in a recording chamber continuously perfused by carbogenated ACSF. If necessary, drugs were

added to the ACSF. Recordings were obtained using 2-4 M Ω glass electrodes (Science Products GB150TF-8P, Hoffenheim, Germany) filled with the corresponding internal solution. Data were collected with an Axopatch amplifier (Axon instruments) and digitized at 5 kHz with the Digidata 1322 controlled by the software pCLAMP 9.2. A test pulse of -5 mV was applied to the cells after obtained whole-cell configuration and only cells analyzed with an input resistance lower than 20 M Ω .

Paired-Pulse-Facilitation (PPF)

Whole cell recordings were obtained from CA1 neurons in acute hippocampal brain slices. To block inhibitory neurotransmission 100 μ M picrotoxin was added to external ACSF. AMPA EPSC were evoked with an interevent interval of 40 ms. The paired-pulse ratio was determined by dividing the second AMPA EPSC amplitude by the first AMPA EPSC amplitude.

Miniature EPSCs (mEPSCs)

Miniature excitatory post-synaptic currents (mEPSC) were recorded from primary hippocampal neurons, CA1 neurons from transfected organotypic hippocampal brain slices as well as from CA1 neurons of acute hippocampal brain slices. The ACSF was supplemented with 0.2 μ M tetrodotoxin (TTX; blocks sodium channels), 250 μ M trichlormethiazide (TCM; increases mEPSC frequency) and 100 μ M picrotoxin. mEPSC were recorded in voltage clamp at -70 mV for at least 10 min to make sure that in the end 120 events could be taken for analysis. mEPSC were analyzed and detected off-line and statistically analyzed with a custom written MATLAB routine (MathWorks).

Evoked AMPA Currents

AMPA receptor mediated EPSC were evoked at -70 mV in acute brain slices perfused with carbogenated ACSF supplemented with 100 μ M picrotoxin and 100 μ M APV (R-2-amino-5-phosphonopentanoate, competitive antagonist of NMDA receptors). The AMPA EPSC amplitude was determined by measuring the peak of response.

NMDA Currents

Evoked Isolated NMDA currents were recorded in the presence of 100 μM picrotoxin (blocks inhibitory neurotransmission) and 10 μM NBQX (AMPA and kainite receptor antagonist) supplemented to external ACSF. After obtaining whole-cell configuration and waited for 20-30 sweeps, cells were depolarized to +40 mV and allowed to stabilize for another 2 minutes. Then, NMDA currents were measured at 0.2 Hz frequency. NMDA EPSC amplitude was determined by measuring the current magnitude 70 ms after the stimulation artifact.

MK-801

NMDA currents were measured as described before (Section 2.2.14; NMDA Currents). When stable NMDA currents were evoked, recordings were stopped and 5 μM of MK-801 was washed in. Then, NMDA currents were evoked with a frequency of 0.1 Hz for 130 stimuli (25 min). NMDA EPSC amplitude was determined by measuring the current magnitude 70 ms after the stimulation artifact.

AMPA/NMDA Ratio

AMPA and NMDA currents were evoked in acute brain slices incubated in ACSF supplemented with 100 μM of picrotoxin. First evoked AMPA EPSC were evoked at -70 mV than neurons were depolarized to +40 mV, allowed to stabilize for 2 min, before evoked NMDA currents were obtained. The AMPA EPSC amplitude was determined by measuring the peak of response. NMDA EPSC amplitude was determined by measuring the current magnitude 70 ms after the stimulation artifact. Finally, AMPA/NMDA ratio was calculated from both values.

Decay Time of AMPA and NMDA Currents

Decay time for AMPA and NMDA currents were calculated from the area under the current from peak to 1.3 s after the peak and normalized to the peak amplitude (Cathala et al., 2005).

Miniature IPSCs (mIPSCs)

Miniature inhibitory post-synaptic currents (mIPSCs) were recorded from primary neurons as well as from CA1 neurons in acute hippocampal brain slices. ACSF was supplemented with 10 μM of NBQX (blocks AMPA and kainite receptors) and 0.2 μM TTX (block action potentials). IPSC were recorded at -70 mV holding potential using a high chloride internal for at least 10 minutes to make sure that 120 events could be analyzed. mIPSC were analyzed and detected off-line and statistically analyzed with a custom written MATLAB routine (MathWorks).

2.2.15 Somatic Outside-Out Patches

Outside-out patches were performed from CA1 neurons of acute hippocampal brain slices. Neurons were clamped at -70 mV and AMPA currents evoked by local application of 0.5 m glutamate for 2 seconds in the presence of 250 μM trichlormethiazideto that blocks receptor desensitization.

2.2.16 Data Analysis

Statistical analysis were carried out using GraphPad Prism 5 software and custom written MATLAB routines. Values are given as mean \pm standard error of the mean (s.e.m.).

3 Aim

Post-translational modifications are known to impact on neuronal function by controlling protein interaction, trafficking, localization, and activity. For ubiquitin and SUMO, neuronal target as well as the impact these post-translational modifications exert on neuronal functions have been established in recent years. Besides ubiquitin and SUMO, no other UBLs have been described that are active in the brain or even in synaptic compartments. Since Nedd8 was discovered in neuronal tissue and considering the high structural and sequence homology between Nedd8 and ubiquitin, it is very likely that the Nedd8 pathway also influences neuronal function.

Question 1: Is the Nedd8 Pathway Active in Synaptic Compartments and Does Neddylated Proteins Impact on Neuronal Function?

To answer this question, the presence of neddylated proteins has to be demonstrated in synaptic compartments as well as the enzymes that are involved in the Nedd8 pathway. This identification will allow for the description of the exact Nedd8 pathway and will give insights into the impact neddylation has on neuronal function. Additionally, relevant neddylated proteins should be identified in the synapse. Inhibition of the Nedd8 pathway in general, by pharmacological or genetic approaches, will allow for the studying of neuronal function when no neuronal proteins are neddylated anymore.

Question 2: Which Lysine Residues of PSD-95 are Neddylated and what is the Impact of PSD-95 Neddylation?

Mass spectrometry of PSD-95 was performed to identify neddylated lysine residues in PSD-95. Since Nedd8 and ubiquitin cannot be distinguished by current methods of mass spectrometry,

Nedd8 mutants will be developed that allow for the differentiation between Nedd8 and ubiquitin conjugated residues. These Nedd8 mutants will enable the identification of neddylated lysine residues in PSD-95. Afterwards, these lysines will be mutated to arginines to prevent their modifications by the Nedd8 pathway. The Nedd8 defective mutants of PSD-95 facilitate the studying of neuronal morphology and function when neddylation at PSD-95 is specifically prevented.

Question 3: Does Neddylation Impact on Basal Synaptic Neurotransmission?

Ubiquitylation and sumoylation have been shown to influence neurotransmitter release from the pre-synapse and to alter post-synaptic receptor distribution. Consequently, the probability of pre-synaptic neurotransmitter release will be investigated upon neddylation inhibition. Additionally, the influence of the Nedd8 pathway on the main excitatory receptors in the post-synapse, AMPA and NMDA receptors will be assessed.

In addition to excitatory synapses, the impact of neddylation on inhibitory neurotransmission will be investigated, too.

Question 4: Does Neuronal Activity Change the Pattern of Neddylated Proteins e.g. PSD-95?

Neuronal activity had been shown to be involved in the regulation of protein concentrations in synaptic compartments by ubiquitylation. One goal will be to see whether neddylation of target proteins changes with neuronal activity. More specifically, it will be studied whether the amount of neddylated PSD-95 changes after glutamate treatment.

Question 5: Does Neddylation Impact on Synaptic Plasticity?

The final goal of this thesis will be to examine whether neddylation influences the induction of synaptic plasticity. Therefore, electrophysiological techniques including long-term depression and long-term potentiation will be conducted.

In summary, this thesis will concentrate on the identification of neddylated proteins in post-synaptic compartments. Furthermore, specific effects of PSD-95 neddylation will be examined that will give an idea of the functional impact of neddylation in neurons. To better understand the role of the Nedd8 pathway on synaptic neurotransmission, electrophysiological experiments will be conducted that will describe the impact on pre- as well as on post-synaptic function of excitatory and of inhibitory synapses. Additionally, the role of the Nedd8 pathway in synaptic plasticity will be studied.

4 Results

Previous work by Annette Vogl showed that neddylation is an active post-translational modification in the brain. Furthermore, we demonstrated that neddylation plays an important role during neuronal development and synaptogenesis and affects the stability of mature neurons. Although we detected very strong morphological changes of the synapses upon inhibition of the Nedd8 pathway, the specific compartmental location of neddylated proteins in the neuron remains to be investigated. Therefore, the first aim was to study where neddylated proteins are present in the neuron, especially in neuronal compartments such as the pre- and post-synapse.

4.1 Neddylated Proteins in the Mature Synapse

In the synapse, the post-synaptic density (PSD) of the post-synapse and the active zone of the pre-synapse build up complex protein structures that regulate synaptic neurotransmission. Figure 4.1A depicts the complexity and number of protein interactions in the PSD. Various post-translational modifications have been described that regulate the integrity of these protein interactions and therefore alter synaptic functions (Yi and Ehlers, 2005, Haas and Broadie, 2008). The identification of synapse-specific targets of the Nedd8 pathway remains to be elucidated. To study the neddylation pattern of synaptic proteins, synaptosome fractionation from adult mouse hippocampi were obtained by sucrose gradient centrifugations.

Protein lysates from mouse hippocampi were used as protein input for the synaptosome preparation (Figure 4.1B, lane 1). Crude synaptosomes that contain proteins from the pre- as well as from the post-synapse were blotted in lanes 2-5 (2: crude synaptosomes, 3: pure synaptosomes, 4: synaptic plasma membranes, 5: synaptic heavy membranes). In lanes 6-9, protein fractions

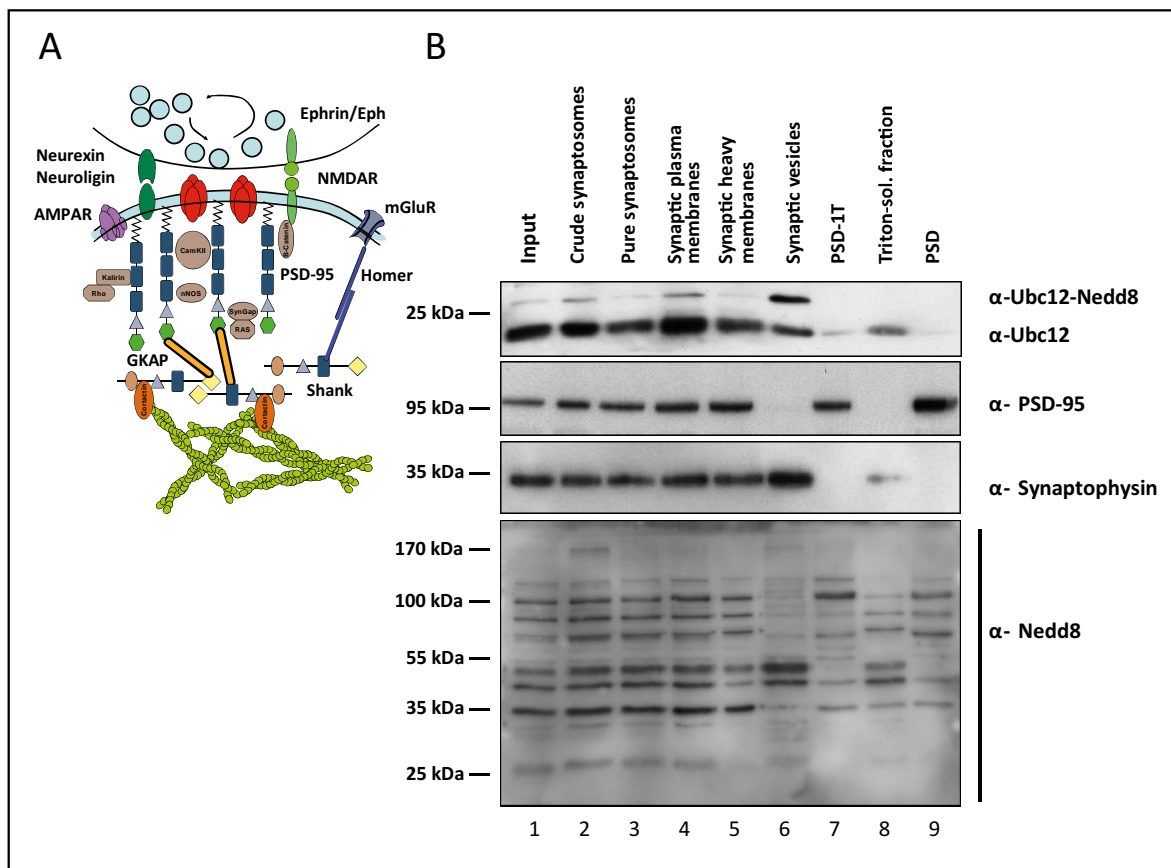


Figure 4.1: Mouse synaptosome preparation reveals that the neddylation pathway is active in pre- and post-synaptic compartments. **A)** Schematic illustration of proteins present in pre- or post-synaptic compartments. **B)** Western blot analysis from synaptic fractions obtained from adult mouse hippocampi show that Ubc12 is expressed in the pre- as well as in the post-synapse and that neddylated proteins can be found in both synaptic compartments.

that contain proteins located in the pre- (6: synaptic vesicles) or in the post-synapse (7: PSD-1T, 8: Triton soluble fraction, 9: PSD) were immunoblotted. To confirm the purity of the obtained synaptic fractionations, all fractionation samples were blotted with antibodies that are specific to the post- (PSD-95) or to the pre-synapse (Synaptophysin) (Fig. 4.1B). Given that lanes 1-5 contain proteins from the pre- as well as from the post-synapse, immunoblottings detected synaptophysin and PSD-95 throughout all lanes. However, in lanes 6-9, synaptophysin was enriched in the synaptic vesicles fraction (Fig. 4.1B, lane 6), whereas PSD-95 detection was restricted to the PSD-1T as well as to the PSD itself (Fig. 4.1B, lanes 7+9). Hence, the immunoblottings with PSD-95 and synaptophysin antibodies confirmed the purity of the synaptosome preparation. Immunoblotting with α -Ubc12 antibodies revealed the presence of Ubc12 in the pre- as well as in

the post-synapse (Fig. 4.1B, lanes 1-6+8). Since Ubc12 is a soluble enzyme, Ubc12 was detected in the triton-soluble fraction, whereas in the PSD fraction, where mainly scaffolding proteins were enriched, Ubc12 was not detected. Additionally, a second band was detected using α -Ubc12 antibodies, representing Ubc12-Nedd8 conjugates. The amount of Ubc12-Nedd8 conjugates was especially high in the synaptic vesicle fraction and might indicate that the Nedd8 pathway is particularly active in this synaptic compartment.

To study the pattern of neddylated proteins throughout the different synaptosomal fractions, western blot experiments were obtained using α -Nedd8 antibodies. Importantly, all bands detected by western blot analysis with α -Nedd8 antibodies present one or more neddylated proteins (Fig. 4.1B) since the covalent bound of Nedd8 and its target proteins remain during SDS-PAGE. Especially in the more purified fractions (Figure 4.1B, lanes 6-9), the pattern of neddylated proteins changed between the different synaptic compartments, suggesting that neddylation was restricted to specific proteins and may thus exert distinct functions.

In summary, the synaptosome preparation shows that Ubc12 is expressed in the pre- as well as in the post-synapse. In addition, Ubc12 seems to be particularly active in the pre-synapse, since the signal of Ubc-12-Nedd8 conjugates is highest in the synaptic vesicle fraction. The pattern of neddylated proteins strongly differed between pre- and post-synaptic fractions and revealed a large number of neddylated proteins in the synapse.

4.2 Interference with the Nedd8 Pathway

To study neddylation and its impact on neuronal function, it is important to block the Nedd8 pathway sufficiently.

In this study, the Nedd8 pathway was inhibited by either genetic or pharmacological approaches. The genetic approach was based on the overexpression of Ubc12-C111S or of shRNAs against Ubc12 or Nedd8, whereas the pharmacological interference used the Nae1-specific inhibitor MLN-4924.

Ubc12-C111S is a dominant negative version of Ubc12, the E2 conjugating enzyme of the Nedd8 pathway. The amino acid exchange from cysteine to serine is sufficient to sequester Nedd8 to

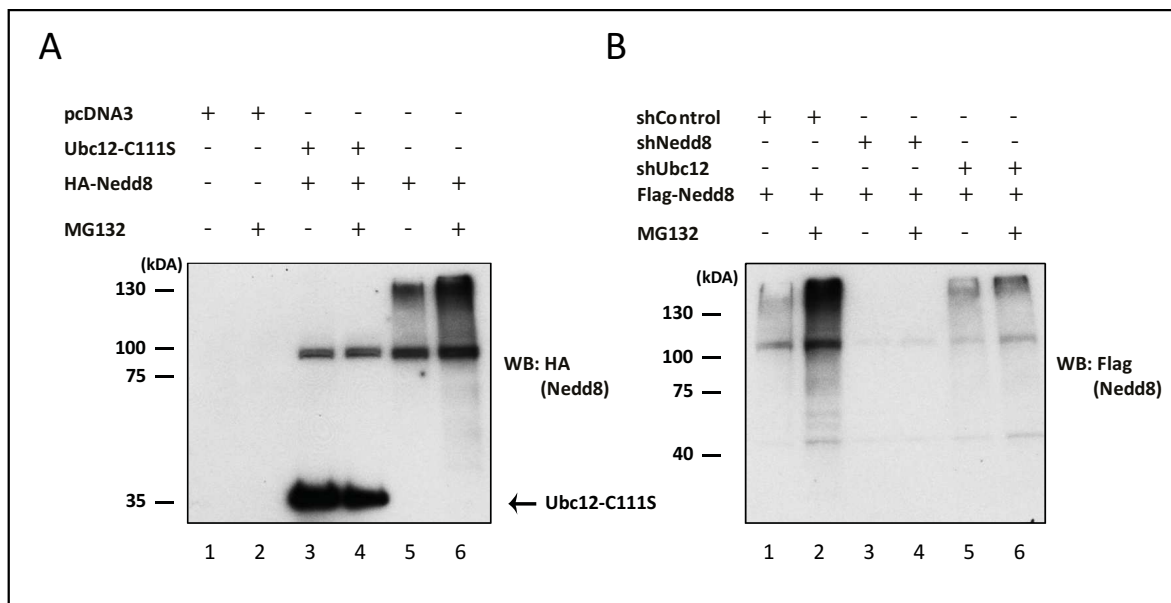


Figure 4.2: Overexpression of Ubc12-C111S, shNedd8 or shUbc12 is sufficient to block the Nedd8 pathway. **A, B)** HEK293 cells were transfected with tagged-Nedd8 and constructs that interfere with the Nedd8 pathway. Samples were analyzed *via* western blots. Additionally, the samples were treated with MG132. **A, B)** MG132 increases the amount of neddylated proteins. **A)** Overexpression of Ubc12-C111S sequesters Nedd8 and thus blocks protein neddylation. **B)** Both, shRNAs against Ubc12 and Nedd8, were sufficient to reduce target protein neddylation.

Ubc12-C111S and thus to inhibit the subsequent transfer from Nedd8 to its target proteins (Wada et al., 2000).

The sequestering function of Ubc12-C111S was tested in HEK293 cells by the overexpression of Ubc12-C111S together with HA-tagged Nedd8 (HA-Nedd8). The expression of HA-Nedd8 resulted in a smear of neddylated proteins when blotting protein lysates with α -HA antibodies (Fig. 4.2A, lanes 5 and 6). Importantly, the smear of neddylated proteins was strongly reduced when Ubc12-C111S was co-transfected (Fig. 4.2A, lanes 3 and 4). Instead of the protein smear, the heterodimeric complex of Ubc12-C111S and Nedd8 appeared in the protein lysates at 35 kDa (Fig. 4.2A, lanes 3 and 4). These results indicate that Ubc12-C111S sufficiently clusters Nedd8 and consequently prevents target protein neddylation.

Furthermore, it was tested whether proteasome inhibition may increase target protein neddylation. Indeed, application of the proteasome inhibitor MG132 resulted in an increased amount of neddylated proteins (Fig. 4.2A, lanes 5+6). This increase in neddylated proteins was sufficiently blocked by Ubc12-C111S co-expression (Fig. 4.2A, lane 4). In conclusion, MG132

treatment increases the amount of neddylated proteins and might thus increase the chances of identifying targets of the Nedd8 pathway.

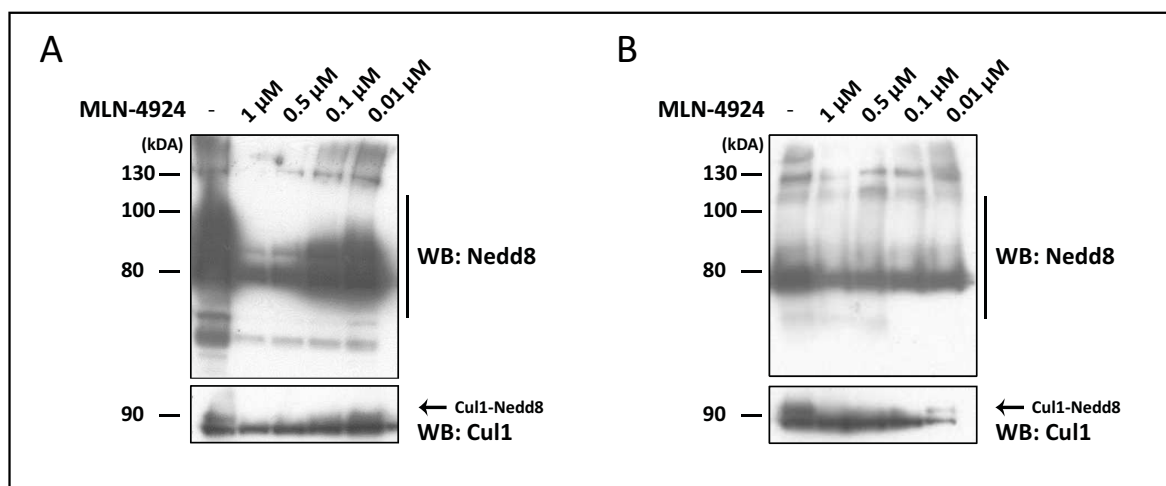


Figure 4.3: MLN-4924 blocks neddylation of target proteins and Cullin1 in HEK293 cells and primary neurons. **A)** Lysates of HEK293 cells treated with 0.01, 0.1, 0.5 and 1 μM MLN-4924 show a dose dependent inhibition of target-protein and Cullin1 (Cul1) neddylation. **B)** Primary neurons treated with MLN-4924, like indicated, display a dose dependent inhibition of protein neddylation and specifically Cullin1 neddylation.

HA-Nedd8 expression resulted in a ~100 kDa band in all transfection conditions which also remained after co-expression of Ubc12-C111S (Fig. 4.2A, lanes 3-6). This band might be a protein that is strongly neddylated or unspecific.

The next approach was to genetically knock down the Nedd8 pathway by the overexpression of short hairpin RNA (shRNA) constructs targeting mouse Ubc12 (shUbc12) or Nedd8 (shNedd8). Different shRNA constructs had been tested and the ones exerting the highest efficiency were selected for further experiments (Vogl, Brockmann et al.). Overexpression of shUbc12 or shNedd8 decreased the smear of neddylated proteins, independent of MG132 treatment (Fig. 4.2B). shUbc12 and shNedd8 sufficiently blocked target protein neddylation.

Recently, MLN-4924, a small molecular inhibitor that selectively inhibits Nedd8-activating enzyme (Nae) activity was described (Soucy et al., 2009). To test the efficiency of MLN-4924, HEK293 cells as well as primary neurons were treated with 0.01, 0.1, 0.5 and 1 μM of MLN-4924 for 24 h. In HEK293 cells and primary neurons, 1 μM MLN-4924 strongly decreased target protein neddylation, whereas 0.01 μM MLN-4924 was not sufficient to reduce the smear of

neddylated target proteins compared to the control (Fig. 4.3A, B). 1 μ M and 0.5 μ M MLN-4924 inhibited neddylation of Cullin1 (Cul1) (Fig. 4.3A, B). Lower concentrations of MLN-4924 did not completely block Cullin1 neddylation.

In conclusion, the genetic approaches, including the overexpression of Ubc12-C111S, shUbc12, and shNedd8, are sufficient to block neddylation. Furthermore, 1 μ M MLN-4924 inhibits target protein neddylation. The genetic and pharmacological approaches will be used in further experiments to prove the specificity of target protein neddylation.

4.3 PSD-95: The First Described Synaptic Target of Neddylation

Inhibiting the Nedd8 pathway results in strong defects on spine morphology during synaptic maturation (Vogl, Brockmann et al.). The morphological defects were described in a batch of experiments where Ubc12-C111S was overexpressed in primary hippocampal neurons. During the course of these experiments, the co-transfection of PSD-95 partially rescued the effects of Ubc12-C111S on spine maturation. The rescue on spine morphology was restricted to PSD-95 overexpression, as the co-transfection of GKAP and PSD-93 did not rescue the morphological spine-defects when neddylation was blocked. Since PSD-95 strongly impacts on spine development and spine maintenance (Schnell et al., 2002, Stein et al., 2003), it is particularly important for synaptic function. We have therefore decided to investigate whether PSD-95 is neddylated.

4.3.1 Neddylation of PSD-95

The neddylation of PSD-95 was tested by co-immunoprecipitation experiments with PSD-95 antibodies. HEK293 cells were transiently transfected with PSD-95 and a 3 x Flag-tagged construct of Nedd8 (3 x Flag-Nedd8). To prove that the transfections were correct, the lysates were analyzed *via* western blot. PSD-95 was expressed in both transfections, as can be seen when blotting the lysates with α -PSD-95 antibodies, whereas 3 x Flag-Nedd8 was just transfected in the second condition, visualized *via* α -Flag antibodies (Fig. 4.4A, Lysate).

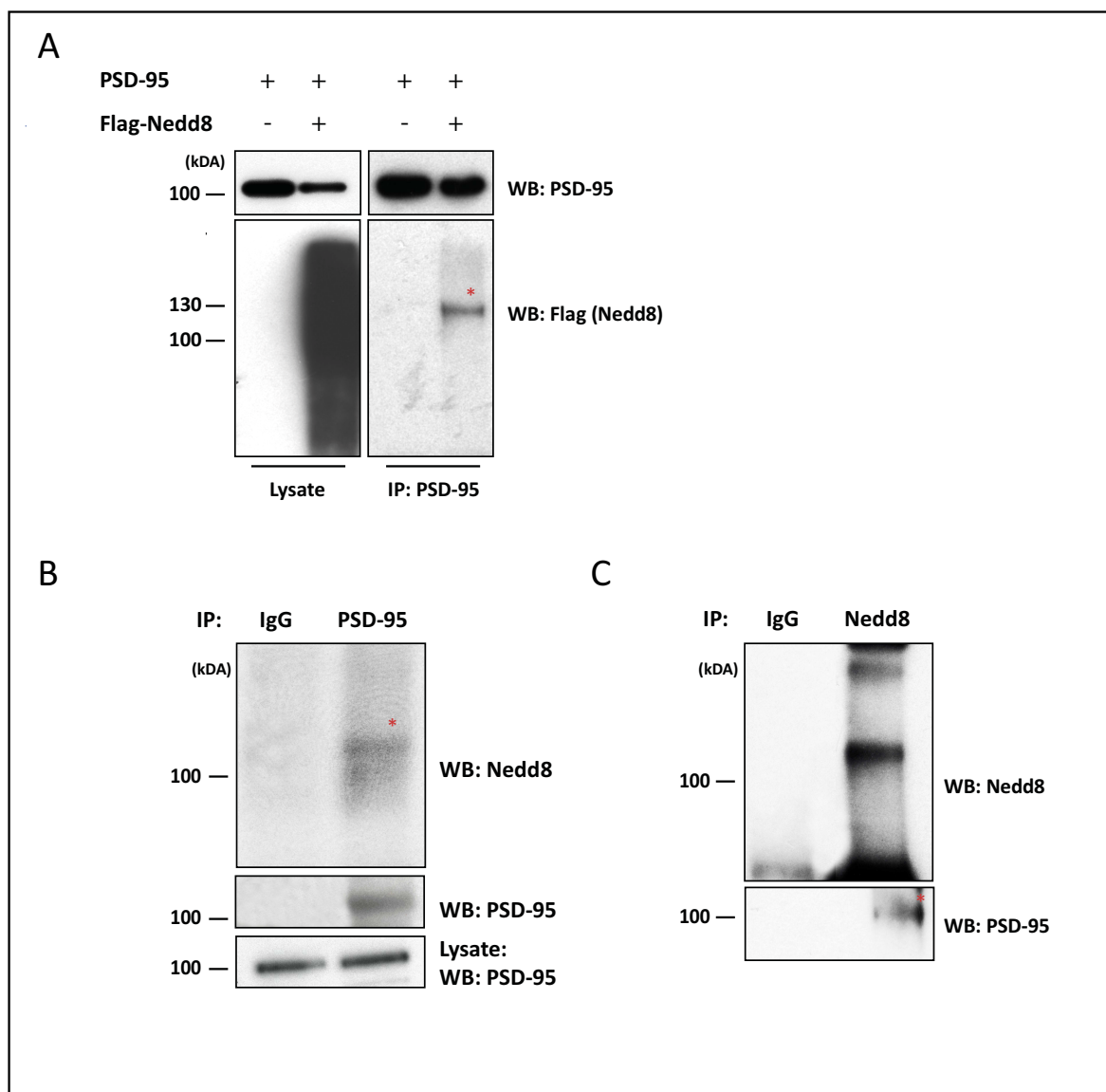


Figure 4.4: PSD-95 is neddylated. **A)** HEK293 cells were transiently transfected with PSD-95 and 3 x Flag-Nedd8 plasmids as indicated. Cell lysates were immunoprecipitated with α -PSD-95 antibodies. Lysates and immunoprecipitation samples were analyzed by immunoblotting and revealed PSD-95 neddylated. **B, C)** Immunoprecipitations from primary cortical neurons (DIV21) with IgG control antibodies and α -PSD-95 (**B**) or α -Nedd8 antibodies (**C**), were analyzed by western blot with α -Nedd8 and α -PSD-95 antibodies. PSD-95 is neddylated under endogenous conditions. Red asterisks represent neddylated PSD-95 bands.

The lysate blotted against α -Flag antibodies revealed a smear of neddylated proteins (Fig. 4.4A, Lysate). To clarify whether one of these neddylated proteins was PSD-95, co-immunoprecipitations were obtained from the lysates using α -PSD-95 antibodies. Blotting

the co-immunoprecipitation samples with α -Flag revealed a band at \sim 130 kDa. This band only appeared when PSD-95 was co-transfected with 3 x Flag-Nedd8 and therefore represented PSD-95-3 x Flag-Nedd8 conjugates (Fig. 4.4A, IP).

Furthermore, co-immunoprecipitations were performed from protein lysates of mature primary neurons DIV21. The detection of endogenously neddylated PSD-95 would prove that PSD-95 neddylation is not dependent on the overexpression of 3 x Flag-Nedd8. To ensure the specificity of the immunoprecipitations, control samples were processed using IgGs. In both co-immunoprecipitation experiments using α -PSD-95 or α -Nedd8 antibodies, no protein signal appeared in the control (IgGs) samples, whereas the samples from the immunoprecipitations with α -PSD-95 or α -Nedd8 showed specific bands (Fig. 4.4B, C, IPs). Immunoprecipitations using the antagonist antibodies (α -PSD-95 or α -Nedd8) revealed bands at \sim 100 kDa (Fig. 4.4B, C, IPs). Co-immunoprecipitations with α -PSD-95 and α -Nedd8 antibodies from primary neurons showed that PSD-95 is neddylated.

In summary, we showed that PSD-95 is neddylated under endogenous conditions in primary neurons as well as in HEK293 cells transiently transfected with PSD-95 and 3 x Flag-Nedd8.

4.3.2 Blocking PSD-95 Neddylation - Genetic Approaches

Section 4.3.1 shows the neddylation of PSD-95. If the neddylation of PSD-95 is specific, PSD-95 has to be neddylated by the enzymes of the Nedd8 pathway. Showing that the inhibition of the Nedd8 pathway prevents PSD-95 neddylation would prove the specificity of this modification.

In a first set of experiments, the Nedd8 pathway was blocked by the overexpression of Ubc12-C111S (Section 4.2). In the lysate of Figure 4.5A (central lane) a smear of neddylated proteins was observed when 3 x Flag-Nedd8 was expressed in HEK293 cells. The co-expression of Ubc12-C111S reduced the smear of neddylated proteins (Fig. 4.5A, Lysate, right lane). These results indicate that Ubc12-C111S blocks the neddylation of target proteins. Additionally, the concentration of PSD-95 was decreased in the lysate when Ubc12-C111S was co-transfected.

In the co-immunoprecipitations obtained with α -PSD-95 antibodies and blotted with α -Flag antibodies, PSD-95-3 x Flag-Nedd8 conjugates were detected when PSD-95 was co-expressed with 3 x Flag-Nedd8 (Fig. 4.5A, IP, red asterisk). When Ubc12-C111S was added to the transfection

conditions, no band was detected at ~130 kDA (Fig. 4.5, IP, right lane), indicating that PSD-95 neddylation was blocked by the overexpression of Ubc12-C111S.

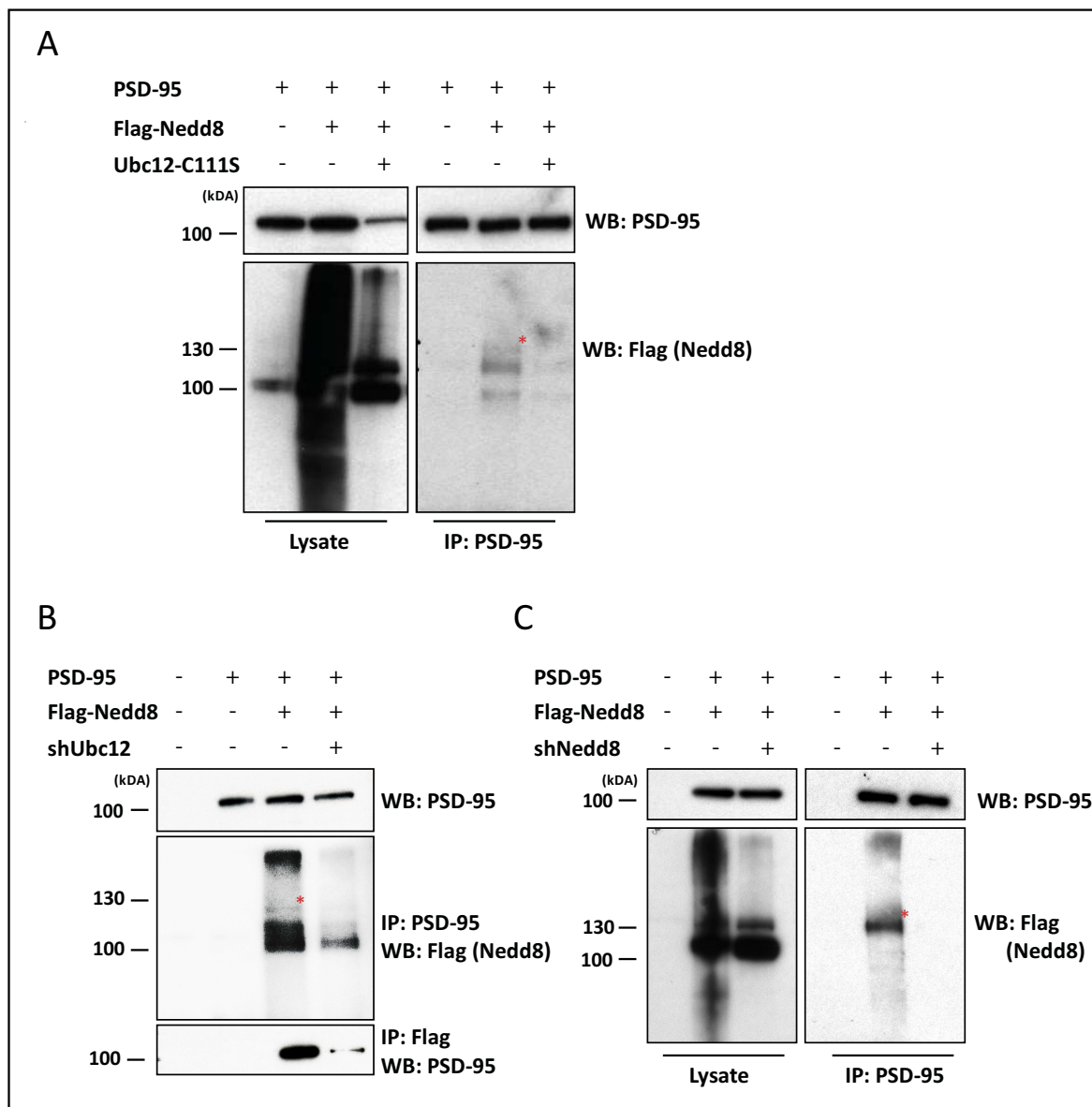


Figure 4.5: PSD-95 neddylation is reversed by genetically blocking the neddylation pathway. HEK293 cells were transiently transfected with PSD-95, Flag-Nedd8 and Ubc12-C111S, or shUbc12, or shNedd8 plasmids as indicated. Cell lysates were immunoprecipitated with α -PSD-95 and analyzed *via* western blot. **A)** Ubc12-C111S sufficiently blocks PSD-95 neddylation. **B, C)** PSD-95 neddylation is reversed by the co-expression of shRNAs against Ubc12 as well as Nedd8. Red asterisks represent neddylated PSD-95 bands.

The next approach aimed to genetically interfere with the Nedd8 pathway by overexpressing short hairpin RNA (shRNA) constructs targeting mouse Ubc12 and Nedd8. Again, the efficiency of the shNedd8 construct was confirmed by the reduced smear of neddylated proteins in the lysates (Fig. 4.5C, Lysate, right lane) as previously shown in section 4.2. To test whether shUbc12 and shNedd8 expression also prevents the neddylation of PSD-95, the same experimental design was chosen as for the Ubc12-C111S experiment.

As expected, the co-expression of PSD-95 and 3 x Flag-Nedd8 revealed PSD-95 neddylation (Fig. 4.5B+C, IP, red asterisks). The amount of neddylated PSD-95 was strongly reduced when shRNAs against Ubc12 or Nedd8 were co-transfected for 48 hours (Fig. 4.5B+C, IP, right lane). Taken together, overexpression of Ubc12-C111S, as well as shNedd8 and shUbc12, proved that PSD-95 neddylation is specific and that Ubc12 is the conjugating enzyme (E2) mediating PSD-95 neddylation.

4.3.3 Blocking PSD-95 Neddylation - Pharmacological Approach

To see whether PSD-95 neddylation is specific, genetic approaches from section 4.3.2 show that Ubc12 is needed for PSD-95 neddylation. In the next set of experiments, it was tested whether the activating enzyme Nae1 is necessary for PSD-95 neddylation. Nae1 can be pharmacological blocked by MLN-4924, as tested in section 4.2.

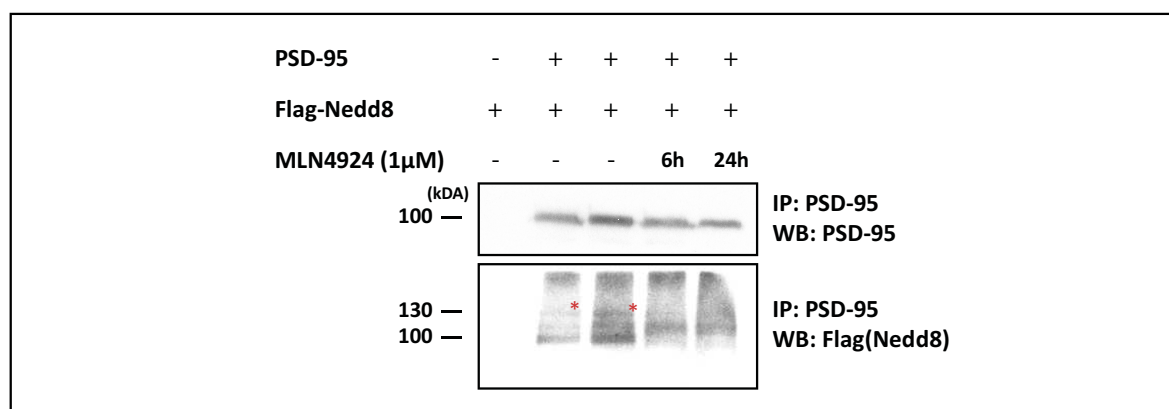


Figure 4.6: PSD-95 neddylation is blocked by the Nae1 inhibitor MLN-4924. Co-immunoprecipitations from HEK293 lysates transiently transfected with PSD-95 and 3 x Flag-Nedd8 show neddylation of PSD-95 that was blocked by MLN-4924 application for 6 h or 24 hours. Red asterisks represent neddylated PSD-95 bands for HEK293 cells treated with vehicle for 6 hours or 24 hours.

The blocking of PSD-95 neddylation by MLN-4924 was tested by co-immunoprecipitation experiments. HEK293 cells were transiently transfected with PSD-95 and 3 x Flag-Nedd8 and treated with vehicle or 1 μ M MLN-4924 for 6 hours or 24 hours. Afterwards, the vehicle and MLN-4924 treated cells were lysed, immunoprecipitated with α -PSD-95, and analyzed by western blotting.

As expected, co-immunoprecipitations revealed PSD-95 neddylation in vehicle-treated cells (Fig. 4.6, IP, red asterisks). Co-immunoprecipitations samples from cells treated for 6 hours with MLN-4924 showed a diminished intensity of the neddylated PSD-95 band. Furthermore, the decrease in PSD-95 neddylation was even more pronounced when MLN-4924 treatment was extended to 24 hours (Fig. 4.6, IP).

In conclusion, MLN-4924 prevents PSD-95 neddylation by inhibiting the E1 enzyme of the Nedd8 pathway.

4.3.4 PSD-95 Neddylation is Mediated via the E3 Ligase Mdm2

Many E3 ligases have already been described for the Ubiquitin pathway. In contrast, for the Nedd8 pathway only a few E3 ligases have been identified. Interestingly, some E3 ligases have been described to mediate ubiquitylation as well as neddylation of the same target proteins (Haupt et al., 1997, Oved et al., 2006).

Previously, Colledge et al. showed that PSD-95 is ubiquitylated by the E3 ligase Mdm2 upon NMDA stimulation (Colledge et al., 2003). Additionally, Mdm2 has been shown to mediate ubiquitylation and neddylation of p53 (Xirodimas et al., 2004). These findings raised the question of whether Mdm2 might also mediate the neddylation of PSD-95.

A RING-finger domain mutant of Mdm2 that contains an alanine at position 464 instead of a cysteine (Mdm2-C464A) lacks the ligase activity of Mdm2 (Boyd et al., 2000). Mdm2-C464A was chosen to test whether neddylation of PSD-95 is blocked when the E3 ligase Mdm2 is not functional.

As in the previous experiments, co-immunoprecipitations of HEK293 lysates co-transfected with PSD-95 and 3 x Flag-Nedd8 revealed PSD-95 neddylation (Fig. 4.7, IP, red asterisk). When Mdm2-C464A was added to the transfection, no specific band was detected at \sim 130 kDA,

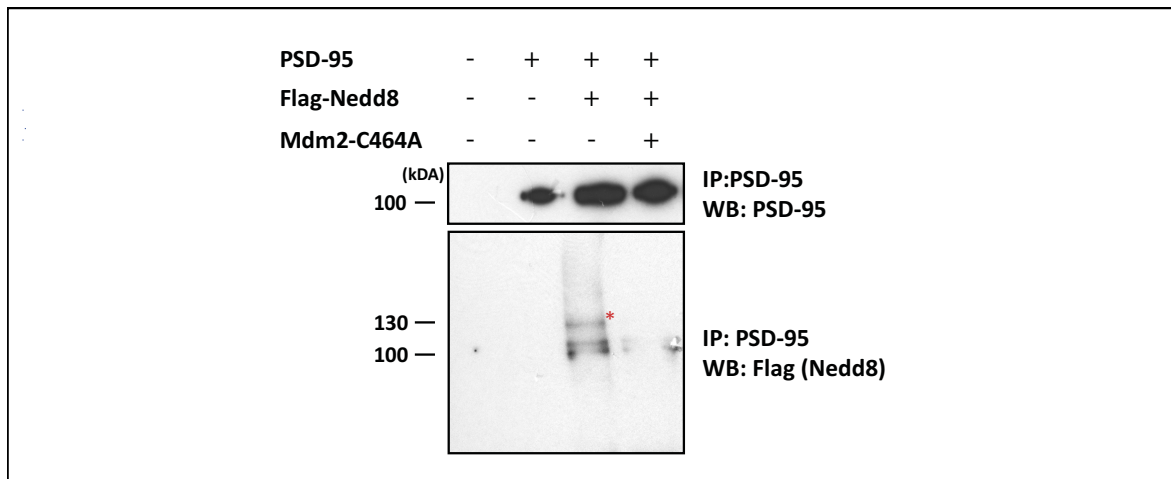


Figure 4.7: PSD-95 is neddylated by the E3 Ligase Mdm2. Overexpression of the RING-finger mutant of Mdm2 (Mdm2-C464A) in HEK293 cells sufficiently blocked PSD-95 neddylation. Red asterisk represents neddylated PSD-95 band.

the size that would correspond to neddylated PSD-95 (Fig. 4.7, IP, right lane), meaning that Mdm2-C464A lacks the ability to conjugate Nedd8 to PSD-95.

In summary, section 4.3 shows that the Nedd8 pathway is active in synaptic compartments and proteins from the pre- and the post-synapse are neddylated. Additionally, the results describe the first synapse-specific target of the Nedd8 pathway: PSD-95.

Moreover, the exact pathway that is responsible for the neddylation of PSD-95 was identified, including Nae1 as the activating enzyme E1, Ubc12 as the conjugating enzyme E2, and Mdm2 as the E3 ligase.

4.4 GKAP is not Neddylated

As previously shown in section 4.3, PSD-95 is targeted by the Nedd8 pathway. To understand the importance of PSD-95 neddylation, the question arose as to whether neddylation is a general synaptic protein modification or whether neddylation is specific to some proteins including PSD-95.

To test whether neddylation is restricted to some synaptic proteins, it was validated whether GKAP is neddylated too. Like PSD-95, GKAP is a well-described scaffold protein of the PSD

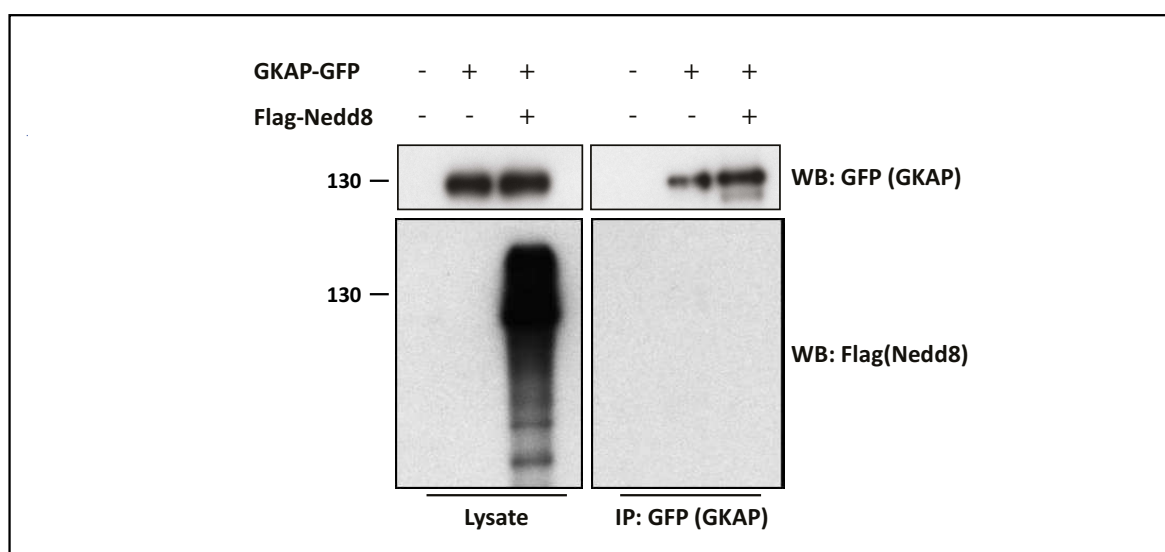


Figure 4.8: GKAP is not neddylated. Co-immunoprecipitations of lysates from HEK293 cells, transiently transfected with GKAP-GFP and 3 x Flag-Nedd8 plasmids, revealed that GKAP is not neddylated.

and has been described as being ubiquitylated (Kim et al., 1997).

GKAP-GFP was transiently transfected with 3 x Flag-Nedd8 in HEK293 cells and cells lysed after 48 h. α -GFP antibodies were used to co-immunoprecipitate GKAP-GFP. Western blot analysis of the immunoprecipitates using α -GFP proved the purification of GFP-tagged GKAP (Fig. 4.8, IP). No signal was obtained after immunoblotting the immunoprecipitated samples with α -Flag antibodies (Fig. 4.8, IP). These findings imply that no GKAP-GFP-3 x Flag-Nedd8 conjugates had been formed.

GKAP is not a target of the Nedd8 pathway, given that no GKAP-GFP-3 x Flag-Nedd8 conjugates were detected.

In conclusion, the Nedd8 pathway does not target every scaffolding protein of the post-synaptic density rather neddylated is restricted to specific proteins.

4.5 Structural Characteristics of PSD-95 Promote its Neddylation

PSD-95 is ubiquitylated upon NMDA receptor activation and thus removed from synaptic sites by degradation (Colledge et al., 2003). The ubiquitylation of PSD-95 is dependent on its PEST domain, which is located at the N-terminus of PSD-95 (amino acid 14-23).

In order to check whether the PEST domain of PSD-95 is also involved in its neddylation, two different constructs were used that both lack a functional PEST domain. In the first construct (PSD-95 deltaPEST) amino acids 10-25 and consequently the complete PEST-domain was cut out from the PSD-95 protein sequence (Colledge et al., 2003), whereas in the second construct (PSD-95 mutPEST) the original PEST motif (RYQDEDTPPLEH) was mutated by site-directed mutagenesis (RRAEQKLISEEDLGRA). The freeware epestfind (<http://emboss.bioinformatics.nl/cgi-bin/emboss/epestfind>; 2013) enables the prediction of PEST motifs and confirmed the successful elimination of the PEST domain from both constructs (Fig. 4.9A).

Transfected with the indicated plasmids, HEK293 cells were lysed, co-immunoprecipitated with α -PSD-95 antibodies, and analyzed *via* western blot (Fig. 4.9B+C). The immunoblotting with α -PSD-95 antibodies showed the correct expression of PSD-95 deltaPEST and PSD-95 mutPEST (Fig. 4.9C, Lysate). The elimination of the PEST domain in PSD-95 deltaPEST resulted in a decreased mass compared to PSD-95. In contrast to the control immunoprecipitations where PSD-95 was again shown to be neddylated (Fig. 4.9B+C, IP, red asterisks), no bands were detected for both mutants of PSD-95 (Fig. 4.9B+C, IP, right lanes). Both PSD-95 mutants demonstrate that the loss of the PEST domain prevented the formation of PSD-95-3 x Flag-Nedd8 conjugates. These results indicate that the PEST domain of PSD-95 is mandatory for PSD-95 neddylation.

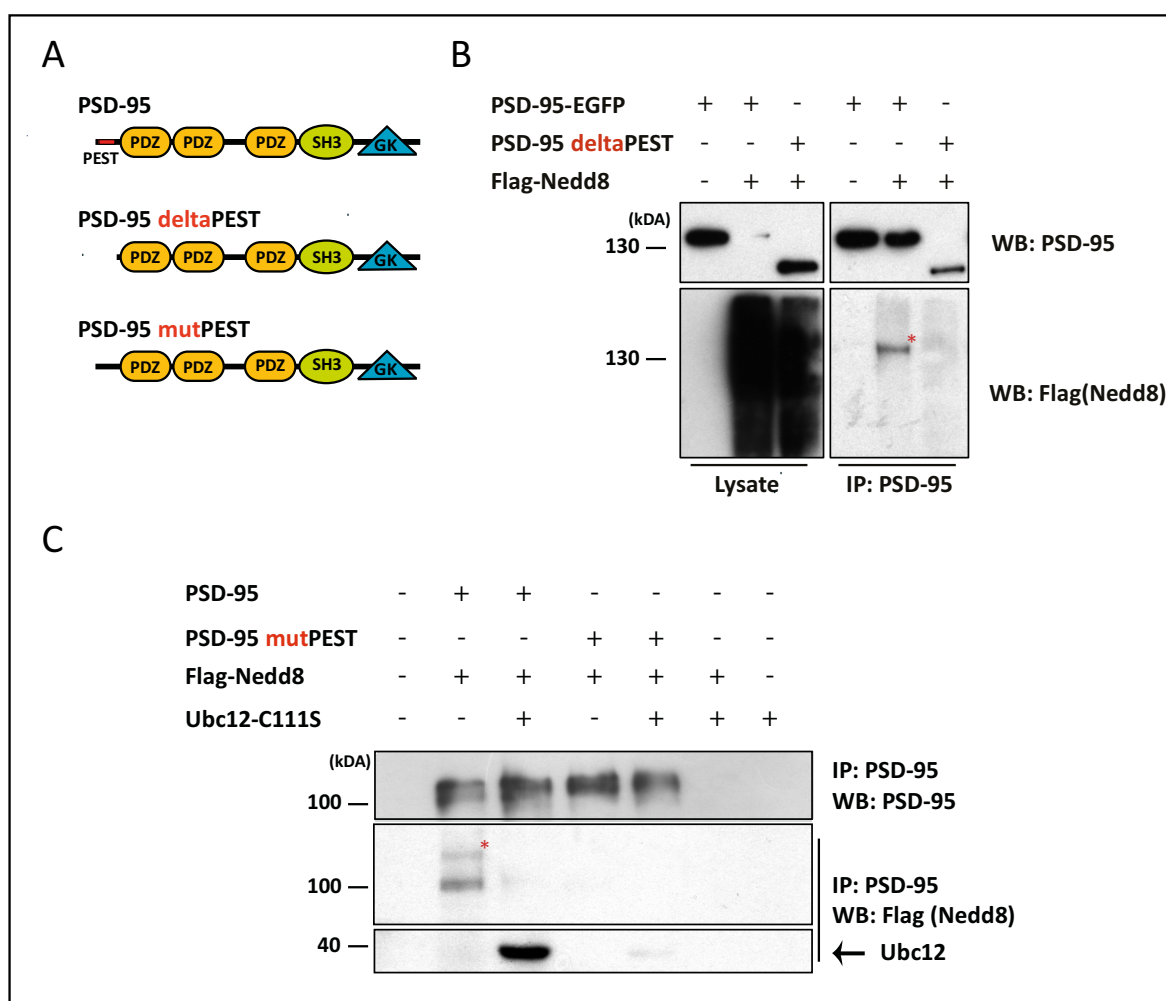


Figure 4.9: PSD-95 is neddylated *via* its PEST domain by interacting with Ubc12. **A)** Schematic illustration of PSD-95 PEST mutants. **B)** HEK293 cells were transiently transfected with either PSD-95-EGFP or PSD-95deltaPEST and 3 x Flag-Nedd8 plasmids. Co-immunoprecipitations were obtained using α -PSD-95 antibodies. The immunoprecipitates and lysates were analyzed and showed that PSD-95deltaPEST is not neddylated. **C)** HEK293 cells were transiently transfected with either PSD-95 or PSD-95mutPEST, 3 x Flag-Nedd8 and Ubc12-C111S plasmids as indicated. Cell lysates were immunoprecipitated with α -PSD-95 antibodies and analyzed by immunoblotting using α -PSD-95 and α -Flag (Nedd8) antibodies. PSD-95mut PEST is not neddylated and does not co-immunoprecipitate Ubc12-C111S. Red asterisks represent neddylated PSD-95 bands.

Moreover, figure 4.9C again shows that co-expressing Ubc12-C111S with PSD-95 and 3 x Flag-Nedd8 prevents PSD-95 neddylated, as previously demonstrated in section 4.3.2. Interestingly, western blots from co-immunoprecipitation samples expressing PSD-95 and Ubc12-C111S revealed a second band at 40 kDa. This second band represents Ubc12-C111S-Nedd8 conjugates which were co-immunoprecipitated with PSD-95 (Fig. 4.9C, lower panel), indicating

that PSD-95 directly interacts with Ubc12-C111S. When PSD-95 mutPEST is transfected instead of PSD-95, co-immunoprecipitated Ubc12-C111S-Nedd8 conjugates were not detected (Fig. 4.9C, lower panel). In conclusion, the interaction of Ubc12-C111S and PSD-95 is mediated *via* the PEST domain.

Taken together, these results demonstrate that the PEST domain of PSD-95 interacts with Ubc12 and thus promotes PSD-95 neddylation.

4.6 PSD-95 is Ubiquitylated

Originally, PSD-95 ubiquitylation was only detected after NMDA receptor activation but not under basal conditions (Colledge et al., 2003). To see whether PSD-95 is ubiquitylated under transfected conditions in HEK293 cells, PSD-95 and HA-Ubiquitin were co-expressed in HEK293 cells.

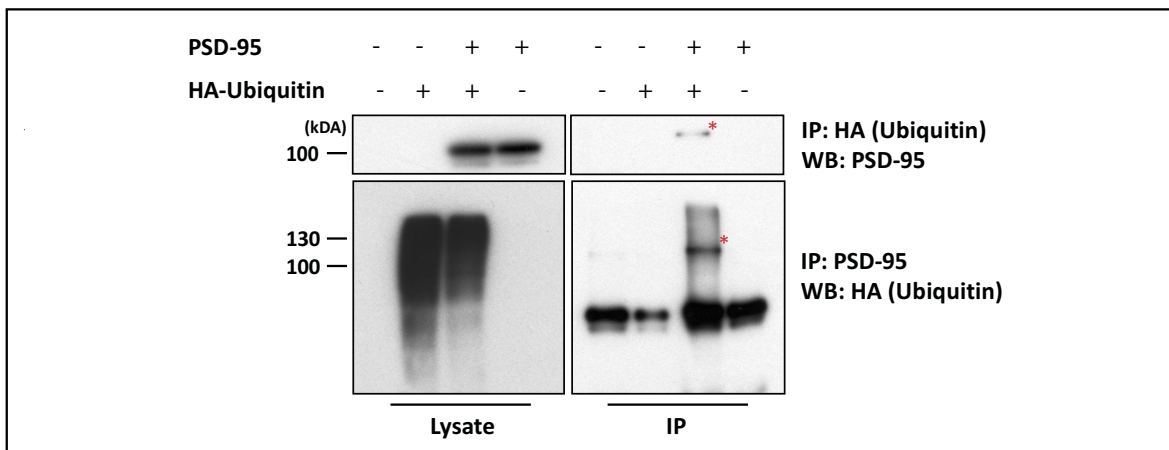


Figure 4.10: PSD-95 is ubiquitylated. PSD-95 and HA-Ubiquitin plasmids were transiently transfected in HEK293 cells. Cell lysates were co-immunoprecipitated with α -HA (Ubiquitin) or α -PSD-95 antibodies and analyzed by immunoblotting. Both experimental conditions revealed PSD-95 ubiquitylation. Red asterisks represent ubiquitylated PSD-95 bands.

To confirm the transfection efficiencies, the lysates were immunoblotted with α -HA and α -PSD-95 antibodies. The lysates revealed a smear of ubiquitylated proteins when blotted against α -HA (Fig. 4.10, Lysate), and thus demonstrated that the HA-Ubiquitin construct was sufficiently bound to target proteins. Co-immunoprecipitations using α -HA and α -PSD-95 antibodies and

immunoblotted vice versa revealed a band at ~130 kDa (Fig. 4.10, IP, red asterisks), representing PSD-95-HA-Ubiquitin conjugates.

In conclusion, PSD-95 ubiquitylation is detectable under basal conditions when overexpressed in HEK293 cells.

4.7 Functional Impact of PSD-95 Neddylolation

For the Nedd8 pathway, neither the neuronal targets nor the function this post-translational modification exerts in the brain are described in the literature. PSD-95 is the first neuronal target that has been described to be neddylated (Section 4.3). To better understand the impact of target protein neddylation, it is essential to understand the impact neddylation has on single proteins. Thus, the question of whether neddylation alters PSD-95 protein function was posed.

4.7.1 PSD-95 Ubiquitylation vs. Neddylation

Given that PSD-95 is neddylated and ubiquitylated and that the E3 ligase Mdm2 is involved in both post-translational modifications, it was of great interest whether Nedd8 and ubiquitin act synergistically or oppositionally on PSD-95. Therefore, it was of great interest whether Nedd8 and ubiquitin can both bind to PSD-95 at the same time, or whether Nedd8 and ubiquitin compete for lysine residues and thus exclusively modify PSD-95.

To receive a first insight of Nedd8 and ubiquitin modification on PSD-95, HEK293 cells were transiently transfected with PSD-95 and 3 x Flag-Nedd8. HA-Ubiquitin was added to the transfections in a 1:1, 1:3, and 1:6 ratio to 3 x Flag-Nedd8. Afterwards, cells were lysed, immunoprecipitated with α -PSD-95 or α -Flag antibodies and analyzed *via* western blot using α -Flag or α -PSD-95 antibodies.

If Nedd8 and ubiquitin compete for PSD-95 modification, the amount of neddylated PSD-95 should decrease with increasing concentrations of HA-Ubiquitin. Whereas, when Nedd8 and ubiquitin work congruously, the amount of neddylated PSD-95 should stay the same with increasing concentrations of HA-Ubiquitin.

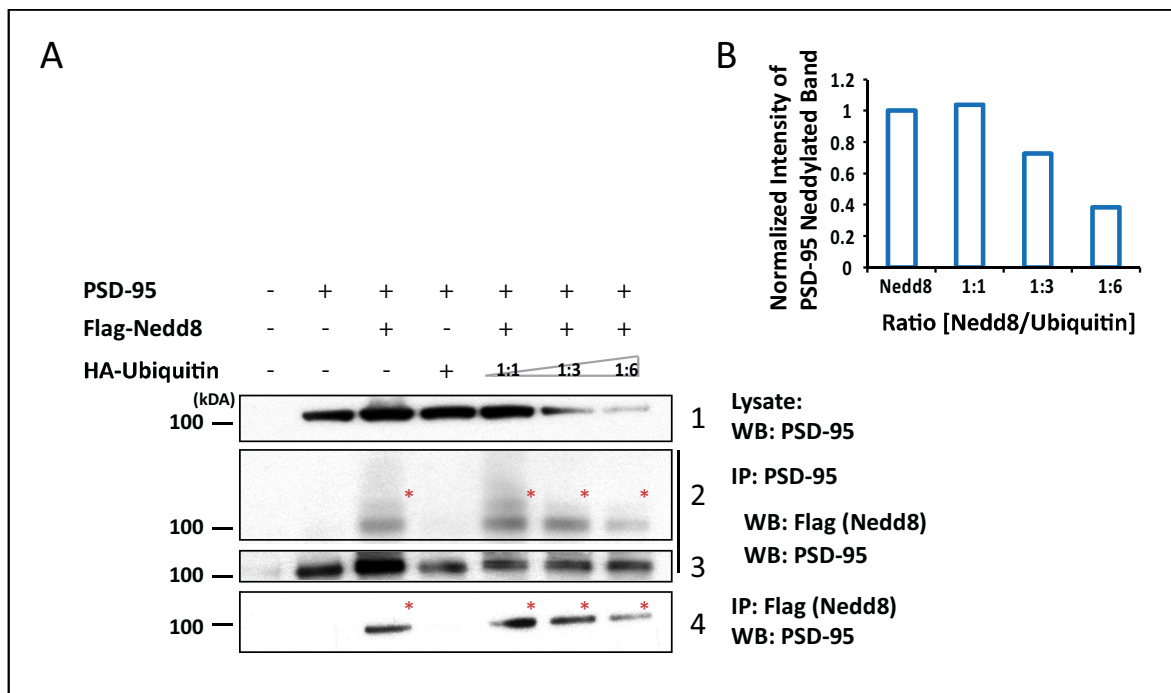


Figure 4.11: Nedd8 and ubiquitin compete for PSD-95 modification. **A)** PSD-95, 3 x Flag-Nedd8 and HA-Ubiquitin plasmids were transiently transfected in HEK293 cells. From the lysates, immunoprecipitations were obtained using α -PSD-95 or α -Flag antibodies. PSD-95 neddylation is decreased when the expression of HA-Ubiquitin is increased. **B)** Quantification of the intensity of neddylation of PSD-95 compared to control (without HA-Ubiquitin transfection). When ubiquitin concentration is increased 6 fold to Nedd8, PSD-95 neddylation is decreased by ~60 %. Red asterisks present neddylation bands.

The lysates in figure 4.11A lane 1, immunoblotted with α -PSD-95 antibodies, show a decrease in PSD-95 concentration with increasing expression of HA-Ubiquitin. This decrease in PSD-95 concentration is induced by increased ubiquitylation and subsequent degradation of PSD-95 (4.11A, Lysate, lane 1). To make sure that the changes in PSD-95 concentration do not influence the results on PSD-95 neddylation, the immunoprecipitation samples were analyzed by western blot using α -PSD-95 antibodies. These results confirmed that in each immunoprecipitation the same amount of PSD-95 was analyzed and thus the differences in PSD-95 protein concentration found in the lysate did not influence the results on PSD-95 neddylation (Fig. 4.11A, IP, lane 3). Immunoblotting from co-immunoprecipitations revealed that PSD-95 neddylation diminished with increasing concentrations of HA-Ubiquitin (Fig. 4.11, IP, lane 2). The same results were obtained by immunoprecipitations of Flag-Nedd8 and immunoblotting with α -PSD-95 antibodies

(Fig. 4.11, IP, lane 4). In both experiments, the concentration of PSD-95-Nedd8 conjugates is reduced when HA-Ubiquitin is co-transfected.

Quantifications showed that when 3 x Flag-Nedd8 and HA-Ubiquitin were transfected in a 1:1 ratio, the amount of neddylated PSD-95 was unaltered compared to control conditions where 3 x Flag-Nedd8 was single transfected (Fig. 4-11B). Transfection of Nedd8 to ubiquitin in a 1:3 ratio decreased PSD-95 neddylation ~30 % and ~60 % when the amount of ubiquitin was increased 6 fold to Nedd8.

These results indicate that Nedd8 and ubiquitin compete for PSD-95 modification. When the amount of ubiquitin is increased, the concentration of neddylated PSD-95 is decreased in a dose-dependent manner.

4.7.2 PSD-95 Multimerization is Diminished after MLN-4924 Treatment

PSD-95 dimerization was shown to stabilize receptors in the synapse e.g. AMPA receptors, and Kv1.4 channels, and to control the assembly of synaptic proteins in a network (Hsueh and Sheng, 1999, Christopherson et al., 2003, Xu et al., 2008). Furthermore, it was shown that PSD-95 ubiquitylation leads to AMPA receptors endocytosis (Colledge et al., 2003). Therefore, PSD-95 ubiquitylation might be an initial step to induce synaptic destabilization.

Since Nedd8 and ubiquitin compete for PSD-95 modification, one hypothesis was that neddylation exerts the opposite effect on PSD-95 function that ubiquitylation does. Hence, PSD-95 neddylation would favor PSD-95 dimerization and would consequently stabilize synapses, whereas PSD-95 ubiquitylation prevents PSD-95 dimerization and destabilizes spines .

To test this hypothesis, the dimerization of PSD-95 was investigated with and without MLN-4924 treatment. PSD-95 was transiently co-transfected with PSD-95-EGFP in HEK293 cells and treated with 1 μ M MLN-4924 as indicated (Fig. 4.12A, Lysate). Cells were lysed, immunoprecipitated with α -GFP antibodies and immunoblotted with α -PSD-95 antibodies. Consequently, PSD-95 was immunoprecipitated when dimerized with PSD-95-EGFP. Figure 4.12A shows that MLN-4924 treatment reduced the pull-down of PSD-95 (Fig. 4.12A, lower panel). The co-immunoprecipitated PSD-95 amount was normalized to the immunoprecipitated PSD-95-EGFP and blotted in a graph bar (Fig. 4.12B) that revealed a decrease of PSD-95-PSD-95-EGFP

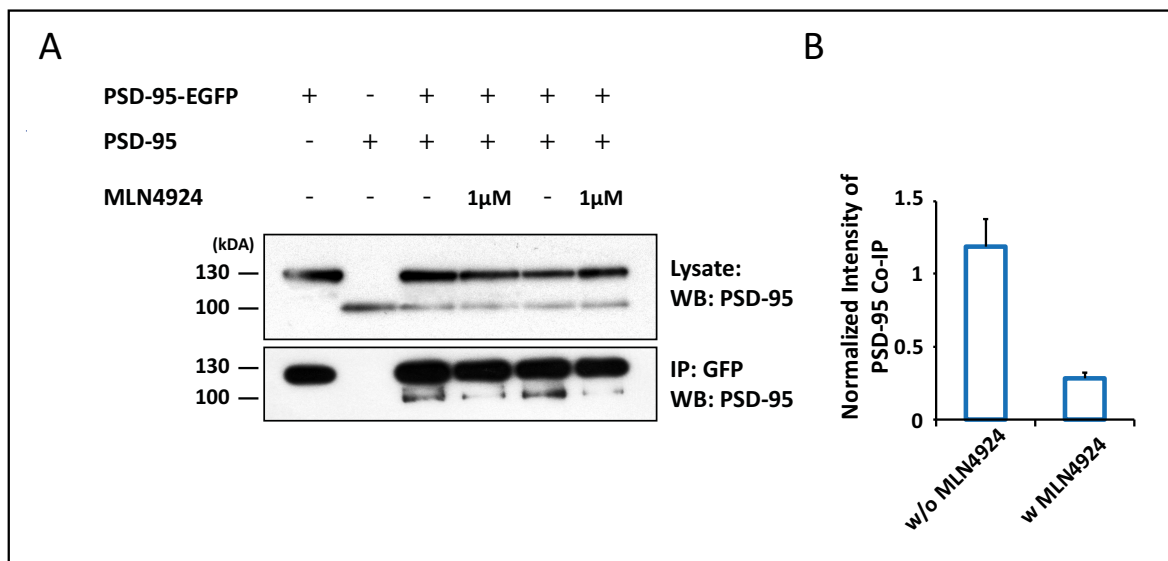


Figure 4.12: PSD-95 - PSD-95 interaction is diminished when blocking the Nedd8 pathway. **A)** HEK293 cells were transiently transfected with PSD-95-EGFP and PSD-95 plasmids. Dimerization of PSD-95 is diminished when cells were treated for 24 hours with 1 μ M MLN-4924, indicated by the reduced co-immunoprecipitation of PSD-95. **B)** Graph bars show the normalized intensity of immunoprecipitated PSD-95 bands with or without MLN-4924 treatment. Upon MLN-4924 treatment, dimerization of PSD-95 is reduced by \sim 60 %.

interaction of \sim 60 % when neddylation was blocked.

The dimerization of PSD-95 is strongly decreased when neddylation is blocked and thus indicating that neddylation is important for PSD-95-PSD-95 interaction.

In summary, section 4.7 showed that Nedd8 and ubiquitin compete for PSD-95 binding and that the inhibition of PSD-95 neddylation prevents its dimerization. This loss of function is one mechanistic insight into the role of PSD-95 neddylation.

4.8 Neddylated Lysine Residues of PSD-95

So far it has been shown that PSD-95 is a specific target of the Nedd8 pathway (Section 4.3). Furthermore, it is known that PSD-95 is ubiquitylated (Colledge et al., 2003) and that ubiquitin and Nedd8 counteract on PSD-95 modification (Section 4.7.1). Additionally, it has been shown that the dimerization of PSD-95 is decreased when the Nedd8 pathway is blocked by MLN-4924 (Section 4.7.2). Nevertheless, the exact lysines of PSD-95 which are neddylated are still unknown.

The identification of the specific lysine residues of PSD-95 is fundamental in order to understand the impact and functional consequences of PSD-95 neddylation. The next step was aimed at the identification of lysine residues of PSD-95 that covalently bind Nedd8 or ubiquitin and the validation whether the same or different Lysine residues are modified by each pathway.

Up to now, studies have used two different approaches to identify ubiquitylated or neddylated lysine residues. On the one hand, lysine residues are mutated to arginines and consequently cannot be modified anymore. The absence of protein modification can be identified by western blot experiments. On the other hand, mass spectrometry can identify modified peptides based on a mass shift due to conjugated Nedd8 or ubiquitin. Given that the protein sequence of PSD-95 comprises 38 lysine residues excludes the feasibility of identifying neddylated proteins by mutation studies. Accordingly, mass spectrometry was chosen to classify neddylated lysine residues in PSD-95.

4.8.1 A new Mass-Spectrometry Method for the Unambiguous Identification of Neddylated Lysine Residues

Routinely, probes for mass spectrometry analysis are trypsin digested to cleave proteins into smaller peptides. Nedd8 is covalently bound to its target proteins and thus PSD-95 remains neddylated during mass spectrometry. Since conjugated Nedd8 to PSD-95 is also cleaved by trypsin, a –GG remnant is left on modified lysines. To identify neddylated lysine residues of PSD-95, all peptides resulting from the trypsin digestion of PSD-95 had to be scanned for –GG remnants. Unfortunately, Nedd8- and ubiquitin-modified peptides cannot be distinguished *via* mass spectrometry, since the identical C-terminal sequence of Nedd8 and ubiquitin (RGG) results in equal –GG remnants after trypsin digestion (Kirkpatrick et al., 2005, Jeram et al., 2010) (illustrated in Fig. 4.13).

To overcome this limitation, C-terminal Nedd8 mutants were generated that result in a change in the trypsin recognition side and consequently allow for the differentiation to ubiquitylated lysine residues. For the first Nedd8 mutant (3 x Flag-Nedd8-L), arginine and leucine at the C-terminus of 3 x Flag-Nedd8 were exchanged to elongate the trypsin digestion side. This mutation increases the remnant size from –GG to –LGG. Elongating the remnant for one amino acid is sufficient

to guarantee the differentiation between -GG and -LGG using mass spectrometry. The second strategy prescribed the insertion of another amino acid, such as alanine (3 x Flag-Nedd8-A) or valine (3 x Flag-Nedd8-V). Both amino acid insertions also increased the size of the remnant after trypsination to -AGG and -VGG (Fig. 4.13).

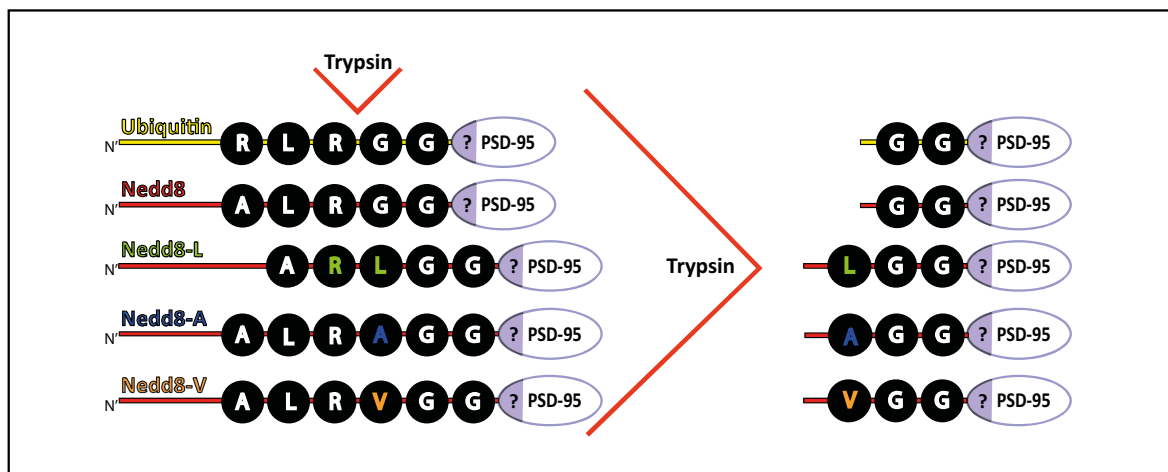


Figure 4.13: Generated Nedd8 mutants for mass spectrometry. Schematic illustration of the C-terminals of ubiquitin, Nedd8, and Nedd8 mutants (3 x Flag-Nedd8-L; 3 x Flag-Nedd8-A, and 3 x Flag-Nedd8-V), and their remnants after trypsin digestion.

To ensure the efficiency of the Nedd8 mutants, 3 x Flag-Nedd8-A, 3 x Flag-Nedd8-L, and 3 x Flag-Nedd8-V were transiently transfected in HEK293 cells together with PSD-95. The lysates, analyzed by immunoblotting using α -Flag antibodies, revealed a smear of neddylated proteins for 3 x Flag-Nedd8-A and 3 x Flag-Nedd8-L (Fig. 4.14B, Lysate). These results confirmed that 3 x Flag-Nedd8-A and 3 x Flag-Nedd8-L can be bound to target proteins like Flag-Nedd8. Only Nedd8-V could not target any protein, indicated by the missing smear in the lysate (Fig. 4.14, Lysate, middle lane). To check whether the 3 x Flag-Nedd8-A and 3 x Flag-Nedd8-L also neddylate PSD-95, co-Immunoprecipitation studies using α -PSD-95 antibodies were obtained and confirmed that 3 x Flag-Nedd8-A and 3 x Flag-Nedd8-L targeted PSD-95 (Fig. 4.14B, IP, red asterisks). In contrast, no band at \sim 130 kDA was detected for 3 x Flag-Nedd8-V (Fig. 4.14, IP, middle lane). Consistently, 3 x Flag-Nedd8-V is not functional since it could not be bound to target proteins including PSD-95.

In summary, analysis of the Nedd8 mutants showed that 3 x Flag-Nedd8-A and

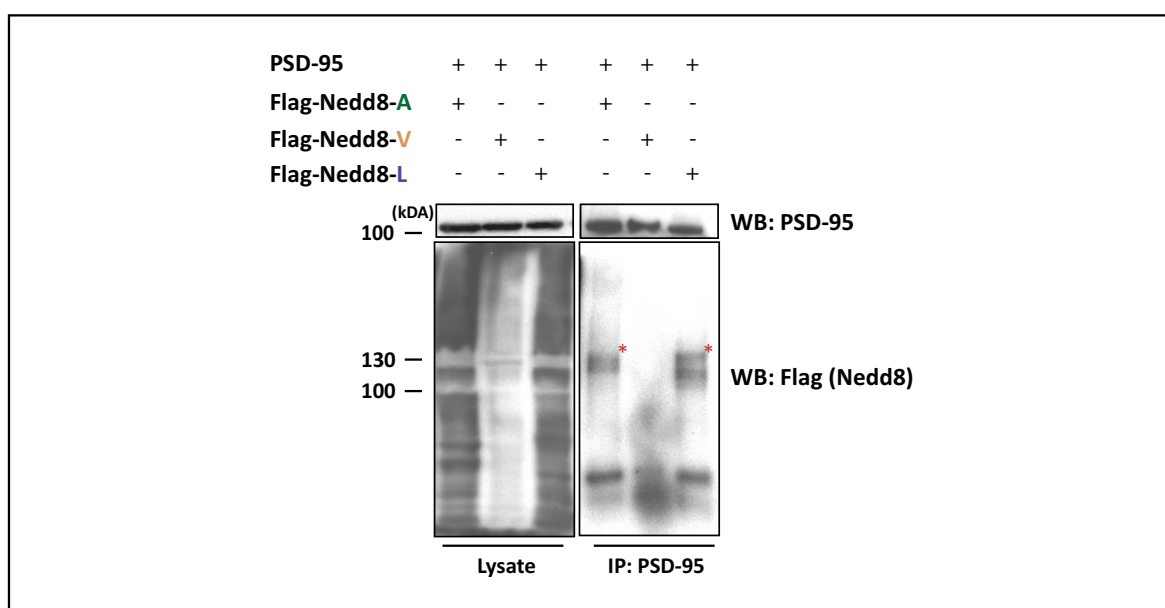


Figure 4.14: Generated Nedd8 mutants are functional and able to neddylate PSD-95. Efficiency of the Nedd8 mutants was tested by Western Blot analysis. HEK293 cells were transiently transfected with PSD-95 and one single Nedd8 mutant, either 3 x Flag-Nedd8-L, 3 x Flag-Nedd8-A or 3 x Flag-Nedd8-V. Western blot analysis show that NEDD8-A as well as Nedd8-L, are bound to target proteins including PSD-95. Red asterisks represent neddylated PSD-95 bands.

3 x Flag-Nedd8-L are bound to target proteins and PSD-95 similar to Flag-Nedd8. This implies that 3 x Flag-Nedd8-A and 3 x Flag-Nedd8-L are candidates for the identification of neddylated lysine residues in PSD-95 using mass spectrometry.

4.8.2 Mass Spectrometry Analysis Revealed Neddylated and Ubiquitylated Lysine Residues of PSD-95

Two experimental setups were chosen that provide cell lysates for mass spectrometry which allow for the identification of neddylated lysines of PSD-95.

In the first set of experiments, PSD-95 as well as 3 x Flag-Nedd8-A or 3xFlag-Nedd8-L were overexpressed in HEK293. Co-Immunoprecipitations with α -PSD-95 antibodies were obtained that allow the identification of specifically neddylated lysines of PSD-95. MLN-4924 and MG132 were partially added to transfected HEK293 cells to challenge the system. For example, MG132 should increase the number of neddylated lysine residues, whereas after MLN-4924 treatment no neddylated lysines should be detected. The challenge of PSD-95 modification allows for

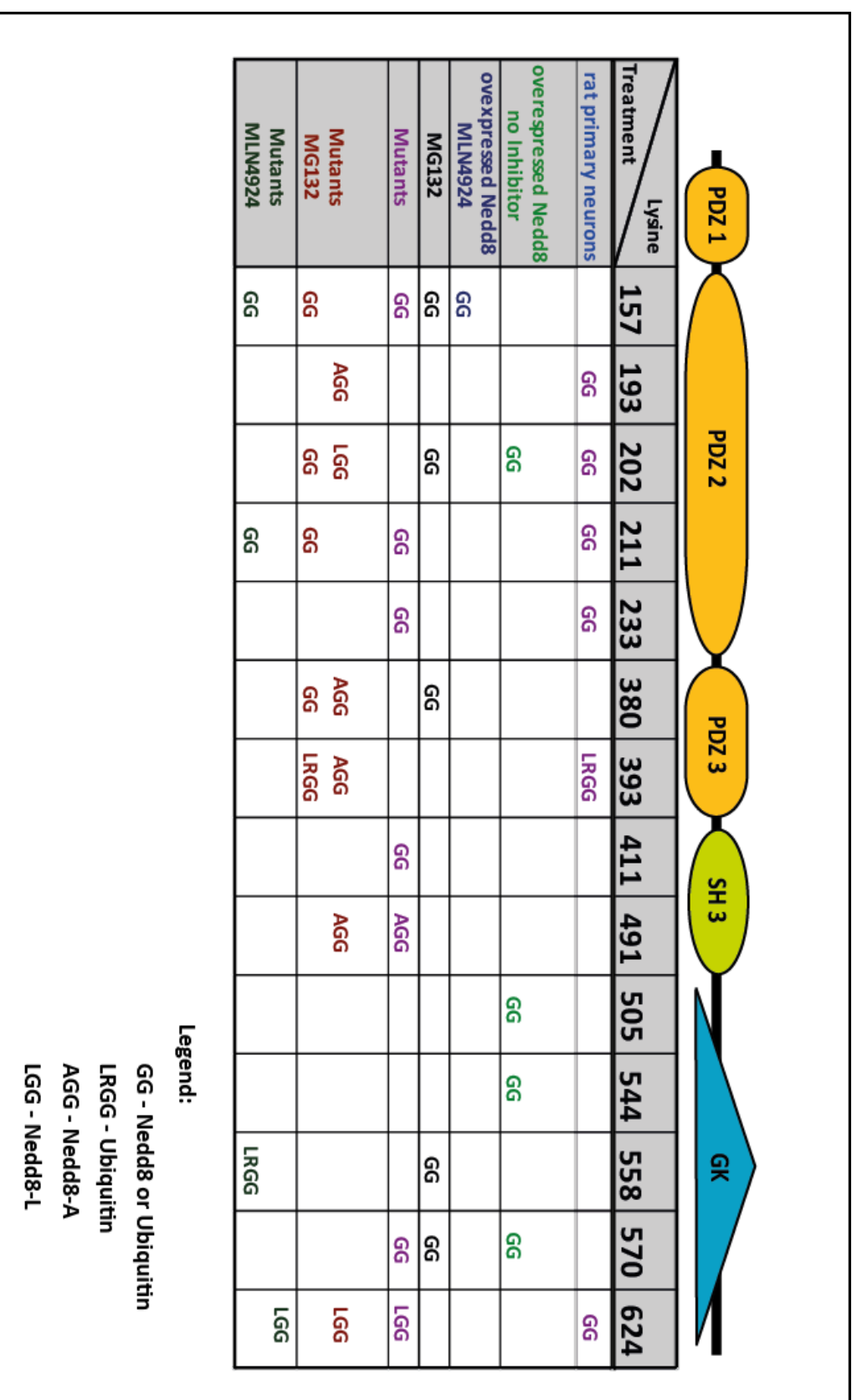


Figure 4.15: Mass spectrometry revealed a number of neddylated and ubiquitylated lysines in PSD-95. To identify modified lysines of PSD-95, mass spectrometry was conducted from primary cell cultures and from overexpression studies in HEK293 cells. The table illustrates lysines of PSD-95 (from left to right) that are found to be neddylated or ubiquitylated throughout different experimental conditions (top down). Above the result table, a schematic illustration of PSD-95 displays the location of modified lysine residues in subunits of PSD-95. Mass spectrometry was obtained by Giuseppe Maccarrone.

the critical evaluation of the identified modifications. In the second set of experiments, cell lysates were obtained from primary cortical neurons. The co-immunoprecipitation samples of endogenously expressed PSD-95 were additionally examined for PSD-95 modifications. Since in primary cortical neurons PSD-95 is modified under endogenous conditions, these results could strengthen the previous findings obtained from the overexpression studies in HEK293 cells.

For all experimental conditions, phosphorylation sites of PSD-95 were detected at Ser-295 and Ser-415. These phosphorylation sites of PSD-95 are well described in the literature and thus proved the detection sensitivity throughout all experiments (Kim et al., 2007, Zhang et al., 2011). When 3 x Flag-Nedd8 was overexpressed in untreated HEK293 cells, K202, K505, K544, and K570 were –GG modified and thus either neddylated or ubiquitylated (Fig. 4.15, lane 2). As soon as the cells were treated with MLN-4924, all lysines that were detected before except K157 did not show up again in the analysis, indicating that these residues of PSD-95 are neddylated. However, K157 modification (–GG) was still detected after MLN-4924 treatment (Fig. 4.15, lane 3), suggesting K157 as a strong candidate for PSD-95 ubiquitylation. To increase the chance of identifying modified lysine residues of PSD-95, MG132 was added to several experiments to block the proteasome and thus prevent protein degradation. MG132 treatment increased the number of –GG modified, lysine residues of PSD-95, including K157, K202, K211, K380, K558, and K570 (Fig. 4.15, lane 4).

So far, all experiments have not allowed for the differentiation between Nedd8 and ubiquitin. Next, the Nedd8 mutants (3 x Flag-Nedd8-A and 3 x Flag-Nedd8-L) were co-expressed to specifically identify neddylated residues of PSD-95. Lysine K193, K380, K393, and K491 were neddylated by Nedd8-A and Lysine K202, and K624 by Nedd8-L (Fig. 4.15, lane 5+6). To prove that the modifications *via* 3 x Flag-Nedd8-A and 3 x Flag-Nedd8-L are functional, neddylation was blocked by MLN-4924. As expected, most –AGG or –LGG modifications were absent after blocking the Nedd8 pathway (K193, K202, K380, K393, and K491) (Fig. 4.15, lane 7). Only lysine K624 was still neddylated after MLN-4924 application and was therefore excluded as a false positive.

In summary, mass spectrometry analyses were obtained from primary neurons examining endogenously modified lysine residues of PSD-95. In these experiments –GG remnants were

detected at K193, K202, K211, K233, and K624 (Fig. 4.15, lane 1). Importantly, all of these lysine residues had already been found in the overexpression studies in HEK293 cells.

In some experiments, miscleavages of trypsin on ubiquitin modifications generated longer remnants -LRGG. These remnants appeared through so-called semi-trypsination and are specific for ubiquitin. LRGG- remnants have been detected at K393 and K558 and thus identified these lysine residues certainly ubiquitylated.

4.8.3 Location of Neddylated and Ubiquitylated Lysine Residues in PSD-95

PSD-95 mutation studies had shown that each subunit of PSD-95 controls specific protein functions, for example protein interactions (Craven et al., 1999, Xu et al., 2008, Shipman et al., 2011). Given that neddylated and ubiquitylated lysine residues have been detected in different subunits of PSD-95 (Section 4.8.2), it is important to determine their exact subunit location to better understand the possible impact each lysine modification might exert. Additionally, it is important to describe the location of modified lysines in the three dimensional protein structure of PSD-95. A surface location of lysine residues is mandatory to enable their modification by enzymes such as Ubc12.

Crystal structures of PSD-95 were analyzed for surface location of modified lysine residues. Unfortunately, the protein size of PSD-95 is too big to accomplish a total crystal structure. Nevertheless, crystal subdomain structures of PSD-95 have been published that allow the exact localization of lysine residues in PSD-95 (McGee et al., 2001, Tavares et al., 2001, Long et al., 2003).

In the PDZ 1 domain of PSD-95 no modified lysine residues were detected *via* mass spectrometry analysis (Fig. 4.15). PDZ domain 2 comprises K157, K193, K202, K211, and K233 (Fig. 4.15). Structural analysis of PDZ 1+2 revealed that K157, K202, and K193 were located at the surface of the protein structure of PSD-95 (Fig. 4.16A+B, green residues). For PDZ 3, the surface location of K380 was depicted in figure 4.16B (green residue) and additionally K393 was found to be neddylated and ubiquitylated in mass spectrometry analysis in PDZ 3 of PSD-95 (Fig. 4.16C). A number of lysine residues were neddylated in the Sh3 and GK domain of PSD-95 (K411, K491, K505, K544, K558, K570, and K624) (Fig. 4.15). Just the position of K544 was visualized at the

protein surface of PSD-95 in figure 4.16D (green residue).

Crystal structure analysis of PSD-95 revealed a number of neddylated and ubiquitylated lysine residues at the protein surface of PSD-95. Lysine residues like K157, K202, K193, K380, and K544 are possible targets for E2 and E3 enzymes of the Nedd8 and ubiquitin pathway.

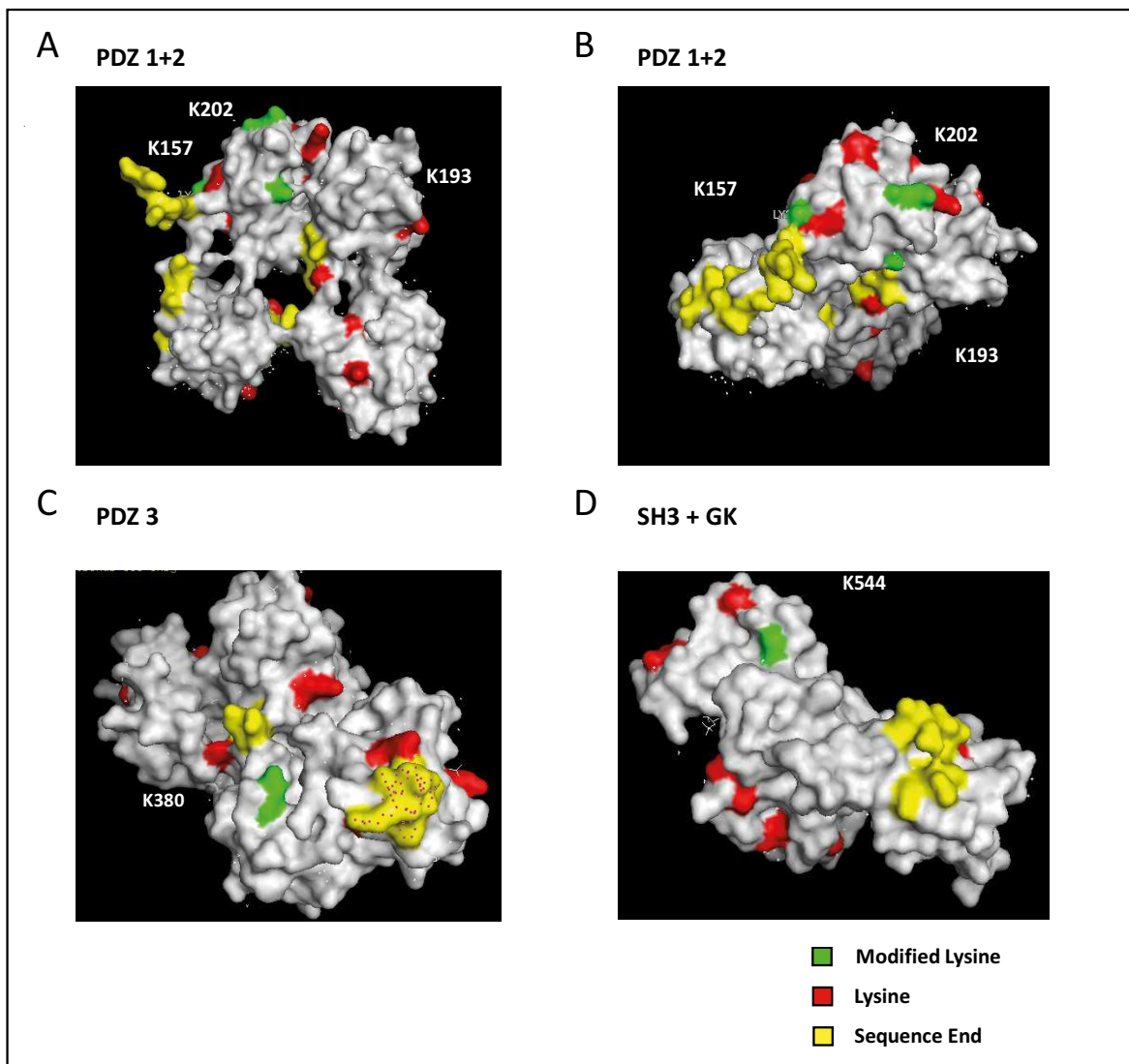


Figure 4.16: Graphic illustration of neddylated and/or ubiquitylated lysine residues in the protein structure of PSD-95. A, B) Graphic illustration of the protein structure of PDZ 1+2 from PSD-95. Highlighted in green are lysine residues K157 ubiquitylated, and K193 and K202 both neddylated. **C)** K380 is neddylated and located in the PDZ 3 of PSD-95. **D)** Protein sequence of Sh3 and GK contains neddylated K544.

4.8.4 Nedd8 and ubiquitin Compete for K393 Modification

Western blot experiments in section 4.7.1 indicate that ubiquitin and Nedd8 compete for PSD-95 neddylation. It was shown that with an increasing amount of ubiquitin, the neddylation of PSD-95 decreases. Mass spectrometry analysis allows for the investigation of whether Nedd8 and ubiquitin compete for the same lysines in PSD-95.

To test whether Nedd8 and ubiquitin bind to the same or different lysine residues, Nedd8 mutants were transfected in different concentrations. Thus, if Nedd8 and ubiquitin compete for lysine modification, increasing amounts of Nedd8 should decrease ubiquitylation of the same lysine residue.

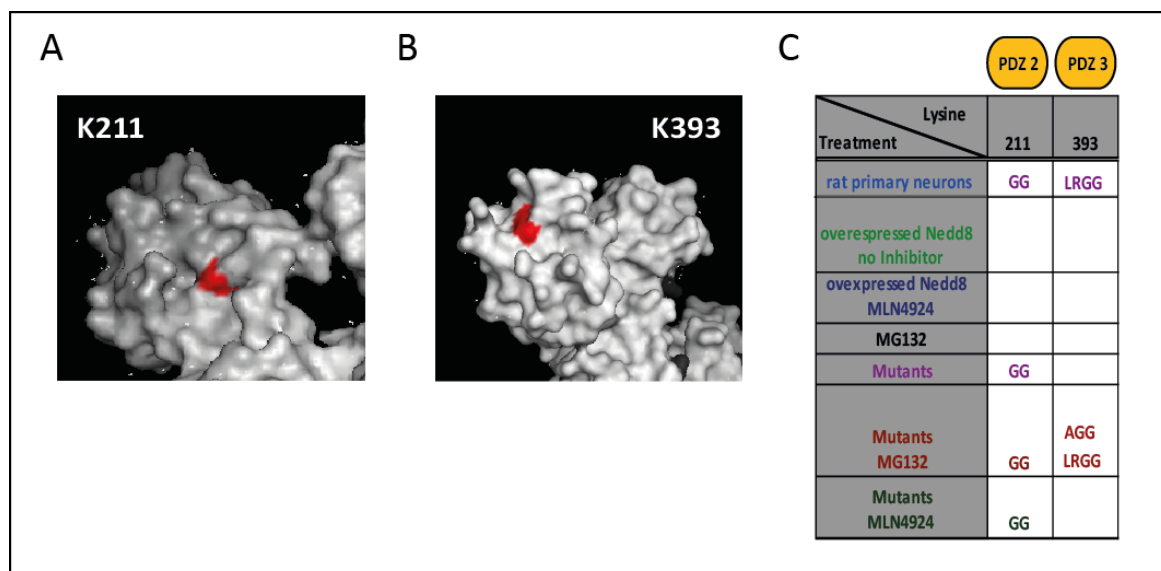


Figure 4.17: K211 and K393 of PSD-95 are modified by Nedd8 and ubiquitin. **A)** Protein structure of the PDZ 2 of PSD-95. The location of K211 is marked in red. **B)** Image of lysine 393 (shown in red), placed in PDZ 3 of PSD-95. **C)** Table shows the specific results of K211 and K393 modification obtained by mass spectrometry.

In primary neurons the –LRGG remnant was detected for K393 (Fig. 4.15C), demonstrating that K393 was ubiquitylated under endogenous conditions. In addition, overexpressing studies of 3 x Flag-Nedd8-A in HEK293 cells also detected -LRGG at K393, confirming the results from primary cell cultures. When Nedd8 mutants were co-transfected in HEK293 cells, besides –LRGG, –AGG remnants were also identified at K393, indicating that despite its ubiquitylation, K393 was also neddylated. This result demonstrated that neddylation and ubiquitylation are not

restricted to different lysine residues, but can be found at same lysines. To check whether there is competition between Nedd8 and ubiquitin for lysine residues modification, mass spectrometry analyses were performed from HEK293 cells transiently transfected with increasing amounts of 3 x Flag-Nedd8-A. If Nedd8 competes with ubiquitin, increasing amounts of Nedd8 should suppress lysine ubiquitylation. Indeed, mass spectrometry analyses of HEK293 cells expressing increased amounts of 3 x Flag-Nedd8 only revealed neddylation of K393. No ubiquitylated K393 was found when the concentration of Nedd8 was increased.

As with the western blot results from section 4.7.1, mass spectrometry analyses using different amounts of 3 x Flag-Nedd8 indicate that Nedd8 and ubiquitin compete for lysine residue modification in PSD-95.

4.8.5 Generation of PSD-95 Neddylation Mutants

The identification of neddylated lysine residues of PSD-95 (Section 4.8.2), raised the question whether the modification of these specific lysines has an impact on PSD-95 function. To answer this question, PSD-95 mutants were generated, that lack the neddylation on specific lysine residues. To prevent lysine residue modification, lysines were exchanged by arginines that cannot be targeted by the Nedd8 pathway. PSD-95 mutants were generated by site-directed mutagenesis.

Before the PSD-95 mutants were used for functional experiments, it was investigated whether single lysine mutations influence the amount of detectable PSD-95 neddylation in western blot experiments.

To test the amount of neddylation in PSD-95 mutants, they were transiently transfected in HEK293 cells. Cells were lysed and immunoprecipitated with α -PSD-95 antibodies and checked for neddylation with western blot analysis using α -Flag antibodies. As expected, PSD-95-WT was neddylated (Fig. 4.18, red asterisk). Also, PSD-95-K157R was still found to be neddylated. PSD-95-K157R neddylation was expected, since K157 was found to be ubiquitylated in mass spectrometry analysis (Fig. 4.18, red asterisk). For PSD-95-K202R and the double mutant PSD-95-K193/393R, the neddylated band of PSD-95 was strongly reduced compared to PSD-95-WT (Fig. 4.18, yellow asterisks). In conclusion, the neddylation of PSD-95 was

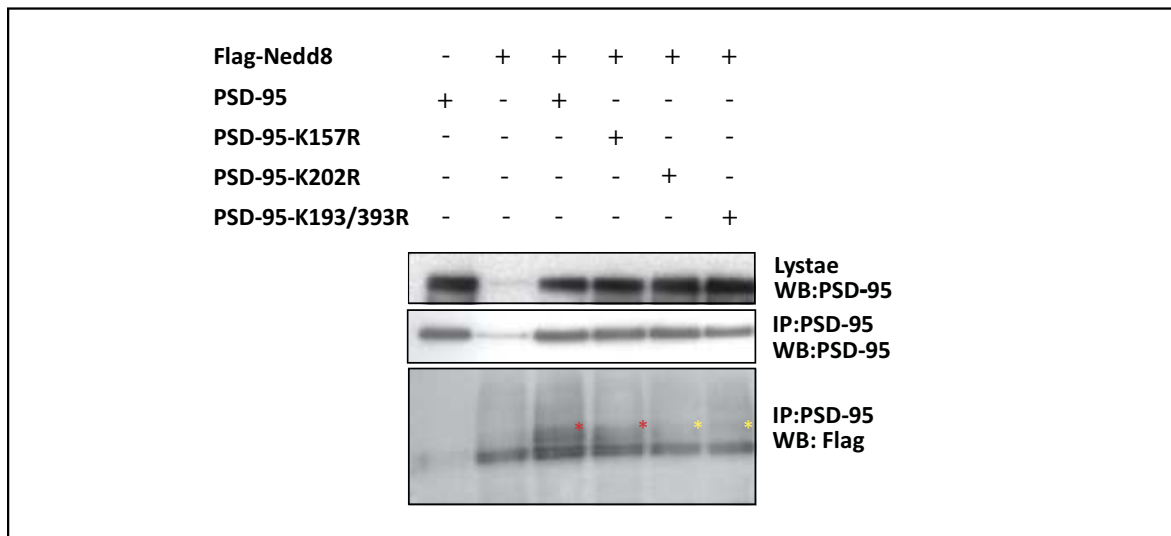


Figure 4.18: PSD-95 mutants are less neddylated compared to PSD-95-WT. PSD-95 and its mutants PSD-95-K157R, PSD-95-K202R, and PSD-95-K193/393R are transiently transfected in HEK293 cells together with the 3 x Flag-Nedd8 construct. Cells were lysed, immunoprecipitated with α -PSD-95 antibodies and analyzed *via* immunoblotting using α -Flag and α -PSD-95 antibodies. Red asterisks present neddylated PSD-95 bands for PSD-95-WT and PSD-95-K157R, yellow asterisks the decreased neddylation of PSD-95-K202R and PSD-95-K193/393R.

diminished when single lysine residues (K202, or K193/393) were mutated to arginines (K202R, K193/393R).

Section 4.8 described the identification of neddylated and ubiquitylated lysine residues of PSD-95. The specificity of these findings was guaranteed by Nedd8 mutants that allow for the differentiation between neddylated and ubiquitylated lysine residues of PSD-95. First analyses described the localization of the modified lysine residues in crystal structures of PSD-95, which will give further hints about their functional impact. Additionally, the decrease in PSD-95 neddylation upon single lysine mutations indicates the importance of the mutated lysine residues.

4.9 Morphological and Functional Analysis of PSD-95 Neddylation Mutants

In Section 4.8 the identification of neddylated and ubiquitylated lysine residues of PSD-95 was described. Within the next set of experiments, the morphology as well as the function of synapses

from neurons overexpressing the mutants of PSD-95 were investigated. These morphological and functional analyses are mandatory in order to clarify the relevance of PSD-95 neddylation.

4.9.1 Morphological Analysis of PSD-95 Mutants in Primary Neurons

One of the best described effects of PSD-95 is its impact on spine size. The overexpression of PSD-95 in primary hippocampal neurons increases spine size and spine number (El-Husseini et al., 2000), whereas the acute knockdown of PSD-95 *via* shRNAs decreases spine size (Ehrlich et al., 2007).

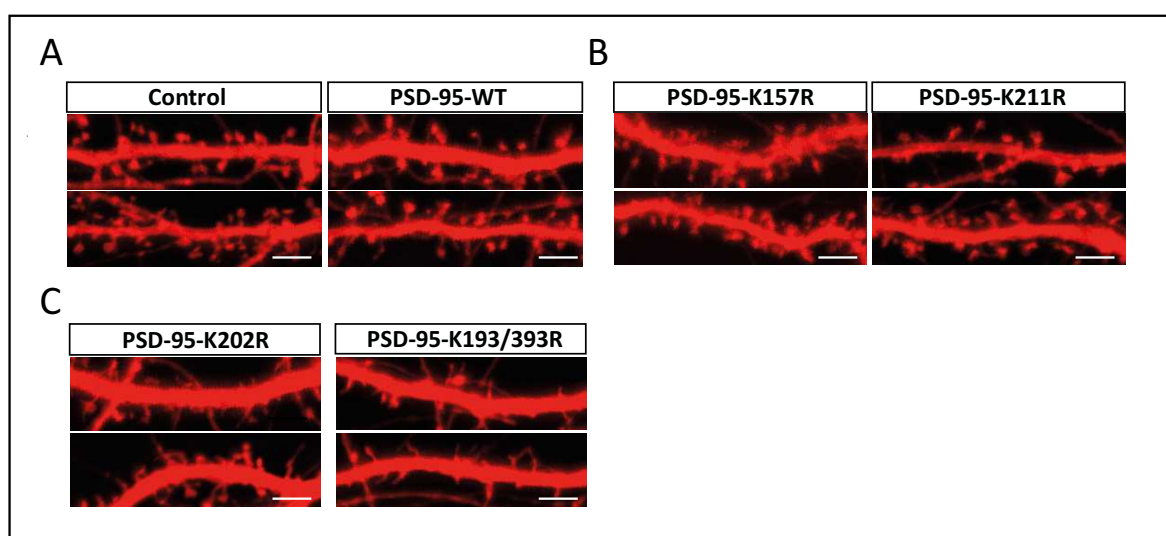


Figure 4.19: PSD-95 mutants exert strong effects on spine morphology in developing primary hippocampal neurons. **A)** Confocal images of primary hippocampal neurons that were transiently transfected with RFP and PSD-95-WT at DIV13. At DIV18 primary neurons were fixed and display mature mushroom shaped spines. **B)** Dendrites of primary neurons expressing PSD-95-K157R or PSD-95-K211R, both mutants that prevent ubiquitylation of PSD-95, are also decorated with mature mushroom shaped spines. **C)** Overexpression of PSD-95-K202R or PSD-95-K193/393R results in dendrites covered with filopodia instead of mature spines. Scale bar, 1 μ m. Data obtained by Annette Vogl.

To analyze the morphological effects of PSD-95 neddylation, primary hippocampal neurons were transiently transfected with PSD-95 mutants to check whether single mutations in PSD-95 are sufficient to alter spine morphology. Primary hippocampal neurons were transiently transfected with PSD-95, or neddylation mutants of PSD-95 (PSD-95-K157R, K202R, K211R, and K193/393R) and RFP at DIV13. Transfected primary neurons were fixed at DIV18 and

prepared for analysis.

As expected, control and PSD-95-WT-expressing neurons were decorated with mature mushroom-shaped spines (Fig. 4.19A). Mushroom-shaped spines were also found in primary hippocampal neurons overexpressing PSD-95-K157R or PSD-95-K211R (Fig. 4.19B). Since PSD-95-K157R and PSD-95-K211R prevent ubiquitylation of PSD-95, these results indicate that PSD-95 ubiquitylation does not impact on spine morphology. In contrast, PSD-95-K202R and PSD-95-K193/393R, the neddylation mutants of PSD-95, showed strong morphological differences compared to control or PSD-95-WT-expressing neurons. Instead of exhibiting mature mushroom-shaped spines, dendrites of PSD-95-K202R and PSD-95-K193/393R-expressing neurons were decorated with filopodia-like structures (Fig. 4.19C).

All experiments analyzing PSD-95 neddylation mutants prove that PSD-95-K202R exerted the strongest phenotype: Lysine 202 had been found to be exclusively neddylated in primary neurons as well as in HEK293 cells. Furthermore, PSD-95-K202 neddylation was detected *via* Nedd8 mutants and PSD-95-K202 neddylation was blocked by MLN-4924 application. In western blot experiments it was shown that the neddylation of PSD-95-K202R is strongly reduced compared to neddylation of PSD-95-WT. Additionally, PSD-95-K202R expression in primary hippocampal neurons particularly effects spine maturation.

Taken together, PSD-95-K202R represents the best candidate to study the functional consequences of PSD-95 neddylation.

4.9.2 Morphological Analysis of PSD-95-K202R during Spine Development in Hippocampal Slices

To analyze the impacts of PSD-95-K202R on spine function, organotypic slice cultures were chosen as a system, since neurons are still embedded in their physiological environment as opposed to primary neuronal cell cultures.

First, the morphological analyses of PSD-95 mutants from section 4.9.2 were repeated in organotypic slice cultures to make sure that PSD-95-K202R also alters spine morphology in a more physiological system. Organotypic slice cultures were infected with Semliki Forest Virus expressing either EGFP, PSD-95-WT-EGFP or PSD-95-K202R-EGFP at DIV2, and

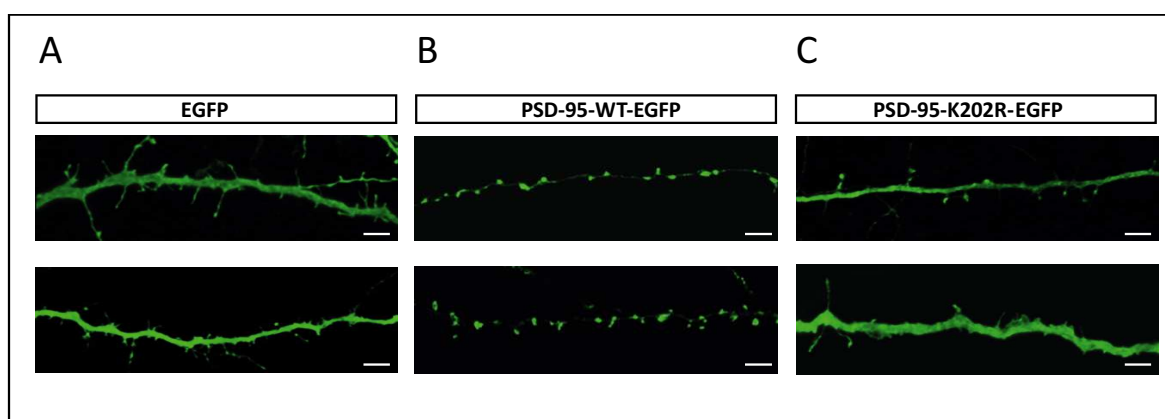


Figure 4.20: PSD-95-K202R strongly affects spine morphology during spine development in young organotypic slice cultures. **A, B, C)** Confocal images were obtained from basal dendrites of CA1 neurons in organotypic slice cultures. Slices were infected at DIV2 with Semliki Forest Virus containing EGFP, Scale bar, 5 μm (**A**), PSD-95-WT-GFP (**B**) or PSD-95-K202R-GFP (**C**) and fixed at DIV3 or DIV4. Whereby the overexpression of PSD-95-WT-EGFP produces mushroom shaped spines compared to EGFP expressing neurons that are decorated with filopodia. Neurons overexpressing PSD-95-K202R-EGFP lack the ability to induce mushroom like spines like PSD-95-WT-EGFP and reduced the spine number compared to EGFP infected neurons.

the spines were analyzed two days later. At the early time of infection, dendrites of young CA1 neurons in organotypic slices cultures are still decorated with filopodia, as can be seen in EGFP-infected cells (Fig. 4.20A). Dendrites from CA1 neurons that overexpressed PSD-95-WT-EGFP exhibited mushroom-shaped spines, a more mature form of developing spines (Fig. 4.20B). Similar to primary hippocampal neurons in section 4.9.2, dendrites from PSD-95-K202R-EGFP-infected neurons displayed more immature filopodia-like structures compared to PSD-95-WT-EGFP overexpression. Additionally, the number of dendritic protrusions was decreased in PSD-95-K202-EGFP-infected neurons compared to EGFP and PSD-95-WT-EGFP-transfected cells (Fig. 4.20C).

The infection of organotypic slice cultures with Semliki Forest Virus containing EGFP, PSD-95-WT, or PSD-95-K202R supports previous findings on spine morphology from primary neurons (Section 4.9.2), showing that neddylation inhibition at K202 of PSD-95 is sufficient to exert a dominant-negative effect on spine morphology.

4.9.3 PSD-95-K202R has a Dominant Negative Effect on Excitatory Synapse Function during Spine Development

Section 4.9.2 demonstrated that PSD-95-K202R overexpression in developing primary neurons decreases the number of mature spines compared to PSD-95-WT overexpression that increases spine number. Hence, one might speculate whether PSD-95-K202R expressing neurons exhibit a reduced number of functional synaptic connections compared to PSD-95-WT expressing neurons. Experimentally, the number of functional synapses can be validated by recording miniature excitatory post-synaptic currents (mEPSC), which are caused by spontaneous vesicle release from the pre-synapse. The released glutamate elicits mEPSC at the post-synapse that is detected *via* whole cell recordings. The amplitude of the recorded mEPSCs correlate to the number of AMPA receptors in the post-synapse and the frequency is a measurement of the amount of functional synapses onto the respective neuron.

To test whether PSD-95-K202R alters synaptic function in developing neurons, mEPSCs were recorded from CA1 neurons of organotypic slice cultures, expressing EGFP, PSD-95-WT-EGFP or PSD-95-K202R-EGFP.

As expected, PSD-95-WT-EGFP infected neurons revealed a significant increase in mEPSC amplitude (EGFP control: 26.01 ± 1.81 pA, $n = 7$; PSD-95-WT-EGFP: 35.30 ± 1.69 pA, $n = 7$; EGFP vs. PSD-95-WT-EGFP $p < 0.05$; Kolmogorov-Smirnov (KS): EGFP vs. PSD-95-WT-EGFP $p < 0.025$) (Fig. 4.21A, B, C), interevent interval, and mean frequency (EGFP control: 0.77 ± 0.14 Hz, $n = 7$; PSD-95-WT-EGFP: 1.25 ± 0.14 Hz, $n = 7$; control vs. PSD-95-WT-EGFP $p < 0.05$; KS: control vs. PSD-95-WT-EGFP $p < 0.0001$) compared to EGFP-expressing neurons (El-Husseini et al., 2000, Ehrlich and Malinow, 2004).

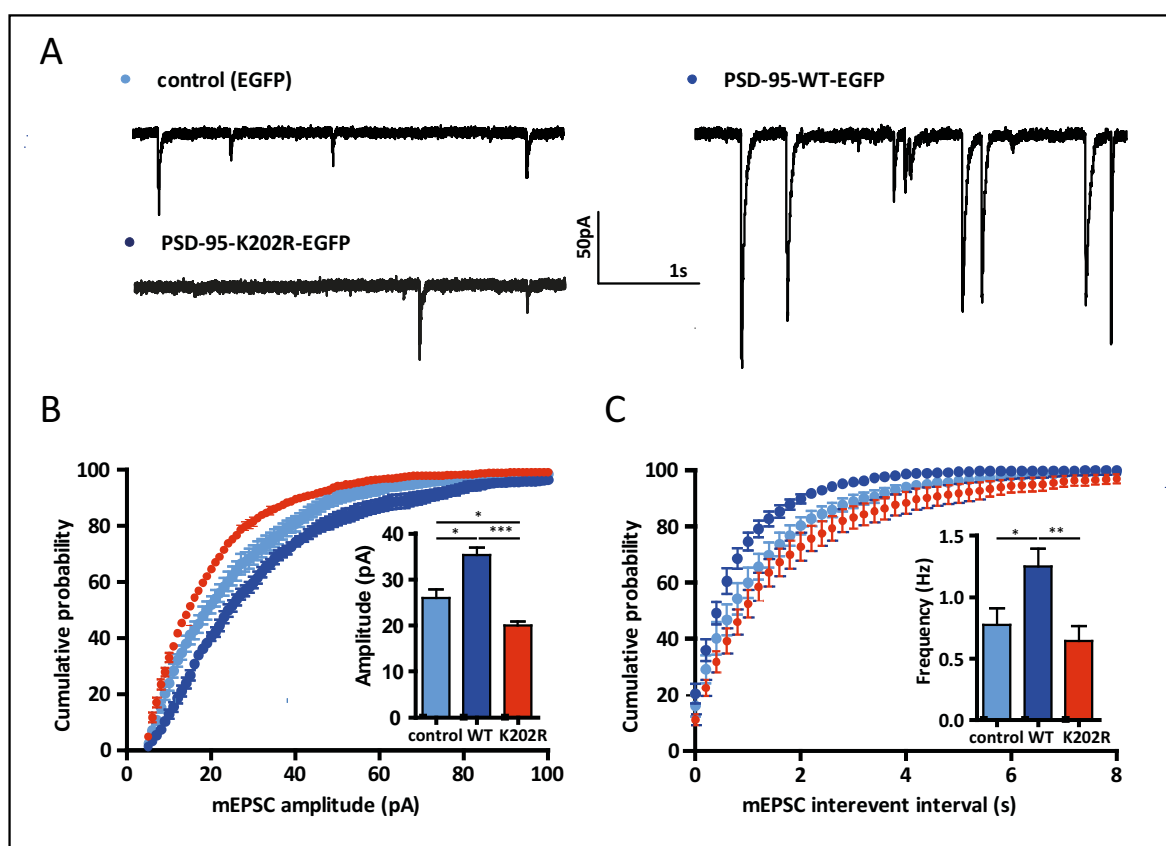


Figure 4.21: PSD-95-K202R has a dominant negative effect on amplitude and interevent interval of mEPSC in developing neurons. **A)** Representative whole cell recordings of mEPSCs from organotypic hippocampal CA1 neurons. Neurons expressed EGFP (control, light blue), PSD-95-WT (dark blue) or PSD-95-K202R (red). Legend and color scheme also apply for **B**, **C**. **B)** Cumulative distribution of mEPSC amplitudes. The graph bar inset depicts mean mEPSC amplitudes. PSD-95-WT increases whereas PSD-95-K202R decreased mEPSC amplitude compared to control neurons. **C)** Cumulative distribution of mEPSC interevent intervals. The bar graph inset depicts mean of mEPSC frequencies. PSD-95-WT overexpression led to a strong increase in mEPSC interevent interval compared to control and PSD-95-K202R expressing neurons.

The cumulative distribution of mEPSC amplitudes demonstrated a strong decrease in mEPSC amplitude when PSD-95-K202R-EGFP was overexpressed compared to EGFP-expressing neurons (KS: EGFP vs. PSD-95-K202R-EGFP $p < 0.005$; KS: PSD-95-WT-EGFP vs. PSD-95-K202R-EGFP $p < 0.0001$) (Fig. 4.21B). This result was reflected in the average mEPSC amplitude also showing a decrease in the mean amplitude of PSD-95-K202R-EGFP-expressing cells compared to control neurons (EGFP control: 26.01 ± 1.81 pA, $n = 7$; PSD-95-WT-EGFP: 35.30 ± 1.69 pA, $n = 7$; PSD-95-K202R-EGFP: 19.99 ± 0.93 pA, $n = 7$; PSD-95-WT-EGFP

vs. PSD-95-K202R-EGFP $p < 0.001$) (Fig. 4.21B inset). PSD-95-K202R overexpression in organotypic slice cultures exerts a dominant negative effect on mEPSC amplitude.

The mEPSC interevent interval of PSD-95-K202R-EGFP-infected cells strongly decreased compared to PSD-95-WT-EGFP expressing neurons (KS: PSD-95-WT-EGFP vs. PSD-95-K202R-EGFP $p < 0.0001$) and to control neurons expressing EGFP (KS: EGFP vs. PSD-95-K202R-EGFP $p < 0.001$). The average mEPSC frequency of PSD-95-K202R-EGFP was only slightly decreased to PSD-95-WT-EGFP but not to EGFP-infected neurons (EGFP control: 0.77 ± 0.14 Hz, $n = 7$; PSD-95-WT-EGFP: 1.25 ± 0.14 Hz, $n = 7$; PSD-95-K202R-EGFP: 0.64 ± 0.12 Hz, $n = 7$; PSD-95-WT-EGFP vs. PSD-95-K202R-EGFP $p < 0.01$) (Fig. 4.21C inset).

In contrast to PSD-95-WT overexpression that increases mEPSC amplitude and mEPSC frequency to control neurons, the overexpression of PSD-95-K202R results in a decreased mEPSC amplitude and mEPSC interevent interval. Remarkably, one amino acid change in PSD-95 that lacks PSD-95 neddylation at K202 not only prevents the increase in mEPSC amplitude and frequency but also has a dominant negative effect on mEPSC amplitude and interevent interval. Accordingly, neddylation inhibition at K202 of PSD-95 completely changes the impact of PSD-95 function on synaptic transmission during neuronal development. The reduction in mEPSC amplitude can be explained by a reduction in AMPA receptors in the post-synaptic membrane induced by PSD-95-K202R expression. The reduction in mEPSC frequency indicates that the number of functional synapses decreased upon PSD-95-K202R expression.

4.9.4 PSD-95-K202R Exerts a Dominant Negative Effect on mEPSC Frequency in Mature Excitatory Synapses

PSD-95-K202R exerts strong effects on spine morphology and synaptic function during spine development (Section 4.9.2 and 4.9.3). Since previous experiments revealed defects in spine development and spine stability upon Nedd8 pathway inhibition and PSD-95-K202R had strong morphological and electrophysiological defects in developing neurons, it was tested whether the overexpression of PSD-95-K202R also influences spine stability in mature neurons.

Organotypic brain slices were infected with Semliki Forest Virus containing EGFP,

PSD-95-WT-EGFP or PSD-95-K202R-EGFP at DIV 7-9. mEPSC from CA1 neurons were recorded 2 days after infection.

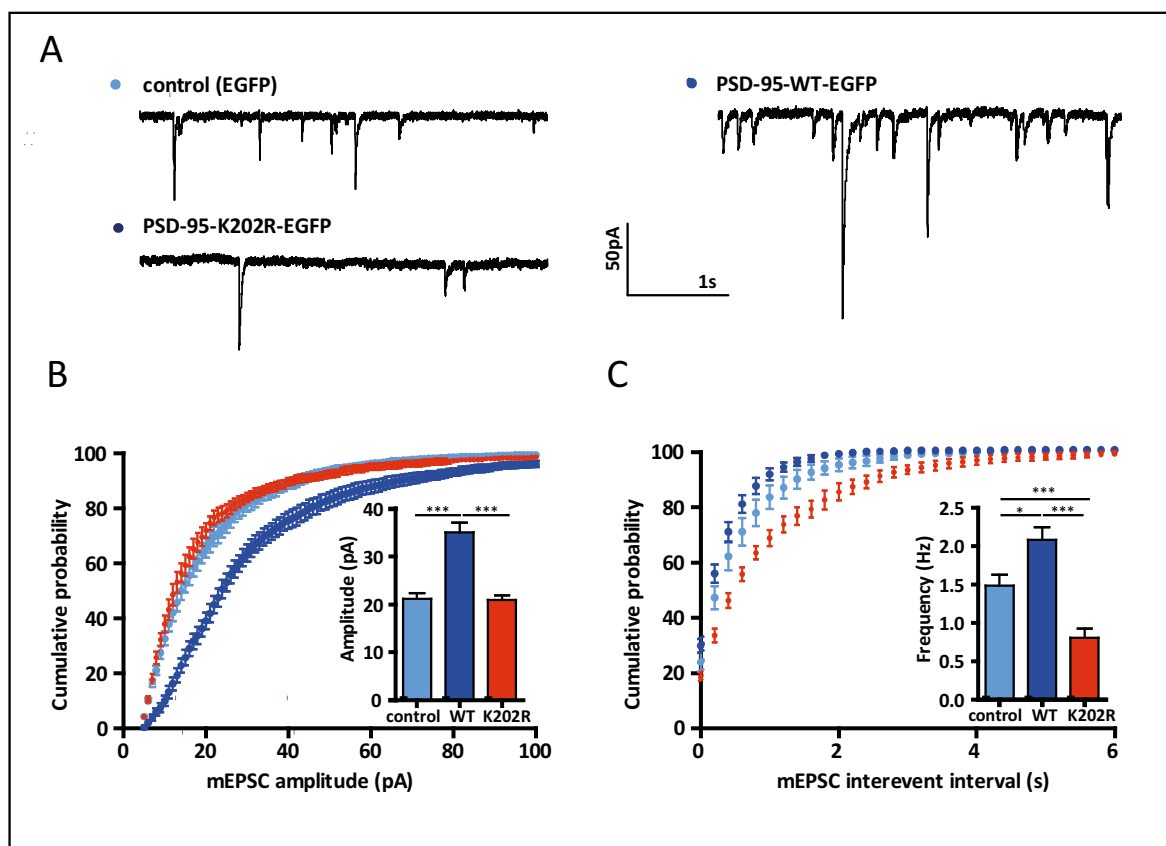


Figure 4.22: PSD-95-K202R has a dominant negative effect on mEPSC frequency in mature neurons. **A)** Representative whole cell recordings of mEPSCs from mature organotypic hippocampal CA1 neurons. Neurons expressed EGFP (control, light blue), PSD-95-WT (dark blue) or PSD-95-K202R (red). Legend and color scheme also apply for **B**, **C**. **B)** Cumulative distribution of mEPSC amplitudes. The graph bar inset depicts mean mEPSC amplitudes. PSD-95-WT mEPSC amplitude increases compared to control and PSD-95-K202R expressing neurons. **C)** Cumulative distribution of mEPSC interevent intervals. The bar graph inset depicts mean of mEPSC frequencies. PSD-95-WT overexpression led to a strong increase in mEPSC frequency whereas PSD-95-K202R decreased mEPSC frequency compared to control neurons expressing EGFP.

The cumulative distribution of mEPSC amplitude from PSD-95-K202R-EGFP-infected neurons was significantly decreased compared to PSD-95-WT-EGFP-infected neurons but did not differ to control neurons expressing EGFP (KS: EGFP vs. PSD-95-WT $p < 0.0001$; $p > 0.1$ EGFP vs. PSD-95-K202R, $p < 0.0001$ PSD-95 WT vs. PSD-95-K202R) (Fig. 4.22B). Additionally, mEPSC amplitude was reduced in PSD-95-K202R-EGFP compared

to PSD-95-WT-EGFP-infected neurons (EGFP control: 21.21 ± 1.14 pA, $n = 10$; PSD-95-WT-EGFP: 35.05 ± 1.97 pA, $n = 10$; PSD-95-K202R-EGFP: 20.90 ± 1.03 pA, $n = 8$; control vs. PSD-95-WT-EGFP $p < 0.0001$; PSD-95-WT-EGFP vs. PSD-95-K202R-EGFP $p < 0.0001$) (Fig. 4.22B inset). Hence, the overexpression of PSD-95-K202R-EGFP had no effect on mEPSC amplitude compared to EGFP-expressing neurons, whereas PSD-95-WT-EGFP overexpression again strongly increased mEPSC amplitude. PSD-95-K202R-EGFP overexpression in organotypic brain slices has no effect on mEPSC amplitude and therefore does not influence the number of AMPA receptors in the post-synapse.

Upon PSD-95-WT-EGFP overexpression the cumulative probability of mEPSC interevent intervals increased compared to PSD-95-K202R or control transfected neurons (KS: EGFP vs. PSD-95-WT $p < 0.005$; KS: EGFP vs. PSD-95-K202R $p < 0.0001$; KS: $p < 0.0001$) (Fig. 4.22C). The average mEPSC frequencies revealed the same result than the mEPSC interevent intervals. The frequency of mEPSPs was significantly increased for PSD-95-WT-EGFP compared to EGFP and PSD-95-K202-EGFP-infected neurons. Additionally, mEPSC frequency exhibited a significant decrease for PSD-95-K202R-EGFP-infected neurons compared to control neurons (EGFP: 1.50 ± 0.14 Hz, $n = 9$; PSD-95 WT: 2.08 ± 0.17 Hz, $n = 10$; PSD-95-K202R: 0.81 ± 0.12 Hz, $n = 7$; EGFP vs. PSD-95-WT-EGFP $p < 0.05$; control vs. PSD-95-K202R-EGFP $p < 0.0001$; PSD-95-WT-EGFP vs. PSD-95-K202R-EGFP $p < 0.01$). These results indicate that PSD-95-WT-EGFP overexpression leads to an increased number of functional synapses in mature hippocampal neurons, whereas the overexpression of PSD-95-K202R-EGFP reduces functional synapses.

Overexpression of the neddylation mutant PSD-95-K202R shows that the lack of neddylation at lysine 202 is not capable of mimicking the effect PSD-95-WT has on synaptic function during spine development as well as on spine stability. More importantly, overexpression of PSD-95-K202R has a dominant negative effect on mEPSC amplitude and frequency during spine development and on mEPSC frequency in adult synapses. The functional analysis of PSD-95-K202R shows that PSD-95 neddylation at K202 is mandatory for synaptic function during spine development and in mature synapses. These results strongly suggest an important role of the Nedd8 pathway on synaptic function.

4.10 Ubc12-C111S in Electrophysiology

Nedd8 pathway inhibition, by the overexpression of Ubc12-C111S exerts a strong effect on spine morphology (Vogl, Brockmann et. all). Overexpressing Ubc12-C111S during the critical time window of spinogenesis or synaptogenesis in primary hippocampal and cortical neurons severely impairs spine formation. Primary neurons expressing Ubc12-C111S were missing mushroom-like spines but were decorated with filopodia instead. To functionally validate this morphological defect, electrophysiological recordings were obtained that allow for a more functional analysis of the morphological changes.

4.10.1 Blocking the Nedd8 Pathway Affects Synaptic Transmission - Genetic Approach

Ubc12-C111S was transfected in primary hippocampal neurons to investigate whether the inhibition of target neddylation has an impact on basal synaptic neurotransmission. Ubc12-C111S and Venus were transfected in neurons at DIV13. The concentration of transfected Ubc12-C111S was much higher than Venus, to guarantee that every green fluorescent cell co-expressed Ubc12-C111S. Five days after transfection, Ubc12-C111S expressing neurons were decorated with filopodia like structures although shaft synapses, visualized by α -synapsin immunostainings, were still observed (Fig. 4.23A).

mEPSC recordings were obtained to verify whether the inhibition of target protein neddylation in the post-synapse has an impact on the number of functional synapses.

mEPSC amplitude and frequency were analyzed from control neurons expressing the fluorescent marker Venus and from Ubc12-C111S and Venus expressing neurons. Whole cell recordings were obtained five days after transfection at DIV18-19. The same experimental design was used for the morphological analysis of Ubc12-C111S expression in primary neurons (Fig. 4.23A). Hence, the functional changes can be directly correlated to the morphological changes. mEPSC amplitude revealed no significant difference between control and Ubc12-C111S-expressing neurons neither in the cumulative probability nor in the mean value of the mEPSC amplitude (control 21.84 ± 2.02 pA, $n = 11$; Ubc12-C111S 18.55 ± 2.25 pA, $n = 10$) (Fig. 4.23B, C).

In contrast to the mEPSC amplitude, the cumulative probability of the interevent interval of the

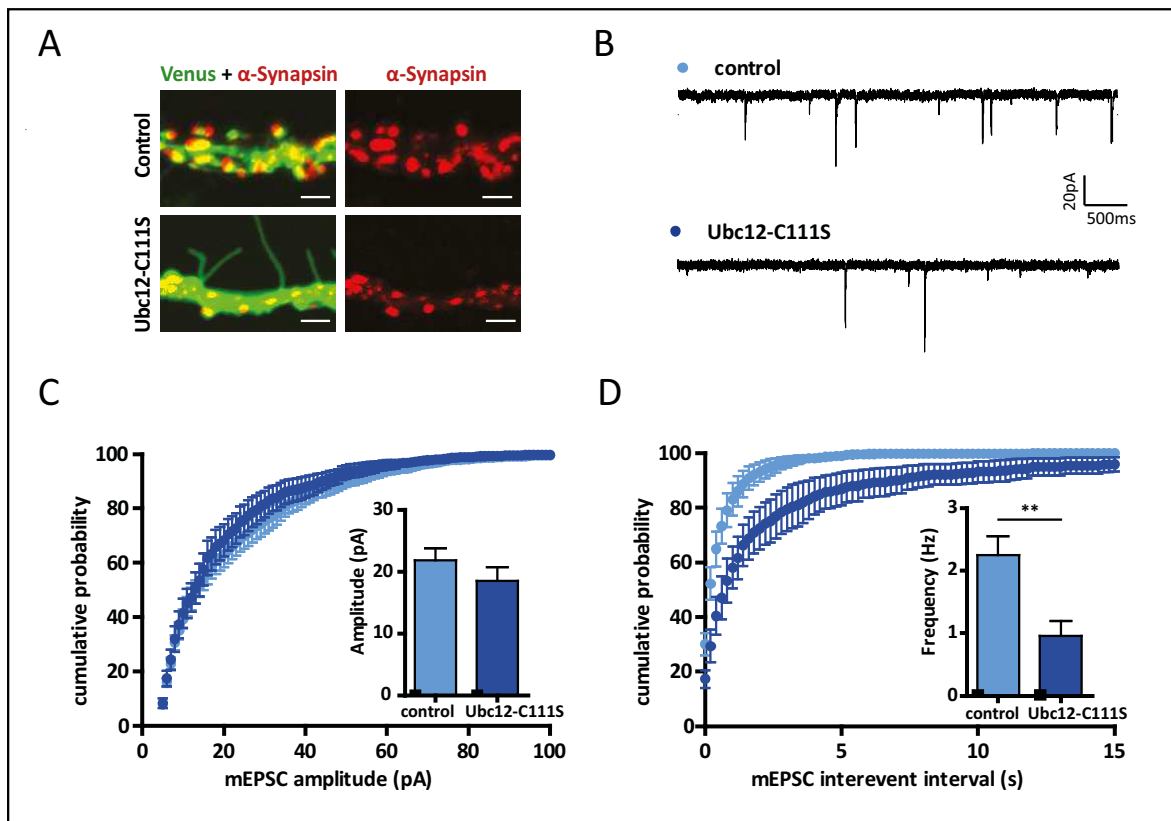


Figure 4.23: The Nedd8 pathway is essential for basal neurotransmission. **A)** Primary hippocampal neurons were transfected with the indicated plasmids at DIV13. At DIV19, neurons were fixed and immunofluorescently stained with α -synapsin antibodies. Scale bar, 2.5 μ m **B)** Representative whole cell recordings from primary hippocampal neurons DIV18-19. **C)** Cumulative distribution of mEPSC amplitude. The inset shows mean mEPSC amplitude. mEPSC amplitude of Ubc12-C111S overexpression primary hippocampal neurons (dark blue) is not significant different compared to control neurons expressing venus (light blue). **D)** Cumulative distribution of mEPSC interevent interval as well as the mean mEPSC frequency, are strongly reduced in Ubc12-C111S expressing primary hippocampal neurons compared to control neurons.

Ubc12-C111S-expressing neurons was significantly reduced compared to controls (KS: Venus vs. Ubc12-C111S $p < 0.001$). Additionally, the mean frequency was diminished in Ubc12-C111S transfected neurons compared to neurons expressing only Venus (control 2.25 ± 0.31 Hz, $n = 11$; Ubc12-C111S 0.96 ± 0.24 Hz, $n = 10$; control vs. Ubc12-C111S $p < 0.01$) (Fig. 4.23B, D).

The morphological changes observed in Ubc12-C111S-expressing neurons were reflected in an altered synaptic neurotransmission. Hence, the strong decrease in mEPSC frequency in Ubc12-C111S expressing neurons indicates that the number of functional synapses is reduced upon neddylation inhibition. The remaining shaft synapses give rise to single events whose

amplitude do not differ to control neurons, indicating that the remaining shaft synapses, detected in the morphological analysis, display normal synaptic transmission.

4.11 Acute Effects of Neddylation Inhibition on Synaptic Transmission - Pharmacological Approach

The section 4.10 showed that the overexpression of Ubc12-C111S and the subsequent inhibition of the Nedd8 pathway strongly effects synaptic neurotransmission. The changes in neurotransmission can be correlated to morphological changes that occur when the Nedd8 pathway is blocked for several days. To functionally understand the effect of neddylation on neurotransmission, it is of great interest whether the inhibition of neddylation impacts on synaptic function even before morphological changes are detected. A fast neddylation inhibition was accomplished with MLN-4924 application, whereby it has to be proven that short MLN-4924 treatment does not affect spine morphology.

4.11.1 Acute MLN-4924 Treatment Affects Spine Morphology and Function in Primary Hippocampal Neurons

The effects of acute neddylation inhibition were first tested in primary hippocampal neurons at DIV19. On that differentiation day, neurons were decorated with mature mushroom-shaped spines. Since the focus of the experiment was to see whether neddylation inhibition alters synaptic function without disturbing spine morphology, we first wanted to test whether MLN-4924 treatment alters spine morphology. Primary hippocampal neurons were treated for 2 h with MLN-4924 and showed a significant difference to vehicle treated neurons. While vehicle treated neurons were still decorated with mushroom-shaped spines, MLN-4924 treated neurons displayed filopodia-like structures (Fig. 4.24A). Hence, acute neddylation inhibition in primary hippocampal neurons for 2 h had similar effects to Ubc12-C111S overexpression (Section 4.10) and severely alters spine morphology.

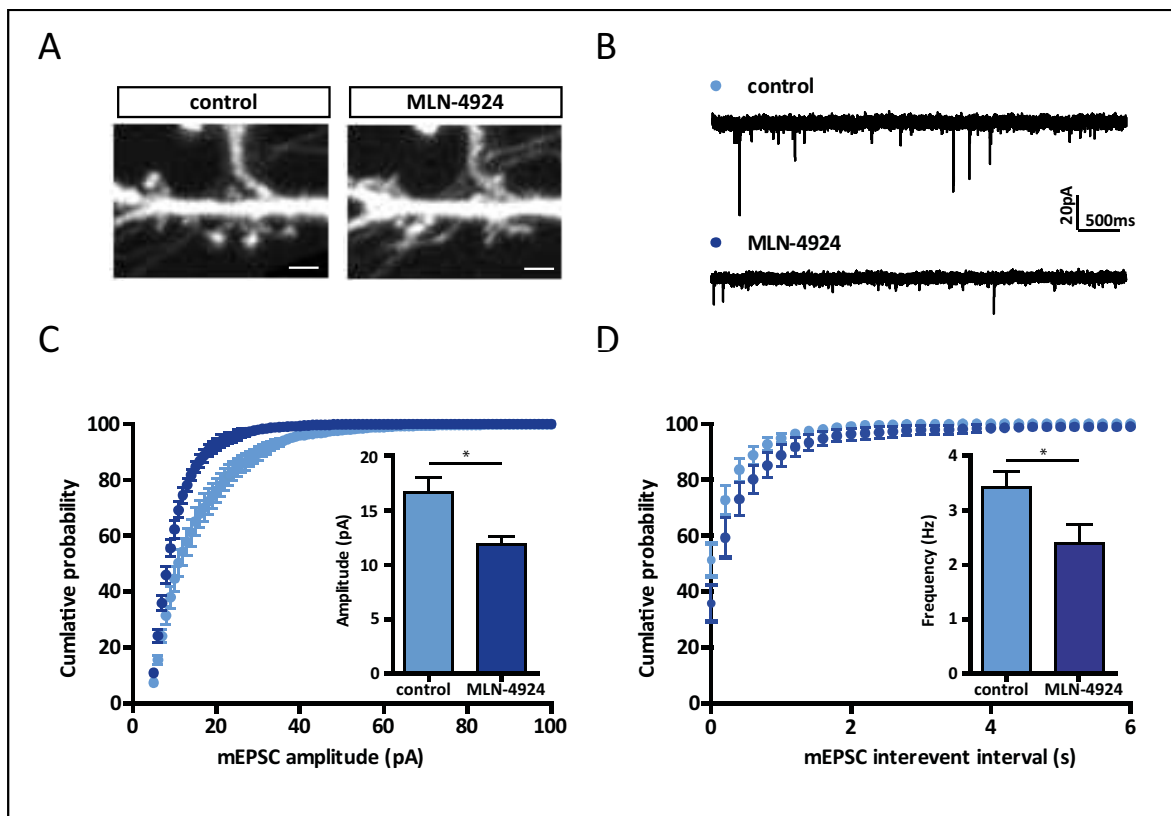


Figure 4.24: MLN-4924 affects spine morphology and basal neurotransmission in primary hippocampal neurons. **A)** Primary hippocampal neurons DIV19 were treated for 2 hours with MLN-4924 or vehicle. Vehicle treated neurons are decorated with mature mushroom shaped spines, whereas MLN-4924 display filopodia like structures. Scale bar, 2.5 μm **B)** Representative whole cell recordings from primary hippocampal neurons DIV19 treated with vehicle or MLN-4924 for 30 min. **C)** Cumulative distribution of mEPSC amplitude. The inset shows mean mEPSC amplitude. mEPSC amplitude of MLN-4924 treated primary hippocampal neurons (dark blue) is significant decreased compared to control neurons (light blue). **D)** Cumulative distribution of mEPSC interevent interval as well as the mean mEPSC frequency are strongly reduced in MLN-4924 treated primary hippocampal neurons compared to control neurons.

mEPSCs were obtained from primary hippocampal neurons DIV19 treated for 30 minutes with MLN-4924. During this short MLN-4924 treatment, no changes on spine morphology were detected. The cumulative distribution of mEPSC amplitude as well as the mean amplitude were significantly decreased in MLN-4924 treated neurons compared to controls treated with vehicle (KS for control amplitude vs. MLN-4924 amplitude $p < 0.001$; bar graph inset: control 16.64 ± 1.40 pA, $n = 13$; MLN-4924 11.89 ± 0.72 pA, $n = 9$; control vs. MLN-4924 $p < 0.05$) (Fig. 4.24B inset, C inset). The decrease of mEPSC amplitude indicates that neddylation inhi-

bition reduces the number of AMPA receptors in the post-synaptic membrane. The mEPSC interevent interval, as well as the mean frequency, were also reduced after MLN-4924 application (KS for control interevent interval vs. MLN-4924 interevent interval $p < 0.001$; bar graph inset: control 3.42 ± 0.30 Hz, $n = 13$; MLN-4924 2.38 ± 0.36 Hz, $n = 9$; control vs. MLN-4924 $p < 0.05$) (Fig. 4.24B, D). MLN-4924 treatment additionally reduced the number of functional synapses compared to control neurons indicated by the decrease in mEPSC frequency.

These results show that MLN-4924 application in primary hippocampal neurons exerts strong effects on AMPA receptor-mediated currents. mEPSC recordings revealed a decrease in functional synapses as well as an decrease in AMPA receptors when neddylation is blocked. Given that MLN-4924 treatment also strongly impacts on spine morphology after 2 h, it is not possible to say whether the functional changes after 30 min of MLN-4924 treatment are independent from the morphological changes.

Since primary hippocampal neurons are not embedded in their physiological surrounding, for example glia cells are missing, it is very likely that synaptic contacts are more unstable compared to synapses in the brain. In the next experiments, acute hippocampal brain slices were chosen as a model system, since neurons are still embedded in their physiological surroundings while physiological characterizations are obtained.

4.11.2 Acute MLN-4924 Treatment has no Effect on Spine Size in Hippocampal Neurons from Acute Brain Slices

The goal of the next set of experiments was to see whether neddylation inhibition has an effect on synaptic neurotransmission before changes in synaptic morphology were detected. For this purpose, acute hippocampal slices were chosen as a model system. In acute brain slices, neurons are embedded in their physiological surrounding and therefore synaptic connections might be more stable after MLN-4924 application than synapses in primary cell cultures.

To test this hypothesis, acute brain slices were obtained from Thy-1 GFP-expressing mice (Fang et al., 2000) at DIV16-21. Spine morphology from GFP-expressing basal dendrites of CA1 pyramidal neurons were analyzed every 5 minutes using by two-photon microscopy. First, a 30 minutes baseline was recorded before $1 \mu\text{M}$ MLN-4924 was applied to the ACSF. Spine vol-

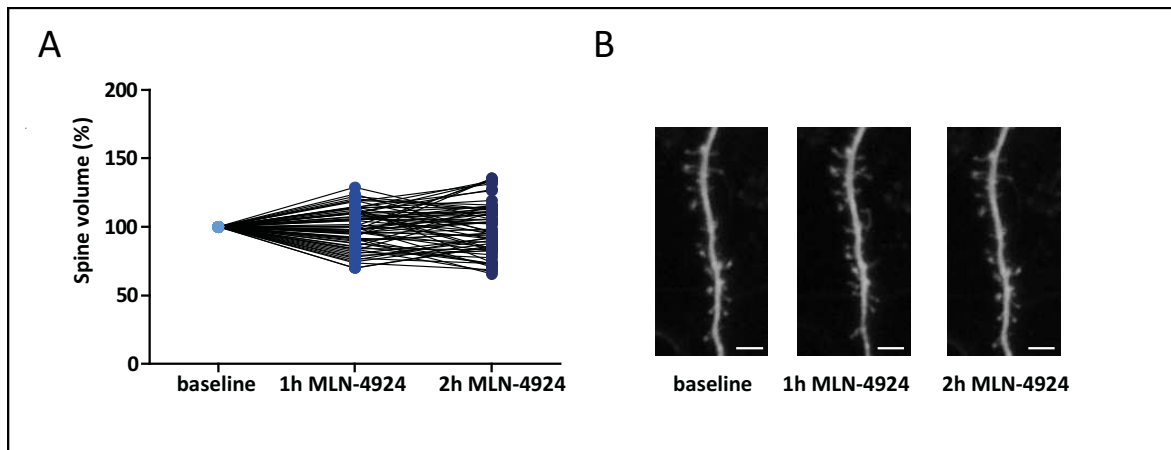


Figure 4.25: Acute MLN-4924 treatment has no effect on spine morphology in acute hippocampal brain slices. A) Acute hippocampal brain slices from thy-1 GFP mice, show no changes in spine volume when treated for 1 hour and 2 hours with 1 μ M MLN-4924. Scale bar, 5 μ m **B)** Representative pictures obtained from two-photon-imaging of dendrites from hippocampal neurons treated with 1 μ M MLN-4924 for 1 hour and 2 hours revealed no effect on spine volume upon neddylation inhibition.

umes of the same spines were analyzed at baseline, 1 hour and 2 hours after 1 μ M MLN-4924 wash-in. 1 hour and 2 hours of MLN-4924 treatment did not alter spine volume of CA1 neurons in acute hippocampal brain slices (n (slices) = 4; n (spines) = 70) (Fig. 4.25A, B).

In conclusion, no morphological changes were observed during short periods of neddylation inhibition in acute hippocampal brain slices. Consequently, acute hippocampal brain slices are an ideal system to study the effect of acute neddylation inhibition on synaptic function.

4.12 Nedd8 Effects on Basal Synaptic Transmission

To see whether neddylation inhibition impacts on basal synaptic transmission, input-output curves were recorded at the CA3-CA1 synapse in acute hippocampal brain slices. Input-output curves measure the intensity of the post-synaptic response after the pre-synaptic neuron was activated with the same stimulus intensity and thus enables the detection of possible defects on basal neurotransmission.

In acute hippocampal brain slices, Schaffer collaterals were stimulated in CA3 and the sum of the post-synaptic responses was recorded in CA1. The number of activated fibers from CA3 to CA1

is reflected in the peak of the fiber volley (FV). To study the effect of neddylation inhibition on basal synaptic neurotransmission, post-synaptic responses in CA1 were recorded upon different stimuli intensities that were set to 0.05, 0.1, 0.15, 0.2, and 0.25 mV (fiber volley peak). Input-output curves were obtained in the same hippocampal slices before and after 30 minutes of 1 μ M MLN-4924 treatment. The sensitivity of the electrical stimulus was unaltered before and after MLN-4924 was washed in, indicating that the excitability of neurons is unaltered upon neddylation inhibition (for each FV slope: control $n = 11$ and MLN-4924 $n = 11$, FV 0.05 mV: control 0.22 ± 0.02 mA, MLN-4924 0.28 ± 0.02 mA; FV 0.1 mV: control 0.42 ± 0.05 mA, MLN-4924 0.46 ± 0.03 mA; FV 0.15 mV: control 0.62 ± 0.06 mA, MLN-4924 0.78 ± 0.10 mA; FV 0.2 mV: control 0.92 ± 0.13 mA, MLN-4924 1.02 ± 0.14 mA; FV 0.25 mV: control 0.99 ± 0.16 mA, $n = 6$, MLN-4924 1.13 ± 0.21 mA, $n = 6$) (Fig. 4.25A, B). Excitatory post-synaptic potential (fEPSP) responses were significantly reduced in MLN-4924 treated slices compared to control conditions, especially for high-stimulation intensities (for each FV slope: control $n = 11$ and MLN-4924 $n = 11$, FV 0.05 mV: control -0.03 ± 0.01 mV/ms, MLN-4924 -0.03 ± 0.01 mV/ms; FV 0.1 mV: control -0.11 ± 0.01 mV/ms, MLN-4924 -0.87 ± 0.01 mV/ms; FV 0.15 mV: control -0.19 ± 0.02 mV/ms, MLN-4924 -0.14 ± 0.02 mV/ms ($p < 0.05$); FV 0.2 mV: control -0.25 ± 0.03 mV/ms, MLN-4924 -0.18 ± 0.02 mV/ms ($p < 0.001$); FV 0.25 mV: control -0.31 ± 0.03 mV/ms, $n = 6$, MLN-4924 -0.19 ± 0.02 mV/ms, $n = 6$ ($p < 0.05$)) (Fig. 4.26A, C).

These results indicate that even after short periods of neddylation inhibition, the input-output relation is effected (Fig. 4.26C). No differences were observed in the excitability of the Schaffer collaterals, or in the number of activated Schaffer collaterals after MLN-4924 application (Fig. 4.26B). Additionally, no changes were seen in spine morphology after short periods of MLN-4924 application (Section 4.11.2). In conclusion, the deficit in the input-output relation can be assigned to altered synaptic transmission and can be related to changes in neurotransmitter release from the pre-synapse, or reduced post-synaptic excitability.

To dissect this phenotype in more detail, additional experiments were performed that exclusively analyzed functional changes in the pre- or post-synapse. All further analyses were performed within 1 hour of 1 μ M MLN-4924 application.

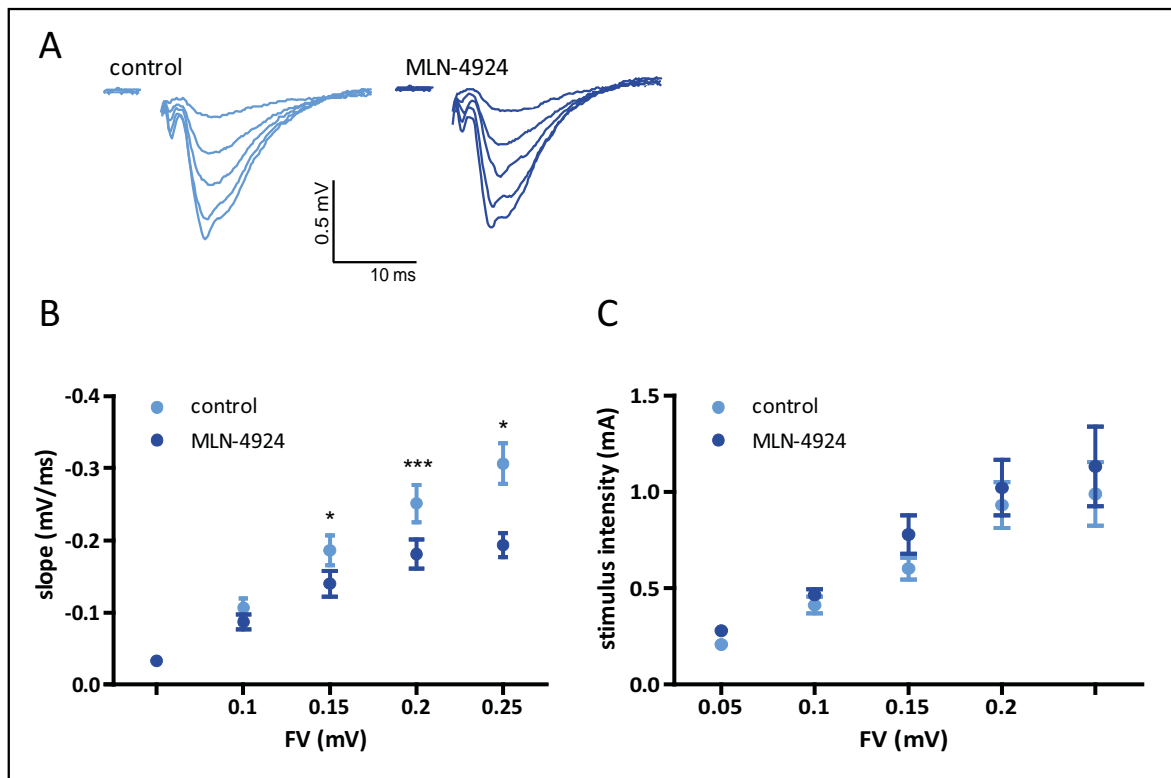


Figure 4.26: Basal synaptic transmission is reduced by blocking the Nedd8 pathway. Input-output curves show a reduced hippocampal basal transmission in acute brain slices after 30 min of MLN-4924 treatment. A) Representative traces of typical input-output curves from slices untreated (light blue) or MLN-4924 treated (dark blue). **B)** The graph displays stimulus intensity (mean \pm SEM) as a function of the pre-synaptic fiber volley (FV). The stimulus intensities are not different for control and MLN-4924 treated slices to elicit the same fiber volley amplitudes. **C)** The graph shows fEPSP slope responses (mean \pm SEM) as a function of the stimulus intensity in CA1. fEPSP slopes are significant lower in MLN-4924 treated slices when stimulated with 0.15, 0.2 and 0.25 mV.

4.13 Neddylated Effects on the Pre-Synapse of Excitatory Synapses

Given that neddylation inhibition decreases basal neurotransmission (Section 4.12) and that synaptosome preparation revealed neddylated protein in the pre-synapse (Section 4.1) the question of whether neddylation impacts on pre-synaptic function was raised.

4.13.1 Pre-Synaptic Neurotransmitter Release is Altered in MLN-4924-Treated Acute Brain Slices

One reason for the decreased synaptic transmission seen in Section 4.12 might be a change in the pre-synaptic neurotransmitter release. To see whether neddylation inhibition leads to an altered release probability, paired-pulse ratios (PPR) were measured in acute hippocampal brain slices before and after 30 minutes of 1 μ M MLN-4924 treatment. For paired-pulse facilitation (PPF) experiments post-synaptic responses were recorded after two stimuli were given within a short interval. During that time interval, residual Ca^{2+} remained in the pre-synapse from the first stimuli and thus facilitated the second stimulus. An increase in paired-pulse facilitation indicates a decreased release probability and vice versa.

Schaffer collaterals were stimulated twice with an interstimulus interval of 20, 40, and 100 ms. Simultaneously, post-synaptic responses were obtained in the CA1 area of the hippocampus and revealed increased fEPSP slopes for the second stimulus compared to the first one, indicated by $\text{PPR} \geq 1$.

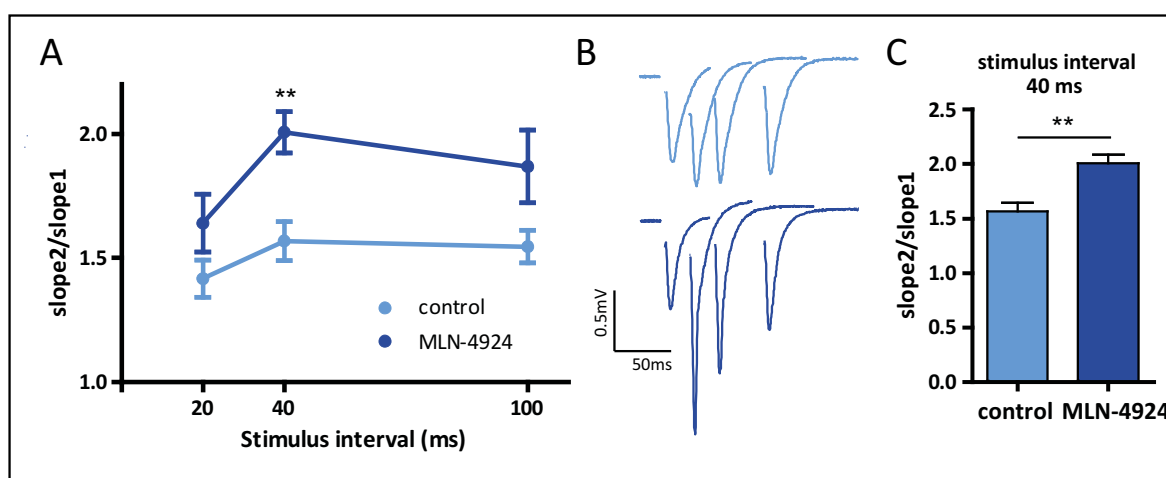


Figure 4.27: Release probability of excitatory synapses is decreased in acute brain slices treated with MLN-4924. **A)** Paired-Pulse facilitation (slope2/slope1) recorded as a function of the interstimulus interval (ms) of excitatory Schaffer collateral/CA1 pyramidal cell synapses show an increased PPF at 40 ms. MLN-4924 treated slices have a decreased release probability compared to control. **B)** Representative traces of typical fEPSP averages of 10 consecutive responses from control and MLN-4924-treated slices. **C)** Graph bar depicts PPF at a stimulus interval of 40 ms, where PPF of MLN-4924 (dark blue) treated slices is significantly higher than in control slices (light blue) ($p < 0.01$).

PPR values for untreated and MLN-4924-treated slices were highest for the stimulus interval of 40 ms compared to stimulus intervals of 20 ms and 100 ms (Fig. 4.27A, B). After 30 minutes of 1 μ M MLN-4924 treatment, PPR values from the interstimulus interval of 40 ms of MLN-4924 treated slices were significantly higher than PPR values from control slices, whereas PPR values at 20 ms and 100 ms were unaltered after MLN-4924-treatment (control n = 8, MLN-4924 n = 8; interstimulus interval: 20 ms: control 1.42 ± 0.08 , MLN-4924 1.64 ± 0.12 ; 40 ms: control 1.57 ± 0.08 , MLN-4924 2.01 ± 0.08 ($p < 0.01$); 100 ms: control 1.55 ± 0.07 , MLN-4924 1.87 ± 0.15) (Fig. 4.27A, B, C).

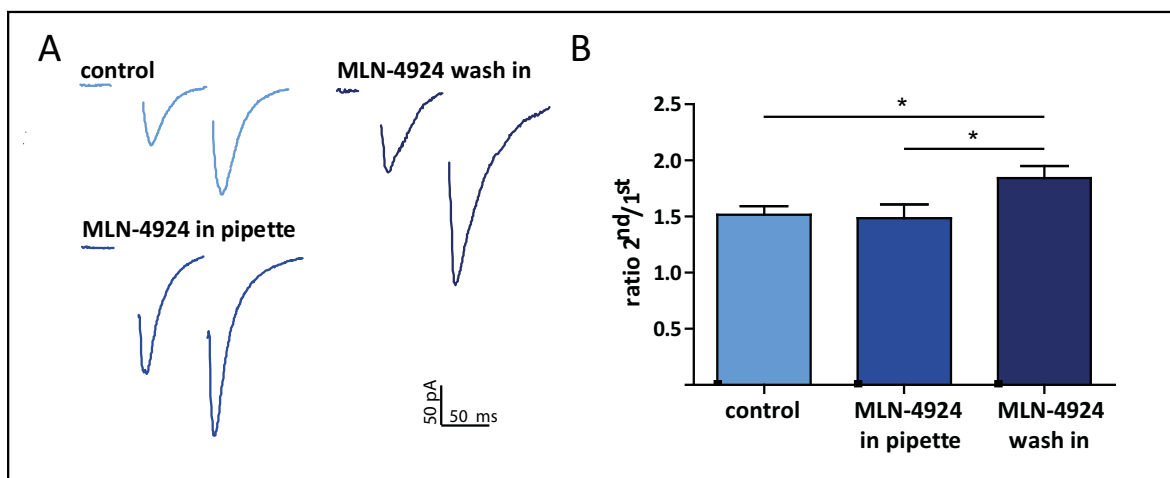


Figure 4.28: Release probability of excitatory synapses is unaltered when MLN-4924 treatment is restricted to the post-synapse. **A)** Representative traces of typical EPSCs averages of 10-15 consecutive responses. **B)** Paired-Pulse facilitation (amplitude₂/amplitude₁) recorded from CA1 neurons in whole cell configuration. PPF values from control neurons (light blue) and neurons where MLN-4924 was infused by the patch pipette (dark blue) have an increased release probability compared to neurons where the pre-synapse is additionally treated with MLN-4924 (black blue).

Increased PPR values for MLN-4924-treated slices revealed that the release probability of excitatory neurons is decreased when neddylation is blocked.

A limitation of the PPF experiment in figure 4.27 was that MLN-4924 was infused into the whole bath and thus acts on the pre- as well as on the post-synapse. To prove that the increased PPR is restricted to MLN-4924 action at the pre-synapse, PPF recordings were repeated from single cell recordings where MLN-4924 was just applied to the post-synapse. In this case, the PPF ratio of MLN-4924-treated neurons should be unchanged compared to control neurons, because neddylation inhibition is restricted to the post-synaptic site whereas the pre-synapse

function should be intact. For these experiments, CA1 neurons were patched and stimulated *via* an electrode in CA3. The interevent interval was set to 40 ms, since this condition caused the biggest effect on PPR in the field recordings (Fig. 4.27). To make sure that MLN-4924 only reached the post-synapse, it was applied directly to the intracellular solution of the patch pipette. After obtaining whole cell configuration, MLN-4924 was allowed to diffuse throughout the whole neuron for 10 minutes before PPF recordings were started. Figure 4.28 shows that MLN-4924 infusion into the post-synapse had no effect on PPR compared to control neurons where vehicle was applied to the patch pipette. To prove that the experimental setup allows the recording of pre-synaptic facilitation, 1 μ M of MLN-4924 was additionally fused into the bath for 30 minutes, again acting on the pre- as well as on the post-synapse. As in the field recordings, the PPF ratio was increased in MLN-4924-treated slices compared to control neurons and to neurons where MLN-4924 was applied using the patch pipette (control: 1.52 ± 0.08 , $n = 10$; MLN-4924 in pipette: 1.50 ± 0.12 , $n = 9$; MLN-4924 wash in: 1.84 ± 0.16 , $n = 9$; control vs. MLN-4924 in pipette $p < 0.05$; MLN-4924 in pipette vs. MLN-4924 wash-in $p < 0.05$) (Fig. 4.28A, B).

In conclusion, neddylation alters the release probability of vesicles from the pre-synapse.

4.13.2 MK-801 Effect is Decreased in MLN-4924-treated Brain Slices

To further specify the effect neddylation inhibition has on pre-synaptic neurotransmitter release, the used-dependent channel blocker for NMDA receptors, MK-801, was applied. In the presence of MK-801, NMDA receptors are blocked upon activation. Therefore, NMDA currents are blocked more efficiently by MK-801 the higher the neurotransmitter release from the pre-synapse is.

Evoked NMDA currents were obtained in acute hippocampal brain slices until stable amplitudes were reached. Afterwards, 60 μ M MK-801 was applied *via* the bath solution without NMDA receptor activation to make sure that a constant MK-801 concentration was reached in the recording chamber for every experiment. Next, Schaffer collaterals were activated with a frequency of 0.1 Hz for 10 minutes (130 stimuli) and NMDA receptor currents recorded at CA1 neurons.

The rate of NMDA receptor inhibition was lower in MLN-4924-treated cells compared to

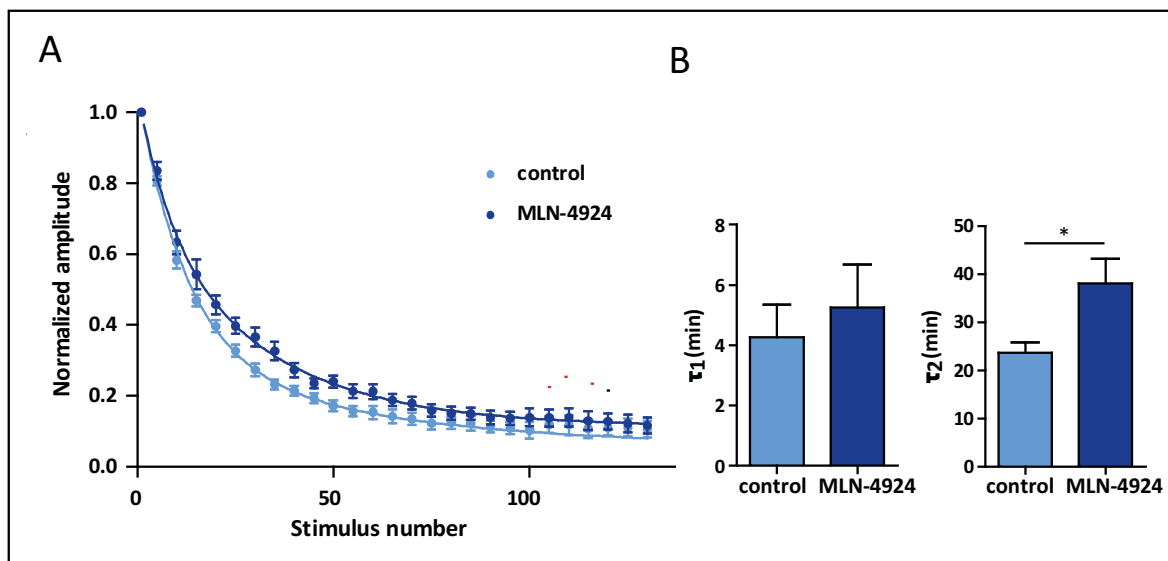


Figure 4.29: Release probability of excitatory synapses is decreased when neddylation is blocked. **A)** Time course of MK-801-dependent inhibition of NMDA-mediated EPSC amplitudes (normalized to baseline) at 0.1 Hz stimulation. MLN-4924 treated cells (light blue) showed a decreased release probability compared to control cells (dark blue). **B)** The rate of blockage was fitted with a two phase decay non-linear regression and revealed an increase in τ_2 for MLN-4924 treated cells compared to control.

control neurons (control: $n = 8$; MLN-4912: $n = 7$) (Fig. 4.29A). This result indicates a reduced neurotransmitter release from the pre-synapse after MLN-4924 treatment. To statistically prove the decrease in neurotransmitter release after neddylation inhibition, the curves in figure 4.29 were nonlinearly fitted by a two-phase decay. In comparison to vehicle treated slices, the slow decay time (τ_2) was increased when the Nedd8 pathway was blocked, whereas the fast decay time (τ_1) was unaltered (τ_1 : control 4.27 ± 1.08 min, $n = 7$, MLN-4924 5.27 ± 1.43 min, $n = 4$; τ_2 : control 23.75 ± 2.08 min, $n = 7$, MLN-4924 38.09 ± 5.07 min, $n = 5$; control τ_2 vs. MLN-4924 τ_2 $p < 0.05$) (Fig. 4.29B).

The nonlinear two-phase decay proved the decreased glutamate release from the pre-synapse after neddylation inhibition. The application of the NMDA antagonist MK801 supports previous findings from Section 4.13.1, showing that neddylation inhibition significantly decreases the release probability of pre-synaptic vesicles.

In summary, both experiments indicate that neddylation strongly impacts on pre-synaptic neurotransmitter release.

4.13.3 Vesicle Depletion and Recovery after High Frequency Stimulation is Reduced in MLN-4924-Treated Slices

The functionality of the pre-synaptic vesicle exocytosis machinery as well as the refilling of vesicles in the pre-synapse is important in order to guarantee the repeated neurotransmitter release during sustained activity. In another set of experiments, the influence of neddylation inhibition on the availability and on the recovery of vesicles upon persistent activity was investigated.

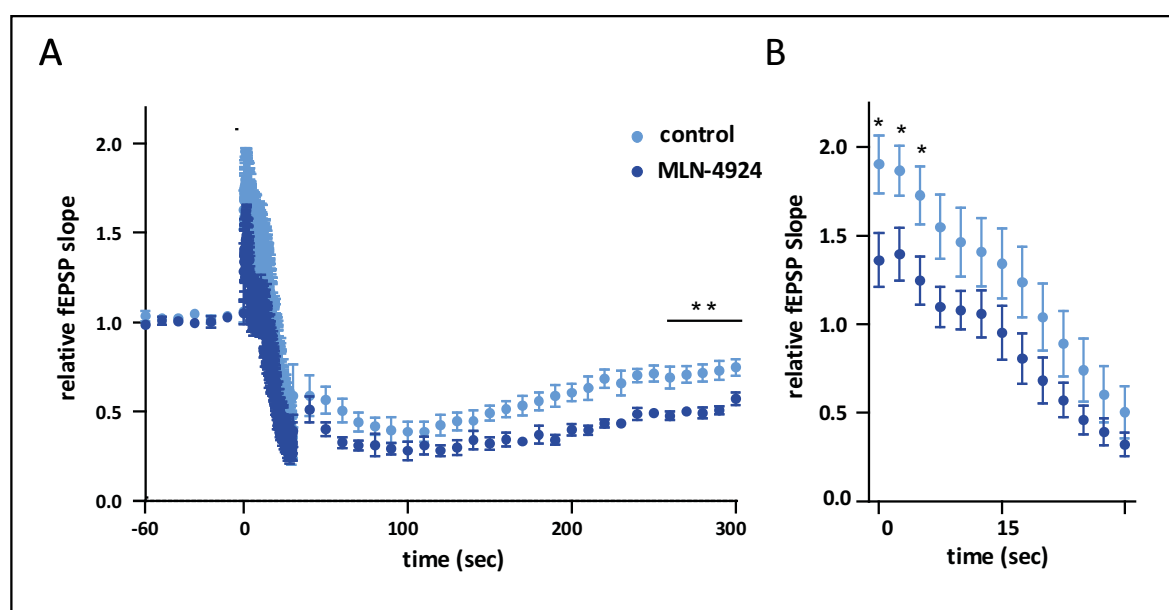


Figure 4.30: The amount of released neurotransmitter upon high stimulation as well as the recovery of the vesicle pool is reduced in MLN-4924 treated slices. A) Relative fEPSP slopes are blotted over time, before and after repetitive stimulation (300 pulses at 10 Hz). MLN-4924 treated slices (dark blue) display a decreased maximum in neurotransmitter release at the start of the repetitive stimulation as well as during the recovery compared to untreated slices (light blue). **B)** Enlargement of the repetitive stimulation time.

A stable baseline of fEPSP slopes was recorded for 10 minutes. Then, cells were stimulated with 300 pulses at 10 Hz, which led to a fast increase in neurotransmitter release that was significantly stronger in control slices compared to slices treated with MLN-4924 (1*: control 1.90 ± 0.16 , $n = 6$, MLN-4924 1.36 ± 1.52 , $n = 5$; control vs. MLN-4924 $p < 0.05$; 2*: control 1.87 ± 0.14 , $n = 6$, MLN-4924 1.40 ± 0.15 , $n = 5$; control vs. MLN-4924 $p < 0.05$; 3*: control 1.73 ± 0.16 , $n = 6$, MLN-4924 1.23 ± 0.13 , $n = 5$; control vs. MLN-4924 $p < 0.05$) (red asterisk in Fig. 4.29A and enlarged in Fig. 4.29B). During the depletion time, the neurotransmitter

release was decreased to the same degree in untreated and MLN-4924-treated slices (Fig. 4.29A, B). The depletion period is followed by the recovery time that allows for the refilling of pre-synaptic vesicles. During the recovery-time fEPSP recordings were obtained every 10 seconds. After 270 seconds the fEPSP slope of control slices had recovered to 75 % whereas MLN-4924-treated slices only reached 50 % of their baseline values. Thus, the vesicle pool recovery was strongly impaired in brain slices where neddylation was blocked (control: 0.74 ± 0.05 , $n = 6$; MLN-4924: 0.49 ± 0.04 , $n = x$; control vs. MLN-4924 $p < 0.01$) (Fig. 4.29A).

This experimental design showed that the availability as well as the refilling of pre-synapse vesicles during and after high frequency stimulation is decreased when neddylation is blocked.

Altogether, the results of section 4.12 indicate that the Nedd8 pathway strongly impacts on pre-synaptic function. Neddylation inhibition results in a decreased release probability of pre-synaptic vesicles. Additionally the recovery of the vesicle pool upon strong activation is reduced when Nedd8 cannot bind to its pre-synaptic targets. Further studies are necessary to define pre-synaptic targets of the Nedd8 pathway to more precisely characterize the molecular mechanisms underlying the facilitator role that neddylation exerts on pre-synaptic function.

4.14 Neddylation Effects on the Post-Synapse of Excitatory Synapses

Western blot experiments have shown that besides the pre-synapse, neddylated proteins are also located in post-synaptic compartments (Section 4.1). Further experiments should reveal whether acute neddylation inhibition by MLN-4924 also impacts on post-synaptic function. Since the scaffold protein PSD-95 is neddylated and PSD-95-K202R strongly reduced AMPA receptor mediated neurotransmission, there is strong evidence that acute neddylation inhibition by MLN-4924 impacts on post-synaptic functions in acute brain slices.

4.14.1 MLN-4924 Reduces Synaptic Transmission in Acute Brain Slices

To test whether neddylation inhibition alters AMPA receptor function, mEPSCs were recorded from CA1 neurons of acute hippocampal brain slices treated for 30 minutes with 1 μ M MLN-4924 or vehicle. mEPSC recordings revealed a significant decrease in mEPSC amplitude in MLN-4924 treated slices compared to control slices, visualized in the cumulative distribution as well as in the mean amplitudes depicted in the graph bar inset (Fig. 4.31B) (KS: $p < 0.001$ for control vs. MLN-4924; bar graph inset: control 15.08 ± 0.57 pA, $n = 11$; MLN-4924 11.09 ± 0.42 pA, $n = 9$; control vs. MLN-4924 $p < 0.001$). The decrease in mEPSC amplitude shows that neddylation inhibition reduces the number of functional AMPA receptors in the post-synaptic membrane.

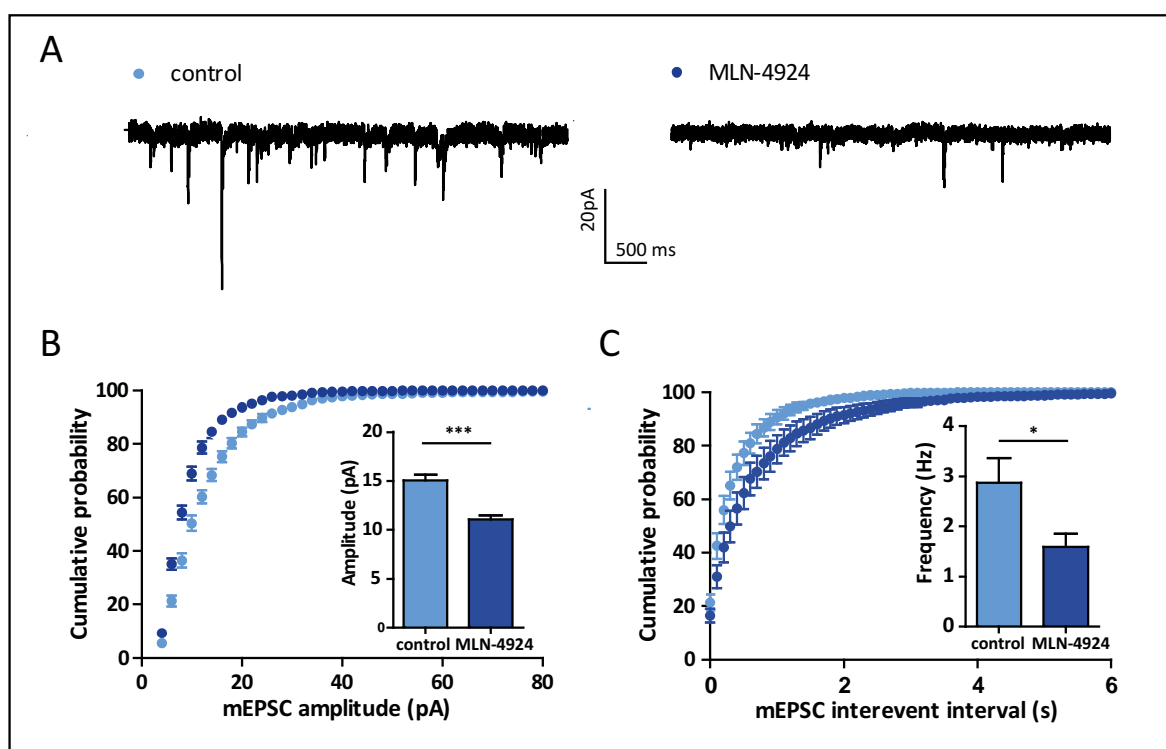


Figure 4.31: MLN-4924 treatment reduces amplitude and frequency of excitatory currents. **A)** Representative traces of mEPSC recordings from P16-21 hippocampal CA1 pyramidal neurons treated with MLN-4924 (dark blue) or vehicle (light blue). **B)** MLN-4924 treatment reduces mEPSC amplitudes of excitatory synapses. Cumulative distribution of mEPSC amplitudes, the bar graph inset depicts mean mEPSC amplitudes. **C)** MLN-4924 treatment decreases mEPSC frequency as shown by the increase in the interevent interval of the cumulative distribution as well as in the graph bar inset displaying the mean frequencies of control and MLN-4924 treated slices.

Additionally, the interevent interval was reduced when MLN-4924 was applied *via* the ACSF (KS: $p < 0.001$ for control interevent interval vs. MLN-4924 interevent interval) (Fig. 4.31C). Additionally, mEPSC frequency was significantly decreased in acute hippocampal brain slices when the Neddy8 pathway was blocked (bar graph inset: control: 2.89 ± 0.50 Hz, $n = 11$; MLN-4924: 1.60 ± 0.26 Hz, $n = 9$; control vs. MLN-4924 $p < 0.05$) (Fig. 4.31C inset). The mEPSC experiments in acute hippocampal brain slices revealed that neddylation inhibition decreases the number in functional synapses as well as the amount of AMPA receptors in the remaining synapses.

Similar to the overexpression of Ubc12-C111S and MLN-4924 treatment in primary neurons, MLN-4924 treatment of acute brain slices also alters the amplitude and frequency of mEPSCs.

4.14.2 AMPA/NMDA Ratios are Increased upon Neddylation Inhibition

The main receptors in the excitatory post-synapse are AMPA and NMDA receptors. The amount of both receptors in the post-synaptic membrane is highly regulated by receptor trafficking and receptor internalization (Fig. Santos et al., 2009, Hunt and Castillo, 2012). The regulation upon changes in neuronal activity is called synaptic plasticity and is dependent on the insertion or internalization of receptors. Especially AMPA receptor trafficking is tightly controlled during synaptic plasticity (Fig. Santos et al., 2009). NMDA receptors are described to be more stable in the synapse. Nevertheless, recent studies have shown that NMDA receptors are also highly mobile in the post-synaptic membrane (Fig. Hunt and Castillo, 2012).

In this section, the influence of neddylation on AMPA and NMDA receptor trafficking was analyzed. Evoked AMPA and NMDA currents were obtained from CA1 neurons in acute hippocampal brain slices that were treated with $1 \mu\text{M}$ MLN-4924 for 30 minutes. AMPA currents were measured at -70 mV, NMDA currents at $+40$ mV. In order to compare the effect MLN-4924 treatment has on both synaptic currents, AMPA/NMDA currents were calculated.

First, AMPA and NMDA currents were evoked in control slices treated with vehicle. In a second batch of experiments, $1 \mu\text{M}$ MLN-4924 was infused with ACSF for 30 minutes before AMPA and NMDA currents were obtained. MLN-4924 treatment led to an increase in the AMPA/NMDA ratio (Fig. 4.32A, B). To exclude that this effect might be dependent on neddylation inhibition in

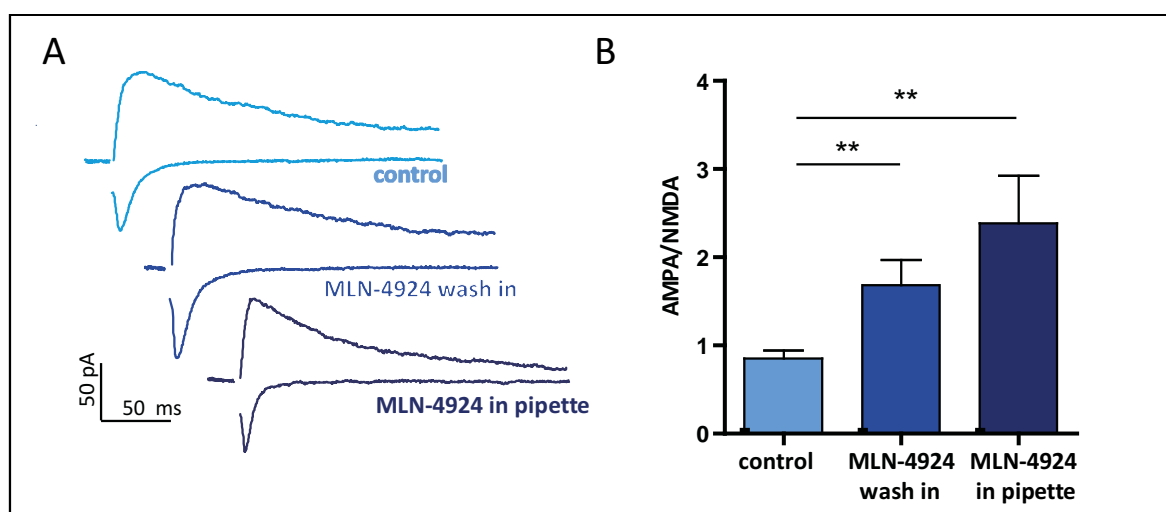


Figure 4.32: MLN-4924 treatment leads to an increase in AMPA/NMDA ratio. **A)** Representative traces of AMPA and NMDA currents from CA1 hippocampal neurons of acute hippocampal slices. Slices were treated with vehicle or MLN-4924 by bath application or MLN-4924 was directly applied to the post-synapse *via* the patch pipette. **B)** AMPA/NMDA ratios are increased in MLN-4924 treated slices (dark blue) compared to control slices (light blue). This effect is even more pronounced when MLN-4924 was applied through the patch pipette (black blue).

the pre-synapse, MLN-4924 was applied to the internal solution of the patch pipette to exclude that the effect MLN-4924 has on pre-synaptic function (Section 4.13) influences the results obtained from the post-synapse. When neddylation is specifically blocked in the post-synapse, the AMPA/NMDA ratio also increases compared to control neurons treated with vehicle, indicating that the result is specific for post-synaptic receptors (control: 0.85 ± 0.10 , $n = 12$; MLN-4924 wash-in: 1.68 ± 0.29 , $n = 11$; MLN-4924 in pipette: 2.39 ± 0.54 , $n = 8$; $p < 0.05$ for control vs. MLN-4924 wash-in; $p < 0.05$ for control vs. MLN-4924 in pipette) (Fig. 4.32A, B). These recordings demonstrate that neddylation inhibition leads to an increase in the AMPA/NMDA ratio, which is more pronounced when MLN-4924 treatment is restricted to the post-synaptic side. These results suggest that MLN-4924 treatment either leads to a decrease in NMDA currents or to an increase in AMPA currents. In conclusion, the changes of the AMPA/NMDA current show that the Nedd8 pathway acts on the receptor densities in the post-synaptic membrane. The next goal was to specifically investigate how AMPA and NMDA currents change during neddylation inhibition. Therefore, evoked AMPA and NMDA currents were recorded during the wash-in of MLN-4924.

4.14.3 AMPA EPSCs are Decreased when the Nedd8 Pathway is Blocked

The mEPSC recordings from section 4.14.1 show that MLN-4924 decreases mEPSC amplitude and frequency and thus exerts an impact on AMPA receptor function. In addition, AMPA/NMDA currents obtained in section 4.14.2 indicate that the Nedd8 pathway impacts on receptor density in the post-synaptic membrane. In an initial experiment, the influence of neddylation on AMPA receptor was studied.

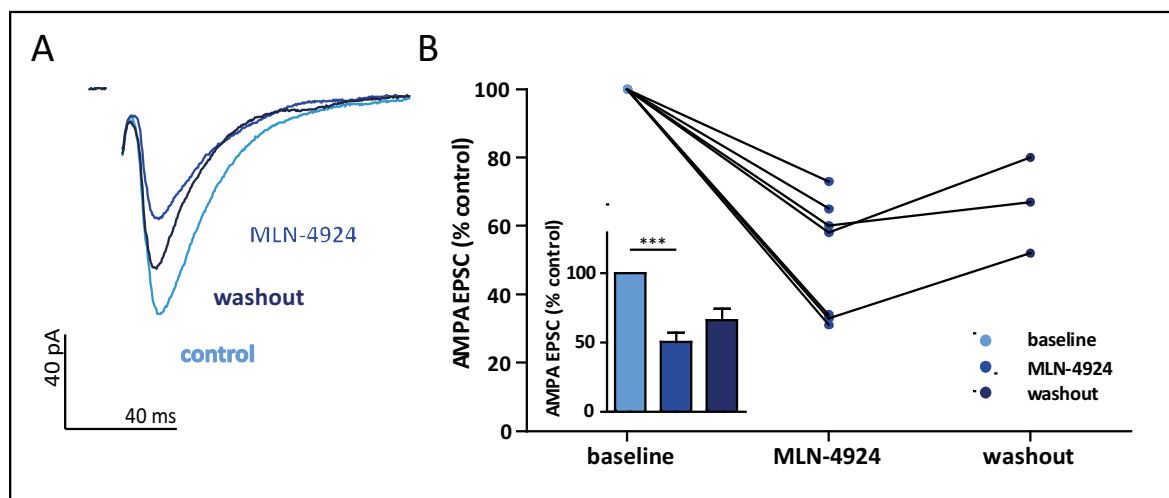


Figure 4.33: 30 minutes of MLN-4924 treatment decreased AMPA current amplitude. Wash-out of MLN-4924 for 30 min partially recovers the decrease of AMPA current amplitude. A) Representative traces of AMPA currents from CA1 hippocampal neurons of acute brain slices before (light blue), during (dark blue) and after MLN-4924 treatment (black blue). **B)** The graph illustrates AMPA currents normalized to baseline for single cell measurements during and after MLN-4924 treatment. AMPA EPSCs decrease during MLN-4924 treatment and partially recover when MLN-4924 is washed out. Graph bar inset shows an overall decrease of 50 % of AMPA EPSC amplitudes and a recovery of the AMPA currents up to 66 % after MLN-4924 wash-out, .

To investigate AMPA current changes during neddylation inhibition, AMPA currents were evoked by Schaffer collateral stimulation and whole cell recordings were obtained from hippocampal CA1 neurons. After reaching a stable baseline for AMPA EPSC amplitude, 1 μ M MLN-4924 was washed in for 30 minutes by the ACSF. During the time of MLN-4924 application, the AMPA current amplitude decreased in all experimental cells (Fig. 4.33A, B). Whereas when MLN-4924 was washed out of the recording chamber, the AMPA EPSC amplitude increased again, showing that the effect of MLN-4924 on AMPA-mediated currents

was **partially** reversible (Fig. 4.33A, B). The graph bar inset illustrates that the AMPA EPSC amplitudes decreased by ~50 % with 30 minutes of MLN-4924 treatment and was reversed to ~66 % of baseline during the wash-out (control: 100, n = 7; MLN-4924: 50.57 ± 6.59 , n = 7; wash-out: 66.33 ± 8.09 , n = 3, $p < 0.001$ for control vs. MLN-4924).

Wash-out experiments were only obtained from half of the recorded cells, because cells had to be excluded when the patch becomes worse during the wash-out. Whole cell recordings are limited in time, since neurons that are filled up with an artificial internal solution suffer and might start to die. Therefore, it might be that AMPA currents might reverse completely after longer time periods. Patch-clamp recordings are limited in answering this question.

In conclusion, AMPA EPSCs decrease upon neddylation inhibition, meaning that AMPA receptors are removed from the post-synaptic membrane. These results give a new insight into the interpretation of the recorded AMPA/NMDA ratios from section 4.14.2. Since MLN-4924 decreases AMPA EPSCs and increases the AMPA/NMDA ratio (Section 4.14.2), NMDA EPSCs have to decrease even stronger during AMPA EPSCs after MLN-4924 treatment. To test this hypothesis, the same experimental design was applied to NMDA EPSC recordings (Section 4.14.4).

4.14.4 NMDA EPSCs are Decreased when the Nedd8 Pathway is Blocked

To test whether NMDA currents decrease upon MLN-4924 application, whole cell recordings were obtained from CA1 neurons in acute hippocampal brain slices.

Cells were clamped on +40 mV and NMDA currents evoked while 1 μ M MLN-4924 was infused. After 30 minutes of MLN-4924 treatment, NMDA current amplitudes were reduced by ~50 %. This effect was not reverted by the wash-out of MLN-4924 for 30 minutes (control: 100, n = 5; MLN-4924 47 ± 1.69 , n = 5; wash-out: 44.00 ± 4.93 , n = 3; for control vs. MLN-4924 $p < 0.05$) (Fig. 4.34A, B). MLN-4924 treatment significantly decreases NMDA receptor currents in the post-synaptic membrane as it was shown for AMPA EPSCs, proving that NMDA receptors are removed from the post-synaptic membrane. In contrast to AMPA currents that partially recover after 30 minutes of MLN-4924 withdrawal, NMDA currents did not recover in 30 minutes. Whether NMDA receptor currents do not recover at all or whether it takes longer

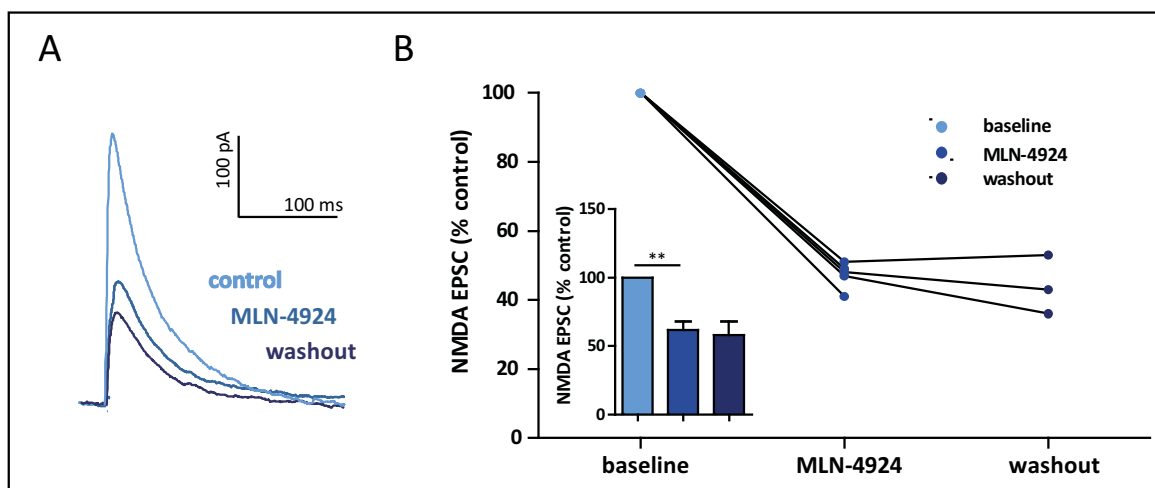


Figure 4.34: MLN-4924 treatment decreases NMDA current amplitude. Wash-out of MLN-4924 for 30 min does not recover the decrease of NMDA current amplitude. **A)** Representative traces of NMDA currents from CA1 hippocampal neurons of acute brain slices before (light blue), during (dark blue) and after MLN-4924 (black blue) treatment. **B)** Graph illustrates NMDA currents normalized to baseline for single cell measurements during and after MLN-4924 treatment. Graph bar inset shows an overall decrease of NMDA EPSCs but no recovery.

than 30 minutes cannot be answered by this experimental design.

The decrease in NMDA EPSCs compared to AMPA EPSCs was not as pronounced as expected based on the results of the AMPA/NMDA ratios under MLN-4924 treatment (Section 4.14.2). AMPA/NMDA ratio was increased stronger when MLN-4924 was applied by the patch-pipette and therefore excluded any pre-synaptic effect. AMPA and NMDA EPSCs recordings should be repeated by applying MLN-4924 with the patch pipette. The strong effect on AMPA EPSCs compared to NMDA EPSCs might be facilitated by a pre-synaptic effect of MLN-4924.

In summary, the last results clearly demonstrate that neddylation inhibition results in a decrease of AMPA and NMDA currents, whereas the effect on NMDA EPSCs might be more pronounced. In conclusion, the Nedd8 pathway is responsible for keeping AMPA and NMDA receptors located in the post-synapse membrane and that neddylation inhibition destabilizes AMPA and NMDA receptors in the post-synaptic membrane.

4.14.5 Decay Times of AMPA and NMDA Currents

Besides the current amplitudes of AMPA and NMDA receptors and thus the number of functional receptors in the post-synapse, the kinetics of both receptors might also change upon neddylation inhibition.

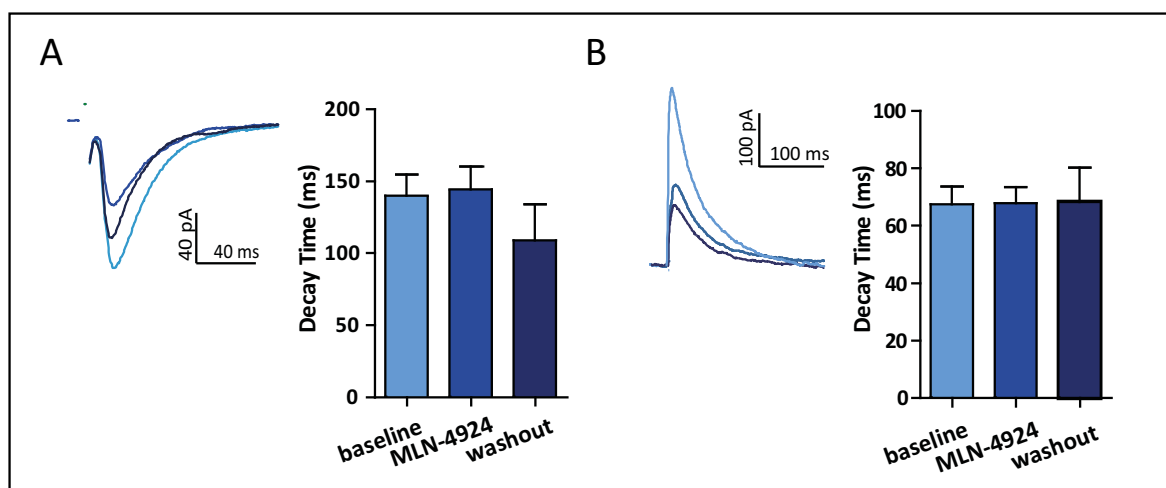


Figure 4.35: MLN-4924 has no effect on AMPA or NMDA kinetics when applied to the bath solution. **A)** On the left side: Representative traces of AMPA currents (like in Figure 4.33). On the right side: The decay time does not change between AMPA currents obtained from the baseline (light blue), MLN-4924 treated slices (dark blue) or during the wash-out (black blue). **B)** On the left side: Representative traces of NMDA currents (like in Figure 4.34). On the right side: The decay time does not change between NMDA currents obtained from the baseline (light blue), MLN-4924 treated slices (dark blue) or during the wash-out (black blue).

A change in the decay time of AMPA receptors can be caused by modifications in the binding of intracellular interaction partners. For instance, a loss of interaction with the well-described AMPA-auxiliary protein stargazing will result in slower GluA1 channel deactivation times (Tomita et al., 2006). For NMDA receptors, the composition of the subunits defines their kinetics. For example, NR2B-containing NMDA receptors have slower decay kinetics compared to NR2A-containing receptors (Cull-Candy and Leszkiewicz, 2004).

AMPA and NMDA decay times (τ) were calculated from the area under the curve from the peak and normalized to the peak amplitude.

Decay times from AMPA and NMDA receptors obtained from MLN-4924 wash-in experiments (Sections 4.33 and 4.34) were analyzed to see whether Nedd8 has an influence on AMPA or

NMDA kinetics. In these experiments 1 μ M MLN-4924 was applied by the ACSF for 30 minutes. No changes were observed for both AMPA and NMDA receptor kinetics when comparing the baseline to MLN-4924-treated conditions or during the wash-out (AMPA: baseline: 139.70 ± 14.71 , $n = 6$; MLN-4924: 144.10 ± 16.11 , $n = 5$; wash-out: 109.00 ± 25.04 , $n = 3$) (NMDA: baseline: 67.50 ± 6.16 , $n = 6$; MLN-4924: 68.00 ± 5.50 , $n = 6$; wash-out: 68.40 ± 11.75 , $n = 3$) (Fig. 4.35A, B).

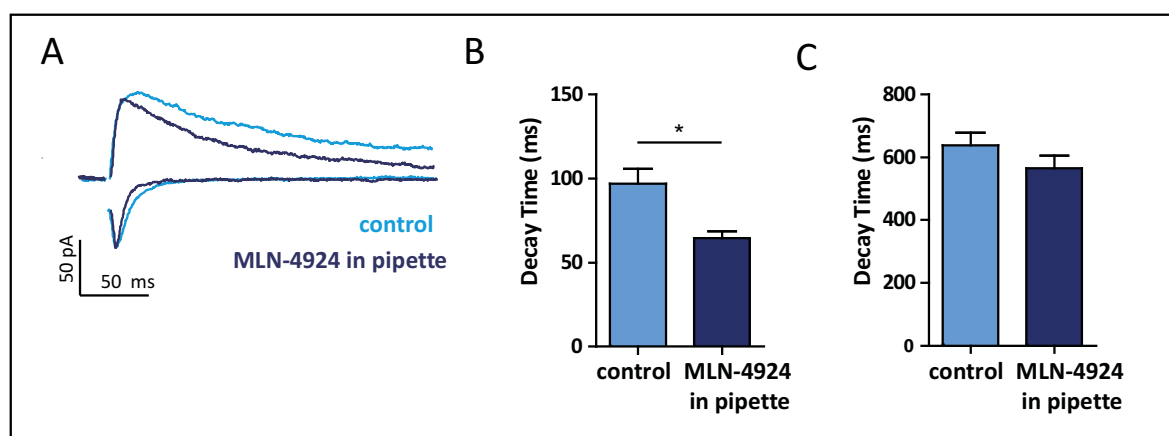


Figure 4.36: MLN-4924 treatment reduces the AMPA decay time when applied to the patch pipette. No differences are found for NMDA EPSCs. A) Representative traces of AMPA and NMDA currents from CA1 hippocampal neurons of acute hippocampal slices (like Figure 4.32). **B)** The decay time of AMPA EPSCs decreases when MLN-4924 is added to the patch pipette. **C)** No changes are found in the NMDA mEPSC decay time after MLN-4924 treatment through the patch pipette.

Additionally, decay times were calculated from AMPA/NMDA ratio experiments when MLN-4924 was directly applied to the patch pipette for 15 minutes (Section 4.14.2). No changes in the decay time were obtained for NMDA EPSCs, thus NMDA receptor composition did not change upon MLN-4924 treatment (control: 638.8 ± 40.09 , $n = 6$; MLN-4924 in pipette: 564.30 ± 41.12 , $n = 7$) (Fig. 4.36A, B). In contrast, the decay time of AMPA EPSCs decreased around ~40 % (control: 97.09 ± 8.80 , $n = 10$; MLN-4924 in pipette: 64.29 ± 4.46 , $n = 8$; $p < 0.01$ for control vs. MLN-4924 in pipette) (Fig. 4.36A, B).

The lack of effect on NMDA receptor kinetics indicates that neddylation does not impact on NMDA receptor subunit composition in the post-synaptic membrane. In contrast, neddylation inhibition does decrease the decay times of AMPA receptor currents. In conclusion, neddylation influences the interaction of AMPA receptors with auxiliary proteins like stargazin. Other

factors, such as pre-synaptic effects, can be excluded, since the decrease in decay time was only detected when MLN-4924 was added to the intracellular solution.

4.14.6 The Current Amplitude of Somatic Outside-Out Patches Increases upon MLN-4924 Treatment

In the previous section 4.14.3 it was shown that AMPA receptors are removed from the post-synaptic membrane upon neddylation inhibition. AMPA receptors are also located at extra-synaptic sites, to enable trafficking of AMPA receptors in and out of the synapse. In the next experiment, it was investigated whether AMPA receptor concentration at extra-synaptic sites changes upon neddylation inhibition. This result will give a more detailed view of the mechanism of neddylation in AMPA receptor localization.

Somatic outside-out patches were recorded before and after 1 μ M MLN-4924 treatment. In this experiment the amount of AMPA receptors at the soma was determined.

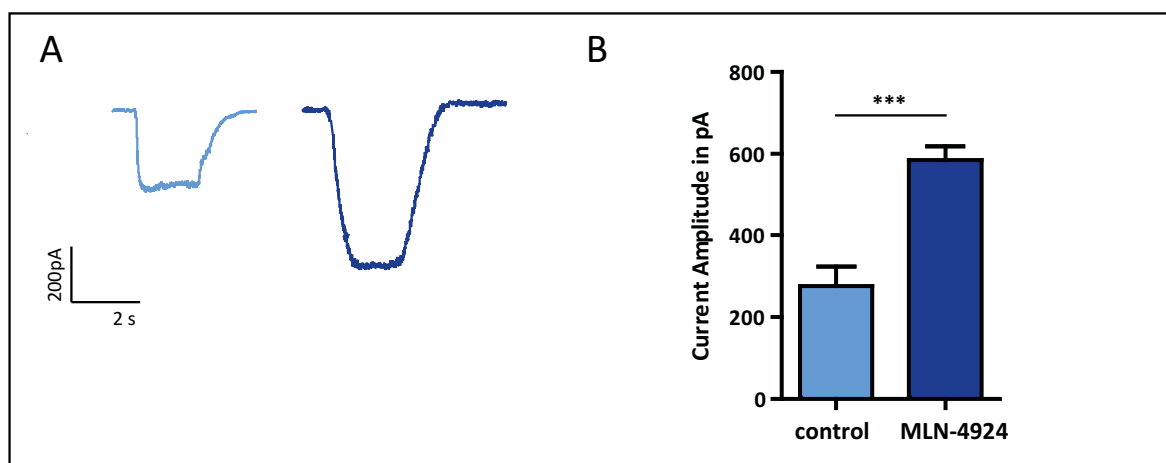


Figure 4.37: MLN-4924 increases somatic expression of AMPA receptors. **A)** Representative current traces from somatic outside-out patches of control (light blue) and MLN-4924-treated CA1 neurons (dark blue) from acute hippocampal brain slices. **B)** Quantification of steady-state current revealed that MLN-4924 significantly increased AMPA current amplitude at extra-synaptic sites.

Figures 4.37A and B show that somatic AMPA receptor currents were increased by ~50 % after 30 minutes of 1 μ M MLN-4924 treatment compared to untreated cells (control: 275.70 ± 48.02 , $n = 6$; MLN-4924: 584.00 ± 33.11 , $n = 5$; $p < 0.001$ for control vs. MLN-4924). Thus, the amount of AMPA receptors in the somatic compartments increased upon neddylation inhibition,

whereas the density of post-synaptic AMPA receptors decreased (Section 4.14.3). Whether the increase is due to lateral diffusion of post-synaptic AMPA receptors to the soma, or whether the increase in somatic AMPA receptors is a compensatory mechanisms to overcome the deficit of AMPA receptors in the post-synapse upon MLN-4924 treatment, will be the focus of further studies.

4.15 Neddylation Effects on Inhibitory Synapses

Given that the inhibition of the Nedd8 pathway has a strong effect on excitatory neurotransmission, the influence of MLN-4924 on neurotransmission of inhibitory synapses was investigated. For these experiments, miniature inhibitory post-synaptic currents (mIPSC) were obtained in primary cell cultures. As for mEPSC recordings, the mIPSC frequency is a measurement of the number of synapses onto the patched neuron and the mIPSC amplitude represents a measurement of the amount of functional receptors in the post-synaptic membrane.

Primary neurons were treated for 30 minutes with vehicle or 1 μ M MLN-4924 before mIPSC were obtained. The cumulative distribution of the mIPSC amplitude is significantly decreased in primary hippocampal neurons treated with MLN-4924 compared to vehicle treated neurons (KS: $p < 0.0001$ for control amplitude vs. MLN-4924 amplitude) (Fig. 4.38A , B). Also, the mean mIPSC amplitude was significantly reduced in MLN-4924-treated neurons, indicating that neddylation inhibition destabilizes GABA_A receptors in the post-synaptic membrane (control: 79.04 ± 8.38 pA, $n = 10$; MLN-4924: 57.56 ± 5.51 pA, $n = 10$; $p < 0.05$ for control vs. MLN-4924) (Fig. 4.38B, graph inset). The mIPSC interevent interval as well as the mean frequency of control and MLN-4924-treated slices did not differ from each other (control: 0.42 ± 0.08 Hz, $n = 10$; MLN-4924: 0.48 ± 0.12 Hz, $n = 10$) (Fig. 4.38A, C). The lack of effect on mIPSC frequency indicates that the number of inhibitory synapses was unaltered when neddylation was blocked.

In addition, mIPSCs were obtained in acute hippocampal brain slices, a system where neurons are embedded in a more physiological condition and might respond differently to MLN-4924 treatment. 30 minutes of 1 μ M MLN-4924 application in acute hippocampal brain slices had the

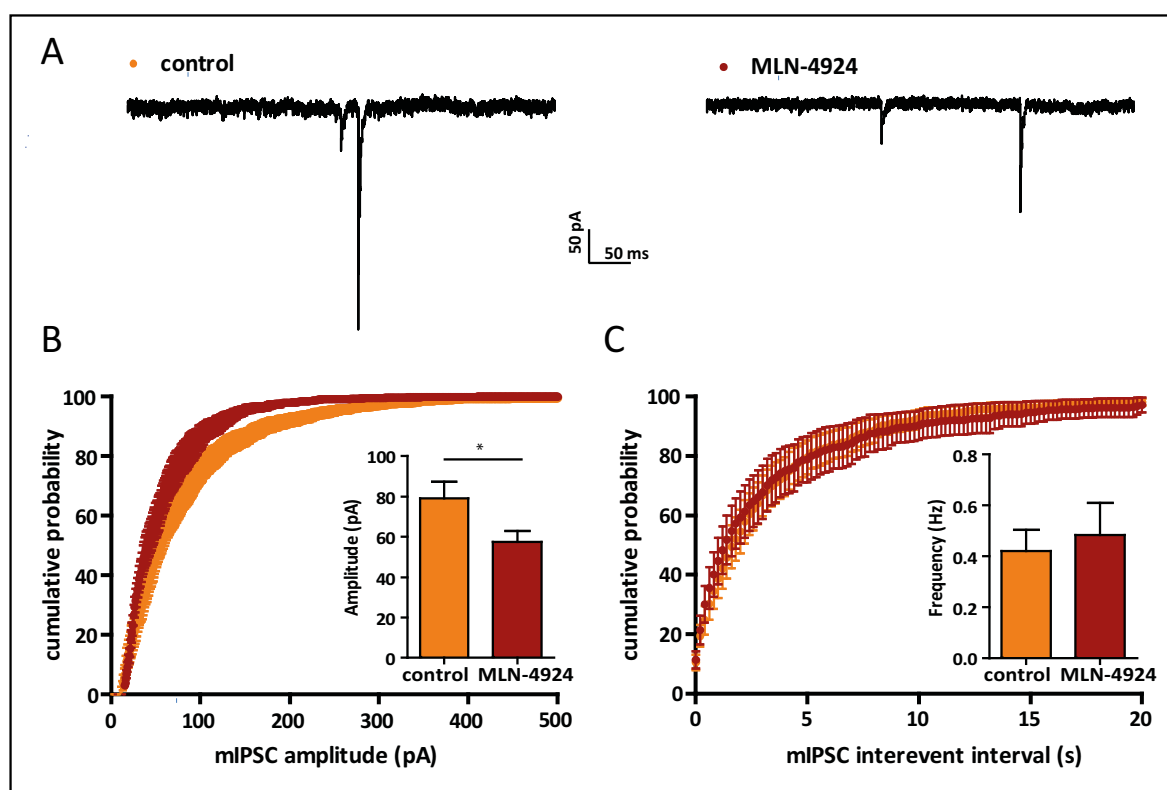


Figure 4.38: The Nedd8 pathway is essential for basal neurotransmission at inhibitory synapses of primary hippocampal neurons. **A)** Representative whole cell recordings from primary hippocampal neurons DIV18-19. **B)** Cumulative distribution of mIPSC amplitude. The inset shows mean mIPSC amplitude. The mIPSC amplitude of MLN-4924-treated primary hippocampal neurons is reduced compared to control neurons. **C)** Cumulative distribution of mIPSC interevent interval as well as the mean mIPSC frequency show no changes between MLN-4924-treated primary hippocampal neurons and control neurons.

same effect on mIPSC as in primary hippocampal neurons. The cumulative probability of mIPSC amplitude as well as the mean amplitude decreased upon MLN-4924 treatment (KS: $p < 0.0001$ for control amplitude vs. MLN-4924 amplitude; control: 45.24 ± 6.24 pA, $n = 10$; MLN-4924: 30.50 ± 1.31 pA, $n = 10$; control vs. MLN-4924 $p < 0.05$) (Fig. 4.39A, B), whereas no differences were found in the interevent interval or in the mean frequency of the obtained mIPSC recordings (control: 5.45 ± 0.56 Hz, $n = 10$; MLN-4924: 5.01 ± 0.84 Hz, $n = 10$) (Fig. 4.39A, C).

mIPSC recordings from CA1 neurons of acute hippocampal brain slices and primary hippocampal neurons indicate that neddylation is important for the receptor distribution at the post-synapse of inhibitory neurons. The number of functional synapses is unaltered upon neddylation inhibition. Whether there are additional effects at the pre-synapse of inhibitory neurons

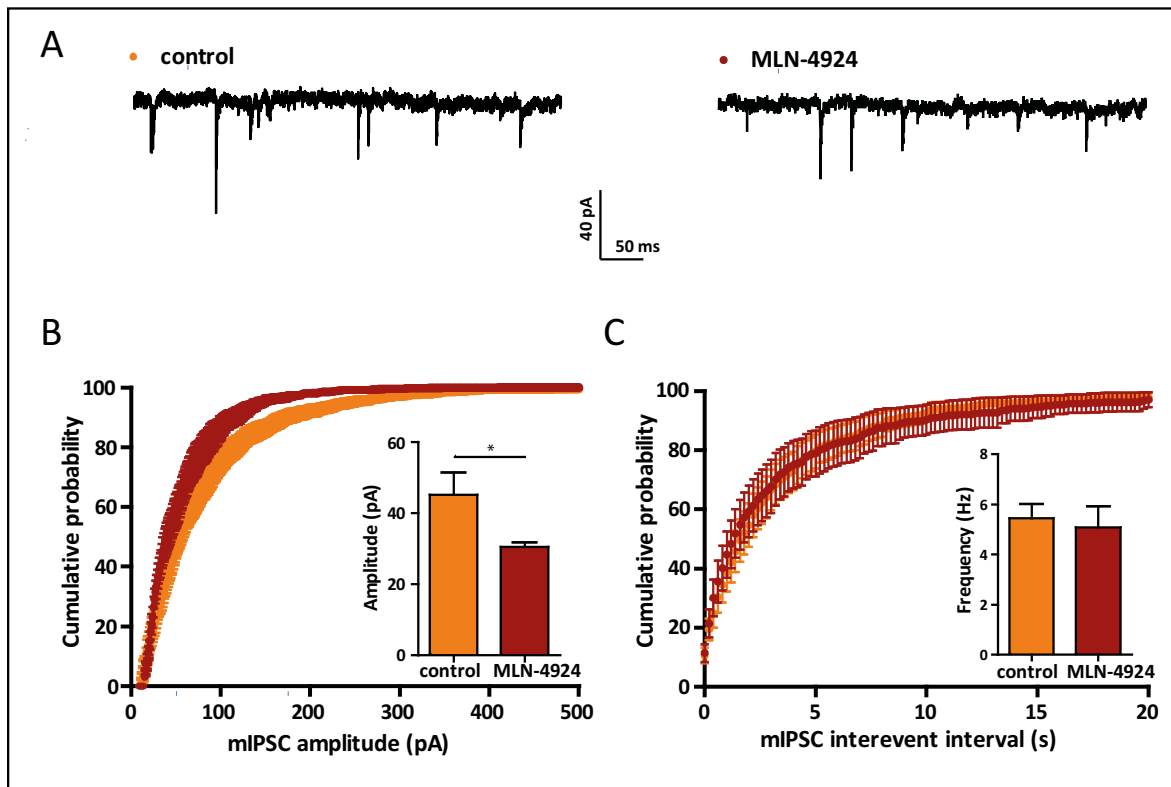


Figure 4.39: The Nedd8 pathway is essential for basal neurotransmission at inhibitory synapses obtained in acute brain slices. **A)** Representative whole cell recordings of mIPSCs in acute brain slices. **B)** Cumulative distribution of mIPSC amplitudes. The inset shows mean mIPSC amplitude. The mIPSC amplitudes of MLN-4924-treated neuron are reduced compared to control neurons. **C)** Cumulative distribution of mIPSC interevent intervals as well as the mean mIPSC frequencies show no changes between MLN-4924 or vehicle treated brain slices.

and how the receptor number of the post-synapse is altered upon neddylation inhibition, is a matter of further studies.

4.16 Neddylation in Synaptic Plasticity

Previous electrophysiological experiments, including recordings of excitatory and inhibitory synapses, focus on the effect neddylation has on basal neurotransmission. Other post-translational modifications, like ubiquitylation, have been shown to be involved in basal neurotransmission as well as in synaptic plasticity (reviewed in Schwartz, 2003). Subsequently, experiments were conducted that study the impact of the Nedd8 pathway on synaptic plasticity.

Two different approaches were chosen to investigate neddylation in synaptic plasticity: On the one hand, biochemical experiments were conducted in primary hippocampal neurons focusing on changes in neddylation upon increased neuronal activity. On the other hand standard electrophysiological tests such as LTP and LTD were obtained in acute brain slices with or without the E1 inhibitor MLN-4924. These experiments indicate whether neddylation is involved in the induction of synaptic plasticity.

4.16.1 Glutamate Treatment Increases PSD-95 Neddylation

Post-translational modifications, such as ubiquitylation, have been shown to alter protein concentrations upon neuronal activity (Ehlers, 2003). To see whether target protein neddylation also changes upon neuronal activity, primary neurons were treated with 10 μ M glutamate for half an hour 1 h, 2 h, 6 h, and 12 hours. From all lysates crude synaptosomes were obtained to study protein and neddylation changes in the synapse. In line with other studies, glutamate application resulted in increased PSD-95 protein concentrations in the synapse, whereas β -actin protein concentrations, a loading control, did not change (Fig. 4.40A). Furthermore, protein lysates were immunoblotted against α -Nedd8 to see whether neuronal activity changes the pattern or the amount of neddylated synaptic proteins. The western blot in Figure 4.40A shows that within the first hour of glutamate treatment, the concentration of neddylated proteins slightly increased. After 1 hour of glutamate application the level of neddylated proteins was reduced to basal levels (Fig. 4.40A). Additionally, the pattern of neddylated protein changes when the Nedd8 pathway was blocked, indicated by the yellow asterisks in figure 4.40A.

In conclusion, increased neuronal activity induced by glutamate application increased the amount of neddylated proteins, including PSD-95, for the first hour. Interestingly, the protein amount of PSD-95 continuously increased within 12 hours of glutamate application, whereas the amount of neddylated proteins in general was back to basal after 1 hour.

Given that the amount of neddylated protein as well as the concentration of PSD-95 changes in the synapse upon glutamate application, co-immunoprecipitations were obtained from synaptosome preparations of primary neuronal lysates that were treated for 4 hours with 10 μ M glutamate in order to see whether the level of neddylated PSD-95 changes upon glutamate treatment.

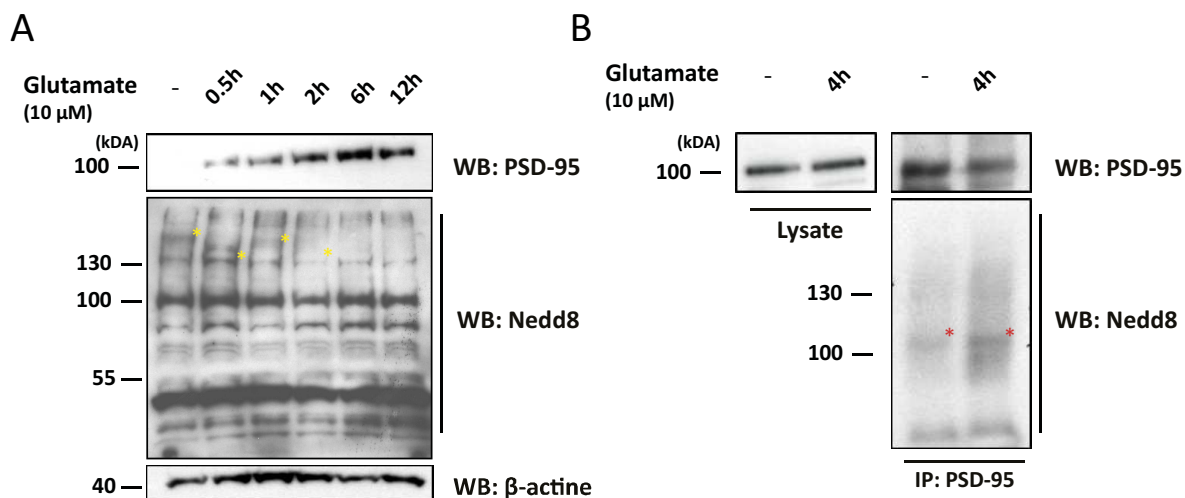


Figure 4.40: Continuous treatment with glutamate increases PSD-95 neddylation. **A)** Primary neurons were treated with 10 μM glutamate for the indicated time points. Western blots show that the amount of neddylated PSD-95 increases upon glutamate treatment. Additionally, the pattern of neddylated proteins changes as well, whereas the protein amount of β-actin shows no difference. Yellow asterisks indicate the changes in the neddylation pattern induced by glutamate treatment. **B)** Co-immunoprecipitation from primary neurons treated with 10 μM of glutamate for 4 hours shows an increase in PSD-95 neddylation compared to cell lysates from untreated neurons. Red asterisks represent neddylated PSD-95 bands.

Figure 4.40B clearly indicates that the amount of neddylated PSD-95 was increased upon glutamate application (Fig. 4.40, red asterisks). Subsequently, one might speculate that the increase in PSD-95 concentration correlates with its neddylation.

A drawback of the last experiment was that primary neurons were treated for 4 hours with glutamate. This long period of glutamate application does not represent any physiological condition and therefore the observed effects are hard to interpret. Consequently, the experiment was repeated with a shorter time interval (10 minutes) of glutamate treatment, a time window also used for chemical LTP induction (Kopec et al., 2007). The obtained results show that 10 minutes of 10 μM glutamate application also increased PSD-95 protein concentration from 10 min up to 1 hour in synaptosomes of primary neurons (Fig. 4.41A). Neddylation of target proteins is slightly increased 0.5 hours after glutamate treatment (Fig. 4.41A). Protein concentrations of tubulin were unchanged upon glutamate application. These experiments show that shorter intervals of glutamate treatment are also sufficient to induce changes in protein levels in the synapse of primary hippocampal neurons. Furthermore, it was tested whether the short application of glutamate also alters the neddylation of synaptic PSD-95. Co-immunoprecipitations from synap-

tosome preparations were obtained from untreated primary neurons and from primary neurons, 1 hour after glutamate treatment, using α -PSD-95 antibodies (10 μ M of glutamate for 10 minutes). The duplicates proved that 10 minutes of 10 μ M glutamate application increased PSD-95 protein levels in the synapse, even 50 minutes after glutamate withdrawal (Fig. 4.41B, Lysate). Additionally, PSD-95 neddylation was increased 50 minutes after glutamate treatment (Fig. 4.41, IP, red asterisks).

In conclusion, 10 minutes of increased neuronal activity induced by glutamate is sufficient to increase PSD-95 concentration as well as PSD-95 neddylation for at least 1 hour.

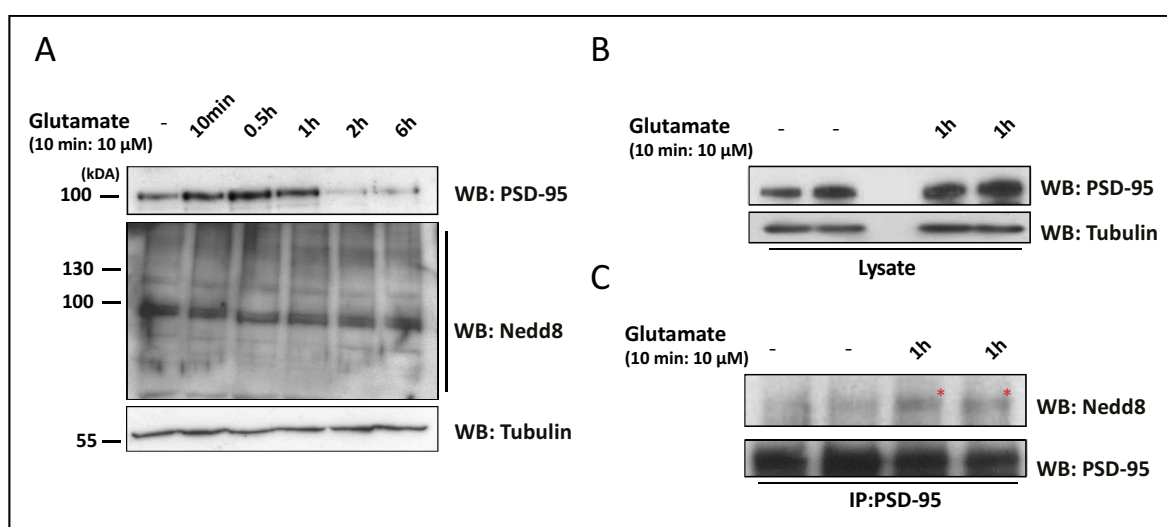


Figure 4.41: Short-term glutamate activation also increases PSD-95 neddylation. **A)** Glutamate treatment for 10 minutes increases PSD-95 concentration for 1 hour. Neddylated proteins as well as tubulin protein concentration do not change upon glutamate treatment. **B)** Protein lysates from primary neurons collected 1 hour after a 10 minutes treatment of glutamate show an increase of PSD-95 concentration compared to untreated protein lysates. **C)** Co-immunoprecipitation samples from the same lysates, reveal an increase of neddylated PSD-95 1 hour after glutamate activation. Red asterisks indicate neddylated PSD-95 bands.

Although glutamate application in primary neuronal cultures cannot be directly related to synaptic plasticity, these experiments demonstrated that high neuronal activity increases neddylation of target proteins. Especially, PSD-95 neddylation is increased upon glutamate treatment.

4.16.2 MLN-4924 Prevents LTP Induction

Synaptic plasticity includes long-term potentiation (LTP) which is induced by high frequency stimulation at a chemical synapse. LTP results in an increased synaptic strength that is characterized by an increased neurotransmission and is associated with learning and memory.

Since Nedd8 strongly influences basal neurotransmission at excitatory synapses, it was tested whether the Nedd8 pathway plays a role in the induction of LTP.

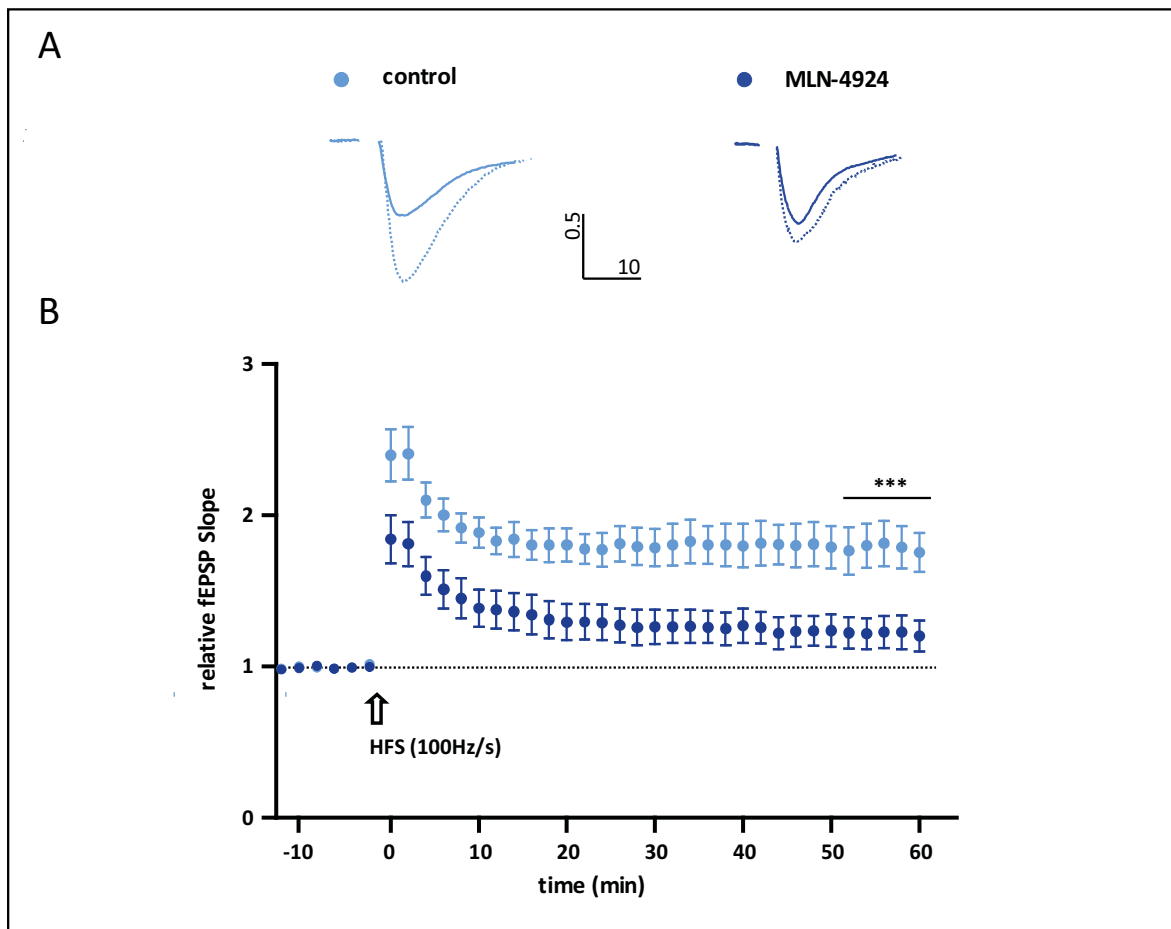


Figure 4.42: MLN-4924 prevents LTP induction in acute hippocampal brain slices. fEPSP were obtained before and after LTP induction in control and MLN-4924 treated brain slices. **A)** Representative traces depict average fEPSP recordings before (solid line) and 50 min after LTP induction (dotted line). **B)** MLN-4924 treatment inhibits the induction of LTP. Dotted line represents baseline. Arrow depicts time of LTP induction.

First, acute hippocampal slices were treated for 30 minutes with 1 μ M MLN-4924 until a stable baseline of fEPSP was obtained. Then, LTP was induced using a high frequency (100 Hz/s)

stimulation for 1 second of the Schaffer collaterals and fEPSP recorded in the CA1 area for another 60 minutes. In control slices fEPSP were significantly increased to the baseline 60 minutes after LTP induction (Fig. 4.42A, B). In contrast, the slope of fEPSPs from MLN-4924-treated slices increased only slightly after LTP induction (control: 1.81 ± 0.01 , $n = 5$; MLN-4924: 1.25 ± 0.003 , $n = 5$; $p < 0.0001$ for control vs. MLN-4924) (Fig. 4.42A, B).

These results indicate that neddylation inhibition prevents LTP induction at the CA3-CA1 synapses in acute brain slices.

4.16.3 Ubc12-C111S Interferes with LTP Induction

Besides the treatment with the E1 inhibitor MLN-4924 (Section 4.16.2), neddylation can also be blocked by the overexpression of Ubc12-C111S. Ubc12-C111S plasmids were electroporated in the hippocampus of CD1 embryos at E14.5 using in utero electroporation. Acute brain slices were obtained from control animals expressing GFP or from neddylation deficient mice expressing Ubc12-C111S at P16-20. LTP was induced in acute hippocampal brain slices expressing GFP or Ubc12-C111S by high frequency stimulation (100 Hz/s) for 1 second. High frequency stimulation increased the size of fEPSP slopes after LTP induction in brain slices expressing GFP. In contrast, the size of fEPSP slopes in Ubc12-C111S-expressing brain slices did not increase after LTP induction compared to baseline fEPSP slopes (control: 1.23 ± 0.001 , $n = 5$; Ubc12-C111S: 1.06 ± 0.003 , $n = 5$; $p < 0.0001$ for control vs. Ubc12-C111S) (Fig. 4.43A). This experiment shows that the overexpression of Ubc12-C111S in acute hippocampal brain slices blocks the induction of LTP.

In this experiment, Ubc12-C111S was already expressed during development. In conclusion, the absence of neddylation during synaptic development prevents LTP induction.

To see whether neddylation inhibition also impairs LTP induction when neddylation is blocked after synaptic development, an inducible vector of Ubc12-C111S was electroporated, allowing timed neddylation inhibition.

For these experiments, inducible Ubc12-C111S was in utero electroporation at E14.5 and expression was induced by tamoxifen injection after P7. Thus, the effect of Ubc12-C111S on synaptic plasticity in mature neurons could be assessed. For control slices, E14.5 pups were in

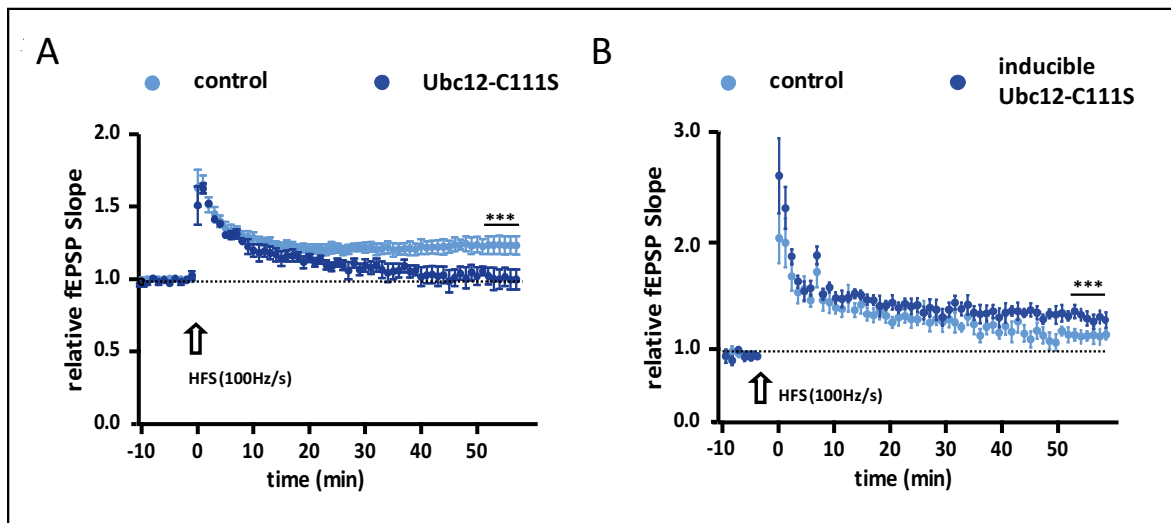


Figure 4.43: Ubc12-C111s expression during development as well as in adult neurons prevents LTP induction. **A)** Ubc12-C111S was electroporated at E14.5 *via* in-utero electroporation. Overexpression of Ubc12-C111S during the development completely blocked LTP induction. Dotted line represents baseline. Arrow depicts time of LTP induction. **B)** Inducible Ubc12-C111S was electroporated at E 14.5 *via* in-utero electroporation in CamK2-Cre-ERT2 mice and overexpression induced by tamoxifen treatment from P35. LTP recordings were performed from P50 animals and also showed an impaired LTP induction when Ubc12-C111S is overexpressed in mature neurons.

utero electroporated with an inducible GFP plasmid.

Control slices expressing GFP showed increased fEPSP slopes after LTP induction whereas the increase in Ubc12-C111S expressing slices were significantly smaller after LTP induction (control: 1.33 ± 0.001 , $n = 7$; Ubc12-C111S: 1.15 ± 0.01 , $n = 7$; $p < 0.0001$ for control vs. Ubc12-C111S) (Fig. 4.43B).

In summary, these results demonstrate that neddylation inhibition *via* the overexpression of Ubc12-C111S, blocks LTP induction. However, the effect on LTP induction is stronger when the Nedd8 pathway is already blocked during synaptic development.

4.16.4 MLN-4924 Prevents LTD Induction

Long-term depression is another form of synaptic plasticity characterized by a decrease in synaptic strength evoked by low frequency stimulation.

To investigate whether neddylation impacts on LTD, acute brain slices were treated for 30 minutes with either vehicle or MLN-4924. LTD was induced *via* slow frequency stimulation (1 Hz

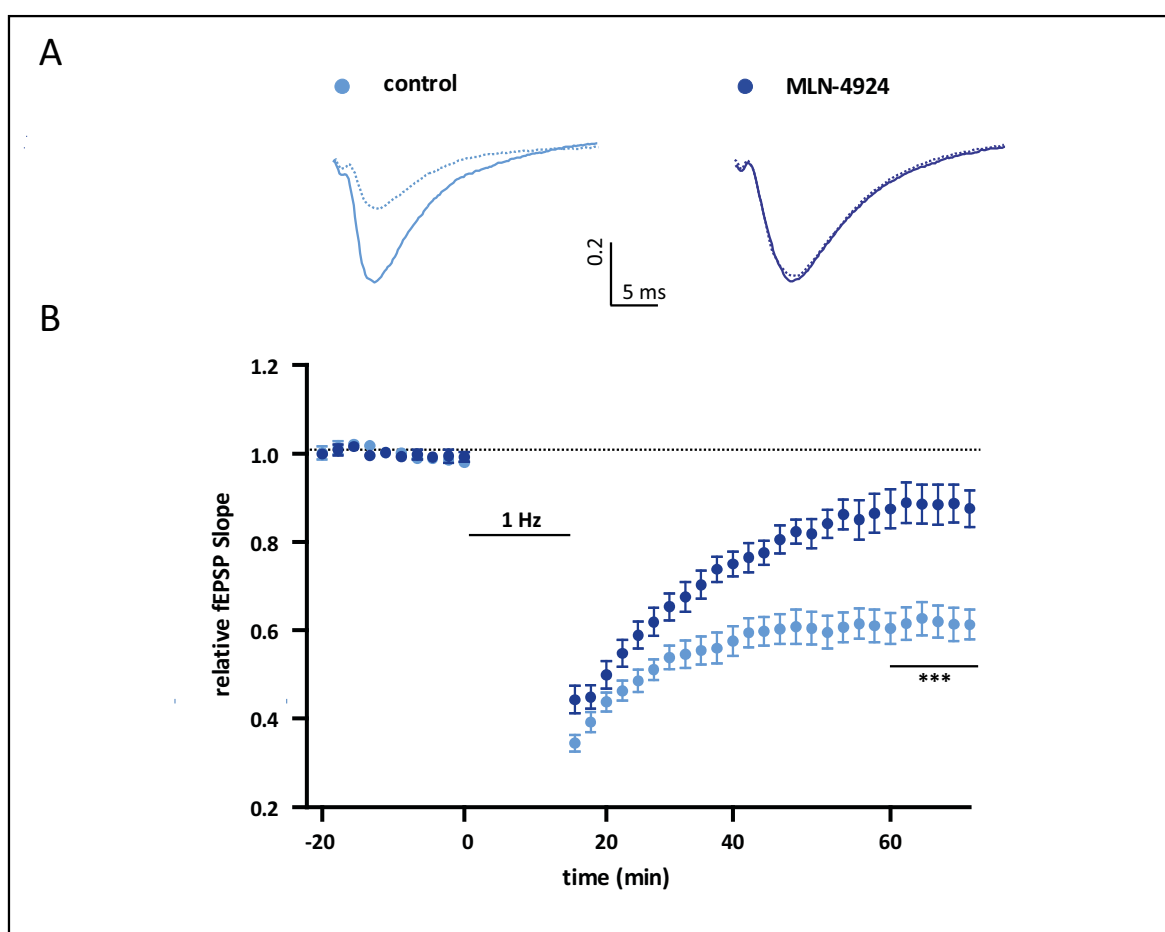


Figure 4.44: MLN-4924 treatment prevents LTD induction. Extracellular field potential recordings (fEPSP) were obtained before and after LTD induction in control and MLN-4924 treated acute brain slices. A) Representative traces depict average fEPSP recordings before (solid line) and 50 min after LTD induction. **B)** LTD is not observed when acute brain slices are pre-treated with MLN-4924. Dotted line represents baseline. Horizontal bar depicts the time of LTD induction.

for 15 min) after obtaining a stable baseline. fEPSP slopes, 40 minutes after LTD induction were significantly smaller for control slices compared to MLN-4924-treated slices (control: 0.62 ± 0.0001 , $n = 5$; MLN-4924: 0.89 ± 0.001 , $n = 5$; $p < 0.0001$ for control vs. MLN-4924) (Fig. 4.44A, B).

In conclusion, these experiments show that MLN-4924 treated slices failed to induce LTD. Consequently, the Nedd8 pathway is essential for intracellular mechanisms inducing the induction of long-term depression.

In summary, the results from section 4.16 show that the Nedd8 pathway plays an important

role in synaptic plasticity. Molecular studies show that the amount and the pattern of neddylated proteins changes during increased neuronal activity. Furthermore, the protein amount of PSD-95 as well as the neddylation of PSD-95 increase upon neuronal activity.

Additionally, electrophysiological studies show that neither LTP nor LTD can be induced when the Nedd8 pathway is blocked. Meaning that AMPA receptors cannot be inserted nor removed sufficiently from the post-synaptic membrane when neuronal activity is changed.

In conclusion, the Nedd8 pathway is essential for synaptic plasticity by targeting proteins in the PSD, like PSD-95.

5 Discussion

The regulation of protein function is a key feature of every eukaryotic cell. In neurons, for example, complex functions such as short-term plasticity and long term plasticity have been associated with post-translation modifications (PTM) that change the protein function or trigger protein synthesis or protein degradation *via* the proteasome (McGaugh, 2000). Many studies describe how PTMs affect neuronal function. Proteins can be modified by the binding of small molecules such as phosphate groups, methyl or acetyl groups, palmitoylation, glycosylation, fucosylation or by direct binding of polypeptides (Pickard et al., 2001, Swank and Sweatt, 2001, El-Husseini Ael et al., 2002, Hochstrasser, 2009). The first protein that was described to change protein function by its binding is ubiquitin. So far, other ubiquitin-like proteins have been described, such as, Nedd8, FubI, Fat10, ISG-15, SUMO1-3, Isg15, Atg8, Atg12, Urm1 and Ufm1 (Hochstrasser, 2009). Of all these modifications, only ubiquitylation and sumoylation have been well-described as active processes in the brain, regulating neuronal functions by protein modification.

In this work, the impact of neddylation on synaptic function was investigated. Until now it has been described that Nedd8 is expressed in the brain (Kumar et al., 1992). Furthermore some studies demonstrated that neddylation can be associated with neurodegenerative diseases. Nedd8 has been found in neuronal and glial inclusions, in Alzheimer's diseases, and in Lewy bodies in Parkinson's disease (Dil Kuazi et al., 2003, Mori et al., 2005). Moreover, it has been shown that the absence of E3–ligase neddylation of the ubiquitin pathway can trigger Parkinson's disease and Huntingtons's disease pathology. The inhibition of the neddylation pathway results in the reduced activity of the E3 ligase parkin that leads to an accumulation of miss/or unfolded proteins in the neuron (Choo et al., 2012). Additionally, it was shown that the neddylation of Cullin3 promotes its interaction with NUB1, which mediates mHTT degradation upon

poly-ubiquitylation (Lu et al., 2013). If neddylation is reduced, neuronal death is increased by increasing amounts of mHTT. All studies describing the impact of neddylation on neuronal diseases do not describe neuron-specific targets of the Nedd8 pathway, although they demonstrate that neuronal diseases can be correlated to a dysfunction of the Nedd8 pathway. None of these studies focuses particularly on the Nedd8 pathway itself. Hence, it is still important to demonstrate that the Nedd8 pathway is active in the brain and whether there are additional targets of the Nedd8 pathway beyond the E3-ligases for ubiquitylation.

5.1 Neddylation is Active in Neurons

Before starting to study the impact of neddylation on neuronal function, it is mandatory to show that Nedd8 and the proteins involved in its conjugating cascade are expressed in neurons.

Nedd8 was first described in the mouse brain in 1992 (Kumar et al., 1992). This finding correlates with our results which show by western blot analysis that Nedd8 is expressed in neuronal lysates. Furthermore, we could demonstrate that Nedd8 is also present in pre- and post-synaptic compartments, indicating that neddylation might also exert its function in the synapse, as it was also shown for ubiquitylation and sumoylation (Yi and Ehlers, 2005, Martin et al., 2007, Mabb and Ehlers, 2010). Nedd8 is coupled to its target proteins *via* an enzymatic cascade. This cascade contains an activating enzyme E1, a conjugating enzyme E2, and an E3 ligase that finally transfers Nedd8 to target proteins. The E1 activation enzyme of the neddylation pathway that is composed of Appbp1, also known as Nae1, and of Uba3 are also present in the brain. As the name β -amyloid precursor protein binding protein 1 indicates, Appbp1 was originally described to bind to β -amyloid precursor protein (APP) (Chow et al., 1996, Chen et al., 2000). Appbp1 and Uba3 is ubiquitously expressed in neurons and are required e.g. for cell cycle progression (Joo et al., 2010). Its expression is increased in the hippocampus of an Alzheimer's diseased brain, which additionally indicates that neddylation is important for neuronal function (Chen et al., 2000, 2003).

The conjugating enzyme of the Nedd8 pathway, Ubc12, is also expressed in neurons (Chen et al., 2000). These findings correlate with our results from mouse hippocampal lysates that showed

Ubc12 expression in neurons and especially in pre- and post-synaptic compartments. Moreover, western blot analysis revealed that neddylation is active in pre- and post-synaptic compartments of the synapse, since Ubc12-Nedd8 conjugates and neddylated proteins were found throughout all synaptic compartments.

The expression of Mdm2, an E3 ligase for the Nedd8 pathway identified in this work, is also well described in the brain (Steinman et al., 2004). However, in contrast to Ubc12 and the Appbp1-Uba3 complex, Mdm2 function is not restricted to the Nedd8 pathway. Mdm2 also acts as an E3 ligase for the ubiquitylation of PSD-95 (Colledge et al., 2003). These results clearly demonstrate that Mdm2 acts as an E3 ligase for synaptic proteins.

Appbp1, Uba3 and Ubc12 are highly specific for neddylation. Although Nedd8 and ubiquitin have high protein similarity, one amino acid at residue 72 where in Nedd8 an alanine is placed and in ubiquitin an arginine determines the interaction of Ubc12 to Nedd8 and not to ubiquitin (Walden et al., 2003). Furthermore, the interaction between the E1 and E2 is highly conserved, since Ubc12 forms docking sites that are highly specific for a groove generated by loops conserved in Uba3 but not in other E1s (Huang et al., 2004). In conclusion, the presence of Appbp1, Uba3 and Ubc12 and their activity in synaptic compartments is sufficient to neddylate synaptic proteins.

In summary, Nedd8 and the proteins involved in the Nedd8 pathway are expressed in the brain and even in synaptic structures. The fact that Uba3 and Ubc12 are highly specific for Nedd8 additionally strengthens the hypothesis that neddylation is relevant for synaptic function. Therefore, the identification of neddylation targets would be the next goal to demonstrate that neddylation is functionally active in the brain and to understand the functional impact on target protein neddylation.

5.2 PSD-95 is a Target of the Nedd8 Pathway

In the literature, many neuronal proteins are described as being modified by ubiquitin or SUMO. Surprisingly, no neuron specific targets of the Nedd8 pathway have been described, although western blot analyses reveal a smear of neddylated proteins in brain lysates.

Cullins are the best described targets of the Nedd8 pathway and it was shown that neddylation increases cullin activity and thereby promotes target protein ubiquitylation. Besides cullins, just a few substrates of the Nedd8 pathway have been described: p53, p73, EGFR and the E3 ligase parkin (Harper, 2004, Oberst et al., 2005, Oved et al., 2006, Um et al., 2012). In this study, we described the first neddylated post-synapse specific protein, PSD-95. Most of the experiments that revealed PSD-95 neddylation were done in HEK293 cells by overexpression of PSD-95 and Flag-Nedd8. However, there are studies claiming that the specificity of the conjugating pathways for Nedd8 and ubiquitin can be altered by changing the ratio of Nedd8 to ubiquitin. Consequently, ubiquitylated substrates would be able to be neddyated by the ubiquitin pathway when Nedd8 is overexpressed (Hjerpe et al., 2012). If this hypothesis is true, PSD-95 neddylation in HEK293 cells might be mediated by the ubiquitin pathway. To disprove these concerns, co-immunoprecipitation studies from primary neurons showed PSD-95 neddylation under endogenous expression of PSD-95 and Nedd8. Additionally, the fact that GKAP was not found to be neddyated after overexpression in HEK293 cells, although it is known that GKAP is ubiquitylated *via* the E3 ligase TRIM3, indicates that the overexpression of Flag-Nedd8 does not automatically promote protein neddylation (Hung et al., 2010). Also, mass spectrometry revealed a number of neddyated lysine residues of PSD-95 that are similar in primary cell culture and transiently transfected HEK293 cells. All these experiments show that the overexpression of Nedd8 does not unspecifically increase the number of neddyated lysine residues or neddyated targets.

Additionally, we showed that Ubc12 mediates the neddylation of PSD-95. Inhibiting the Ubc12 function prevents PSD-95 neddylation and thus demonstrates that Ubc12 is essential to mediate PSD-95 neddylation. Furthermore, the application of the Nae1 inhibitor MLN-4924 blocks the neddylation of PSD-95. All experiments blocking neddylation indicate that the postulated Nedd8 pathway is involved in PSD-95 neddylation and that the overexpression of Nedd8 does not lead to PSD-95 neddylation by using the ubiquitin pathway. The inhibition of the Nedd8 pathway in all experiments resulted in a decreased smear of neddyated proteins in western blot analyses. In conclusion, Nae1 and Ubc12 are also specific for the neddylation of neuronal targets beyond PSD-95.

To discard the possibility that neddylation can be mediated *via* the ubiquitin pathway is especially important for PSD-95 since PSD-95 is neddylated and ubiquitylated *via* the same E3 ligase. Previous studies reported that Mdm2 is involved in the ubiquitylation of PSD-95 (Colledge et al., 2003). The fact that the Ring finger domain mutant of Mdm2 (Mdm2-C464) lacks neddylation of PSD-95 demonstrates that Mdm2 acts also as an E3 ligase for the Nedd8 pathway. Given that PSD-95 is neddylated and ubiquitylated by the same E3 ligase raises the question whether Nedd8 and ubiquitin act synergistically or competitively on PSD-95 function. The competition for the same lysine residues is common for post-translational modifications and was already described for SUMO and ubiquitin that compete for the same lysines (Ulrich, 2005). In the future, the identification of the stimuli that trigger PSD-95 neddylation and/or ubiquitylation could give additional information about the regulatory mechanisms of the post-translation modifications. Previously, it was reported that Mdm2 directly interacts with p53 and thereby promotes its ubiquitylation (Bottger et al., 1997, Haupt et al., 1997, Kubbutat et al., 1997). p53 can be poly-ubiquitylated and thus degraded by the proteasome or mono-ubiquitylated which promotes the nuclear export of p53. In both cases, transcriptional activity of p53 is kept low, for example after stress stimuli such as ultraviolet radiation (UV) (Xirodimas et al., 2004, Kulikov et al., 2010, Lee and Gu, 2010, Liu and Xirodimas, 2010). In p53, 9 lysine residues have been described to be modified, whereby six of them are mono- or poly-ubiquitylated by Mdm2 (Lee and Gu, 2010). Three of the ubiquitylated lysine residues have also been found to be neddylated (Xirodimas et al., 2004, Brooks and Gu, 2006). Two different studies using a fusion construct of p53-Nedd8 for proximal lysine residues show that neddylation of p53 decreases the transcription function compared to wild type p53 (Xirodimas et al., 2004, Abida et al., 2007). Taken together, ubiquitin and Nedd8 modifications exert a synergistic function on p53 by Mdm2-dependent conjugation. Another characterized target for Nedd8 and ubiquitin is the epidermal growth factor receptor (EGFR). EGFR is also neddylated and ubiquitylated by the same E3 ligase c-Cbl, whereby EGFR neddylation increases the efficiency of its ubiquitylation and facilitates lysosomal degradation (Oved et al., 2006). In this example, the ubiquitin and Nedd8 pathway also co-operate on protein function. Both studies indicate that ubiquitin and Nedd8 exert the same effect on the p53 and EGFR function. Nevertheless, the studies are limited, since not all modified lysine

residues have been studied in detail.

In this study we showed that PSD-95 is neddylated and ubiquitylated by Mdm2. Previous studies showed that the p53 neddylation and ubiquitylation by Mdm2 exert the same effect on p53 function. Our results indicate that ubiquitylation or neddylation of PSD-95 can be favored by increasing the available amount of ubiquitin or Nedd8. This means that when ubiquitin is overexpressed, the neddylation of PSD-95 is decreased. This result indicates that ubiquitin and Nedd8 compete for PSD-95 modification. The competition might lead to the hypothesis that neddylation and ubiquitylation act differently on PSD-95 function. Additionally, NMDA treatment increases the ubiquitylation of PSD-95 and thus promotes PSD-95 degradation *via* the proteasome (Colledge et al., 2003). In contrast, glutamate treatment increases PSD-95 neddylation and the protein level of PSD-95 in the synapse. In summary, these results show that neddylation and ubiquitylation of PSD-95 are triggered by different stimuli and that both modifications compete for PSD-95 binding. Additionally, it was shown that the protein amount of PSD-95 was differentially regulated by Nedd8 and ubiquitin.

One main interest in the research of post-translational modifications is to identify sequences that allow for the prediction of whether a protein will be modified by ubiquitin or other UBLs. For example, SUMO substrates could be identified by searching the core motif required for Sumo conjugation, Ω KXE (where Ω is a bulky hydrophobic residue) (Bernier-Villamor et al., 2002, Lin et al., 2002). The E2-conjugating enzyme Ubc9 of the SUMO pathway directly binds to the consensus motif and thereby transfers SUMO to lysine residues. Since the consensus motif is found in over 30 % of all characterized proteins but not all of them could be proven to be sumoylated, there might be false positive proteins that have to be excluded from being targets of the SUMO pathway. Although there are studies that try to identify consensus sequences for ubiquitin, no exact motive has been identified so far (Xu et al., 2010). Nevertheless, a polypeptide sequence enriched in proline (P), glutamate (E), serine (S), and threonine (T), named PEST domain has been described in proteins that are ubiquitylated and degraded *via* the proteasome (Shumway et al., 1999, Spencer et al., 2004). By mutating the PEST domain protein, ubiquitylation is prevented and thus protein stability increased. The same was shown for PSD-95, whose protein sequence contains a PEST domain on its N-terminal that promotes PSD-95 ubiquitylation (Colledge et al.,

2003). Interestingly, we observed that the PEST domain is necessary for PSD-95 neddylation. Hence, the E2-conjugating enzyme Ubc12 interacts with the PEST domain of PSD-95. By mutating or deleting the PEST domain, the interaction of PSD-95 and Ubc12 is lost and PSD-95 is not neddylated anymore. However, the protein sequences from p53 and EGFR do not include a PEST domain (epestfind; <http://emboss.bioinformatics.nl/cgi-bin/emboss/epestfind>), indicating that the PEST motif is not mandatory for the neddylation of every target. Further studies will be needed to understand whether the PEST domain is also involved in the neddylation of other target proteins. In the future it will be interesting to see whether the neddylation or ubiquitylation *via* the PEST domain is dependent on PEST domain phosphorylation as it was shown for the PEST-dependent ubiquitylation of other target proteins (Shumway et al., 1999, Spencer et al., 2004). First results indicate that N-terminal phosphorylation of PSD-95 suppresses PSD-95 multimerization (Nelson et al., 2006) and that the phosphorylation is mediated *via* Cdk5 (Morabito et al., 2004). Additionally, another study reported that NMDA receptor activation activates Cdk5 in a Ca^{2+} /calmodulin-dependent manner (Wei et al., 2005). Taking all the results together, one might speculate whether NMDA receptor activation promotes PSD-95 phosphorylation *via* Cdk5 that will increase PSD-95 ubiquitylation and thereby inhibit PSD-95 multimerization. The potential influence of neddylation on this process is the focus of further studies.

In summary, PSD-95 neddylation is mediated by an enzymatic cascade including Nae1, Ubc12, and Mdm2. Ubc12 and Mdm2 interact with PSD-95 *via* the N-terminal PEST domain and therefore promote PSD-95 neddylation.

5.3 Identification of Neddylated Lysine Residues

In recent years, many studies have concentrated on the identification of ubiquitylated and sumoylated lysine residues (Witze et al., 2007, Jeram et al., 2009, Vertegaal, 2011). The identification of modified lysine residues is essential to understand the functional impact of post-translational modifications. Using mass spectrometry, neddylated and ubiquitylated lysine residues are identified that afterwards can be mutated to arginines to prevent its modifications. This amino acid

exchange prevents protein modification on the mutated amino acid and thus morphological as well as functional changes can be analyzed when post-translational modifications are prevented at specific sites.

Before proteins can be analyzed by mass spectrometry they have to be cleaved into smaller peptides *via* trypsin or lysine C. ubiquitin and UBLs are linked *via* an isopeptide bond to their target proteins. This covalent binding allows UBLs to remain conjugated to lysines during the whole mass spectrometry analysis process. Ubiquitin and UBLs will also be cleaved *via* trypsin or Lysine C and leave a remnant on the modified lysine residue. As a result of their protein sequence and the specific cleavage sites for trypsin which cleaves carboxy-terminals to lysines and arginines, ubiquitylated lysine residues remain GG remnants at modified lysines. In addition, Nedd8 trypsination results in GG remnants that make it impossible to discriminate between ubiquitylated and neddylated lysine residues after trypsin digestion. Lysine C digestion cleaves carboxyl-terminal to lysine residues resulting in larger remnants after trypsination, which differ between Nedd8 and ubiquitin. Nevertheless, this approach is impractical for mass spectrometry analysis, since the resulting remnants are too large to be analyzed.

To overcome this limitation, Nedd8 mutants were generated that result in bigger remnants after trypsination and therefore allow the discrimination between neddylated and ubiquitylated lysine residues. Two of the generated mutants can be coupled to target proteins, and PSD-95 neddylation is abolished when treated with MLN-4924, thus the mutants are functionally processed. Nedd8-V that only differs in one amino acid to the other two Nedd8 mutants could not be coupled to PSD-95 or any other neddylation target. This result indicates that small changes in the sequence of Nedd8 are already sufficient to prevent target neddylation. It underlines previous findings that post-translational modifications, including neddylation, are strictly regulated to prevent fous bindings.

Mass-spectrometry analysis of PSD-95 revealed neddylated and ubiquitylated lysine residues of PSD-95. Lysine residue modifications were detected throughout the whole PSD-95 sequence. Since PSD-95 is a multi-domain protein, neddylation of PSD-95 in different domains might exert multiple functions. The generalized neddylation of PSD-95 indicates that Nedd8 might regulate multiple functions of PSD-95 and that Nedd8 modification is not restricted to controlling

one specific subdomain-dependent function of PSD-95. Additionally, these findings strengthen the importance of identifying the neddylation lysine residues of PSD-95. Mutations that prevent single neddylation events of PSD-95 allow for the investigation of the specific impact of neddylation on PSD-95 function. A general inhibition of PSD-95 neddylation would effect a number of PSD-95 modifications and allows for no conclusion about single neddylation lysine residues. Until now, a number of post-translational modifications have been described in different domains of PSD-95 that alter e.g. PSD-95 stability and therefore synaptic function. Also, studies with truncated versions of PSD-95 that lack different subdomains of PSD-95 have tried to shed light on regulatory mechanisms on PSD-95 (Craven et al., 1999, Xu et al., 2008, Shipman et al., 2011). On the N-terminus of PSD-95, two different post-transcriptional modifications are described: PSD-95 palmitoylation at C3 and C5 (Craven et al., 1999). Palmitoylation of PSD-95 is diminished upon glutamatergic neurotransmission (El-Husseini Ael et al., 2002), while blocking of synaptic activity leads to increased PSD-95 palmitoylation (Noritake et al., 2009). In addition, PSD-95 can also be nitrosylated at the same cysteines. Upon NMDA receptor activation and subsequent Ca^{2+} influx, PSD-95 induces nitric oxide (NO) production by mediating the interaction between NMDA receptors and nitric oxide synthase (nNOS) (Christopherson et al., 1999). Accordingly, nitrosylation of PSD-95 blocks its palmitoylation and subsequently PSD-95 is removed from the post-synapse site (Ho et al., 2011). In the N-terminal domain of PSD-95, K10 had been found to be ubiquitylated (Bianchetta et al., 2011) which is thought to impact on PSD-95 dimerization (Hsueh et al., 1997, Morabito et al., 2004). The phosphorylation of N-terminal serine and threonine residues had also been shown to negatively regulate the clustering of PSD-95 (Morabito et al., 2004). Furthermore, our results clearly demonstrate that PSD-95 oligomerization is diminished when neddylation is blocked. However, they did not reveal any ubiquitylated or neddylation lysine residues at the N-terminus of PSD-95. This result might be due to low protein coverage during mass spectrometry analysis in the N-terminal protein sequence of PSD-95.

PDZ 1 of PSD-95 is weakly modified by post-translational modifications and also in this study no lysine residues were found to be ubiquitylated or neddylation in this protein domain.

NMDA receptors have been shown to interact with PDZ 2 of PSD-95 (Cui et al., 2007). In this

domain, 5 lysine residues are modified by ubiquitin or Nedd8, whereby two of them are certainly neddylated and two of them ubiquitylated. Since no phosphorylation sites were identified in PDZ 2 of PSD-95, ubiquitin and Nedd8 are the only post-translational modifications in this protein domain.

PDZ 3 of PSD-95 where 2 modified lysine residues were found, has been described interacting with DHCC5 a palmitoyltransferase which alters hippocampal dependent learning (Li et al., 2010). Furthermore, PRR7, a membrane protein with a still unclear function (Murata et al., 2005) and neuroligins have been found to interact with PDZ 3 (Irie et al., 1997). The interaction of neuroligins and PSD-95 regulates the development of excitatory and inhibitory synapses (Levinson and El-Husseini, 2005). Since PSD-95-K393R is located in PDZ 3 of PSD-95 and displays strong effects on spine development, the protein interaction of PSD-95 with PRR7 or neuroligins might be altered upon neddylation inhibition.

In the SH3 domain, two modified lysines have been identified that might impact on PSD-95 function. SH3 mainly interacts with Pyk2, whose clustering and activation is required during long-term potentiation mediated by NMDARs at CA3-CA1 synapses (Seabold et al., 2003, Bartos et al., 2010). Additionally, the SH3 domain of PSD-95 interacts with EB3, which is important during dendritic development while interacting with microtubules (Sweet et al., 2011).

The GK domain of PSD-95 contains a high number of possible ubiquitylation, neddylation, and phosphorylation sites. GK is the fundamental domain of PSD-95 to build up the core structure of the post-synapse by interacting with other scaffold proteins, such as GKAP (Kim et al., 1997, Takeuchi et al., 1997), and other proteins like MAP1 (Reese et al., 2007), S-Cam (Hirao et al., 2000), and SPAR (Pak et al., 2001).

PSD-95 as a scaffold for the post-synapse has multiple interaction partners and the interactions are highly regulated. Depending on the subdomain-location of neddylated lysine residues, neddylation might differentially alter PSD-95 function. Further studies with PSD-95 mutants that specifically lack neddylation at specific sites, are needed to characterize the influence neddylation has on PSD-95 function.

In this study a number of lysine residues have been described that might exert a functional impact on PSD-95. When blocking the neddylation of PSD-95 in general by MLN-4924, PSD-95

oligomerization is disturbed. Since PSD-95 dimerization is depending on the N-terminus of PSD-95, altered neddylation in this domain might be responsible for the impaired clustering. However, K157 is the most proximal lysine residues to the N-terminus of PSD-95 and is already located in the PDZ 2. Consequently, no lysine residue for the N-terminus was described in our study that might explain the observed defect in dimerization. Another study that identified ubiquitylated sites in PSD-95 showed that K10 is modified by GG remnants (Bianchetta et al., 2011). Also, the protein coverage for the N-terminus of PSD-95 was low compared to other parts of PSD-95 and thus we might have missed PSD-95 modification at the N-terminus. It is even possible that the lack of dimerization is not due to the absence of PSD-95 neddylation. Since MLN-4924 blocks neddylation of all proteins that are involved in synaptic function, neddylation inhibition of other target proteins might be responsible for the missing dimerization of PSD-95.

Additionally, one has to consider that although the PDZ 1 and PDZ 2 are structurally different, they functionally work as a molecular tandem and are often referred to as PDZ 1+2. PDZ 1+2 work as a molecular tandem, since the two domains remain in close proximity and form intramolecular interactions (Sainlos et al., 2011). As a consequence, neddylation of PDZ 2, as it was shown for K193 and K202, might indirectly affect the structure of PDZ 1 and therefore alter the molecular function of the entire PDZ 1+2 tandem.

To overcome these limitations in interpretation, it is necessary to investigate single PSD-95 mutants beyond K202 in which the neddylation is prevented specifically at one or more lysine residues.

5.4 PSD-95-K202R Impact on Neuronal Morphology and Function

Lysine 202 of PSD-95 showed up in mass spectrometry experiments. It was shown that K202 is modified by the Nedd8 mutants and that its neddylation is blocked when MLN-4924 was added, implying that the modification is functional. PSD-95-K202 modification also appeared

in primary neurons under endogenous conditions. These findings were supported by a study by Wagner et al. which already found K202 to be modified by –GG remnants (Wagner et al., 2012), but does not allow for the differentiation of ubiquitin or Nedd8 modification.

Given that K202 of PSD-95 is neddylated, we wanted to know which functional impact neddylation at K202 might exert on PSD-95 function.

One important finding for PSD-95 was that its overexpression leads to an increased spine density and spine size in primary neurons (El-Husseini et al., 2000) as well as in organotypic slice cultures (Stein et al., 2003, Ehrlich and Malinow, 2004), whereas acute knockdown of PSD-95 decreases spine size (Ehrlich et al., 2007). In contrast to the overexpression of PSD-95-WT, PSD-95-K202R overexpression does not increase spine size although it is integrated into the post-synapse. Thus, the lack of effect does not depend on a de-localization of PSD-95-K202R out of the synapse but on the function it exerts in the post-synaptic compartment. K202 is located in PDZ 2 of PSD-95 which had already been shown to be involved in PSD-95 function. Its mutation decreases the size of PSD-95 clusters and spine morphology in young neurons (Nonaka et al., 2006). These results are in line with our findings showing that PSD-95-K202R does not mimic the function of PSD-95-WT overexpression in primary hippocampal neurons.

In addition, it was shown that the overexpression of PDZ 1 and PDZ 2 of PSD-95 enhances AMPA dependent neurotransmission (Schnell et al., 2002). In contrast, Migaud and colleagues (Migaud et al., 1998) did not see any changes in AMPA receptor transmission using truncated PSD-95 PDZ 1+2. The different results can be explained by the experimental design of each group. In the experimental set-up of Schnell et al. truncated PSD-95 is overexpressed in neurons expressing endogenous PSD-95, whereas Migaud et al. used neurons from knockout mice. Thus, in neurons still expressing the full-length PSD-95, an increase in AMPA neurotransmission can still be observed when truncated and endogenous PSD-95 act in duo. The more important aspect of our experiments is that the overexpression of PSD-95-K202R has a dominant negative effect on AMPA mEPSC amplitude in developing neurons, although endogenous PSD-95 is still expressed.

A dominant negative effect on AMPA currents was already described for other scaffold proteins, such as SAP97. SAP97-I38G had been shown to alter the dimerization of SAP97. Hence,

AMPA EPSCs are decreased when SAP-I38G is overexpressed in organotypic brain slices, since AMPA receptors cannot be stabilized in the post-synapse (Nakagawa et al., 2004). Whether this effect is also true for PSD-95-K202R is still unknown, but the fact that MLN-4924 blocks the oligomerization of PSD-95 and decreases the amplitude of AMPA currents might point towards a similar mechanism.

Furthermore, it might be that the lack of neddylation induces conformational changes or precludes certain interactions during spine formation that might explain the decrease in AMPA mEPSC amplitude. In summary, de-neddylation of PSD-95-K202 in developing neurons leads to a decrease of AMPA receptors in the post-synaptic membrane. The frequency of the mEPSC is unaltered compared to control neurons but decreased compared to PSD-95-WT-expressing neurons. Thus PSD-95-K202R does not decrease the number of spines but decreases the number of functional AMPA receptors in the post-synaptic membrane.

The opposite effect of PSD-95 K202R overexpression is found in mature neurons that are already decorated with mature spines. Here, the overexpression of PSD-95-K202R does not influence the amplitude of AMPA mEPSC compared to control, but had a dominant negative effect on the interevent interval. Thus, PSD-95-K202R is not able to increase the number of AMPA receptors in the post-synapse compared to PSD-95-WT. Additionally, PSD-95-K202R overexpression decreases the number of functional spines. This reduction in mEPSC frequency was observed when PSD-95 was knockdown by shRNAs (Ehrlich et al., 2007) and might be explained by the formation of AMPA-lacking synapses, called silent synapses.

The deficits in AMPA mEPSC observed upon PSD-95-K202R overexpression might be explained by a loss of protein interaction or by conformational changes that appear when neddylation is blocked. TARPs and especially stargazin are the best characterized proteins that interact with PSD-95 and stabilize AMPA receptors in the post-synaptic membrane. Mutants of stargazin that lack the C-terminal protein sequence and consequently lose PDZ binding result in a decrease in AMPA mEPSC frequency and amplitude (Chen et al., 2000, Bats et al., 2007). Besides stargazin, a lot of other proteins have been described as interacting with PSD-95 by PDZ 1 and PDZ 2 for example Kalrinin-7, Presco, SynGap, and neuroligins (Xie et al., 2007, Lee et al., 2008, Kim et al., 2009, Mondin et al., 2011). Down-regulation of these proteins results

in altered AMPA mEPSCs. To further dissect the effect of PSD-95-K202R on AMPA mEPSCs, additional interaction studies are needed that might explain the functional background.

5.5 Functional Impact of Neddylation on Basal Synaptic-Transmission at Excitatory Synapses

Neurons and especially synapses are highly dynamic structures that have the ability to respond to differences in signal strength by regulating the neurotransmitter released from the pre-synapse or receptor density in the post-synapse. Those regulatory mechanisms are controlled by post-translational modifications like phosphorylation and ubiquitylation (Yokoi et al., 2012). Poly-ubiquitylation in neurons plays an important role during neuronal development and differentiation, but also mature neurons can rapidly adapt to external stimuli by the ubiquitin pathway (Yi and Ehlers, 2005). This can be achieved by protein poly-ubiquitylation and subsequent degradation *via* the proteasome, or by mono-ubiquitylation of e.g. AMPA receptors (Lin et al., 2011, Schwarz et al., 2010). Mono-ubiquitylation induces a change in protein function and lead to AMPA receptor endocytosis. Nevertheless, it has been shown that proteasome inhibition does not influences basal neurotransmission (Fonseca et al., 2006). In conclusion, the effect of the ubiquitin pathway and protein degradation *via* the proteasome is an important mechanism for synaptic plasticity but apparently not relevant for basal neurotransmission.

In this study we have shown that MLN-4924 diminishes basal neurotransmission. These changes in neurotransmission are obtained before morphological defects were observed. Therefore, the activity of the Nedd8 pathway is needed to maintain synaptic function under basal conditions. Nevertheless, the experiments done in the presence of MG132 and MLN-4924 are hard to compare, since MG132 does not block the ubiquitylation of target proteins but the subsequent degradation. An E1 inhibitor of the ubiquitin pathway, PYR-41, that reduces target protein ubiquitylation has been published (Yang et al., 2007). But so far it has not been investigated whether this inhibitor also alters basal neurotransmission. Additionally, PYR-41 treatment leads to an accumulation of sumoylated proteins (Ulrich, 2005) and the effect of PYR-41 cannot be restricted to

the inhibition of the ubiquitin pathway. Consequently, PYR-41 is not suitable for investigating the effect of ubiquitylation.

Since neddylation impacts on basal neurotransmission, further analyses were conducted to specify the impact of the Nedd8 pathway on pre- and post-synaptic functions.

5.5.1 Neddylation is Involved in Pre-Synaptic Functions

Although several studies in mice did not observe an impact on basal synaptic transmission when the proteasome system is blocked, some invertebrate studies showed changes in pre-synaptic strength when the degradation of proteins is blocked. In *Aplysia*, proteasome inhibition in the pre- or in the post-synapse increases synaptic strength *via* protein synthesis in 24 hours (Zhao et al., 2003). In primary neurons it was shown that proteasome inhibition for 1-2 hours increased the size of the vesicle pool upon neuronal activity (Willeumier et al., 2006). Furthermore, proteasome inhibition results in an increase in fEPSP slope and decreased PPF ratios (Yao et al., 2007). Given that several studies show that post-translational modifications can alter synaptic strength and that neddylation decreases basal neurotransmission, the impact of neddylation on pre-synaptic function was investigated.

In this study, short-term pre-synaptic plasticity was investigated with different stimulation protocols. The first approach, measuring paired-pulse facilitation, is based on residual calcium in pre-synapse boutons. During PPF, two stimuli are given briefly to the pre-synapse, whereby the second response is facilitated by residual calcium in the pre-synapse. Neddylation inhibition increases paired pulse facilitation which is associated with a decreased release probability of vesicles from the pre-synapse. Decreased release probability has been associated with the dysfunction or loss of many pre-synaptic proteins (Takahashi et al., 1996, Yao et al., 2007). The number of pre-synaptic proteins that alter paired-pulse facilitation is enormous and indicates the fine tuning and complexity of pre-synaptic neurotransmitter release. Since so many proteins are involved in neurotransmitter release, the increases paired-pulse facilitation upon neddylation inhibition does not allow for a conclusion about possible target proteins for the Nedd8 pathway.

A number of studies claim that pre-synaptic facilitation is not just dependent on residual calcium in pre-synaptic boutons, but is caused by acting on pre-synaptic calcium sensors (Bain and Quas-

tel, 1992, Atluri and Regehr, 1996). Synaptotagmin rapidly binds calcium with low affinity and is therefore suited to quickly bind calcium and evoke vesicle fusion. The quick turnover of synaptotagmin does not make it a first choice calcium sensor to explain facilitation. Nevertheless, synaptotagmin is described to be poly-ubiquitylated by the E3 ligase parkin (Huynh et al., 2003). Since synaptotagmin is important for vesicle formation and docking, this suggests a role for Parkin and thus ubiquitylation in the regulation of the synaptic vesicle pool and vesicle release from pre-synaptic sites. Synaptotagmin knockouts display an increase in PPF ratio similar to neddylation inhibition. In conclusion, one might speculate whether neddylation controls synaptotagmin function and thereby impacts on synaptic vesicle release. Synaptotagmin function might be regulated *via* the neddylation of Parkin or directly by synaptotagmin modification as it was described for ubiquitin.

Another mechanism to control pre-synaptic vesicle release involves depression followed by a tetanic stimulation. The tetanic stimulation is sufficient to deplete all vesicle pools, including the fast and slow ready-releasable pool, the recycling pool, and the reserve pool. Additionally, the frequency of the sustained stimulation is too high to allow replenishment or recycling pre-synaptic vesicles. The amount of neurotransmitter release during the sustained stimulus is reduced by blocking the Nedd8 pathway, which again shows that the release probability is decreased after neddylation inhibition. Also it might be that MLN-4924 disrupts the actin structure in the pre-synapse that is needed to guide vesicles from the reserve pool to the active zone upon sustained stimulation (Kuromi and Kidokoro, 2000). Therefore, neddylation inhibition might disrupt actin filaments or disturb actin-vesicle interaction and consequently decrease the neurotransmitter release.

Additionally, MLN-4924 treatment impairs the recycling of the vesicle pool resulting in decreased neurotransmitter release compared to control which recover much faster. After high frequency stimulation, endocytic intermediates are required to reform vesicles. When the reserve pool is depleted, the recovery needs slow endocytosis that proceeds through the formation of infoldings. Rab5 is expressed on endosomes and therefore regulates endosome trafficking through the synaptic compartment. Previous studies showed that ubiquitylation regulates the Rab5 binding protein Rabex-5 (Mattera et al., 2006). Ubiquitylation controls

endosome fusion and allows for the speculation of whether neddylation, as a post-translational modification, also impacts on vesicle pool recovery *via* endosome regulation. Nevertheless, the refilling of the vesicle pool is a complex function that involves many steps, and neddylation might also influence other proteins involved in this process.

For the post-synapse, a lot of targets have been described as being modified by ubiquitin or SUMO. For the pre-synapse just a few targets are known like, for example RIM-1 (rab3-interacting molecule 1) an active zone protein that is ubiquitylated by the E3 ligase SCRAPPER and thus regulates pre-synaptic neurotransmitter release (Yao et al., 2007). Additionally, the E3 ligase Staring ubiquitylates and therefore alters Syntaxin-1 levels in the pre-synapse. Also the degradation of synaptophysin is mediated *via* its ubiquitylation by the E3 ligase Siah-1A and Siah-2A (Wheeler et al., 2002). Most of these studies only describe the ubiquitylation of target proteins and the consequent degradation of synaptic proteins *via* the proteasome upon poly-ubiquitylation. The functional consequences or regulatory mechanisms that alter pre-synaptic function also *via* mono-ubiquitylation has been described less, or even not at all so far.

For sumoylation, no pre-synaptic targets have been described. However, some studies have revealed that sumoylation modulates calcium influx into the pre-synapse and therefore regulates glutamate release from pre-synaptic terminals (Feligioni et al., 2009). Additionally, it was shown that mGluAs control pre-synaptic glutamate release through G-protein-mediated regulation of ion channels (Ferraguti and Shigemoto, 2006) and that mGluA8 is sumoylated in HEK293 cells (Tang et al., 2005, Scheschonka et al., 2007). In conclusion, there is strong evidence that sumoylation regulates pre-synaptic neurotransmitter release. Neddylation is also involved in pre-synaptic glutamate release, and since SUMO has been described to control mGluA function, mGluAs might be a promising target to look for regulatory mechanisms of post-transcriptional modifications, including neddylation.

Pre-synaptic function, for example the neurotransmitter release from pre-synaptic terminals, is highly regulated by mechanisms that are poorly described. However, there is strong evidence that ubiquitylation and sumoylation are mandatory to control pre-synaptic function. This study demonstrates that neddylated targets in the pre-synapse also strongly impact on pre-synaptic

function. Further studies will focus on the identification of pre-synaptic targets of the Nedd8 pathway. Since little is known about the impact other post-translational modifications have on pre-synaptic function, it would be interesting to add them into further analyses.

5.5.2 Nedd8 Controls AMPA Receptor Distribution

In the post-synaptic membrane, the two main excitatory receptors are the AMPA and NMDA receptor families. Under basal conditions, AMPA receptors open upon glutamate binding to depolarize the excitatory post-synapse, blocking neddylation for 30 minutes in the post-synapse reduces AMPA receptor currents. Meaning that AMPA receptors are removed or not sufficiently integrated into the post-synapse when neddylation is blocked.

Trafficking and stabilization of AMPA receptors in the post-synapse are fine-tuned mechanisms that have been intensively studied recently, and neddylation is one additional mechanism that controls AMPA receptor concentration in the synapse. Since neddylation inhibition reduced AMPA receptors in the post-synaptic membrane one hypothesis is that neddylation of AMPA receptors or AMPA receptor-interacting molecules stabilizes AMPA receptors in the post-synaptic membrane. From our previous results it is known that PSD-95 is neddylated and thus the change in PSD-95 function upon neddylation inhibition might be responsible for the decrease in AMPA currents. Similar results showed that PSD-95-4c acutely inactivates PSD-95 by photo-activation and thus decreases GluA2 subunit concentration in the post-synaptic membrane in 15 minutes (Yudowski et al., 2013). Furthermore, it was shown that neddylation inhibition decreases PSD-95 oligomerization that was also shown to be important for targeting PSD-95 to the post-synaptic site to stabilize AMPA receptors *via* stargazin (Sturgill et al., 2009). This finding indicates that the loss of neddylation of PSD-95 and the implicated loss of oligomerization destabilizes the post-synaptic density and therefore AMPA receptors cannot sustain in the post-synaptic membrane.

Since MLN-4924 inhibits the activating enzyme of the Nedd8 pathway, a number of post-synaptic proteins are not neddylated anymore. In conclusion, the effect on AMPA current might be dependent on a loss of PSD-95 neddylation but might also be influenced by other de-neddylated proteins.

A decrease in AMPA receptor current might result from the destabilization of AMPA receptors in the post-synaptic membrane or from an impairment of exocytosis or lateral diffusion that transports AMPA receptors to extra-synapse sites and into the spine. It is well described, that AMPA receptors are very dynamic in synapses. Within 10 minutes 30 % of all AMPA receptors in the post-synapse are exchanged (Heine et al., 2008, Frischknecht et al., 2009, Kerr and Blanpied, 2012). The decline in AMPA receptor currents upon MLN-4924 treatment might be dependent on impaired stabilization of new AMPA receptors in the post-synapse. This loss of stability might result from impaired protein interaction between AMPA receptors and proteins that link the receptor to the actin cytoskeleton, such as N-cadherins, α -actinin, and BAND 4.1N (Shen et al., 2000, Zhou et al., 2001, Cingolani and Goda, 2008). Since PSD-95 clustering is altered upon MLN-4924 treatment, other protein interactions might also be affected for example by conformational changes. Thus, AMPA receptor protein interactions to PICK or SAP97 or PSD-95 *via* stargazin might also be diminished.

AMPA receptor subunits have been shown to be highly regulated in their localization by post-translational modifications such as phosphorylation, palmitoylation, and ubiquitylation. Consequently, it is possible that subunits neddylate themselves. The high number of post-translational modifications described in each subunit of the AMPA receptors demonstrates the relevance of the fine tuning of AMPA receptor localization and concentration in the post-synaptic membrane. On the one hand, GluA1 is phosphorylated at S818, S831, and S845, all positioned at the C-terminus of GluA1 that guide AMPA receptors to the neuronal surface, whereby S818 additionally favors the GluA1 interaction with the 4.1N protein to stabilize the receptor in the post-synapse (Lin et al., 2009). On the other hand, phosphorylation of S567 located in the loop1 of GluA1 promotes receptor insertion in the post-synaptic membrane (Lu et al., 2010). The core domain as well as the C-terminus of GluA1 is also palmitoylated, which prevents its degradation *via* ubiquitylation (Hayashi et al., 2005). GluA1 and GluA2 were shown to be targets of the ubiquitin pathway (Schwarz et al., 2010, Lin et al., 2011, Lussier et al., 2011). The GluA1 receptor is poly-ubiquitylated upon AMPA receptor activation and therefore triggers AMPA receptor endocytosis and degradation (Patrick et al., 2003). In contrast, GluA2 is ubiquitylated after its endocytosis (Lussier et al., 2011).

In recent years it has been well established that different post-translational modifications cross-talk with each other to provide fine tuning of the function and the trafficking of receptors (Pickering et al., 1995, Moffett et al., 1996, Hayashi et al., 2009). For example, it was shown that the phosphorylation of GluA1 prevents its degradation *via* the lysosomes and thus suggests a cross-modulation between AMPA receptor phosphorylation and ubiquitylation (Kessels et al., 2009).

Since AMPA receptor currents are increased in extra-synaptic sites, it can be excluded that neddylation inhibition completely disturbs AMPA receptor stabilization in membranes. In fact, the decrease in the AMPA receptor number in the post-synapse seems to be specific for the stabilization of AMPA receptors in the post-synaptic membrane. Interestingly, the acute knock-down of PSD-95 showed the same phenotype, expressing less AMPA receptors in the post-synapse, whereas extra-synaptic AMPA currents increase (Elias et al., 2006). These results might strengthen the hypothesis that neddylation inhibition impairs the interaction between PSD-95 and AMPA receptors *via* stargazin. Whether the increase in AMPA receptors in extra-synaptic sites is caused by lateral diffusion of AMPA receptors out of the synapse or whether it is a compensatory mechanism from the cell trying to overcome the loss of AMPA receptors in the post-synapse is the focus of future studies. Additionally, it will be mandatory to identify the proteins that are modulated by Nedd8 that are involved in AMPA receptor stabilization in the post-synaptic membrane and whether one or more subdomains of the AMPA receptor are directly neddylated.

More importantly, the reduction of AMPA receptors in the post-synapse after MLN-4924 treatment is reversed when the drug is washed out. This indicates that neddylation is a functional process in the post-synapse to regulate AMPA receptor trafficking in and out of the synapse. The wash-out experiment indicates that neddylation supports AMPA receptor stabilization in the post-synaptic membrane whereas de-neddylation destabilizes AMPA receptors and therefore decreases AMPA receptor concentration in the spine.

5.5.3 Nedd8 Control AMPA Receptor Kinetics

Besides the number of AMPA receptors in the post-synapse, the kinetics of AMPA receptors are also regulated. Glutamate receptors were shown to contain auxiliary subunits that modulate trafficking and/or channel properties. For example, AMPA receptors interact with TARPs and CNIHs and therefore alter the kinetics of AMPA receptors (Rouach et al., 2005).

In this study, neddylation inhibition fastens the deactivation of AMPA receptor currents. These results might suggest that when neddylation is blocked, protein interaction of AMPA and TARPs is disturbed since TARPs slow the deactivation of the receptor (Tomita et al., 2005a). The same could be shown for CNIHs. The loss of CNIH binding to AMPA receptors decreases the deactivation time (Kato et al., 2010, Shi et al., 2010). The increase in deactivation time upon neddylation inhibition indicates that protein interactions between AMPA receptor and their auxiliary subunits TARPs or CNIHs might be affected.

Additionally, TARPs as well as CNIHs were shown to promote the trafficking from AMPA receptors to the post-synaptic membrane (Tomita et al., 2003, Ziff, 2007, Tomita et al., 2012). Since neddylation inhibition results in a decrease in AMPA receptors in the post-synapse, it supports the statement that Nedd8 facilitates AMPA receptor interaction with its auxiliary subunits.

5.5.4 Nedd8 Controls NMDA Receptor Distribution

Like AMPA receptors, NMDA receptors concentration also decreases in the post-synaptic membrane through neddylation inhibition. Although NMDA receptors have been described as being more stable in synapses compared to the high regulated AMPA receptors, recent studies showed that NMDA receptors concentrations can also be rapidly regulated. Especially during spine development, the exchange of NMDA receptors upon different stimuli is regulated within minutes (Washbourne et al., 2004, Bellone and Nicoll, 2007). Different studies had shown that the regulation of NMDA receptors is dependent on the C-terminus of NR2B- and NR2A-containing receptors and their interacting intracellular partners as well as on differences in phosphorylation (Roche et al., 2001, Carroll and Zukin, 2002, Chen et al., 2006).

One of the best described interaction partners of NMDA receptors is PSD-95, which interacts

with NR2B *via* PDZ 2. Deletion of the PDZ-domain binding motif in NR2B increases NMDA receptor internalization (Yamada et al., 1999, Roche et al., 2001). Neddylated lysine residues of PSD-95, including K202, are located in PDZ 2 of PSD-95 and therefore might facilitate the interaction of NMDA receptor and PSD-95 and the subsequent stabilization of the receptor in the post-synaptic membrane. Thus, the loss of neddylation might destabilize the interaction between PSD-95 and NMDA receptors and consequently result in a decrease in post-synaptic NMDA receptors.

The main idea behind the speculation that neddylation inhibition prevents PSD-95-NMDA interaction is that neddylation is important for protein interaction as it was shown for PSD-95 oligomerization. Another possible explanation might be that neddylation leads to conformational changes and therefore inhibits protein-protein interactions. A possible example for increased protein interaction upon neddylation inhibition might be that neddylation inhibition favors NR2B-AP-2 interaction and consequently favors NMDA receptor internalization. A recent study proved the necessity of AP-2 NMDA interaction for NMDA internalization (Prybylowski et al., 2005).

Endocytosis zones for NMDA receptors are located tangentially to the synapse, thus NMDA receptors have to be diffused laterally before they are removed from the surface (Groc et al., 2004). Since NMDA receptor kinetics do not differ between MLN-4924 and untreated neurons, neddylation inhibition seems to act similarly on NR2A and NR2B containing NMDA receptors. Consequently, neither the removal nor insertion of certain NMDA receptor subunits seems to be specifically regulated by neddylation.

The decrease in NMDA receptor currents might also be caused by defects in the delivery of NMDA receptors to the post-synapse. Under physiological conditions, PKC activation enhances NMDA channel opening and therefore delivers new NMDA channels to the membrane by SNARE-dependent exocytosis (Lan et al., 2001). Since MLN-4924 had been shown to alter pre-synaptic neurotransmitter release in pre-synaptic compartments in a SNARE-dependent manner that is similar to the exocytosis of NMDA receptors in the post-synapse, the same effect of neddylation inhibition might be responsible for the decreased release probability from the

pre-synapse and decreased NMDA receptors in the post-synaptic membrane (Groc et al., 2004). Only a few studies have been published that describe direct post-translational modifications of NMDA subunits. In one study, NMDA subunits NR1 and NR2B were described to be ubiquitinated and that protein concentrations of NR2B are increased after MG132 application after amphetamine treatment (Mao et al., 2009). Therefore, NMDA receptor ubiquitylation alters NMDA receptor concentration in the synapse upon external stimuli. Additionally, parkin had been shown to directly interact with NR2B, but whether parkin directly ubiquitylates NR2B has not been described yet. In general, little is known about the influences of post-translational modifications have on NMDA receptor regulation.

From our results we can conclude that neddylation inhibitions result in decreased AMPA and NMDA receptors in the post-synaptic membrane. In contrast, NMDA receptor distribution in the spine is not reversible after neddylation inhibition and therefore fewer NMDA receptors remain in the synapses after neddylation inhibition, whereas AMPA receptor currents recover.

5.6 Functional Impact of Neddylation on Synaptic-Neurotransmission at Inhibitory Synapses

Little is known about the impact of post-translational modification on the function of inhibitory synapses and especially on GABA dependent neurotransmission.

This study demonstrates that neddylation inhibition has no influence on the number of inhibitory synapses, but decreases the number of functional GABA_A receptors in post-synaptic sites or reduces neurotransmitter release from the pre-synapse. Since no experiments were conducted that would exclusively investigate neddylation effects on the pre-synapse, it cannot be concluded whether GABA release from the pre-synapse is altered. GABA release is mediated *via* pre-synaptic vesicle exocytosis such as glutamate release from excitatory pre-synaptic terminals. Consequently, it might be that similar mechanisms in pre-synaptic release are altered by neddylation inhibition in inhibitory synapses as we demonstrated for excitatory pre-synaptic glutamate release. Whether this is true or whether the defects in gabaergic neurotransmission

are restricted to post-synaptic mechanisms is the focus of future studies.

For the post-synapse of inhibitory synapses, it was shown that GABA_A receptors are ubiquitinated in an activity-dependent manner. Chronic inhibition of neuronal activity increases GABA_A receptors ubiquitination in the ER and thus prevents receptor insertion into the plasma membrane. The effect could be reversed, meaning that increased neuronal activity decreased GABA_A receptors ubiquitination and therefore favors receptor insertion into the membrane (Saliba et al., 2007, Yi and Ehlers, 2007). Also, the stability of GABA_A receptors in the post-synaptic membrane might be altered by ubiquitination. Gephyrin, a scaffold protein of the inhibitory post-synapse, has been associated with ubiquitin (Forstera et al., 2010). Furthermore, a reduction of gephyrin was shown to decrease GABA_A receptor currents. Thus, gephyrin ubiquitination and the subsequent degradation *via* the proteasome might decrease GABA_A receptor concentration in the post-synapse. The fact that the protein sequence of gephyrin comprises two PEST domains (aa 181-202, aa 258-272) strengthens the possibility of gephyrin being a target of the ubiquitin pathway. Since neddylation of PSD-95 is mediated *via* the PEST domain, the two PEST domains in gephyrin might also regulate the neddylation of gephyrin. Neddylation of gephyrin would counteract the destabilization of gephyrin in the post-synapse upon ubiquitination. Thus, neddylation might favor gephyrin multimerization and consequently stabilize GABA_A receptors in the post-synaptic membrane.

If this hypothesis is true, the Nedd8 pathway might have similar control mechanisms for synaptic functions. In this case, neddylation would favor scaffold protein interaction that increases receptor stabilization in the post-synapse and thereby strengthens synaptic connections.

5.7 Activity-Dependent Changes of Target Protein Neddylation

Basal synaptic neurotransmission is important to transfer information from one neuron to another neuron. This study demonstrated that neddylation strongly impacts basal synaptic transmission and thus showed that the Nedd8 pathway is essential for normal synaptic function.

Furthermore, it was checked whether the Nedd8 pathway also impacts on synaptic plasticity. So far, the ubiquitin pathway is described regulating synaptic plasticity by its subsequent degradation of proteins *via* the proteasome and by regulating the trafficking of synaptic receptors (DiAntonio and Hicke, 2004, Mabb and Ehlers, 2010).

Sustained activity or inactivation changes protein turnover and consequently alters synapse remodeling and signaling. In response to increased activity, proteins in the PSD are highly ubiquitylated and the protein turnover is increased. In contrast, activity deprivation reduces ubiquitylation of target proteins (Ehlers, 2003). Interestingly, not all proteins are involved in activity dependent changes. Consequently, protein ubiquitylation upon activity changes is not a general process but specifically regulated. The limitation of Ehler's work is that treatment times with TTX and bicuculline are extended to several days. These long application times do not mimic any physiological condition and therefore the experiments could not be correlated to any physiological condition. Nevertheless, the results give a first insight into protein concentration regulation upon neuronal activity.

Our study shows that the pattern and amount of neddylated proteins change upon neuronal activity, meaning that glutamate treatment increases the amount of neddylated proteins. Especially PSD-95 neddylation is increased upon glutamate treatment. Additionally, short periods of neuronal activity are sufficient to increase PSD-95 neddylation. More interestingly, PSD-95 concentration also increases upon glutamate treatment similarly to PSD-95 neddylation (Shen and Meyer, 1999, Kim et al., 1997, Steiner et al., 2008). These results strongly suggest that the increased concentration of PSD-95 is correlated to its neddylation. Since PSD-95 concentrations were obtained from synaptosome fractions, it cannot be concluded whether the elevation in PSD-95 concentration is due to increased protein stability in general or to the stabilization of PSD-95 in post-synaptic compartments.

Remarkably, NMDA treatment, which causes chemical long-term depression (LTD), increases the ubiquitylation of PSD-95 and consequently decreases the amount of PSD-95. Taken together, these results suggest that neddylation and ubiquitylation are activated by different external stimuli and therefore regulate protein stability and function.

Interestingly, synaptic stimulation induces the translocation of the proteasome from the dendritic

shaft to the spine, where the proteasome subsequently becomes more active (Bingol and Schuman, 2006). The redistribution as well as the increased activity of the proteasome is mainly regulated by CaMKII (Djakovic et al., 2009). Investigating the translocation of the proteasome upon neddylation inhibition might give further evidence about stimuli dependent control of the Nedd8 pathway. Furthermore, the finding of whether neddylation would induce proteasome localization in the spine or in the dendritic shaft would additionally show whether neddylation stabilizes or destabilizes proteins in synaptic compartments.

5.8 The Nedd8 Pathway is Involved in the Induction of Synaptic Plasticity

Synaptic activity results in altered post-translational modifications by the activation or inhibition of post-translational modification machineries. Since post-translational modifications alter protein stability and function, which is mandatory for synaptic plasticity, it is very likely that post-translational modifications impact on synaptic plasticity.

In this study, electrophysiological recordings were performed that show a decrease in LTP and LTD induction after short and long periods of neddylation inhibition, indicating that the Nedd8 pathway plays an important part in the induction of LTP and LTD. The limitation of the performed experiments is that neddylation was blocked 30 minutes before LTP or LTD was induced. Thus the decrease in AMPA and more importantly NMDA receptors, which are necessary for the induction of synaptic plasticity, might already be sufficient to block LTP and LTD induction. Also, the pre-synaptic effect of neddylation inhibition might be involved in decreased LTP induction, since fewer neurotransmitter can be released upon neddylation inhibition. Nevertheless, the fact that Ubc12-C111S expression in post-synaptic neurons also decreases LTP induction supports the idea that neddylation inhibition of the post-synapse results in synaptic plasticity defects. Additionally, after Ubc12-C111S expression the number of functional synapses decreases whereas the remaining synapses still exert normal AMPA function. Nevertheless, LTP induction was still impaired, suggesting that under basal conditions and upon the induction of synaptic

plasticity different mechanisms are altered when neddylation is blocked.

Previous publications have already established that the ubiquitin pathway and consequently protein degradation strongly impact on activity-dependent synaptic plasticity (Fonseca et al., 2006, Karpova et al., 2006, Dong et al., 2008, Mabb and Ehlers, 2010). In these experiments, the time point of inhibiting protein degradation is important for blocking LTP. LTP is only blocked *via* proteasome inhibition during the LTP induction time (Karpova et al., 2006).

Further studies are needed to describe the impact of neddylation on LTP and LTD induction, whereby the time and side of MNL-4924 application has to be fine tuned to receive clear results about neddylation action. More interestingly, PSD-95-K202R will be used to study the effect of PSD-95 neddylation on synaptic plasticity.

5.9 The Impact of MLN-4924 on Different Synaptic Sites

Neddylation is a post-translational modification that acts on different, until now almost undefined, synaptic proteins. Like other post-translational modifications such as phosphorylation or ubiquitylation, neddylation is not restricted to specific synaptic compartments but is active in the whole neuron.

To characterize the impact of protein neddylation it is important to over-activate or to inhibit the neddylation of target proteins. The over-activation of the Nedd8 pathway has not been possible so far, since Ubc12 overexpression has a dominant negative effect. Only the inhibition of the Nedd8 pathway allows for the analysis of altered neddylation.

MLN-4924 application acutely blocks the neddylation of target proteins and therefore allows for the study of the impact of neddylation on basal neurotransmission. Nevertheless, it is important to keep in mind that wash-in experiments with MLN-4924 always act on the pre- and on the post-synapse. For example, if you want to investigate neddylation inhibition on AMPA receptor function, it is important to consider that neddylation effects on the pre-synaptic or even on inhibitory synapses might also influence the results. Besides, an impact of neddylation on glial cells that also regulate neurotransmitter concentration in the synaptic cleft cannot be excluded. Experimental designs where MLN-4924 was applied *via* the patch pipette restrict MLN-4924

action to the post-synaptic site, as could be shown in several experiments and therefore was able to prove the strong effects neddylation inhibition exerts on pre- as well as on post-synaptic function. Nevertheless, to completely understand the impact neddylation has on pre- as well as on post-synaptic function it will be mandatory to block neddylation more specifically.

PSD-95-K202 is a good example for showing that protein neddylation strongly influences synaptic morphology and function. In this line, the goal of future studies must be to identify additional neuronal targets of the Nedd8 pathway as well as the specific lysine residues that are neddylated. The identification of neddylated lysine residues allow for mutation studies, such as for PSD-95-K202R. This detailed analysis is necessary to specifically describe the impact of the Nedd8 pathway on neuronal function.

6 Conclusion

Taken together, this thesis shows that the Nedd8 pathway strongly impacts on synaptic function. The first part of this thesis illustrated that the Nedd8 pathway is active in the synapse and that neddylated proteins are present in pre- and post-synaptic compartments. To specify the impact neddylation has on synaptic function, the main goal was to describe the neddylation of one synaptic protein. In this thesis, we identified the first synaptic protein that is neddylated: PSD-95. In addition, we proved that PSD-95 neddylation is specific, by showing that Nae1, Ubc12 and Mdm2 are involved in PSD-95 neddylation. Furthermore, Nedd8 mutants were developed that allow to differentiate between neddylated and ubiquitylated lysines *via* mass spectrometry and demonstrated lysine 202 of PSD-95 to be neddylated. Mutation of K202 to arginine significantly reduces PSD-95 neddylation. PSD-95-K202R displayed strong defects in spine development, indicated by morphological defects, and changes in mEPSC amplitude and interevent interval. In conclusion, we identified the first brain specific target of the Nedd8 pathway and showed that PSD-95 neddylation impacts on synaptic function.

To further describe the impact of the Nedd8 pathway on synaptic function, electrophysiological studies were obtained that determined a decrease in AMPA and NMDA receptors in the post-synaptic membrane when neddylation was blocked. In contrast, AMPA receptor concentration increased in extra-synaptic sides. In addition, a change in AMPA receptor kinetics was described when neddylation was blocked in the post-synaptic compartment.

Besides excitatory synapses, neddylation also reduces the expression of GABA_A receptors in the post-synaptic membrane of inhibitory synapses.

Moreover, we showed that neddylation also impacts on synaptic plasticity. Neither LTP nor LTD could be induced when neddylation was blocked. In addition, neddylation in general and

PSD-95 neddylation increased upon neuronal activity. These findings suggest that neddylation is important to induce synaptic plasticity by stabilizing proteins in the post-synapse.

In summary, this thesis gives a broad overview about the impact neddylation has on neuronal function. Therefore, molecular- and electrophysiological-methods were combined to analyze the neddylation of synaptic proteins and to understand their functional impact. The identification of another post-translational modification that besides ubiquitylation and sumoylation modifies synaptic proteins, illustrates the importance of post-translational modifications in the regulation of synaptic functions. This thesis opens a broad field in neuroscience research that will help to understand the impact neddylation has on synaptic function.

List of Figures

1.1	Physiological and morphological properties of AMPA receptors.	12
1.2	Physiological properties of AMPA and NMDA receptors.	13
1.3	The Ubiquitin pathway.	20
1.4	The Nedd8 pathway and its interaction with the ubiquitin pathway. . . .	22
1.5	Simple schematic illustration of the projections and connections in the hippocampus.	26
1.6	Illustration of extracellular recordings in the hippocampus by Schaffer collaterals activation.	28
1.7	Sample trace for extracellular field recording.	29
1.8	Illustration of a patched CA1 neuron and patch-clamp configurations. . .	30
4.1	Mouse synaptosome preparation reveals that the neddylation pathway is active in pre- and post-synaptic compartments.	66
4.2	Overexpression of Ubc12-C111S, shNedd8 or shUbc12 is sufficient to block the Nedd8 pathway.	68
4.3	MLN-4924 blocks neddylation of target proteins and Cullin1 in HEK293 cells and primary neurons.	69
4.4	PSD-95 is neddylated.	71
4.5	PSD-95 neddylation is reversed by genetically blocking the neddylation pathway.	73
4.6	PSD-95 neddylation is blocked by the Nae1 inhibitor MLN-4924.	74
4.7	PSD-95 is neddylated by the E3 Ligase Mdm2.	76
4.8	GKAP is not neddylated.	77

4.9	PSD-95 is neddylated <i>via</i> its PEST domain by interacting with Ubc12. . . .	79
4.10	PSD-95 is ubiquitylated.	80
4.11	Nedd8 and ubiquitin compete for PSD-95 modification.	82
4.12	PSD-95 - PSD-95 interaction is diminished when blocking the Nedd8 pathway.	84
4.13	Generated Nedd8 mutants for mass spectrometry.	86
4.14	Generated Nedd8 mutants are functional and able to neddylate PSD-95.	87
4.15	Mass spectrometry revealed a number of neddylated and ubiquitylated lysines in PSD-95.	88
4.16	Graphic illustration of neddylated and/or ubiquitylated lysine residues in the protein structure of PSD-95.	91
4.17	K211 and K393 of PSD-95 are modified by Nedd8 and ubiquitin.	92
4.18	PSD-95 mutants are less neddylated compared to PSD-95-WT.	94
4.19	PSD-95 mutants exert strong effects on spine morphology in developing primary hippocampal neurons.	95
4.20	PSD-95-K202R strongly affects spine morphology during spine development in young organotypic slice cultures.	97
4.21	PSD-95-K202R has a dominant negative effect on amplitude and interevent interval of mEPSC in developing neurons.	99
4.22	PSD-95-K202R has a dominant negative effect on mEPSC frequency in mature neurons.	101
4.23	The Nedd8 pathway is essential for basal neurotransmission.	104
4.24	MLN-4924 affects spine morphology and basal neurotransmission in primary hippocampal neurons.	106
4.25	Acute MLN-4924 treatment has no effect on spine morphology in acute hippocampal brain slices.	108
4.26	Basal synaptic transmission is reduced by blocking the Nedd8 pathway.	110
4.27	Release probability of excitatory synapses is decreased in acute brain slices treated with MLN-4924.	111

4.28	Release probability of excitatory synapses is unaltered when MLN-4924 treatment is restricted to the post-synapse.	112
4.29	Release probability of excitatory synapses is decreased when neddylation is blocked.	114
4.30	The amount of released neurotransmitter upon high stimulation as well as the recovery of the vesicle pool is reduced in MLN-4924 treated slices.	115
4.31	MLN-4924 treatment reduces amplitude and frequency of excitatory currents.	117
4.32	MLN-4924 treatment leads to an increase in AMPA/NMDA ratio.	119
4.33	MLN-4924 treatment decreased AMPA current amplitude.	120
4.34	30 min of MLN-4924 treatment decreases NMDA current amplitude. Wash-out of MLN-4924 for 30 min does not recover the decrease of NMDA current amplitude.	122
4.35	MLN-4924 has no effect on AMPA or NMDA kinetics when applied to the bath solution.	123
4.36	MLN-4924 treatment reduces the AMPA decay time when applied to the patch pipette. No differences are found for NMDA EPSCs.	124
4.37	MLN-4924 increases somatic expression of AMPA receptors.	125
4.38	The Nedd8 pathway is essential for basal neurotransmission at inhibitory synapses of primary hippocampal neurons.	127
4.39	The Nedd8 pathway is essential for basal neurotransmission at inhibitory synapses obtained in acute brain slices.	128
4.40	Continuous treatment with glutamate increases PSD-95 neddylation.	130
4.41	Short-term glutamate activation also increases PSD-95 neddylation.	131
4.42	MLN-4924 prevents LTP induction in acute hippocampal brain slices.	132
4.43	Ubc12-C111s expression during development as well as in adult neurons prevents LTP induction.	134

4.44 **MLN-4924 treatment prevents LTD induction. Extracellular field potential recordings (fEPSP) were obtained before and after LTD induction in control and MLN-4924 treated acute brain slices. 135**

List of Tables

2.1	Media for General Cell Culture and Primary Cell Culture	33
2.2	Media for Bacteria Cultures	34
2.3	Buffers for Biochemistry	34
2.4	Media for Organotypic Slice Cultures and SFV generation	35
2.5	Media used for Electrophysiology	35
2.6	Chemicals and Reagents	36
2.7	Primary Antibodies	37
2.8	Secondary Antibodies	37

Nomenclature

A	Ampere
ACSF	Artificial Cerebrospinal Fluid
AMPA	Amino-3-hydroxy-5-methylisoxazole-4- propionic acid
APP	Amyloid precursor protein
Appbp1	β -Amyloid precursor protein binding protein 1 (also called Nae1)
APV	R-2-amino-5-phosphonopentanoate
ATP	Adenosine triphosphate
BHK-21	Baby hamster kidney cells
Bp	Basepair
CA	Cornu ammonis, region in the hippocampus
CaCl ₂	Calcium Chloride
CaMKII	Calcium/calmodulin-dependent protein kinase II
CAZ	Cytomatrix of the active zone
C	Cysteine
cDNA	Complementary DNA
CNQX	6-cyano-7-nitroquinoxaline-2,3-dione
COP	Constitutive photomorphogenesis 9
CRL	Cullin RING ligase C-terminus Carboxyl terminus
Da	Dalton
DH5 α	DaltonE.coli strain DH5 α
DIV	Days in vitro

DMEM	Dulbecco's Modified Eagle Medium
DMSO	Dimethylsulfoxide dNTPs Desoxyribonucleotide triphosphate
DUB	Deubiquitinating enzymes
EPSC	Excitatory post-synaptic current
EPSP	Excitatory post-synaptic potential
FCS	Fetal calf serum
fEPSP	Field EPSP G Gramm
GFP	Green fluorescent protein
GKAP	Guanylate kinase-associated protein
GluN	Glutamate receptor subunit N,, formally called NR
HEK	Human embryonic kidney
HEPES	4-(2-Hydroxyethyl)piperazine-1-ethanesulfonic acid
HZ	Hertz
Ig	Immunoglobulin
IPSC	Inhibitory postsynaptic currents
kDA	Kilodalton
K	Lysine
KS	Kolmogorov-Smirnov
L	Leucine
LTD	Long-term-depression
LTP	Long-term-potential
MAGUK	Membrane associated guanylate kinase
mEPSC	Miniature excitatory post-synaptic current
mEPSP	Miniature excitatory post-synaptic potential
mg	Milligram
min	Minute

ml	Milliliter
M	Molar concentration
N-terminus	Amino terminus
Nae	Nedd8-activating enzyme
Nedd8	Neural precursor cell expressed, developmentally down-regulated 8
NMDA	N-methyl-D-aspartate
NOS	Nitric oxide synthase
NP-40	Nonidet P-40
o.n.	Overnight
PBS	Phosphate buffered saline
PCR	Polymerase chain reaction
PD	Parkinson Disease
PP1	Protein Phosphatase 1
PPF	Paired-Pulse-Facilitation
PSD-95	Post-synaptic density protein 95
PSD	Post-synaptic density
PTX	Picrotoxin
Rbx	Ring box protein
Rpm	Rounds per minute
R	Arginine
RT	Room temperature
SDS	Sodium dodecyl sulfate
SEM	Standard error of the mean
SFV	Semiliki Forest Virus
Shank1	SH3 and multiple ankyrin repeat domains protein 1
SOC medium	Suboptimal broth with catabolite repression

S	Serine
SUMO	Small ubiquitin-like modifier
SV	Synaptic Vesicles
TAE	Tris acetate with EDTA
TARPs	Transmembrane AMPA receptor regulatory proteins
TCM	Trichlormethiazide
TMs	Trichlormethiazide Transmembrane domains
TRIS	Tris[hydroxymethyl]aminomethane
TTX	Tetrodotoxin
UBL	Ubiquitin-like protein

References

- W. M. Abida, A. Nikolaev, W. Zhao, W. Zhang, and W. Gu. Fbxo11 promotes the neddylation of p53 and inhibits its transcriptional activity. *J Biol Chem*, 282(3):1797–804, 2007.
- H. C. Ardley and P. A. Robinson. E3 ubiquitin ligases. *Essays Biochem*, 41:15–30, 2005.
- P. P. Atluri and W. G. Regehr. Determinants of the time course of facilitation at the granule cell to purkinje cell synapse. *J Neurosci*, 16(18):5661–71, 1996.
- C. H. Bailey and E. R. Kandel. Structural changes accompanying memory storage. *Annu Rev Physiol*, 55:397–426, 1993.
- A. I. Bain and D. M. Quastel. Multiplicative and additive Ca^{2+} -dependent components of facilitation at mouse endplates. *J Physiol*, 455:383–405, 1992.
- T. G. Banke, D. Bowie, H. Lee, R. L. Huganir, A. Schousboe, and S. F. Traynelis. Control of glur1 ampa receptor function by camp-dependent protein kinase. *J Neurosci*, 20(1):89–102, 2000.
- G. Banker, L. Churchill, and C. W. Cotman. Proteins of the postsynaptic density. *J Cell Biol*, 63 (2 Pt 1):456–65, 1974.
- J. A. Bartos, J. D. Ulrich, H. Li, M. A. Beazely, Y. Chen, J. F. Macdonald, and J. W. Hell. Post-synaptic clustering and activation of pyk2 by psd-95. *J Neurosci*, 30(2):449–63, 2010.
- C. Bats, L. Groc, and D. Choquet. The interaction between stargazin and psd-95 regulates ampa receptor surface trafficking. *Neuron*, 53(5):719–34, 2007.
- T. Bawa-Khalfe and E. T. Yeh. Sumo losing balance: Sumo proteases disrupt sumo homeostasis to facilitate cancer development and progression. *Genes Cancer*, 1(7):748–752, 2010.
- M. F. Bear and R. C. Malenka. Synaptic plasticity: Ltp and ltd. *Curr Opin Neurobiol*, 4(3):389–99, 1994.
- J. C. Beique and R. Andrade. Psd-95 regulates synaptic transmission and plasticity in rat cerebral cortex. *J Physiol*, 546(Pt 3):859–67, 2003.
- C. Bellone and R. A. Nicoll. Rapid bidirectional switching of synaptic nmda receptors. *Neuron*, 55(5):779–85, 2007.

-
- V. Bernier-Villamor, D. A. Sampson, M. J. Matunis, and C. D. Lima. Structural basis for e2-mediated sumo conjugation revealed by a complex between ubiquitin-conjugating enzyme ubc9 and rangap1. *Cell*, 108(3):345–56, 2002.
- B. Bettler and J. Y. Tiao. Molecular diversity, trafficking and subcellular localization of gabab receptors. *Pharmacol Ther*, 110(3):533–43, 2006.
- S. Bhattacharyya, V. Biou, W. Xu, O. Schluter, and R. C. Malenka. A critical role for psd-95/akap interactions in endocytosis of synaptic ampa receptors. *Nat Neurosci*, 12(2):172–81, 2009.
- M. J. Bianchetta, T. T. Lam, S. N. Jones, and M. A. Morabito. Cyclin-dependent kinase 5 regulates psd-95 ubiquitination in neurons. *J Neurosci*, 31(33):12029–35, 2011.
- B. Bingol and E. M. Schuman. Activity-dependent dynamics and sequestration of proteasomes in dendritic spines. *Nature*, 441(7097):1144–8, 2006.
- J. Bormann and A. Feigenspan. Gabac receptors. *Trends Neurosci*, 18(12):515–9, 1995.
- A. Bottger, V. Bottger, A. Sparks, W. L. Liu, S. F. Howard, and D. P. Lane. Design of a synthetic mdm2-binding mini protein that activates the p53 response in vivo. *Curr Biol*, 7(11):860–9, 1997.
- S. D. Boyd, K. Y. Tsai, and T. Jacks. An intact hdm2 ring-finger domain is required for nuclear exclusion of p53. *Nat Cell Biol*, 2(9):563–8, 2000.
- D. S. Bredt and R. A. Nicoll. Ampa receptor trafficking at excitatory synapses. *Neuron*, 40(2):361–79, 2003.
- C. L. Brooks and W. Gu. p53 ubiquitination: Mdm2 and beyond. *Mol Cell*, 21(3):307–15, 2006.
- M. Burbea, L. Dreier, J. S. Dittman, M. E. Grunwald, and J. M. Kaplan. Ubiquitin and ap180 regulate the abundance of glr-1 glutamate receptors at postsynaptic elements in *c. elegans*. *Neuron*, 35(1):107–20, 2002.
- N. Burnashev, H. Monyer, P. H. Seeburg, and B. Sakmann. Divalent ion permeability of ampa receptor channels is dominated by the edited form of a single subunit. *Neuron*, 8(1):189–98, 1992.
- J. Callis, T. Carpenter, C. W. Sun, and R. D. Vierstra. Structure and evolution of genes encoding polyubiquitin and ubiquitin-like proteins in *arabidopsis thaliana* ecotype columbia. *Genetics*, 139(2):921–39, 1995.
- R. C. Carroll and R. S. Zukin. Nmda-receptor trafficking and targeting: implications for synaptic transmission and plasticity. *Trends Neurosci*, 25(11):571–7, 2002.
- R. C. Carroll, D. V. Lissin, M. von Zastrow, R. A. Nicoll, and R. C. Malenka. Rapid redistribution of glutamate receptors contributes to long-term depression in hippocampal cultures. *Nat Neurosci*, 2(5):454–60, 1999.

- L. Cathala, N. B. Holderith, Z. Nusser, D. A. DiGregorio, and S. G. Cull-Candy. Changes in synaptic structure underlie the developmental speeding of ampa receptor-mediated epscs. *Nat Neurosci*, 8(10):1310–8, 2005.
- N. L. Chan and C. P. Hill. Defining polyubiquitin chain topology. *Nat Struct Biol*, 8(8):650–2, 2001.
- H. W. Chao, C. J. Hong, T. N. Huang, Y. L. Lin, and Y. P. Hsueh. Sumoylation of the maguk protein cask regulates dendritic spinogenesis. *J Cell Biol*, 182(1):141–55, 2008.
- B. S. Chen, S. Braud, 2nd Badger, J. D., J. T. Isaac, and K. W. Roche. Regulation of nr1/nr2c n-methyl-d-aspartate (nmda) receptors by phosphorylation. *J Biol Chem*, 281(24):16583–90, 2006.
- L. Chen, D. M. Chetkovich, R. S. Petralia, N. T. Sweeney, Y. Kawasaki, R. J. Wenthold, D. S. Brecht, and R. A. Nicoll. Stargazin regulates synaptic targeting of ampa receptors by two distinct mechanisms. *Nature*, 408(6815):936–43, 2000.
- M. Chen, X. Hou, and G. Zhang. Tyrosine kinase and tyrosine phosphatase participate in regulation of interactions of nmda receptor subunit 2a with src and fyn mediated by psd-95 after transient brain ischemia. *Neurosci Lett*, 339(1):29–32, 2003.
- L. S. Chin, J. P. Vavalle, and L. Li. Staring, a novel e3 ubiquitin-protein ligase that targets syntaxin 1 for degradation. *J Biol Chem*, 277(38):35071–9, 2002.
- K. O. Cho, C. A. Hunt, and M. B. Kennedy. The rat brain postsynaptic density fraction contains a homolog of the drosophila discs-large tumor suppressor protein. *Neuron*, 9(5):929–42, 1992.
- Y. S. Choo, G. Vogler, D. Wang, S. Kalvakuri, A. Iliuk, W. A. Tao, R. Bodmer, and Z. Zhang. Regulation of parkin and pink1 by neddylation. *Hum Mol Genet*, 21(11):2514–23, 2012.
- N. Chow, J. R. Korenberg, X. N. Chen, and R. L. Neve. App-bp1, a novel protein that binds to the carboxyl-terminal region of the amyloid precursor protein. *J Biol Chem*, 271(19):11339–46, 1996.
- K. S. Christopherson, B. J. Hillier, W. A. Lim, and D. S. Brecht. Psd-95 assembles a ternary complex with the n-methyl-d-aspartic acid receptor and a bivalent neuronal no synthase pdz domain. *J Biol Chem*, 274(39):27467–73, 1999.
- K. S. Christopherson, N. T. Sweeney, S. E. Craven, R. Kang, D. El-Husseini Ael, and D. S. Brecht. Lipid- and protein-mediated multimerization of psd-95: implications for receptor clustering and assembly of synaptic protein networks. *J Cell Sci*, 116(Pt 15):3213–9, 2003.
- L. A. Cingolani and Y. Goda. Actin in action: the interplay between the actin cytoskeleton and synaptic efficacy. *Nat Rev Neurosci*, 9(5):344–56, 2008.

-
- M. Colledge, E. M. Snyder, R. A. Crozier, J. A. Soderling, Y. Jin, L. K. Langeberg, H. Lu, M. F. Bear, and J. D. Scott. Ubiquitination regulates psd-95 degradation and ampa receptor surface expression. *Neuron*, 40(3):595–607, 2003.
- T. J. Craig and J. M. Henley. Protein sumoylation in spine structure and function. *Curr Opin Neurobiol*, 22(3):480–7, 2012.
- S. E. Craven, A. E. El-Husseini, and D. S. Bredt. Synaptic targeting of the postsynaptic density protein psd-95 mediated by lipid and protein motifs. *Neuron*, 22(3):497–509, 1999.
- H. Cui, A. Hayashi, H. S. Sun, M. P. Belmares, C. Cobey, T. Phan, J. Schweizer, M. W. Salter, Y. T. Wang, R. A. Tasker, D. Garman, J. Rabinowitz, P. S. Lu, and M. Tymianski. PdZ protein interactions underlying nmda receptor-mediated excitotoxicity and neuroprotection by psd-95 inhibitors. *J Neurosci*, 27(37):9901–15, 2007.
- S. G. Cull-Candy and D. N. Leszkiewicz. Role of distinct nmda receptor subtypes at central synapses. *Sci STKE*, 2004(255):re16, 2004.
- R. J. Deshaies and C. A. Joazeiro. Ring domain e3 ubiquitin ligases. *Annu Rev Biochem*, 78:399–434, 2009.
- A. DiAntonio and L. Hicke. Ubiquitin-dependent regulation of the synapse. *Annu Rev Neurosci*, 27:223–46, 2004.
- A. Dil Kuazi, K. Kito, Y. Abe, R. W. Shin, T. Kamitani, and N. Ueda. Nedd8 protein is involved in ubiquitinated inclusion bodies. *J Pathol*, 199(2):259–66, 2003.
- S. N. Djakovic, L. A. Schwarz, B. Barylko, G. N. DeMartino, and G. N. Patrick. Regulation of the proteasome by neuronal activity and calcium/calmodulin-dependent protein kinase ii. *J Biol Chem*, 284(39):26655–65, 2009.
- C. Dong, S. C. Upadhyaya, L. Ding, T. K. Smith, and A. N. Hegde. Proteasome inhibition enhances the induction and impairs the maintenance of late-phase long-term potentiation. *Learn Mem*, 15(5):335–47, 2008.
- C. G. Dotti, C. A. Sullivan, and G. A. Banker. The establishment of polarity by hippocampal neurons in culture. *J Neurosci*, 8(4):1454–68, 1988.
- L. Dreier, M. Burbea, and J. M. Kaplan. Lin-23-mediated degradation of beta-catenin regulates the abundance of glr-1 glutamate receptors in the ventral nerve cord of *c. elegans*. *Neuron*, 46(1):51–64, 2005.
- D. M. Duda, L. A. Borg, D. C. Scott, H. W. Hunt, M. Hammel, and B. A. Schulman. Structural insights into nedd8 activation of cullin-ring ligases: conformational control of conjugation. *Cell*, 134(6):995–1006, 2008.
- T. C. Dumas. Developmental regulation of cognitive abilities: modified composition of a molecular switch turns on associative learning. *Prog Neurobiol*, 76(3):189–211, 2005.

- B. T. Dye and B. A. Schulman. Structural mechanisms underlying posttranslational modification by ubiquitin-like proteins. *Annu Rev Biophys Biomol Struct*, 36:131–50, 2007.
- M. D. Ehlers. Reinsertion or degradation of ampa receptors determined by activity-dependent endocytic sorting. *Neuron*, 28(2):511–25, 2000.
- M. D. Ehlers. Activity level controls postsynaptic composition and signaling via the ubiquitin-proteasome system. *Nat Neurosci*, 6(3):231–42, 2003.
- I. Ehrlich and R. Malinow. Postsynaptic density 95 controls ampa receptor incorporation during long-term potentiation and experience-driven synaptic plasticity. *J Neurosci*, 24(4):916–27, 2004.
- I. Ehrlich, M. Klein, S. Rumpel, and R. Malinow. Psd-95 is required for activity-driven synapse stabilization. *Proc Natl Acad Sci U S A*, 104(10):4176–81, 2007.
- A. E. El-Husseini, E. Schnell, D. M. Chetkovich, R. A. Nicoll, and D. S. Bredt. Psd-95 involvement in maturation of excitatory synapses. *Science*, 290(5495):1364–8, 2000.
- D. El-Husseini Ael, E. Schnell, S. Dakoji, N. Sweeney, Q. Zhou, O. Prange, C. Gauthier-Campbell, A. Aguilera-Moreno, R. A. Nicoll, and D. S. Bredt. Synaptic strength regulated by palmitate cycling on psd-95. *Cell*, 108(6):849–63, 2002.
- Z. M. Eletr, D. T. Huang, D. M. Duda, B. A. Schulman, and B. Kuhlman. E2 conjugating enzymes must disengage from their e1 enzymes before e3-dependent ubiquitin and ubiquitin-like transfer. *Nat Struct Mol Biol*, 12(10):933–4, 2005.
- G. M. Elias, L. Funke, V. Stein, S. G. Grant, D. S. Bredt, and R. A. Nicoll. Synapse-specific and developmentally regulated targeting of ampa receptors by a family of maguk scaffolding proteins. *Neuron*, 52(2):307–20, 2006.
- G. M. Elias, L. A. Elias, P. F. Apostolides, A. R. Kriegstein, and R. A. Nicoll. Differential trafficking of ampa and nmda receptors by sap102 and psd-95 underlies synapse development. *Proc Natl Acad Sci U S A*, 105(52):20953–8, 2008.
- M. Feligioni, A. Nishimune, and J. M. Henley. Protein sumoylation modulates calcium influx and glutamate release from presynaptic terminals. *Eur J Neurosci*, 29(7):1348–56, 2009.
- F. Ferraguti and R. Shigemoto. Metabotropic glutamate receptors. *Cell Tissue Res*, 326(2):483–504, 2006.
- R. Fonseca, U. V. Nagerl, and T. Bonhoeffer. Neuronal activity determines the protein synthesis dependence of long-term potentiation. *Nat Neurosci*, 9(4):478–80, 2006.
- B. Forstera, A. A. Belaidi, R. Juttner, C. Bernert, M. Tsokos, T. N. Lehmann, P. Horn, C. Dehnicke, G. Schwarz, and J. C. Meier. Irregular rna splicing curtails postsynaptic gephyrin in the cornu ammonis of patients with epilepsy. *Brain*, 133(Pt 12):3778–94, 2010.

-
- R. Frischknecht, M. Heine, D. Perrais, C. I. Seidenbecher, D. Choquet, and E. D. Gundelfinger. Brain extracellular matrix affects ampa receptor lateral mobility and short-term synaptic plasticity. *Nat Neurosci*, 12(7):897–904, 2009.
- J. M. Fritschy, D. K. Johnson, H. Mohler, and U. Rudolph. Independent assembly and subcellular targeting of gaba(a)-receptor subtypes demonstrated in mouse hippocampal and olfactory neurons in vivo. *Neurosci Lett*, 249(2-3):99–102, 1998.
- L. Funke, S. Dakoji, and D. S. Bredt. Membrane-associated guanylate kinases regulate adhesion and plasticity at cell junctions. *Annu Rev Biochem*, 74:219–45, 2005.
- L. Ghoda, D. Sidney, M. Macrae, and P. Coffino. Structural elements of ornithine decarboxylase required for intracellular degradation and polyamine-dependent regulation. *Mol Cell Biol*, 12(5):2178–85, 1992.
- T. Giesemann, G. Schwarz, R. Nawrotzki, K. Berhorster, M. Rothkegel, K. Schluter, N. Schrader, H. Schindelin, R. R. Mendel, J. Kirsch, and B. M. Jockusch. Complex formation between the postsynaptic scaffolding protein gephyrin, profilin, and mena: a possible link to the microfilament system. *J Neurosci*, 23(23):8330–9, 2003.
- C. G. Giraud, W. S. Eng, T. J. Melia, and J. E. Rothman. A clamping mechanism involved in snare-dependent exocytosis. *Science*, 313(5787):676–80, 2006.
- S. J. Goldenberg, T. C. Cascio, S. D. Shumway, K. C. Garbutt, J. Liu, Y. Xiong, and N. Zheng. Structure of the cand1-cul1-roc1 complex reveals regulatory mechanisms for the assembly of the multisubunit cullin-dependent ubiquitin ligases. *Cell*, 119(4):517–28, 2004.
- L. Gong and E. T. Yeh. Identification of the activating and conjugating enzymes of the nedd8 conjugation pathway. *J Biol Chem*, 274(17):12036–42, 1999.
- L. Groc, M. Heine, L. Cognet, K. Brickley, F. A. Stephenson, B. Lounis, and D. Choquet. Differential activity-dependent regulation of the lateral mobilities of ampa and nmda receptors. *Nat Neurosci*, 7(7):695–6, 2004.
- A. J. Groffen, S. Martens, R. Diez Arazola, L. N. Cornelisse, N. Lozovaya, A. P. de Jong, N. A. Goriounova, R. L. Habets, Y. Takai, J. G. Borst, N. Brose, H. T. McMahon, and M. Verhage. Doc2b is a high-affinity ca²⁺ sensor for spontaneous neurotransmitter release. *Science*, 327(5973):1614–8, 2010.
- A. L. Haas, J. V. Warmes, A. Hershko, and I. A. Rose. Ubiquitin-activating enzyme. mechanism and role in protein-ubiquitin conjugation. *J Biol Chem*, 257(5):2543–8–, 1982.
- A. L. Haas, P. Ahrens, P. M. Bright, and H. Ankel. Interferon induces a 15-kilodalton protein exhibiting marked homology to ubiquitin. *J Biol Chem*, 262(23):11315–23, 1987.
- K. F. Haas and K. Broadie. Roles of ubiquitination at the synapse. *Biochim Biophys Acta*, 1779(8):495–506, 2008.

- K. Haglund, P. P. Di Fiore, and I. Dikic. Distinct monoubiquitin signals in receptor endocytosis. *Trends Biochem Sci*, 28(11):598–603, 2003.
- O. P. Hamill, A. Marty, E. Neher, B. Sakmann, and F. J. Sigworth. Improved patch-clamp techniques for high-resolution current recording from cells and cell-free membrane patches. *Pflugers Arch*, 391(2):85–100, 1981.
- J. G. Han, H. Zhu, G. D. Chen, P. Chen, L. M. Luo, X. N. Liu, and C. B. Wang. [the expression of bdnf and psd-95 in hippocampal ca1 region of morphine-withdrawn rat with different dependent times]. *Sichuan Da Xue Xue Bao Yi Xue Ban*, 39(2):253–5, 2008.
- J. W. Harper. Neddylation of the guardian; mdm2 catalyzed conjugation of nedd8 to p53. *Cell*, 118(1):2–4, 2004.
- Y. Haupt, R. Maya, A. Kazaz, and M. Oren. Mdm2 promotes the rapid degradation of p53. *Nature*, 387(6630):296–9, 1997.
- T. Hayashi, G. Rumbaugh, and R. L. Huganir. Differential regulation of ampa receptor subunit trafficking by palmitoylation of two distinct sites. *Neuron*, 47(5):709–23, 2005.
- T. Hayashi, G. M. Thomas, and R. L. Huganir. Dual palmitoylation of nr2 subunits regulates nmda receptor trafficking. *Neuron*, 64(2):213–26, 2009.
- M. Heine, L. Groc, R. Frischknecht, J. C. Beique, B. Lounis, G. Rumbaugh, R. L. Huganir, L. Cognet, and D. Choquet. Surface mobility of postsynaptic ampars tunes synaptic transmission. *Science*, 320(5873):201–5, 2008.
- A. Hershko and A. Ciechanover. The ubiquitin system. *Annu Rev Biochem*, 67:425–79, 1998.
- K. Hirao, Y. Hata, I. Yao, M. Deguchi, H. Kawabe, A. Mizoguchi, and Y. Takai. Three isoforms of synaptic scaffolding molecule and their characterization. multimerization between the isoforms and their interaction with n-methyl-d-aspartate receptors and sap90/psd-95-associated protein. *J Biol Chem*, 275(4):2966–72, 2000.
- R. Hjerpe, Y. Thomas, J. Chen, A. Zemla, S. Curran, N. Shpiro, L. R. Dick, and T. Kurz. Changes in the ratio of free nedd8 to ubiquitin triggers neddylation by ubiquitin enzymes. *Biochem J*, 441(3):927–36, 2012.
- G. P. Ho, B. Selvakumar, J. Mukai, L. D. Hester, Y. Wang, J. A. Gogos, and S. H. Snyder. S-nitrosylation and s-palmitoylation reciprocally regulate synaptic targeting of psd-95. *Neuron*, 71(1):131–41, 2011.
- M. Hochstrasser. Ubiquitin-dependent protein degradation. *Annu Rev Genet*, 30:405–39, 1996.
- M. Hochstrasser. Origin and function of ubiquitin-like proteins. *Nature*, 458(7237):422–9, 2009.
- S. B. Hofer, T. D. Mrsic-Flogel, T. Bonhoeffer, and M. Hubener. Experience leaves a lasting structural trace in cortical circuits. *Nature*, 457(7227):313–7, 2009.

-
- M. Hollmann and S. Heinemann. Cloned glutamate receptors. *Annu Rev Neurosci*, 17:31–108, 1994.
- T. Hoppe. Multiubiquitylation by e4 enzymes: 'one size' doesn't fit all. *Trends Biochem Sci*, 30(4):183–7, 2005.
- T. Hori, F. Osaka, T. Chiba, C. Miyamoto, K. Okabayashi, N. Shimbara, S. Kato, and K. Tanaka. Covalent modification of all members of human cullin family proteins by nedd8. *Oncogene*, 18(48):6829–34, 1999.
- S. K. Hotton and J. Callis. Regulation of cullin ring ligases. *Annu Rev Plant Biol*, 59:467–89, 2008.
- Y. P. Hsueh and M. Sheng. Requirement of n-terminal cysteines of psd-95 for psd-95 multimerization and ternary complex formation, but not for binding to potassium channel kv1.4. *J Biol Chem*, 274(1):532–6, 1999.
- Y. P. Hsueh, E. Kim, and M. Sheng. Disulfide-linked head-to-head multimerization in the mechanism of ion channel clustering by psd-95. *Neuron*, 18(5):803–14, 1997.
- D. T. Huang and B. A. Schulman. Expression, purification, and characterization of the e1 for human nedd8, the heterodimeric appbp1-uba3 complex. *Methods Enzymol*, 398:9–20, 2005.
- D. T. Huang, D. W. Miller, R. Mathew, R. Cassell, J. M. Holton, M. F. Roussel, and B. A. Schulman. A unique e1-e2 interaction required for optimal conjugation of the ubiquitin-like protein nedd8. *Nat Struct Mol Biol*, 11(10):927–35, 2004.
- D. T. Huang, O. Ayrault, H. W. Hunt, A. M. Taherbhoy, D. M. Duda, D. C. Scott, L. A. Borg, G. Neale, P. J. Murray, M. F. Roussel, and B. A. Schulman. E2-ring expansion of the nedd8 cascade confers specificity to cullin modification. *Mol Cell*, 33(4):483–95, 2009.
- A. Y. Hung, C. C. Sung, I. L. Brito, and M. Sheng. Degradation of postsynaptic scaffold gkap and regulation of dendritic spine morphology by the trim3 ubiquitin ligase in rat hippocampal neurons. *PLoS One*, 5(3):e9842, 2010.
- D. L. Hunt and P. E. Castillo. Synaptic plasticity of nmda receptors: mechanisms and functional implications. *Curr Opin Neurobiol*, 22(3):496–508, 2012.
- D. P. Huynh, D. R. Scoles, D. Nguyen, and S. M. Pulst. The autosomal recessive juvenile parkinson disease gene product, parkin, interacts with and ubiquitinates synaptotagmin xi. *Hum Mol Genet*, 12(20):2587–97, 2003.
- Y. Ichimura, T. Kirisako, T. Takao, Y. Satomi, Y. Shimonishi, N. Ishihara, N. Mizushima, I. Tanida, E. Kominami, M. Ohsumi, T. Noda, and Y. Ohsumi. A ubiquitin-like system mediates protein lipidation. *Nature*, 408(6811):488–92, 2000.
- M. Irie, Y. Hata, M. Takeuchi, K. Ichtchenko, A. Toyoda, K. Hirao, Y. Takai, T. W. Rosahl, and T. C. Sudhof. Binding of neuroligins to psd-95. *Science*, 277(5331):1511–5, 1997.

- T. C. Jacob, Y. D. Bogdanov, C. Magnus, R. S. Saliba, J. T. Kittler, P. G. Haydon, and S. J. Moss. Gephyrin regulates the cell surface dynamics of synaptic gabaa receptors. *J Neurosci*, 25(45):10469–78, 2005.
- S. M. Jeram, T. Srikumar, P. G. Pedrioli, and B. Raught. Using mass spectrometry to identify ubiquitin and ubiquitin-like protein conjugation sites. *Proteomics*, 9(4):922–34, 2009.
- S. M. Jeram, T. Srikumar, X. D. Zhang, H. Anne Eisenhauer, R. Rogers, P. G. Pedrioli, M. Matunis, and B. Raught. An improved summon-based methodology for the identification of ubiquitin and ubiquitin-like protein conjugation sites identifies novel ubiquitin-like protein chain linkages. *Proteomics*, 10(2):254–65, 2010.
- M. Jiang and G. Chen. High ca²⁺-phosphate transfection efficiency in low-density neuronal cultures. *Nat Protoc*, 1(2):695–700, 2006.
- Y. Joo, S. Ha, B. H. Hong, Ja Kim, K. A. Chang, H. Liew, S. Kim, W. Sun, J. H. Kim, Y. H. Chong, Y. H. Suh, and H. S. Kim. Amyloid precursor protein binding protein-1 modulates cell cycle progression in fetal neural stem cells. *PLoS One*, 5(12):e14203, 2010.
- P. Juo and J. M. Kaplan. The anaphase-promoting complex regulates the abundance of glr-1 glutamate receptors in the ventral nerve cord of *c. elegans*. *Curr Biol*, 14(22):2057–62, 2004.
- R. Jurd, C. Thornton, J. Wang, K. Luong, K. Phamluong, V. Kharazia, S. L. Gibb, and D. Ron. Mind bomb-2 is an e3 ligase that ubiquitinates the n-methyl-d-aspartate receptor nr2b subunit in a phosphorylation-dependent manner. *J Biol Chem*, 283(1):301–10, 2008.
- S. Kaech and G. Banker. Culturing hippocampal neurons. *Nat Protoc*, 1(5):2406–15, 2006.
- K. Kameyama, H. K. Lee, M. F. Bear, and R. L. Huganir. Involvement of a postsynaptic protein kinase a substrate in the expression of homosynaptic long-term depression. *Neuron*, 21(5):1163–75, 1998.
- T. Kamitani, K. Kito, H. P. Nguyen, and E. T. Yeh. Characterization of nedd8, a developmentally down-regulated ubiquitin-like protein. *J Biol Chem*, 272(45):28557–62, 1997.
- T. Kamura, M. N. Conrad, Q. Yan, R. C. Conaway, and J. W. Conaway. The rbx1 subunit of scf and vhl e3 ubiquitin ligase activates rub1 modification of cullins cdc53 and cul2. *Genes Dev*, 13(22):2928–33, 1999.
- E. R. Kandel and J. H. Schwartz. Molecular biology of learning: modulation of transmitter release. *Science*, 218(4571):433–43, 1982.
- A. Karpova, M. Mikhaylova, U. Thomas, T. Knopfel, and T. Behnisch. Involvement of protein synthesis and degradation in long-term potentiation of schaffer collateral ca1 synapses. *J Neurosci*, 26(18):4949–55, 2006.

-
- A. Kato, N. Rouach, R. A. Nicoll, and D. S. Bredt. Activity-dependent nmda receptor degradation mediated by retrotranslocation and ubiquitination. *Proc Natl Acad Sci U S A*, 102(15):5600–5, 2005.
- A. S. Kato, M. B. Gill, M. T. Ho, H. Yu, Y. Tu, E. R. Siuda, H. Wang, Y. W. Qian, E. S. Nisenbaum, S. Tomita, and D. S. Bredt. Hippocampal ampa receptor gating controlled by both tarp and cornichon proteins. *Neuron*, 68(6):1082–96, 2010.
- H. Kawabe and N. Brose. The role of ubiquitylation in nerve cell development. *Nat Rev Neurosci*, 12(5):251–68, 2011.
- T. Keck, T. D. Mrsic-Flogel, M. Vaz Afonso, U. T. Eysel, T. Bonhoeffer, and M. Hubener. *Massive restructuring of neuronal circuits during functional reorganization of adult visual cortex*, volume 11, pages 1162–7. United States, 2008.
- K. Keinanen, W. Wisden, B. Sommer, P. Werner, A. Herb, T. A. Verdoorn, B. Sakmann, and P. H. Seeburg. A family of ampa-selective glutamate receptors. *Science*, 249(4968):556–60, 1990.
- J. M. Kerr and T. A. Blanpied. Subsynaptic ampa receptor distribution is acutely regulated by actin-driven reorganization of the postsynaptic density. *J Neurosci*, 32(2):658–73, 2012.
- O. Kerscher, R. Felberbaum, and M. Hochstrasser. Modification of proteins by ubiquitin and ubiquitin-like proteins. *Annu Rev Cell Dev Biol*, 22:159–80, 2006.
- H. W. Kessels, C. D. Kopec, M. E. Klein, and R. Malinow. Roles of stargazin and phosphorylation in the control of ampa receptor subcellular distribution. *Nat Neurosci*, 12(7):888–96, 2009.
- E. Kim and M. Sheng. PdZ domain proteins of synapses. *Nat Rev Neurosci*, 5(10):771–81, 2004.
- E. Kim, S. Naisbitt, Y. P. Hsueh, A. Rao, A. Rothschild, A. M. Craig, and M. Sheng. Gkap, a novel synaptic protein that interacts with the guanylate kinase-like domain of the psd-95/sap90 family of channel clustering molecules. *J Cell Biol*, 136(3):669–78, 1997.
- J. H. Kim, K. C. Park, S. S. Chung, O. Bang, and C. H. Chung. Deubiquitinating enzymes as cellular regulators. *J Biochem*, 134(1):9–18, 2003.
- K. Kim, J. Yang, X. P. Zhong, M. H. Kim, Y. S. Kim, H. W. Lee, S. Han, J. Choi, K. Han, J. Seo, S. M. Prescott, M. K. Topham, Y. C. Bae, G. Koretzky, S. Y. Choi, and E. Kim. Synaptic removal of diacylglycerol by dgkzeta and psd-95 regulates dendritic spine maintenance. *EMBO J*, 28(8):1170–9, 2009.
- M. J. Kim, K. Futai, J. Jo, Y. Hayashi, K. Cho, and M. Sheng. Synaptic accumulation of psd-95 and synaptic function regulated by phosphorylation of serine-295 of psd-95. *Neuron*, 56(3):488–502, 2007.
- S. Kins, H. Betz, and J. Kirsch. Collybistin, a newly identified brain-specific gef, induces sub-membrane clustering of gephyrin. *Nat Neurosci*, 3(1):22–9, 2000.

- D. S. Kirkpatrick, C. Denison, and S. P. Gygi. Weighing in on ubiquitin: the expanding role of mass-spectrometry-based proteomics. *Nat Cell Biol*, 7(8):750–7, 2005.
- J. T. Kittler, P. Thomas, V. Tretter, Y. D. Bogdanov, V. Haucke, T. G. Smart, and S. J. Moss. Huntingtin-associated protein 1 regulates inhibitory synaptic transmission by modulating gamma-aminobutyric acid type a receptor membrane trafficking. *Proc Natl Acad Sci U S A*, 101(34):12736–41, 2004.
- M. Kneussel, A. Hermann, J. Kirsch, and H. Betz. Hydrophobic interactions mediate binding of the glycine receptor beta-subunit to gephyrin. *J Neurochem*, 72(3):1323–6, 1999.
- C. D. Kopec, E. Real, H. W. Kessels, and R. Malinow. Glur1 links structural and functional plasticity at excitatory synapses. *J Neurosci*, 27(50):13706–18, 2007.
- M. H. Kubbutat, S. N. Jones, and K. H. Vousden. Regulation of p53 stability by mdm2. *Nature*, 387(6630):299–303, 1997.
- R. Kulikov, J. Letienne, M. Kaur, S. R. Grossman, J. Arts, and C. Blattner. Mdm2 facilitates the association of p53 with the proteasome. *Proc Natl Acad Sci U S A*, 107(22):10038–43, 2010.
- S. Kumar, Y. Tomooka, and M. Noda. Identification of a set of genes with developmentally down-regulated expression in the mouse brain. *Biochem Biophys Res Commun*, 185(3):1155–61, 1992.
- H. Kuromi and Y. Kidokoro. Tetanic stimulation recruits vesicles from reserve pool via a camp-mediated process in drosophila synapses. *Neuron*, 27(1):133–43, 2000.
- J. Y. Lan, V. A. Skeberdis, T. Jover, S. Y. Grooms, Y. Lin, R. C. Araneda, X. Zheng, M. V. Bennett, and R. S. Zukin. Protein kinase c modulates nmda receptor trafficking and gating. *Nat Neurosci*, 4(4):382–90, 2001.
- L. F. Lau, A. Mammen, M. D. Ehlers, S. Kindler, W. J. Chung, C. C. Garner, and R. L. Huganir. Interaction of the n-methyl-d-aspartate receptor complex with a novel synapse-associated protein, sap102. *J Biol Chem*, 271(35):21622–8, 1996.
- H. W. Lee, J. Choi, H. Shin, K. Kim, J. Yang, M. Na, S. Y. Choi, G. B. Kang, S. H. Eom, H. Kim, and E. Kim. Preso, a novel psd-95-interacting ferm and pdz domain protein that regulates dendritic spine morphogenesis. *J Neurosci*, 28(53):14546–56, 2008.
- J. T. Lee and W. Gu. The multiple levels of regulation by p53 ubiquitination. *Cell Death Differ*, 17(1):86–92, 2010.
- J. N. Levinson and A. El-Husseini. Building excitatory and inhibitory synapses: balancing neurotransmitter partnerships. *Neuron*, 48(2):171–4, 2005.
- Y. Li, J. Hu, K. Hofer, A. M. Wong, J. D. Cooper, S. G. Birnbaum, R. E. Hammer, and S. L. Hofmann. Dhhc5 interacts with pdz domain 3 of post-synaptic density-95 (psd-95) protein and plays a role in learning and memory. *J Biol Chem*, 285(17):13022–31, 2010.

-
- D. Liakopoulos, G. Doenges, K. Matuschewski, and S. Jentsch. A novel protein modification pathway related to the ubiquitin system. *EMBO J*, 17(8):2208–14, 1998.
- A. Lin, Q. Hou, L. Jarzylo, S. Amato, J. Gilbert, F. Shang, and H. Y. Man. Nedd4-mediated ampa receptor ubiquitination regulates receptor turnover and trafficking. *J Neurochem*, 119(1):27–39, 2011.
- D. Lin, M. H. Tatham, B. Yu, S. Kim, R. T. Hay, and Y. Chen. Identification of a substrate recognition site on ubc9. *J Biol Chem*, 277(24):21740–8, 2002.
- D. T. Lin, Y. Makino, K. Sharma, T. Hayashi, R. Neve, K. Takamiya, and R. L. Huganir. Regulation of ampa receptor extrasynaptic insertion by 4.1n, phosphorylation and palmitoylation. *Nat Neurosci*, 12(7):879–87, 2009.
- G. Liu and D. P. Xirodimas. Nub1 promotes cytoplasmic localization of p53 through cooperation of the nedd8 and ubiquitin pathways. *Oncogene*, 29(15):2252–61, 2010.
- J. Liu, M. Furukawa, T. Matsumoto, and Y. Xiong. Nedd8 modification of cul1 dissociates p120(cand1), an inhibitor of cul1-skp1 binding and scf ligases. *Mol Cell*, 10(6):1511–8, 2002.
- Y. C. Liu, J. Pan, C. Zhang, W. Fan, M. Collinge, J. R. Bender, and S. M. Weissman. A mhc-encoded ubiquitin-like protein (fat10) binds noncovalently to the spindle assembly checkpoint protein mad2. *Proc Natl Acad Sci U S A*, 96(8):4313–8, 1999.
- K. R. Loeb and A. L. Haas. The interferon-inducible 15-kda ubiquitin homolog conjugates to intracellular proteins. *J Biol Chem*, 267(11):7806–13, 1992.
- J. F. Long, H. Tochio, P. Wang, J. S. Fan, C. Sala, M. Niethammer, M. Sheng, and M. Zhang. Supramodular structure and synergistic target binding of the n-terminal tandem pdz domains of psd-95. *J Mol Biol*, 327(1):203–14, 2003.
- B. Lu, I. Al-Ramahi, A. Valencia, Q. Wang, F. Berenshteyn, H. Yang, T. Gallego-Flores, S. Ichcho, A. Lacoste, M. Hild, M. DiFiglia, J. Botas, and J. Palacino. Identification of nub1 as a suppressor of mutant huntington toxicity via enhanced protein clearance. *Nat Neurosci*, 16(5):562–70, 2013.
- H. Lu, P. L. Cheng, B. K. Lim, N. Khoshnevisrad, and M. M. Poo. Elevated bdnf after cocaine withdrawal facilitates ltp in medial prefrontal cortex by suppressing gaba inhibition. *Neuron*, 67(5):821–33, 2010.
- W. Lu, H. Man, W. Ju, W. S. Trimble, J. F. MacDonald, and Y. T. Wang. Activation of synaptic nmda receptors induces membrane insertion of new ampa receptors and ltp in cultured hippocampal neurons. *Neuron*, 29(1):243–54, 2001.
- M. P. Lussier, Y. Nasu-Nishimura, and K. W. Roche. Activity-dependent ubiquitination of the ampa receptor subunit glua2. *J Neurosci*, 31(8):3077–81, 2011.

- S. Lyapina, G. Cope, A. Shevchenko, G. Serino, T. Tsuge, C. Zhou, D. A. Wolf, N. Wei, A. Shevchenko, and R. J. Deshaies. Promotion of nedd-cul1 conjugate cleavage by cop9 signalosome. *Science*, 292(5520):1382–5, 2001.
- A. M. Mabb and M. D. Ehlers. Ubiquitination in postsynaptic function and plasticity. *Annu Rev Cell Dev Biol*, 26:179–210, 2010.
- A. K. Majewska, J. R. Newton, and M. Sur. Remodeling of synaptic structure in sensory cortical areas in vivo. *J Neurosci*, 26(11):3021–9, 2006.
- R. C. Malenka and M. F. Bear. Ltp and ltd: an embarrassment of riches. *Neuron*, 44(1):5–21, 2004.
- A. Mammoto, T. Sasaki, T. Asakura, I. Hotta, H. Imamura, K. Takahashi, Y. Matsuura, T. Shirao, and Y. Takai. Interactions of drebrin and gephyrin with profilin. *Biochem Biophys Res Commun*, 243(1):86–9, 1998.
- L. M. Mao, W. Wang, X. P. Chu, G. C. Zhang, X. Y. Liu, Y. J. Yang, M. Haines, C. J. Pappasian, E. E. Fibuch, S. Buch, J. G. Chen, and J. Q. Wang. Stability of surface nmda receptors controls synaptic and behavioral adaptations to amphetamine. *Nat Neurosci*, 12(5):602–10, 2009.
- S. Martin, A. Nishimune, J. R. Mellor, and J. M. Henley. Sumoylation regulates kainate-receptor-mediated synaptic transmission. *Nature*, 447(7142):321–5, 2007.
- R. Mattera, Y. C. Tsai, A. M. Weissman, and J. S. Bonifacino. The rab5 guanine nucleotide exchange factor rabex-5 binds ubiquitin (ub) and functions as a ub ligase through an atypical ub-interacting motif and a zinc finger domain. *J Biol Chem*, 281(10):6874–83, 2006.
- J. L. McGaugh. Memory—a century of consolidation. *Science*, 287(5451):248–51, 2000.
- A. W. McGee, S. R. Dakoji, O. Olsen, D. S. Bredt, W. A. Lim, and K. E. Prehoda. Structure of the sh3-guanylate kinase module from psd-95 suggests a mechanism for regulated assembly of maguk scaffolding proteins. *Mol Cell*, 8(6):1291–301, 2001.
- G. Meyer, J. Kirsch, H. Betz, and D. Langosch. Identification of a gephyrin binding motif on the glycine receptor beta subunit. *Neuron*, 15(3):563–72, 1995.
- M. Migaud, P. Charlesworth, M. Dempster, L. C. Webster, A. M. Watabe, M. Makhinson, Y. He, M. F. Ramsay, R. G. Morris, J. H. Morrison, T. J. O’Dell, and S. G. Grant. Enhanced long-term potentiation and impaired learning in mice with mutant postsynaptic density-95 protein. *Nature*, 396(6710):433–9, 1998.
- U. Misgeld, R. A. Deisz, H. U. Dodt, and H. D. Lux. The role of chloride transport in postsynaptic inhibition of hippocampal neurons. *Science*, 232(4756):1413–5, 1986.
- N. Mizushima, T. Noda, T. Yoshimori, Y. Tanaka, T. Ishii, M. D. George, D. J. Klionsky, M. Ohsumi, and Y. Ohsumi. A protein conjugation system essential for autophagy. *Nature*, 395(6700):395–8, 1998.

-
- S. Moffett, L. Adam, H. Bonin, T. P. Loisel, M. Bouvier, and B. Mouillac. Palmitoylated cysteine 341 modulates phosphorylation of the beta2-adrenergic receptor by the camp-dependent protein kinase. *J Biol Chem*, 271(35):21490–7, 1996.
- M. Mondin, V. Labrousse, E. Hossy, M. Heine, B. Tessier, F. Levet, C. Poujol, C. Blanchet, D. Choquet, and O. Thoumine. Neurexin-neuroigin adhesions capture surface-diffusing ampa receptors through psd-95 scaffolds. *J Neurosci*, 31(38):13500–15, 2011.
- H. Monyer, P. H. Seeburg, and W. Wisden. Glutamate-operated channels: developmentally early and mature forms arise by alternative splicing. *Neuron*, 6(5):799–810, 1991.
- M. A. Morabito, M. Sheng, and L. H. Tsai. Cyclin-dependent kinase 5 phosphorylates the n-terminal domain of the postsynaptic density protein psd-95 in neurons. *J Neurosci*, 24(4):865–76, 2004.
- F. Mori, M. Nishie, Y. S. Piao, K. Kito, T. Kamitani, H. Takahashi, and K. Wakabayashi. Accumulation of nedd8 in neuronal and glial inclusions of neurodegenerative disorders. *Neuropathol Appl Neurobiol*, 31(1):53–61, 2005.
- M. Morimoto, T. Nishida, R. Honda, and H. Yasuda. Modification of cullin-1 by ubiquitin-like protein nedd8 enhances the activity of scf(skp2) toward p27(kip1). *Biochem Biophys Res Commun*, 270(3):1093–6, 2000.
- J. Mosbacher, R. Schoepfer, H. Monyer, N. Burnashev, P. H. Seeburg, and J. P. Ruppersberg. A molecular determinant for submillisecond desensitization in glutamate receptors. *Science*, 266(5187):1059–62, 1994.
- D. Mukhopadhyay and H. Riezman. Proteasome-independent functions of ubiquitin in endocytosis and signaling. *Science*, 315(5809):201–5, 2007.
- Y. Murata, T. Doi, H. Taniguchi, and Y. Fujiyoshi. Proteomic analysis revealed a novel synaptic proline-rich membrane protein (prp7) associated with psd-95 and nmda receptor. *Biochem Biophys Res Commun*, 327(1):183–91, 2005.
- T. Nakagawa, K. Futai, H. A. Lashuel, I. Lo, K. Okamoto, T. Walz, Y. Hayashi, and M. Sheng. Quaternary structure, protein dynamics, and synaptic function of sap97 controlled by l27 domain interactions. *Neuron*, 44(3):453–67, 2004.
- E. Nakahira and S. Yuasa. Neuronal generation, migration, and differentiation in the mouse hippocampal primordium as revealed by enhanced green fluorescent protein gene transfer by means of in utero electroporation. *J Comp Neurol*, 483(3):329–40, 2005.
- R. F. Nelson, K. A. Glenn, V. M. Miller, H. Wen, and H. L. Paulson. A novel route for f-box protein-mediated ubiquitination links chip to glycoprotein quality control. *J Biol Chem*, 281(29):20242–51, 2006.
- R. A. Nicoll, S. Tomita, and D. S. Bredt. Auxiliary subunits assist ampa-type glutamate receptors. *Science*, 311(5765):1253–6, 2006.

- A. Nishimune, J. T. Isaac, E. Molnar, J. Noel, S. R. Nash, M. Tagaya, G. L. Collingridge, S. Nakanishi, and J. M. Henley. Nsf binding to glur2 regulates synaptic transmission. *Neuron*, 21(1): 87–97, 1998.
- C. M. Niswender and P. J. Conn. Metabotropic glutamate receptors: physiology, pharmacology, and disease. *Annu Rev Pharmacol Toxicol*, 50:295–322, 2010.
- M. Nonaka, T. Doi, Y. Fujiyoshi, S. Takemoto-Kimura, and H. Bito. Essential contribution of the ligand-binding beta b/beta c loop of pdz1 and pdz2 in the regulation of postsynaptic clustering, scaffolding, and localization of postsynaptic density-95. *J Neurosci*, 26(3):763–74, 2006.
- J. Noritake, Y. Fukata, T. Iwanaga, N. Hosomi, R. Tsutsumi, N. Matsuda, H. Tani, H. Iwanari, Y. Mochizuki, T. Kodama, Y. Matsuura, D. S. Bredt, T. Hamakubo, and M. Fukata. Mobile dhhc palmitoylating enzyme mediates activity-sensitive synaptic targeting of psd-95. *J Cell Biol*, 186(1):147–60, 2009.
- A. Oberst, M. Rossi, P. Salomoni, P. P. Pandolfi, M. Oren, G. Melino, and F. Bernassola. Regulation of the p73 protein stability and degradation. *Biochem Biophys Res Commun*, 331(3):707–12, 2005.
- F. Osaka, H. Kawasaki, N. Aida, M. Saeki, T. Chiba, S. Kawashima, K. Tanaka, and S. Kato. A new nedd8-ligating system for cullin-4a. *Genes Dev*, 12(15):2263–8, 1998.
- S. Oved, Y. Mosesson, Y. Zwang, E. Santonico, K. Shtiegman, M. D. Marmor, B. S. Kochupurakkal, M. Katz, S. Lavi, G. Cesareni, and Y. Yarden. Conjugation to nedd8 instigates ubiquitylation and down-regulation of activated receptor tyrosine kinases. *J Biol Chem*, 281(31): 21640–51, 2006.
- D. T. Pak, S. Yang, S. Rudolph-Correia, E. Kim, and M. Sheng. Regulation of dendritic spine morphology by spar, a psd-95-associated rapgap. *Neuron*, 31(2):289–303, 2001.
- Z. Q. Pan, A. Kentsis, D. C. Dias, K. Yamoah, and K. Wu. Nedd8 on cullin: building an expressway to protein destruction. *Oncogene*, 23(11):1985–97, 2004.
- P. Paoletti. Molecular basis of nmda receptor functional diversity. *Eur J Neurosci*, 33(8):1351–65, 2011.
- M. Passafaro, V. Piech, and M. Sheng. Subunit-specific temporal and spatial patterns of ampa receptor exocytosis in hippocampal neurons. *Nat Neurosci*, 4(9):917–26, 2001.
- G. N. Patrick, B. Bingol, H. A. Weld, and E. M. Schuman. Ubiquitin-mediated proteasome activity is required for agonist-induced endocytosis of glurs. *Curr Biol*, 13(23):2073–81, 2003.
- R. S. Petralia, Y. X. Wang, and R. J. Wenthold. Nmda receptors and psd-95 are found in attachment plaques in cerebellar granular layer glomeruli. *Eur J Neurosci*, 15(3):583–7, 2002.

-
- L. Pickard, J. Noel, J. K. Duckworth, S. M. Fitzjohn, J. M. Henley, G. L. Collingridge, and E. Molnar. Transient synaptic activation of nmda receptors leads to the insertion of native ampa receptors at hippocampal neuronal plasma membranes. *Neuropharmacology*, 41(6):700–13, 2001.
- D. S. Pickering, F. A. Taverna, M. W. Salter, and D. R. Hampson. Palmitoylation of the glur6 kainate receptor. *Proc Natl Acad Sci U S A*, 92(26):12090–4, 1995.
- A. Priel, A. Kollerker, G. Ayalon, M. Gillor, P. Osten, and Y. Stern-Bach. Stargazin reduces desensitization and slows deactivation of the ampa-type glutamate receptors. *J Neurosci*, 25(10):2682–6, 2005.
- K. Prybylowski, K. Chang, N. Sans, L. Kan, S. Vicini, and R. J. Wenthold. The synaptic localization of nr2b-containing nmda receptors is controlled by interactions with pdz proteins and ap-2. *Neuron*, 47(6):845–57, 2005.
- M. L. Reese, S. Dakoji, D. S. Bredt, and V. Dotsch. The guanylate kinase domain of the maguk psd-95 binds dynamically to a conserved motif in map1a. *Nat Struct Mol Biol*, 14(2):155–63, 2007.
- F. E. Reyes-Turcu, K. H. Ventii, and K. D. Wilkinson. Regulation and cellular roles of ubiquitin-specific deubiquitinating enzymes. *Annu Rev Biochem*, 78:363–97, 2009.
- K. W. Roche, S. Standley, J. McCallum, C. Dune Ly, M. D. Ehlers, and R. J. Wenthold. Molecular determinants of nmda receptor internalization. *Nat Neurosci*, 4(8):794–802, 2001.
- C. Rosenmund, Y. Stern-Bach, and C. F. Stevens. The tetrameric structure of a glutamate receptor channel. *Science*, 280(5369):1596–9, 1998.
- N. Rouach, K. Byrd, R. S. Petralia, G. M. Elias, H. Adesnik, S. Tomita, S. Karimzadegan, C. Kealey, D. S. Bredt, and R. A. Nicoll. Tarp gamma-8 controls hippocampal ampa receptor number, distribution and synaptic plasticity. *Nat Neurosci*, 8(11):1525–33, 2005.
- U. Rudolph and H. Mohler. Analysis of gabaa receptor function and dissection of the pharmacology of benzodiazepines and general anesthetics through mouse genetics. *Annu Rev Pharmacol Toxicol*, 44:475–98, 2004.
- A. Saha and R. J. Deshaies. Multimodal activation of the ubiquitin ligase scf by nedd8 conjugation. *Mol Cell*, 32(1):21–31, 2008.
- M. Sainlos, C. Tigaret, C. Poujol, N. B. Olivier, L. Bard, C. Breillat, K. Thiolon, D. Choquet, and B. Imperiali. Biomimetic divalent ligands for the acute disruption of synaptic ampar stabilization. *Nat Chem Biol*, 7(2):81–91, 2011.
- R. S. Saliba, G. Michels, T. C. Jacob, M. N. Pangalos, and S. J. Moss. Activity-dependent ubiquitination of gaba(a) receptors regulates their accumulation at synaptic sites. *J Neurosci*, 27(48):13341–51, 2007.

- N. Sans, C. Racca, R. S. Petralia, Y. X. Wang, J. McCallum, and R. J. Wenthold. Synapse-associated protein 97 selectively associates with a subset of ampa receptors early in their biosynthetic pathway. *J Neurosci*, 21(19):7506–16, 2001.
- S. D. Santos, A. L. Carvalho, M. V. Caldeira, and C. B. Duarte. Regulation of ampa receptors and synaptic plasticity. *Neuroscience*, 158(1):105–25, 2009.
- J. R. Schaub, X. Lu, B. Doneske, Y. K. Shin, and J. A. McNew. Hemifusion arrest by complexin is relieved by ca²⁺-synaptotagmin i. *Nat Struct Mol Biol*, 13(8):748–50, 2006.
- A. Scheschonka, Z. Tang, and H. Betz. Sumoylation in neurons: nuclear and synaptic roles? *Trends Neurosci*, 30(3):85–91, 2007.
- E. Schnell, M. Sizemore, S. Karimzadegan, L. Chen, D. S. Bredt, and R. A. Nicoll. Direct interactions between psd-95 and stargazin control synaptic ampa receptor number. *Proc Natl Acad Sci U S A*, 99(21):13902–7, 2002.
- S. Schoch and E. D. Gundelfinger. Molecular organization of the presynaptic active zone. *Cell Tissue Res*, 326(2):379–91, 2006.
- S. M. Schork, M. Thumm, and D. H. Wolf. Catabolite inactivation of fructose-1,6-bisphosphatase of *saccharomyces cerevisiae*. degradation occurs via the ubiquitin pathway. *J Biol Chem*, 270(44):26446–50, 1995.
- A. L. Schwartz and A. Ciechanover. Targeting proteins for destruction by the ubiquitin system: implications for human pathobiology. *Annu Rev Pharmacol Toxicol*, 49:73–96, 2009.
- J. H. Schwartz. Ubiquitination, protein turnover, and long-term synaptic plasticity. *Sci STKE*, 2003(190):pe26, 2003.
- L. A. Schwarz, B. J. Hall, and G. N. Patrick. Activity-dependent ubiquitination of glua1 mediates a distinct ampa receptor endocytosis and sorting pathway. *J Neurosci*, 30(49):16718–29, 2010.
- W. B. Scoville and B. Milner. Loss of recent memory after bilateral hippocampal lesions. *J Neurol Neurosurg Psychiatry*, 20(1):11–21, 1957.
- G. K. Seabold, A. Burette, I. A. Lim, R. J. Weinberg, and J. W. Hell. Interaction of the tyrosine kinase pyk2 with the n-methyl-d-aspartate receptor complex via the src homology 3 domains of psd-95 and sap102. *J Biol Chem*, 278(17):15040–8, 2003.
- K. Shen and T. Meyer. Dynamic control of camkii translocation and localization in hippocampal neurons by nmda receptor stimulation. *Science*, 284(5411):162–6, 1999.
- L. Shen, F. Liang, L. D. Walensky, and R. L. Huganir. Regulation of ampa receptor glur1 subunit surface expression by a 4. 1n-linked actin cytoskeletal association. *J Neurosci*, 20(21):7932–40, 2000.

-
- L. N. Shen, H. Liu, C. Dong, D. Xirodimas, J. H. Naismith, and R. T. Hay. Structural basis of nedd8 ubiquitin discrimination by the deneddylating enzyme nedp1. *EMBO J*, 24(7):1341–51, 2005.
- S. Shi, Y. Hayashi, J. A. Esteban, and R. Malinow. Subunit-specific rules governing ampa receptor trafficking to synapses in hippocampal pyramidal neurons. *Cell*, 105(3):331–43, 2001.
- S. H. Shi, Y. Hayashi, R. S. Petralia, S. H. Zaman, R. J. Wenthold, K. Svoboda, and R. Malinow. Rapid spine delivery and redistribution of ampa receptors after synaptic nmda receptor activation. *Science*, 284(5421):1811–6, 1999.
- Y. Shi, Y. H. Suh, A. D. Milstein, K. Isozaki, S. M. Schmid, K. W. Roche, and R. A. Nicoll. Functional comparison of the effects of tarps and cornichons on ampa receptor trafficking and gating. *Proc Natl Acad Sci U S A*, 107(37):16315–9, 2010.
- S. L. Shipman, E. Schnell, T. Hirai, B. S. Chen, K. W. Roche, and R. A. Nicoll. Functional dependence of neuroligin on a new non-pdz intracellular domain. *Nat Neurosci*, 14(6):718–26, 2011.
- S. D. Shumway, M. Maki, and S. Miyamoto. The pest domain of ikappabalpha is necessary and sufficient for in vitro degradation by mu-calpain. *J Biol Chem*, 274(43):30874–81, 1999.
- B. Sommer, K. Keinanen, T. A. Verdoorn, W. Wisden, N. Burnashev, A. Herb, M. Kohler, T. Takagi, B. Sakmann, and P. H. Seeburg. Flip and flop: a cell-specific functional switch in glutamate-operated channels of the cns. *Science*, 249(4976):1580–5, 1990.
- T. A. Soucy, P. G. Smith, M. A. Milhollen, A. J. Berger, J. M. Gavin, S. Adhikari, J. E. Brownell, K. E. Burke, D. P. Cardin, S. Critchley, C. A. Cullis, A. Doucette, J. J. Garnsey, J. L. Gaulin, R. E. Gershman, A. R. Lublinsky, A. McDonald, H. Mizutani, U. Narayanan, E. J. Olhava, S. Peluso, M. Rezaei, M. D. Sintchak, T. Talreja, M. P. Thomas, T. Traore, S. Vyskocil, G. S. Weatherhead, J. Yu, J. Zhang, L. R. Dick, C. F. Claiborne, M. Rolfe, J. B. Bolen, and S. P. Langston. An inhibitor of nedd8-activating enzyme as a new approach to treat cancer. *Nature*, 458(7239):732–6, 2009.
- S. D. Speese, N. Trotta, C. K. Rodesch, B. Aravamudan, and K. Broadie. The ubiquitin proteasome system acutely regulates presynaptic protein turnover and synaptic efficacy. *Curr Biol*, 13(11):899–910, 2003.
- M. L. Spencer, M. Theodosiou, and D. J. Noonan. Npdc-1, a novel regulator of neuronal proliferation, is degraded by the ubiquitin/proteasome system through a pest degradation motif. *J Biol Chem*, 279(35):37069–78, 2004.
- V. Stein, D. R. House, D. S. Bredt, and R. A. Nicoll. Postsynaptic density-95 mimics and occludes hippocampal long-term potentiation and enhances long-term depression. *J Neurosci*, 23(13):5503–6, 2003.

- P. Steiner, M. J. Higley, W. Xu, B. L. Czervionke, R. C. Malenka, and B. L. Sabatini. Destabilization of the postsynaptic density by psd-95 serine 73 phosphorylation inhibits spine growth and synaptic plasticity. *Neuron*, 60(5):788–802, 2008.
- H. A. Steinman, E. Burstein, C. Lengner, J. Gosselin, G. Pihan, C. S. Duckett, and S. N. Jones. An alternative splice form of mdm2 induces p53-independent cell growth and tumorigenesis. *J Biol Chem*, 279(6):4877–86, 2004.
- L. Stoppini, P. A. Buchs, and D. Muller. A simple method for organotypic cultures of nervous tissue. *J Neurosci Methods*, 37(2):173–82, 1991.
- J. F. Sturgill, P. Steiner, B. L. Czervionke, and B. L. Sabatini. Distinct domains within psd-95 mediate synaptic incorporation, stabilization, and activity-dependent trafficking. *J Neurosci*, 29(41):12845–54, 2009.
- T. C. Sudhof and J. Rizo. Synaptic vesicle exocytosis. *Cold Spring Harb Perspect Biol*, 3(12), 2011.
- M. W. Swank and J. D. Sweatt. Increased histone acetyltransferase and lysine acetyltransferase activity and biphasic activation of the erk/rsk cascade in insular cortex during novel taste learning. *J Neurosci*, 21(10):3383–91, 2001.
- E. S. Sweet, M. L. Previtiera, J. R. Fernandez, E. I. Charych, C. Y. Tseng, M. Kwon, V. Starovoytov, J. Q. Zheng, and B. L. Firestein. Psd-95 alters microtubule dynamics via an association with eb3. *J Neurosci*, 31(3):1038–47, 2011.
- H. C. Tai and E. M. Schuman. Ubiquitin, the proteasome and protein degradation in neuronal function and dysfunction. *Nat Rev Neurosci*, 9(11):826–38, 2008.
- T. Takahashi, I. D. Forsythe, T. Tsujimoto, M. Barnes-Davies, and K. Onodera. Presynaptic calcium current modulation by a metabotropic glutamate receptor. *Science*, 274(5287):594–7, 1996.
- M. Takeuchi, Y. Hata, K. Hirao, A. Toyoda, M. Irie, and Y. Takai. Sapaps, a family of psd-95/sap90-associated proteins localized at postsynaptic density. *J Biol Chem*, 272(18):11943–51, 1997.
- Z. Tang, O. El Far, H. Betz, and A. Scheschonka. Pias1 interaction and sumoylation of metabotropic glutamate receptor 8. *J Biol Chem*, 280(46):38153–9, 2005.
- S. J. Tavalin, M. Colledge, J. W. Hell, L. K. Langeberg, R. L. Huganir, and J. D. Scott. Regulation of glur1 by the α -kinase anchoring protein 79 (akap79) signaling complex shares properties with long-term depression. *J Neurosci*, 22(8):3044–51, 2002.
- G. A. Tavares, E. H. Panepucci, and A. T. Brunger. Structural characterization of the intramolecular interaction between the sh3 and guanylate kinase domains of psd-95. *Mol Cell*, 8(6):1313–25, 2001.

-
- J. S. Thrower, L. Hoffman, M. Rechsteiner, and C. M. Pickart. Recognition of the polyubiquitin proteolytic signal. *EMBO J*, 19(1):94–102, 2000.
- K. Tomita, M. Sperling, S. B. Cambridge, T. Bonhoeffer, and M. Hubener. *A Molecular Correlate of Ocular Dominance Columns in the Developing Mammalian Visual Cortex*. 2012.
- S. Tomita, L. Chen, Y. Kawasaki, R. S. Petralia, R. J. Wenthold, R. A. Nicoll, and D. S. Bredt. Functional studies and distribution define a family of transmembrane ampa receptor regulatory proteins. *J Cell Biol*, 161(4):805–16, 2003.
- S. Tomita, H. Adesnik, M. Sekiguchi, W. Zhang, K. Wada, J. R. Howe, R. A. Nicoll, and D. S. Bredt. Stargazin modulates ampa receptor gating and trafficking by distinct domains. *Nature*, 435(7045):1052–8, 2005a.
- S. Tomita, V. Stein, T. J. Stocker, R. A. Nicoll, and D. S. Bredt. Bidirectional synaptic plasticity regulated by phosphorylation of stargazin-like tarps. *Neuron*, 45(2):269–77, 2005b.
- S. Tomita, M. Sekiguchi, K. Wada, R. A. Nicoll, and D. S. Bredt. Stargazin controls the pharmacology of ampa receptor potentiators. *Proc Natl Acad Sci U S A*, 103(26):10064–7, 2006.
- J. R. Topinka and D. S. Bredt. N-terminal palmitoylation of psd-95 regulates association with cell membranes and interaction with k⁺ channel kv1.4. *Neuron*, 20(1):125–34, 1998.
- S. F. Traynelis, L. P. Wollmuth, C. J. McBain, F. S. Menniti, K. M. Vance, K. K. Ogden, K. B. Hansen, H. Yuan, S. J. Myers, and R. Dingledine. Glutamate receptor ion channels: structure, regulation, and function. *Pharmacol Rev*, 62(3):405–96, 2010.
- D. Turetsky, E. Garringer, and D. K. Patneau. Stargazin modulates native ampa receptor functional properties by two distinct mechanisms. *J Neurosci*, 25(32):7438–48, 2005.
- H. D. Ulrich. Mutual interactions between the sumo and ubiquitin systems: a plea of no contest. *Trends Cell Biol*, 15(10):525–32, 2005.
- J. W. Um, K. A. Han, E. Im, Y. Oh, K. Lee, and K. C. Chung. Neddylation positively regulates the ubiquitin e3 ligase activity of parkin. *J Neurosci Res*, 90(5):1030–42, 2012.
- B. van Zundert, A. Yoshii, and M. Constantine-Paton. Receptor compartmentalization and trafficking at glutamate synapses: a developmental proposal. *Trends Neurosci*, 27(7):428–37, 2004.
- A. C. Vertegaal. Uncovering ubiquitin and ubiquitin-like signaling networks. *Chem Rev*, 111(12):7923–40, 2011.
- H. Wada, E. T. Yeh, and T. Kamitani. A dominant-negative ubc12 mutant sequesters nedd8 and inhibits nedd8 conjugation in vivo. *J Biol Chem*, 275(22):17008–15, 2000.
- S. A. Wagner, P. Beli, B. T. Weinert, C. Scholz, C. D. Kelstrup, C. Young, M. L. Nielsen, J. V. Olsen, C. Brakebusch, and C. Choudhary. Proteomic analyses reveal divergent ubiquitylation site patterns in murine tissues. *Mol Cell Proteomics*, 11(12):1578–85, 2012.

- H. Walden, M. S. Podgorski, D. T. Huang, D. W. Miller, R. J. Howard, Jr. Minor, D. L., J. M. Holton, and B. A. Schulman. The structure of the appbp1-uba3-nedd8-atp complex reveals the basis for selective ubiquitin-like protein activation by an e1. *Mol Cell*, 12(6):1427–37, 2003.
- P. Washbourne, X. B. Liu, E. G. Jones, and A. K. McAllister. Cycling of nmda receptors during trafficking in neurons before synapse formation. *J Neurosci*, 24(38):8253–64, 2004.
- M. W. Waung, B. E. Pfeiffer, E. D. Nosyreva, J. A. Ronesi, and K. M. Huber. Rapid translation of arc/arg3.1 selectively mediates mglur-dependent ltd through persistent increases in ampar endocytosis rate. *Neuron*, 59(1):84–97, 2008.
- F. Y. Wei, K. Tomizawa, T. Ohshima, A. Asada, T. Saito, C. Nguyen, J. A. Bibb, K. Ishiguro, A. B. Kulkarni, H. C. Pant, K. Mikoshiba, H. Matsui, and S. Hisanaga. Control of cyclin-dependent kinase 5 (cdk5) activity by glutamatergic regulation of p35 stability. *J Neurochem*, 93(2):502–12, 2005.
- R. L. Welchman, C. Gordon, and R. J. Mayer. Ubiquitin and ubiquitin-like proteins as multifunctional signals. *Nat Rev Mol Cell Biol*, 6(8):599–609, 2005.
- T. C. Wheeler, L. S. Chin, Y. Li, F. L. Roudabush, and L. Li. Regulation of synaptophysin degradation by mammalian homologues of seven in absentia. *J Biol Chem*, 277(12):10273–82, 2002.
- F. G. Whitby, G. Xia, C. M. Pickart, and C. P. Hill. Crystal structure of the human ubiquitin-like protein nedd8 and interactions with ubiquitin pathway enzymes. *J Biol Chem*, 273(52):34983–91, 1998.
- K. A. Wilkinson and J. M. Henley. Analysis of metabotropic glutamate receptor 7 as a potential substrate for sumoylation. *Neurosci Lett*, 491(3):181–6, 2011.
- K. A. Wilkinson, A. Nishimune, and J. M. Henley. Analysis of sumo-1 modification of neuronal proteins containing consensus sumoylation motifs. *Neurosci Lett*, 436(2):239–44, 2008.
- K. Willeumier, S. M. Pulst, and F. E. Schweizer. Proteasome inhibition triggers activity-dependent increase in the size of the recycling vesicle pool in cultured hippocampal neurons. *J Neurosci*, 26(44):11333–41, 2006.
- A. L. Williams, N. Bielopolski, D. Meroz, A. D. Lam, D. R. Passmore, N. Ben-Tal, S. A. Ernst, U. Ashery, and E. L. Stuenkel. Structural and functional analysis of tomosyn identifies domains important in exocytotic regulation. *J Biol Chem*, 286(16):14542–53, 2011.
- E. S. Witze, W. M. Old, K. A. Resing, and N. G. Ahn. Mapping protein post-translational modifications with mass spectrometry. *Nat Methods*, 4(10):798–806, 2007.
- K. Wu, K. Yamoah, G. Dolios, T. Gan-Erdene, P. Tan, A. Chen, C. G. Lee, N. Wei, K. D. Wilkinson, R. Wang, and Z. Q. Pan. Den1 is a dual function protease capable of processing the c terminus of nedd8 and deconjugating hyper-neddylated cul1. *J Biol Chem*, 278(31):28882–91, 2003.

-
- L. G. Wu, T. A. Ryan, and L. Lagnado. Modes of vesicle retrieval at ribbon synapses, calyx-type synapses, and small central synapses. *J Neurosci*, 27(44):11793–802, 2007.
- J. Xia, X. Zhang, J. Staudinger, and R. L. Huganir. Clustering of ampa receptors by the synaptic pdz domain-containing protein pick1. *Neuron*, 22(1):179–87, 1999.
- Z. Xie, D. P. Srivastava, H. Photowala, L. Kai, M. E. Cahill, K. M. Woolfrey, C. Y. Shum, D. J. Surmeier, and P. Penzes. Kalirin-7 controls activity-dependent structural and functional plasticity of dendritic spines. *Neuron*, 56(4):640–56, 2007.
- D. P. Xirodimas, M. K. Saville, J. C. Bourdon, R. T. Hay, and D. P. Lane. Mdm2-mediated nedd8 conjugation of p53 inhibits its transcriptional activity. *Cell*, 118(1):83–97, 2004.
- G. Xu, J. S. Paige, and S. R. Jaffrey. Global analysis of lysine ubiquitination by ubiquitin remnant immunoaffinity profiling. *Nat Biotechnol*, 28(8):868–73, 2010.
- W. Xu. Psd-95-like membrane associated guanylate kinases (psd-maguks) and synaptic plasticity. *Curr Opin Neurobiol*, 21(2):306–12, 2011.
- W. Xu, O. M. Schluter, P. Steiner, B. L. Czervionke, B. Sabatini, and R. C. Malenka. Molecular dissociation of the role of psd-95 in regulating synaptic strength and ltd. *Neuron*, 57(2):248–62, 2008.
- Y. Yamada, Y. Chochi, K. Takamiya, K. Sobue, and M. Inui. Modulation of the channel activity of the epsilon2/zeta1-subtype n-methyl d-aspartate receptor by psd-95. *J Biol Chem*, 274(10):6647–52, 1999.
- H. Yamahachi, S. A. Marik, J. N. McManus, W. Denk, and C. D. Gilbert. Rapid axonal sprouting and pruning accompany functional reorganization in primary visual cortex. *Neuron*, 64(5):719–29, 2009.
- K. Yamoah, K. Wu, and Z. Q. Pan. In vitro cleavage of nedd8 from cullin 1 by cop9 signalosome and deneddylase 1. *Methods Enzymol*, 398:509–22, 2005.
- Y. Yang, J. Kitagaki, R. M. Dai, Y. C. Tsai, K. L. Lorick, R. L. Ludwig, S. A. Pierre, J. P. Jensen, I. V. Davydov, P. Oberoi, C. C. Li, J. H. Kenten, J. A. Beutler, K. H. Vousden, and A. M. Weissman. Inhibitors of ubiquitin-activating enzyme (e1), a new class of potential cancer therapeutics. *Cancer Res*, 67(19):9472–81, 2007.
- I. Yao, H. Takagi, H. Ageta, T. Kahyo, S. Sato, K. Hatanaka, Y. Fukuda, T. Chiba, N. Morone, S. Yuasa, K. Inokuchi, T. Ohtsuka, G. R. Macgregor, K. Tanaka, and M. Setou. Scrapper-dependent ubiquitination of active zone protein rim1 regulates synaptic vesicle release. *Cell*, 130(5):943–57, 2007.
- E. T. Yeh, L. Gong, and T. Kamitani. Ubiquitin-like proteins: new wines in new bottles. *Gene*, 248(1-2):1–14, 2000.

- J. J. Yi and M. D. Ehlers. Ubiquitin and protein turnover in synapse function. *Neuron*, 47(5): 629–32, 2005.
- J. J. Yi and M. D. Ehlers. Emerging roles for ubiquitin and protein degradation in neuronal function. *Pharmacol Rev*, 59(1):14–39, 2007.
- N. Yokoi, M. Fukata, and Y. Fukata. Synaptic plasticity regulated by protein-protein interactions and posttranslational modifications. *Int Rev Cell Mol Biol*, 297:1–43, 2012.
- G. A. Yudowski, O. Olsen, H. Adesnik, K. W. Marek, and D. S. Bredt. Acute inactivation of psd-95 destabilizes ampa receptors at hippocampal synapses. *PLoS One*, 8(1):e53965, 2013.
- J. Zhang, C. M. Petit, D. S. King, and A. L. Lee. Phosphorylation of a pdz domain extension modulates binding affinity and interdomain interactions in postsynaptic density-95 (psd-95) protein, a membrane-associated guanylate kinase (maguk). *J Biol Chem*, 286(48):41776–85, 2011.
- Y. Zhao, A. N. Hegde, and K. C. Martin. The ubiquitin proteasome system functions as an inhibitory constraint on synaptic strengthening. *Curr Biol*, 13(11):887–98, 2003.
- Q. Zhou, M. Xiao, and R. A. Nicoll. Contribution of cytoskeleton to the internalization of ampa receptors. *Proc Natl Acad Sci U S A*, 98(3):1261–6, 2001.
- E. B. Ziff. Tarps and the ampa receptor trafficking paradox. *Neuron*, 53(5):627–33, 2007.
- N. E. Ziv and C. C. Garner. Cellular and molecular mechanisms of presynaptic assembly. *Nat Rev Neurosci*, 5(5):385–99, 2004.

Acknowledgments

This thesis would never have been possible without the support of several people.

First of all, I thank Prof. Dr. Wolfgang Wurst for giving me the opportunity to do my PhD thesis at the Helmholtz-Zentrum München and for all his support.

I want to express my gratitude to the examination board, Prof. Dr. Wolfgang Wurst, Prof. Dr. Valentin Stein and Prof. Dr. Erwin Grill, for evaluating and examining my thesis.

Moreover, I am grateful to Prof. Dr. Dr. Dr. h.c. Florian Holsboer for the opportunity to conduct my PhD thesis at the Max Planck Institute of Psychiatry.

Foremost I thank my supervisor Dr. Damian Refojo for giving me the opportunity to start my PhD thesis in his group. I am very grateful for his support, his constructive suggestions and critical discussions. Damian taught me to understand and to design scientific experiments. In addition, I am very thankful that Damian gave me the possibility to collaborate with Prof. Dr. Valentin Stein and enabling my stay at the University of Bonn.

I am very grateful to Prof. Dr. Valentin Stein, who welcomed me in his laboratory. I am very thankful to Valentin for supporting me in my electrophysiological studies and for training me in preparing and presenting talks. Our fruitful discussion strengthened my scientific view.

Also, I would like to thank Dr. Giuseppina Maccarrone for the great collaboration.

My special thanks are dedicated to the members of AG Refojo, Dr. Annette Vogl, Dr. Sebastián Giusti, Anna Möbus, Dr. Boldizsar Czéh and to the members of AG Stein, Nils Körber, Dorit

Glass, Michael Döngi, and Ira Indrakusuma for great assistant and friendly working atmosphere. Also I want to thank Dr. Jan Deussing and his group for great discussions in all seminars. In particular, I want to thank Nils, Sandra, Nina , and Dorit for their friendship and support whenever it was needed.

Finally, I thank my parents and my sister, who supported me during all this time. Vielen Dank!

Curriculum Vitae

Marisa Brockmann

geb. in Braunschweig

November 25th, 1983

School

2003 | Abitur, Otto-Hahn-Gymnasium Gifhorn

University

2003–2007 | Bachelor of Science in "Molecular Medicin" at the University of Göttingen

2007–2009 | Master of Science in "Experimental and Clinical Neuroscience" at the University of Regensburg

2009–2013 | PhD-Thesis in the lab of Dr. Damian Refojo "Molecular Neurobiology" at the MPI of Psychatrie; Technical University of Munich

2014 | Post-doc in the lab of Prof. Dr. Valentin Stein at the University of Bonn

Scholarship

2007 | IFMSA - Research Exchange, Fukushima, Japan

2008–2009 | Max Weber-Programm Bayern, Studienstiftung des deutschen Volkes

Theses

- 2007 **Bachelor Thesis** at the University of Göttingen - "Sensibilisierung von strahlenresistenten Prostatakarzinomzellen"
- 2009 **Master Thesis** at the National Institute of Health, Bethesda - "The anxiolytic effect of oxytocin"
- 2001–2005 **PhD Thesis** at the MPI of Psychatrie "Nedd8 in the brain – Its impact on neuronal function and the role of PSD-95"

Publications

Milenkovic VM, **Brockmann M**, Stöhr H, Weber BH, Strauss O. (2010) Evolution and functional divergence of the anoctamin family of membrane proteins. *BMC Evol Biol.* *BMC Evol Biol* 10: 319

Milenkovic VM, **Brockmann M**, Meyer C, Desch M, Schweda F, Kurtz A, Todorov V, Strauss O. (2010) Regulation of the renin expression in the retinal pigment epithelium by systemic stimuli. *Am J Physiol Renal Physiol.* 299(2): F396-403

Meetings and Conferences

43rd annual meeting of the Society for Neuroscience, San Diego, Abstract/Poster

10th Göttingen Meeting of the German Neuroscience Society, Abstract/Poster

XXVI CINP Congress 2008, Munich, Germany,

Publications

Brockmann MM*, Annette Vogl*, Sebastian A. Giusti¹, Giuseppina Maccarrone, Anna J. Moebus, Julia Richter, Claudia A. Vercelli, Francesco Roselli¹, Gerhard Rammes, Daniela M. Vogt-Weisenhorn, Christoph W. Turck, Valentin Stein, Jan M. Deussing, Damian Refojo (2013) The Nedd8 pathway controls dendritic spine maturation and stability: critical role of PSD-95 neddylation; submitted to Nature Neuroscience

*contributed equally to this work

Milenkovic VM, **Brockmann MM**, Stöhr H, Weber BH, Strauss O. (2010) Evolution and functional divergence of the anoctamin family of membrane proteins. BMC Evol Biol. BMC Evol Biol 10: 319

Milenkovic VM, **Brockmann MM**, Meyer C, Desch M, Schweda F, Kurtz A, Todorov V, Strauss O. (2010) Regulation of the renin expression in the retinal pigment epithelium by systemic stimuli. Am J Physiol Renal Physiol. 299(2): F396-403